TROPICAL FOREST MAPPING AT REGIONAL SCALE USING THE GRFM SAR MOSAICS OVER THE AMAZON IN SOUTH AMERICA

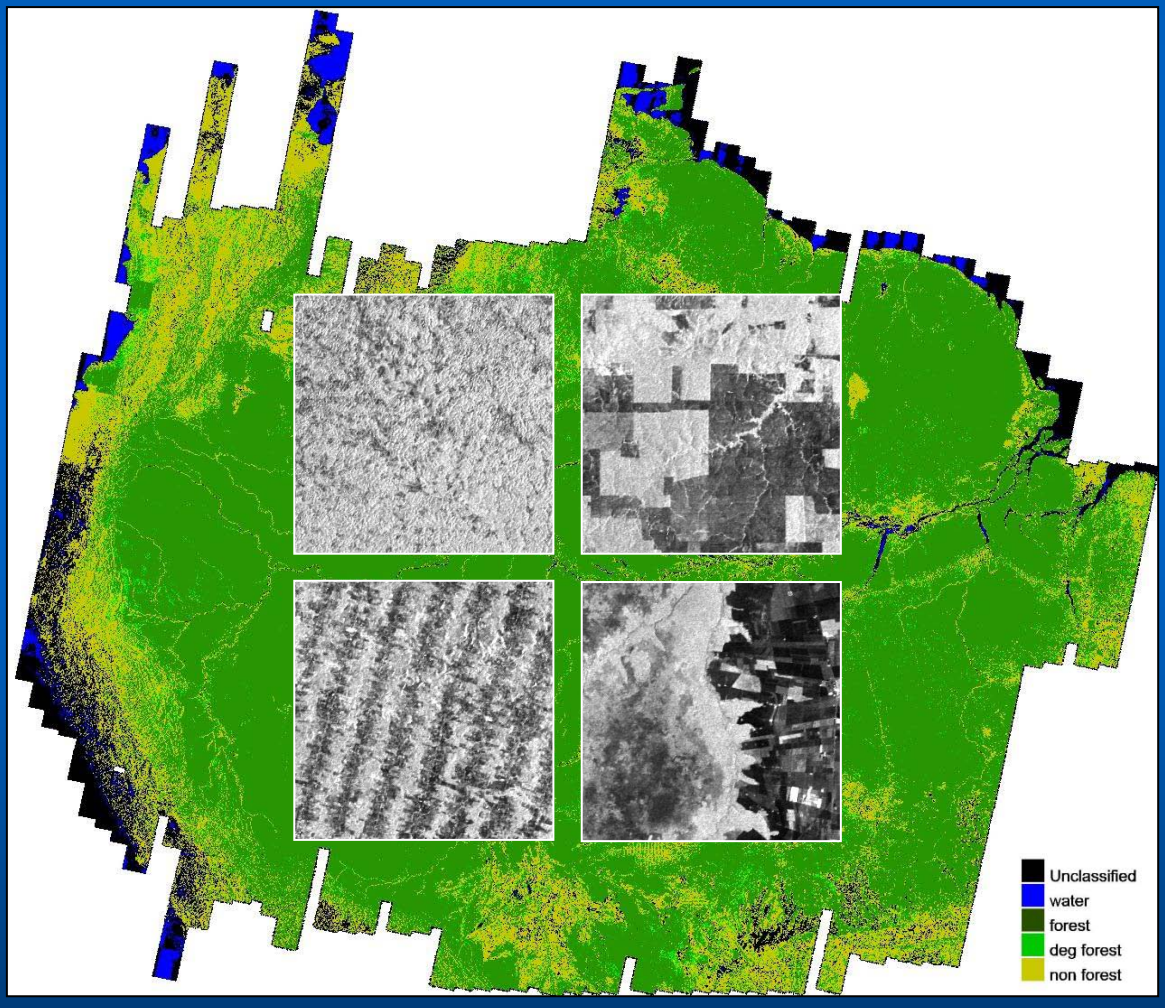

Matteo Sgrenzaroli

TROPICAL FOREST MAPPING AT REGIONAL SCALE USING THE GRFM SAR MOSAICS OVER THE AMAZON IN SOUTH AMERICA

Promotor: Prof. dr. ir. R.A. Feddes
Chair Soil Physics, Agrohydrology and Groundwater Management
Department of Environmental Sciences,
Sub-Department Water Resources,
Wageningen University

Co-promotor: Dr. Dirk H. Hoekman
Department of Environmental Sciences,
Wageningen University

Dr. Ing. Gianfranco De Grandi, Fellow IEEE
Global Vegetation Monitoring Unit,
Institute for Environment and Sustainability,
European Commission, DG Joint Research Centre

Samenstelling promotiecommissie:
Prof. ir. P. Hoogeboom (Technische Universiteit Delft)
Prof. dr. M. E. Schaepman (Wageningen Universiteit)
Prof. dr. A. de Gier (ITC, Enschede)
Dr. ir. C. Varekamp (Philips Research, Eindhoven)

TROPICAL FOREST MAPPING AT REGIONAL SCALE USING THE GRFM SAR MOSAICS OVER THE AMAZON IN SOUTH AMERICA

Matteo Sgrenzaroli

Proefschrift
ter verkrijging van de graad van doctor
op gezag van de rector magnificus
van Wageningen Universiteit,
prof. dr. ir. L. Speelman
in het openbaar te verdedigen
op woensdag 25 februari 2004
des namiddags om 16.00 uur in de Aula

ISBN 90-5808-995-9

Abstract

The work described in this thesis concerns *the estimation of tropical forest vegetation cover in the Amazon region using a continental scale high resolution (100 m) radar mosaic as data source.* The radar mosaic was compiled by the Jet Propulsion Laboratory (Caltech/NASA JPL) using approximately 2500 JERS-1 L-band scenes acquired in the context of the Global Rain Forest Mapping project by the National Agency for Space Development of Japan (NASDA).

A novel classification scheme was developed for this purpose. The underpinning method is based on a wavelet signal decomposition/reconstruction technique. In the wavelet reconstruction algorithm, *an adaptive wavelet coefficient threshold is introduced* to distinguish wavelet maxima related to the transition between classes from maxima related to textural within-class variation.

Two image-labeling techniques are tested and compared: i) a region-growing algorithm and ii) a per-pixel two-stage hybrid classifier.

The large data volume problem was tackled by developing a special purpose processing chain that works on partially overlapping tiles extracted from the mosaic

Quantitative validation and error analysis of the classifiers' performance and their generalization capability to regional scale are carried out using, as reference, maps derived from Landsat Thematic Mapper. A first result of the validation process is that the wavelet classifier provides a *classification accuracy of 87% in forest/non-forest mapping.* The analysis by site reveals that *class degraded-forest is the major source of classification errors.* The *discrepancy between TM maps and SAR maps increases with increasing landscape spatial fragmentation.*

A test on relative performances between the wavelet-based region growing segmentation technique and a conventional clustering technique (ISODATA) shows

that the wavelet-based technique provides better accuracy and is capable of generalizing over the entire data set.

The issue of *detecting the degraded-forest class* - generally ignored by Amazonian deforestation mapping programs - is *tackled using data acquired by both optical and SAR instruments*. For optical data, a three-stage classification procedure is developed for detecting degraded forest classes in Landsat TM images. For SAR data, a multi-temporal speckle filtering technique is used to improve the signal to noise ratio. Forest degradation, characterized by small isolated and elongated bare soil regions regularly distributed in forest areas, is visually detectable in the filtered imagery.

Starting from the consideration that the discrepancy between TM maps and SAR maps increases with the landscape spatial fragmentation, *an inductive learning methodology, capable of correcting SAR regional-scale maps using local classification estimates at a higher resolution* is tested.

Finally some ideas and projects are put forward which are meant to be working hypotheses for future actions and practical approaches to reduce the pressure over the tropical forest ecosystem.

Samenvatting

Het werk beschreven in dit proefschrift betreft *de schatting van het areaal tropisch bos in het Amazonegebied door middel van een radarmozaïek met hoge resolutie (100 m) en continentale bedekking als databron.* Het radarmozaïek is door het Jet Propulsion Laboratory (NASA JPL) samengesteld uit ongeveer 2500 JERS-1 L-band radarbeelden die opgenomen zijn door het National Agency for Space Development of Japan (NASDA) ten behoeve van het Global Rain Forest Mapping project.

Voor dit doel is een nieuwe classificatie methode ontwikkeld. Deze methode is gebaseerd op een wavelet signaalontbinding en –reconstructie techniek. Binnen het wavelet reconstructiealgoritme wordt *een adaptieve wavelet coëfficiënt drempel geïntroduceerd* om wavelet maxima gerelateerd aan de ruimtelijke overgang tussen klassen te kunnen onderscheiden van maxima gerelateerd aan textuurvariaties binnen een klasse.

Twee beeldkenmerkbenoemingstechnieken zijn getest en vergeleken: i) een gebiedsaangroei algoritme en ii) een per beeldelement twee-traps hybride classificeerder.

Het probleem van het grote data volume is aangepakt door de ontwikkeling van een speciaal voor dit doel vervaardigde verwerkingsketen die werkt op de gedeeltelijk overlappende deelgebieden waaruit het mozaïek is samengesteld.

Kwantitatieve validatie en foutenanalyse van de prestaties van de classificeerders, en hun mogelijkheden voor generalisatie naar een regionale schaal, zijn uitgevoerd met behulp van kaarten afgeleid uit Landsat Thematic Mapper beelden als referentie. Een eerste resultaat van dit prestatiebeoordelingsproces laat zien dat de wavelet classificeerder *een nauwkeurigheid van 87% haalt voor kartering*

van bossen versus niet-bossen. De analyseresultaten op het niveau van individuele testgebieden laten zien dat *de klasse gedegradeerd bos de voornaamste oorzaak is van classificatiefouten. De discrepantie tussen TM-kaarten and SAR-kaarten neemt toe met toenemende fragmentatie van het landschap.*

Een vergelijkende test naar de relatieve prestaties van de op wavelets gebaseerde techniek van segmentatie door gebiedsgroei en een conventionele cluster techniek (ISODATA) laat zien dat de op wavelets gebaseerde techniek een hogere nauwkeurigheid geeft en in staat is een generalisatie te leveren voor de gehele dataset.

Het probleem van *de detectie van de klasse gedegradeerd bos* – in het algemeen veronachtzaamd binnen programma's voor kartering van ontbossing in de Amazone – *wordt aangepakt door zowel optische als SAR data te gebruiken*. Voor optische data is een drie-traps classificatieprocedure ontwikkeld voor detectie van gedegradeerd bos in Landsat TM beelden. Voor SAR data is een multitemporele speckle filteringtechniek gebruikt om de signaal-ruis verhouding te verbeteren. Bosdegradatie, gekarakteriseerd door kleine langwerpige en geïsoleerde gebieden zonder vegetatiebedekking, en met een regelmatige verdeling binnen bosgebieden, is visueel waarneembaar in gefilterde beelden.

Uitgaande van de veronderstelling dat de discrepantie tussen TM-kaarten en SAR-kaarten toeneemt met de mate van landschapsfragmentatie *is een inductieve leermethode getest. Deze methode blijkt de mogelijkheid te hebben om lokale classificatieschattingen bij een hogere resolutie te gebruiken voor de correctie van SAR-kaarten met regionale schaal.*

Tenslotte worden enkele ideeën en aanbevelingen gegeven die bruikbaar kunnen zijn als werkhypothesen of als praktische benaderingen om de druk op het tropisch bosecosysteem te verlichten.

Acknowledgments

First of all I would like to thank my co-promotor Dr. Gianfranco De Grandi for what he taught me, for his fundamental help in carrying out my research work at the JRC and his sincere friendship.

I express my gratitude to my promotor Prof. dr. ir. Reinder Feddes, and to my co-promoter Dr. Dirk Hoekman, for accepting me as part of the Ph.D. Program at Wageningen University and for their fundamental help in the thesis revision.

The work reported in this thesis was carried out at the Global Vegetation Monitoring Unit (GVM), Institute for Environment and Sustainability, DG Joint Research Centre (JRC) of the European Commission and it was supported by a JRC category 20 grant. I wish to express my gratitude for all the support I had from this Institution, particularly by Alan Belward, GVM Head of Unit and by Jean Paul Malingreau, former GVM Head of Unit.

Also my gratitude goes to Wageningen University for the support in preparing and defending my Ph.D. thesis.

During the years spent at JRC, a lot people have personally helped me, contributing to the final result. I wish to mention in the following each of those people not in order of importance but trying to follow the chronology of my life as a student and as a researcher.

First of all my gratitude goes to Prof. Ing. Giovanmaria Lechi and Prof. Rudolf Winter who introduced me to the remote sensing world.

Special thanks to Frederic Achard for exposing me to the TREES Project technical and historical issues. It was also a pleasure for me to ski and climb with him the Italian Alps.

Thanks to Hugh Eva, whose great experience with the South American environment was instrumental for my work, in particular in connection with the data set selections, thematic class definition and validation problems.

To Bruce Chapman of JPL, who gave me the possibility to work hands-on on the "first" GRFM South America radar mosaic.

To Ake Rosenqvist, for his contribution in retrieving JERS-1 historical data for time-series analysis.

To Elisabetta Franchino and Giorgio Perna, the software gurus, without whom the IDL language would still be a mystery for me.

To Tim Richards, whose great experience in geo-referencing problems was fundamental in the data-set preparation.

To Paul Siqueira of JPL, for his help with SAR data processing and with fond memories of our joint trip to the Amazon Forest.

To Andrea Baraldi, who introduced me to the image classification secrets. Discussing with him on image processing issues was worth while attending a full university course.

To Philippe Mayaux, for his help in building a model for correcting global estimates from local ones.

I would like to express my gratitude to the entire GVM research group. It was really important for me to have expert remote sensing researchers available and ready too answer my questions when I knocked at their doors.

I wish finally to thank Prof. Giorgio Vassena of University Brescia and my present colleagues in Brescia for their patient support during the last period of the thesis's correction and defence preparation.

During these years my family has been constantly present to encourage me and to give me the serenity of mind that is a key ingredient for research work. My mother's and father's passion for life were an inspiration for me and established a framework

to look in the due perspective at scientific problems. A special thank to my sister Paola for her loving and supporting presence at my side during these years.

Contents

Chapter 1
Introduction

1.1 Background

Tropical rainforests form an irregular vegetation belt comprised between the Tropic of Cancer to the North and the Tropic of Capricorn to the South. Rainforests can exist only in high rainfall areas (precipitation > 110 mm/month) having a short or non-existent dry season, at an altitude lower than 1300 m where the soil's physical properties ensure high levels of available soil moisture and the mean annual temperature is around 24° C.

The Amazon river basin in South America, the Congo river basin in Africa and the Borneo and Papua New Guinea in South East Asia are in order of size the world widest geographical regions covered by tropical rainforests (see figure 1.1).

Tropical forests represent important pools of biological, ecological and economic resources. Covering less than 7% of the earth, they contain half of the planet's species. For instance, in a half hectare of Amazonian forest, 200 different tree species can be found while in the whole of North America the amount of different tree species is around 400.

Moreover, these ecosystems have constituted for millennia the natural habitat of native populations. Many archeological finds, discovered in wide areas within the Amazon basin, prove the intensive but sustainable usage of forest resources from indigenous populations in the past (Fisher, 1990).

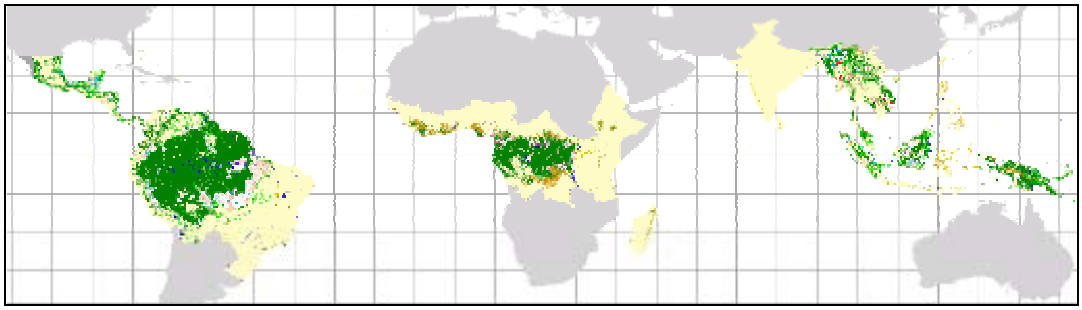

Figure 1.1: Geographical location of the Tropical forest belt (see color Figure B.1 - Annex B, pp. 201).

1.2 Deforestation and related consequences

Tropical rainforests are particularly threatened by the rapid increase, worldwide, in the demand for new agricultural, ranching or farming land, by selective and intensive logging, by mining or oil/gas extraction, by settlements or tourism programs, water diversion and dam building (figure 2.2 shows the effect of a fire event) (Meyers 1980, 1996, and 2000; Lanly, 1982, Jerry, 1986).

Figure 1.2: The photo, taken in Brazilian Amazonia, shows a deforested area where the ground was cleared by fire (see color Figure B.2 - Annex B, pp. 201).

In many rainforest regions the native populations have been decimated; anthropologists calculate that 8 million South American Indians lived in Brazil before the discovery of the New World and nowadays only 230,000 Indians survive. About half of the tropical rainforest on earth have been destroyed and the remaining coverage is about 9 million square kilometers.

A total of 5.1 million ha of forest was lost per year in tropical South and Central America over the period 1990 to 1995 (FAO, 1997). 500,000 square kilometers of primary forest in Brazil's Legal Amazon were converted to ranching, agriculture, hydroelectric dams and other land uses at a rate of 20,000 square kilometers per year during the 1978-1988 period (Fearnside, 1993a)**,** 19,000 square kilometers per year for the 1988-1989 period, 14,000 square kilometers per year for the 1989-1990 period, 11,000 square kilometers per year for 1990-1991 (Fearnside, 1993b)**,** 14,000 square kilometers per year for 1991-1992 and 15,000 square kilometers per year for 1992-1994 (INPE, 1996), 29,000 square kilometers per year for 1995, 18,000 square kilometers per year for 1996, 13,000 square kilometers per year for 1997 and 17,000 square kilometers per year for 1997 (INPE, 1998).

These deforestation phenomena are related to another important aspect: the tropical rainforests role in the atmosphere – biosphere exchange processes, and in particular for the carbon cycle and the green house gases flow - such as carbon dioxide and methane. This issue is linked to global climate change, a problem of great political and scientific relevance (Mellillo *et al.,* 1996; Devol, 1998)

Large conversion of tropical forest into pastures or annual crops could lead to changes in the climate. Numerical models of the global atmosphere and biosphere, used for simulating the effects of the Amazonian tropical forest replacements by degraded grass (pasture), have revealed a significant increase in the mean surface temperature (about 2.5° C) and a decrease in the annual evapo-transpiration (39%

reduction), precipitation (25% reduction), and runoff (20 % reduction) in the region (Nobre *et al.,* 1991).

Continuous collection of climate and soil moisture data at different sites within forest and pasture in the Amazon basin has confirmed the model results demonstrating the local-scale, meso-scale, and large-scale climatic impacts of deforestation (Gash and Nobre, 1997).

Moreover tropical forest conversion, shifting cultivation and clearing of secondary vegetation make significant contributions to the global emission of greenhouse gases today, and have the potential for large additional emissions in future decades (Zhang *et al*., 1996). Although the discrepant estimations of the total net emission of carbon from the tropical land use (i.e. for the 1981-1990 period: 2.4 million t C per year according to INPA (Fearnside, 2000) or 1.6 million t C per year according to Intergovernmental Panel of Climate Change (IPCC), they all indicate that continued deforestation would produce greater impact on global carbon emission

The recent Protocol to the Framework Convention on Climate Change agreed in Kyoto has but stressed the critical nature of the situation, confirming general awareness and the need for political action towards a long-term solution (UNEP/IUC., 1999)

1.3 Objectives

This research work addresses *the problem of deriving and validating regional scale estimates of the tropical forest cover in South America using a wide area high resolution (100 m) L-band radar mosaic.* This data set was compiled in the context of the Global Rain Forest Mapping (GRFM).project, an initiative of the Agency for Space Development of Japan (see section 1.5).

1.4 Remote sensing for forest monitoring

A correct evaluation of tropical forest resources implies a response to a set of simple questions (Mayaux, 1998).

1) Where are the forested areas?
2) How much tropical forest remains?
3) What are the changes that have affected and will affect those ecosystems?

Delivering accurate estimates of tropical forest coverage is therefore a key component to give an answer to these questions.

A related question is: which instruments are available for this purpose?

Earth observations by satellite provide a unique technology to acquire quantitative information on forest cover, particularly on a regional scale (Kummer, 1992; Looyen, 1993; Mayaux *et al.,* 2000).

Field-based inventories have in fact many technical restrictions: the vastness and the wilderness of the tropical ecosystem would limit extrapolation from a discreet sampling over a continuous spatial dimension.

Airborne sensors may offer a higher spatial, spectral and radiometric resolution, or the possibility of selecting the time of image acquisition. But due to expensive and spatially limited acquisitions they are more suitable for local forest survey (Hoekman and Varekamp, 2001; Hoekman and Quiñones, 2002; Van der Sanden and Hoekman, 1999)

Moreover, the cost of satellite images is usually much lower than that of digital airborne images. Lower spatial resolution of satellite images (image resolution of the most widely employed sources of remotely sensed data goes from 18m of SPOT images to 1.1 km of NOAA-AVHRR) (D'Souza *et al.,* 1985) although in a way a restriction, facilitates the analyses of wider areas. The higher sensor stability (i.e. compared to the airborne sensor) facilitates relative image registration for monitoring

in time. In some cases, the coarse spatial resolution may give more stable and representative measurements when there is very high heterogeneity.

Satellite remote sensing offers different sensors for measuring different ground parameters at different scales. The imaging instruments can be divided into two main categories: active and passive instruments. A typically active sensor is radar (Radio Detection and Ranging), which measures the strength and round-trip time of the microwave signals that are emitted by a radar antenna and reflected off a distant surface or object. The radar antenna alternately transmits and receives pulses at particular microwave wavelengths (in the range 1 cm to 1 m, which corresponds to a frequency range of about 300 MHz to 30 GHz) and polarizations (waves polarized on a single vertical or horizontal plane). Passive instruments generally work in the visible or thermal domains (approximately from 0.35 micron to 15 micron) measuring the Sun reflected energy or the target emitted energy.

Parameters to be estimated are the forest cover extension compared to the anthropic or natural non-forest area. This objective implies the extraction of thematic information on vegetation cover by classifying satellite images.

The geographical extension of deforestation phenomena calls for regional scale mapping, which requires imagery with wide and continuous geographical coverage.

Inconsistencies in the methods, legends and frequency of national surveys have led to the use of optical remotely sensed data to monitor tropical forests at national (INPE, 1996), pan-tropical (Skole, 1993; Achard *et al*., 1998) and global (FAO, 1993) levels. Despite offering synoptic views of the changes, these approaches all suffer from major logistical problems in processing the data, and in a lack of completeness due to cloud cover.

Radar data offer all weather, 24 hour acquisition and allows to obtaining wall-to-wall coverage in tropical area affected by cloud coverage. Despite this advantage the

specific knowledge required for image formation and raw data processing, historically hindered the radar data usage for global scale problems.

The usage of satellite data set - both from optical and radar sensors - for global scale problems call for adequate geometric, radiometric, geocoding and data analysis tools due to the massive data volume involved.

1.5 Approaches and techniques for forest monitoring by satellite

1.5.1 Optical remote sensing approaches

Optical remote sensing approaches, as recommended by Myers (Myers, 1989) to improve world tropical forest assessment, became the basis for several initiatives launched in the early 1990s by organizations such as the Food and Agriculture Organization of the United Nations (FAO), the World Conservation Union (IUCN), the European Commission (EC) Joint Research Centre (JRC), the National Aeronautics and Space Administration (NASA) and the Woods Hole Research Center (WHRC).

More recently and specifically for the Amazon region the Instituto National de Pesquisas Espaciais (INPE) has initiated a remote sensing-based program for tropical forest assessment at national level (INPE, 1996). A Landsat TM wall-to-wall coverage at national level is adopted by INPE in this project.

FAO Forest Resource Information System (FAO-FORIS), the geographical information system developed by FAO and IUNC Conservation Atlas of the Tropical Forest (Collins *et al.,* 1991; Sayer *et al.,* 1992; Harcourt and Sayer, 1996) approach the problem through compilation of existing national surveys that often differ from country to country.

FAO Remote Sensing Survey (FAO-RS) adopts a statistical sampling with Landsat TM 30 m spatial resolution optical images.

NASA's Landsat Pathfinder Tropical Forest Inventory Project (Skole and Tucker, 1993; Chomentowski *et al.,* 1994) is designed to map the rates of deforestation in the tropical forest by a Landsat TM wall-to-wall coverage of the early 1970s, mid 1980s and mid 1990s.

The TREES (Tropical Forest Ecosystem Environments monitoring by Satellites) project developed by EC JRC is based on a NOAA AVHRR wall-to-wall coverage (1.1 km ground resolution) and samples of Landsat TM data (30 m ground resolution) for area correction (Mayaux *et al*., 1998; Mayaux and Lambin, 1995, 1997).

Comparing results from these different forest assessment projects Mayaux *et al*. (Mayaux *et al.,* 1998) have spotted discrepancies than can be ascribed to the following methodological elements.

First, different forest-resource assessments do not share the same definition of forests. Forest definition can refer to spectral response of the adopted sensor, or to the inventory requirements.

Spatial resolution and acquisition frequency are the two parameters of the optical remote sensing data sets that cause major discrepancies among the forest survey projects which have been here mentioned. High spatial resolution optical sensors (e.g. Landsat TM 30 m pixel size) suffer from low frequency of acquisition especially in tropical cloudy regions. On the other hand, despite the nearly day by day coverage, coarse spatial resolution optical sensors (i.e. NOAA AVHRR 1.1 km pixel size) lead to loss of spatial detail with respect to the spatial structure of the landscape (Woodcock and Strahler, 1987).

These difficulties in obtaining wall-to-wall high-resolution coverage call for statistical sampling in space to extrapolate global coverage statistics (i.e. FAO-RS

approach) or for correcting proportional errors of coarse resolution coverage (i.e. TREES approach).

Finally differences in forest statistics are also related to the different methodologies adopted for image interpretation. The satellite data can be analyzed by visual interpretation or by automatic classification. Batista and Tucker (Batista and Tucker, 1991) found that visual interpretation of Landsat TM images, coupled with digitizing the results into a geographic information system, is the best tropical deforestation determination technique. A confirmation is given by Mas and Ramirez (Mas and Ramirez, 1996) who maintain that visual classification presents a higher overall accuracy than the best digital classification. On the other hand there is evidence that visual interpretation tends to overestimate the forest cover in heavily-forested areas (Mayaux *et al.,* 1998) and to underestimate the forest that has been impoverished (i.e., degraded) each year (Nepstad *et al.,* 1999). In any case detection of deforestation phenomena on regional scales and high spatial resolutions still depends to a large extent on human photo-interpretation (i.e. FAO-RS, INPE), (Stone and Lefebvre, 1998); TREES and Landsat Pathfinder adopt a mixed procedure, combining an automatic classification of the raw images and a visual labeling of the resultant classes (Mayaux *et al.,* 1998; TRFIC)**.**

Finally it is worth noticing that even though in the image analysis and pattern recognition literature there has been a great development of new methods for image labeling in recent years, many labeling techniques have had a minor impact, owing to their functional, operational and computational limitations. (Zamperoni, 1996; Jain and Dubes, 1988; Jain and Binford, 1991; Kunt, 1991).

Within the limits imposed by the intrinsic difficulties mentioned above, global tropical forest area estimation can be improved by the use of radar remote sensing. Indeed, in contrast to optical sensors, radar sensors can provide on-demand high

resolution acquisitions with a frequency that is independent from the weather conditions.

1.5.2 Radar remote sensing approaches

Thematic information extraction on the vegetation cover from radar data, either by visual inspection or by automatic classification, indicates that these data can provide a new and important characterization of some geophysical parameters related to tropical forests (Bijker and Hoekman, 1994, Conway *et al.,* 1996, Hoekman, 1995; Hoekman, 1997b; Hoekman and Quiñones, 2000; Van der Sanden and Hoekman, 1995; Varekamp and Hoekman, 2001; Woodhouse and Hoekman, 1996; Van der Sanden, 1997b; De Grandi, 1997a).

Much research work was recently devoted to tropical forest assessment using radar remote sensing. This work however is limited to the radar mapping at national and local level. Some examples in bibliography specifically related to Amazon forest are listed in table 1.1; other important examples are reported in (De Araujo, 1999; Dutra *et al.,* 1999; Hoekman, 1995; Salas *et al.,* 2002; Sgrenzaroli *et al.,* 2000)

Due to the extent of tropical forest area, space-borne radar sensors are ideal vehicles for tropical forest assessment at continental/regional level.

Initiatives for radar applications at regional level are still very few. Among these the NASDA Global Rain Forest Mapping (GRFM) can be considered the first international project, that has overcome the two constraints that historically hindered radar data usage for global scale problems: i) the heavy requirements of data processing and ii) the massive data volume involved.

Table 1.1: Examples of radar (satellite and airborne) mapping applications at local and national level.

Author	Study area	Type of sensor and resolution	Thematic context	Classification methodology
Haschimoto and Tsuchiya, 1995	Center Amazonia, Rondonia, Sena Madureira (Brazil)	JERS-1 SAR L-band, 12.5 m	Forest, clear-cuts mapping	Images backscatter thresholding and visual interpretation
Freeman *et al.,* 1995	Manu National Park (Peru)	JERS-1 SAR L-band, 100 m	Forest (different types)/non forest	Bayesian Maximum likelihood classifier (feature vector: backscatter and texture)
Schmidt *et al.,* 1996	Rondonia (Brazil)	ERS-1 SAR C-band, 25 m	Forest / non forest	Maximum likelihood classifier applied on filtered images. Texture classifier (EBIS) on unfiltered images
Keil *et al.,* 1997	Acre and Rondonia (Brazil)	SIR-C/X L-band and C-band	Forest, non forest, degraded forest	Maximum likelihood classifier applied on filtered images. Texture classifier (EBIS) on unfiltered images
Yanasse *et al.,* 1997	Tapajos National Forest (Brazil)	SIR-C/X L-band and C-band	Secondary forest regrowth stages	Visual interpretation
Saatchi *et al.,* 1997	Rondonia (Brazil)	SIR-C/X L-band and C-band	Deforestation	Supervised maximum a posteriori Bayesian classifier

Table 1.1: Examples of radar (satellite and airborne) mapping applications at local and national level.

Author	Study area	Type of sensor and resolution	Thematic context	Classification methodology
Van der Sanden, 1997a	Mabura Hill (Guyana) San Jose' del Guaviare (Colombia)	CCRS Airborne SAR C-band and X band Pixel size around 4 m NASA/JPL Airborne SAR (AIRSAR) P-, L- and C-bands Pixel size 6-8 m ERS-1 SAR C-band 25 m, single	Forest (different types), other land cover	Maximum likelihood on radiometric and textural attributes
Bijker, 1997	San Jose' del Guaviare (Colombia)	ERS-1 SAR C-band 25 m	Forest, pasture, grasslands, secondary vegetation	Decision rule classifier Multi-channel segmentation algorithm (RCSEG)
Dutra *et al.,* 1999	Para' (Brazil)	Multitemporal JERS-1 SAR L-band, 12.5 m	Deforestation	Region growing technique
Grover *et al.,* 1999	Tapajos National Forest (Brazil)	Multi-temporal ERS-1 SAR C-band 25 m, single JERS-1 SAR L-band, 12.5 m	Forest, non forest, regrowth	Multi-temporal segmentation on ERS-1 data, image thresholding on JERS-1 data

1.5.3 The Global Rain Forest Mapping (GRFM) project

GRFM was an initiative launched in 1995 by the National Space Development Agency of Japan (NASDA) (Rosenqvist, 1996; Rosenqvist *et al.,* 2000). Goal of the project was to produce wall-to-wall geometrically corrected and radiometrically balanced mosaics of radar backscatter over the tropical rainforests using data acquired by the L-band Synthetic Aperture Radar (SAR) on board the JERS-1 spacecraft (De

Grandi *et al.,* 2000b; Siqueira *et al*., 2000; Shimada *et al.,* 2000). These radar mosaics are spatially and temporally contiguous at a resolution of 100 m. Coverage includes South East Asia, Central Africa and the Amazon basin. As far as our research is concerned, the work is focused on the South America tropical area.

The starting idea of a large-area seasonal mapping by JERS-1 over the entire Amazon Basin originated in 1994 from the Jet Propulsion Laboratory (JPL) evolved at NASDA to cover the entire equatorial belt, and culminated in 1995 with the establishment of the GRFM project. Later on NASDA extended the collaboration to the Joint Research Centre (JRC) of the European Commission (EC), where experience in tropical forest monitoring by radar remote sensing had been already developed through the TREES ERS-1 Project and the ERS-1 Central Africa Mosaic Projects (CAMP) (Malingreau and Duchassois, 1995; De Grandi *et al.*, 1999c).

It has to be noted that the TREES ERS-1 ’94 Project (Malingreau and Duchassois, 1995) systematically assesses for the first time the relevance and usefulness of space-borne SAR (ERS-1) within a series of representative forest areas around the tropical belt. Eight tropical rain forest test sites in South America were selected. A related study on the use of ERS-1 in deforestation detection and monitoring is presented in (Hoekman, 1997). A synopsis of these studies is given table 1.2.

Table 1.2: Radar mapping applications at local and national level for the Latin American Site of *the TREES ERS-1 Study '94.*

Author	Study area	Type of sensor and resolution	Thematic context	Classification methodology
Huising and Lemoine, 1997	Cost Rica	ERS-1 SAR C-band, 25 m, multi-temporal dataset	Forest / non forest	Multi-temporal signature extraction and supervised classification
Keil M. *et al.,* 1997	Sena Madureira, Acre (Brazil)	ERS-1 SAR C-band, 25 m	Forest / non forest	Supervised image thresholding Maximum likelihood EBIS classifier
Conway, 1997	Acre (Brazil)	ERS-1 SAR C-band, 100 m, mono and multi-temporal	Forest / non forest	K-K' Nearest Neighbors
Corves *et al.,* 1997	Manaus region (Brazil)	ERS-1 SAR C-band, 30 m	Forest / non forest	Minimum Euclidean Distance
Wooding and Batts, 1997	Rondonia (Brazil)	ERS-1 SAR C-band, 25 m, multi-temporal dataset	Forest, Scrub/grass, Cultivated	Visual interpretation of multi-temporal color composites
Grover *et al.,* 1997	Tapajos National Park (Brazil)	ERS-1 SAR C-band, 25 m, multi-temporal dataset	Forest (different types), secondary forest, pasture, bare soil	Image filtering and interactive thresholding
Hoekman, 1997a	Aracuara (Colombia)	ERS-1 SAR C-band, 25 m, multi-temporal dataset NASA/JPL Airborne SAR (AIRSAR) P-, L- and C-bands Pixel size 6-8 m	Forest / non forest Shifting Cultivation	Texture analyses, filtering processing, backscattering modelling
Van der Sanden, 1997a	Mabura Hill (Guyana)	ERS-1 SAR C-(SAR.PRI and SAR.SLC multitemporal)	Forest (different types), Logged forest, Non forest, Secondary forest	Visual interpretation of SAR.PRI Textural analysis of SAR.SLC
Bijker and Hoekman, 1997	San Jose' del Guaviare (Colombia)	ERS-1 SAR C-band, 25 m, multi-temporal dataset	Forest , non-forest, savannah, pasture	Filtering and image segmentation

The TREES Central Africa Mosaic Project (CAMP) is one of the first attempts to bring high-resolution SAR data from the role of gap–filler and local hot spot analyses to the role of global mapping on a semi continental scale. Within this project a Central Africa radar mosaic was assembled at 100 m pixel spacing using 477 ERS-1 scenes and covering an area of more than 3,000,000 square km (De Grandi *et al.,* 1999c). This project can be considered a predecessor of the GRFM Project in terms of new perspectives on using SAR data but also for the development of a mosaicking machine software.

An important example of large SAR dataset mosaicking can be found in the work by Jean-Paul Rudant *et al*. [http://earth.esa.int/symposia/papers/tonon/].

An accurate geometric model by block triangulation has been achieved over the whole set French Guyana with a RMS (Root Means Square) plan metric accuracy of 15 m, checked by a differential GPS field campaign led by a French military survey team.

Related to the GRFM project and to thematic information extraction at local level from wide-area radar mosaics, it is important to mention some results obtained by the GRFM science program. This program involves the agencies that generate the radar mosaics (NASA ASF and JPL, NASDA, JRC) but also a large number of organizations, universities and individuals who perform field activities and data analyses at different levels. In table 1.3 we schematically report some of these results that use the GRFM products on a local scale level.

As to regional/continental scale, the generation of thematic products from the high resolution GRFM radar mosaics poses challenging problems with respect to the estimation of relevant geophysical parameters at global scale and the determination of the accuracy of these estimates.

Only a few examples can be found in the literature with reference to the use of radar mosaics for global/regional scale mapping.

De Grandi (De Grandi *et al*., 2000a) present very promising results about a thematic map of the swamp and lowland rain forests in the entire Congo River basin at 200 m pixel size. This map constitutes a significant update in the information on biomes like the swamp forests in the Congo floodplain that were so far not well documented on a continental scale.

Table 1.3: Radar mapping applications at local and national level for South America within the *JERS-1 Science Program '99.*

Author	Study area	Type of sensor and resolution	Thematic context	Classification methodology
Beaulieu N. *et al.*, 1999.	Puerto Lopez (Colombia) Pucallpa (Peru')	JERS-1 SAR L-band, 12.5 m, single and multi-temporal dataset	Gallery forest Flooded areas extension	Image filtering and thresholding Visual interpretation
Dobson *et al.,* 1999.	Cabaliana (Brazil)	JERS-1 SAR L-band and ERS-1 SAR C combination (12.5 m)	Forest (different type), non forest (different classes)	Edge preserving filtering Unsupervised clustering followed by a supervised maximum likelihood cluster labeling
Dutra L. V. *et al.,* 1999.	Acre, Rondonia, Para', Monte Alegre Lake area (Brazil)	JERS-1 SAR L-band, 12.5 m	Relationship forest biomass – radar backscatter Deforestation Flooded areas extension	Texture analyses and minimum distance (Mahalanobis) classifier
Hess L. *et al.,* 1999.	16 test area within the entire Amazon basin	JERS-1 SAR L-band, 100 m	20 forest and savanna types	Visual interpretation
Salas W. S. *et al.,* 1999.		JERS-1 SAR L-band, 12.5 m, multi-temporal dataset	Deforestation, biomass estimates, impact of Faraday rotation	Filtering and ISODATA clustering

In the same thematic context two other studies propose solutions hinging on multi-sensor (radar and optical) regional scale mosaics.

De Grandi *et al*. (De Grandi *et al.,* 1998) illustrate the potential of a synergic combination of the CAMP ERS-1 (C-band) and the GRFM JERS-1 (L-band) mosaics to supply complementary information - the first related to the vegetation cover only, the second to the flooding extent -, and they generate a classification map of the entire Congo floodplain at 200 m pixel size. A simple supervised maximum likelihood classification that works on a two component feature vector (pixel radiometric value and the normalized standard deviation of amplitude data) is used to delineate the swamp and lowland forests. Stratification of the classification map using a-priori knowledge of the vegetation distribution contained in the TREES project GIS is also used to resolve some class ambiguities. Accuracy evaluation of the swamp forest map has been preformed by comparison with interpretation of 6 Landsat TM scenes over the Congo flood-plain.

In the second research work (De Grandi *et al.*, 2001b) the different properties of the composite microwave (ERS-1 C-band, JERS-1 L-band) and optical observations (imaging spectrometer VEGETATION on board SPOT 4) are exploited to achieve a vegetation map of the Central Congo basin. Thematic information on swamp, lowland and flooded forest is derived by a rule-based hierarchical classifier applied on radar data. Secondary forest information that cannot be consistently detected by radar instruments is derived from the optical data using non-contextual clustering algorithms. Information fusion is achieved at the level of the classification maps independently derived from optical and radar data.

The Podest and Saatchi (Podest and Saatchi, 2002) work refers to the GRFM project and to mapping of the Amazonian rainforest and so it is specifically linked to the geographical and thematic context of this thesis. They adopt a multi-scale texture-based classifier for mapping tropical forest land cover types (forest, non forest, terra firme, floodplain, grassland and woodland savanna). Various combinations of first order statistic as texture measures at different scales are used as feature vector into a

supervised multi-scale maximum likelihood classifier. Interesting for the purposes of our work, the JERS-1 backscatter and texture measures can discriminate forest from non forest with very high accuracy (above 90%) while the radar data may have limited sensitivity to separate old secondary regrowth from mature dense forest and various types of herbaceous savanna vegetation.

This bibliographic survey, although non exhaustive of all the scientific work in this field, highlights the fact that a rigorous methodology for an operational usage of global scale radar data and in particular quantitative validation and error analysis of regional scale estimation still need to be worked out and consolidated.

Research work presented here tries to make progress along this line. Results achieved so far can lay the groundwork for future use of radar mosaics in an operational way and in synergy with optical satellite imagery to improve the reliability, timeliness and accuracy of estimates of tropical forest cover change.

We are anyway aware that satellite cannot provide information on all the parameters related to changes in a forest cover. A purely satellite-based system may miss significant features or events, which indicate on-going or impending changes. Such knowledge is usually available locally where first-hand information is gathered by foresters, scientists, project managers and local inhabitants. In our opinion this last component must be more and more involved in the knowledge process and in the decisions for sustainable usage of their land resources. One of the problems is to insert such local knowledge into a broader context where it can be interpreted and linked to information at more generalized levels. The Tropical Forest Information System (TFIS) within the TREES Project context is an example that demonstrates the feasibility of applying space observation techniques towards better monitoring of tropical forest area.

Local initiatives for testing and teaching to local people techniques for forest sustainable usage are the other complementary ways of attacking the problem. We

personally think in fact, that only if the tropical forest ecosystem is conceived by local people as an important resource to be maintained and used in a sustainable way, there will be hope to save this threatened ecosystem.

1.6 Highlights and novel aspects

1.6.1 Data set

The high-resolution (100 m) *Global Rain Forest L-band JERS-1 radar mosaic over South America provides a unique and unprecedented snapshot of the humid tropical ecosystem of the Amazon Basin*. The coverage extends from 14° S to 12° N in latitude and from 50° W to 80° W in longitude.

Several features have made JERS-1 space-borne *SAR* particularly suitable for tropical forest monitoring. Most notably the all weather acquisition capability, an important asset in the tropical belt that is frequently affected by cloud coverage. The low L-band frequency is more sensitive to aboveground biomass. The orbital configuration - adjacent passes on two consecutive days – is particularly suitable for large-area mapping and yields a temporally homogenous data coverage.

1.6.2 Thematic information extraction

Few research works (Saatchi *et al.,* 2000; De Grandi *et al.,* 1998; De Grandi *et al.,* 2000a, De Grandi *et al.,* 2001b; Hoekman and Quiñones, 1997d) are geared to mapping bio-physical parameters in this ecosystem by radar remote sensing on a regional scale and high spatial resolution.

A new classification scheme for producing a high-resolution (100 m) regional scale forest-non-forest thematic map using the GRFM mosaic is developed here. In

the specific thematic context regional scale image segmentation into a limited set of classes (e.g. forest, non-forest, and degraded forest) is obtained.

The underpinning method is based *on a wavelet signal approximation technique* developed by the Global Vegetation Monitoring (GVM) unit for the Joint Research Center (JRC) that can lend support to SAR image processing problems, such as speckle filtering and segmentation. In our specific case we must take into account the following characteristics of the radar imagery:

1) The SAR signal is affected by multiplicative noise
2) Some classes of interest (e.g. *forest*) correspond to highly textured regions.

These signal characteristics make conventional clustering techniques ill suited calling for novel image processing techniques.

In the *wavelet reconstruction algorithm* we introduce *an adaptive wavelet coefficient threshold* applied to the scale where the wavelet coefficients carry predominantly information on strong persistent edges and the noise influence has decayed significantly. In that way we can distinguish the local maxima related to the transition between classes of interest we want to separate (i.e. *Forest/Non-forest* transitions) from local maxima related to textural within-class variation.

Per-pixel (non contextual) and *segment-based* (contextual) clustering technique *are tested*. A non-conventional clustering technique appears to be near-optimal and stable, and performs better in terms of quantization error minimization than several clustering technique found in the literature.

Moreover a *processing chain capable of facing the computational load* due to data volume is developed.

1.6.3 Results validation

Quantitative validation and error analysis of regional area scale estimation are carried out comparing JERS-1 SAR maps with Landsat Thematic Mapper (TM)

optical maps used as reference. This comparison reveals spectral and spatial differences between the optical and SAR imaging systems, which detect different wave scattering mechanisms.

Class *degraded forest* is the major source of classification error. The discrepancy between TM maps and SAR maps increases with the increment of the landscape spatial fragmentation.

SAR maps are derived using a new SAR image wavelet-based clustering technique; the relative performance between the wavelet-based technique and a conventional clustering technique (ISODATA) is then assessed.

The issue of detecting the degraded-forest class - generally ignored by Amazonian deforestation mapping programs - is attacked using data acquired by both optical and SAR instruments. A novel three-stage classification scheme for forest degradation phenomena detection in Landsat TM images is proposed. A multi temporal speckle filtering technique is applied to a time-series of a full-resolution JERS-1 SAR images (12.5 m pixels size) to catch those small isolated and elongated bare soil regions regularly distributed in the forest and related to selective logging degradation.

Starting from the consideration that the discrepancy between TM maps and SAR maps increases with the increment of the landscape spatial fragmentation we test an inductive learning methodology, capable of correcting SAR regional-scale maps using local classification estimates at a higher resolution.

1.7 Structure of the thesis

The data sets used in this work, including remote sensing imagery, reference maps, training and test data, are presented in Chapter 2. The South America GFRM radar mosaic characteristics are given together with a short overview of the basic processing engine for the mosaic generation. Problems related to training and testing

data set compilation using GRFM Mosaic as semi-continental geographical reference are then detailed. Criteria for the selection of these training and testing sets are also highlighted.

The classification problem is the subject of Chapter 3. Both classification methods and the thematic class definition are dealt with. At first an overview is given of the basic underlying theory and the state of the art of classification in the context of applied remote sensing. The focus is then narrowed on the specific methods conceived and adopted for the task pertinent to this research work. A special purpose classification method, suitable for large area radar mosaics, such as the GRFM one, is introduced. An important component of the method is a pre-processing step based on a wavelet decomposition / reconstruction algorithm that generates piece-wise smooth approximations of the SAR imagery. This method is not part of the original developments of this thesis and is therefore only summarized for the sake of completeness. On the other hand, an original extension of the method to cope with within-class textural edges was devised, and is described next. Finally a detailed description of the classes of interest is given. On one side, this description gives an appreciation of the vast amount of ecological and geographical information content of the GRFM South America mosaic. On the other side, it helps in better understanding the technical problems that have to be overcome to detect the classes of interest in our thematic context.

Validations of the classification map and error analysis are reported in Chapter 4. Causes of discrepancy between maps derived from radar and optical data are also discussed. *Class degraded forest is identified as the major source of misclassification, using both optical and SAR imaging system.*

The relative performance of a wavelet-based region growing technique and a conventional clustering technique (ISODATA) is assessed in Chapter 5.

An extension of the thematic problem to include the *degraded-forest* class, generally ignored by Amazonian deforestation mapping programs, is discussed in Chapter 6.

In Chapter 7, an inductive learning methodology, capable of correcting SAR regional-scale maps starting from local classification estimates at higher resolution is proposed.

Chapter 8 gives a summary of the results obtained in this research work. Advantages of forest monitoring by radar remote sensing and future perspectives are discussed. Finally some ideas and projects are put forward which are meant to be working hypotheses for future actions and projects aimed at reducing the pressure over the tropical forest ecosystem.

An application for mapping swamp forests in the Amazonian basin using the GRFM radar mosaic is also described in Appendix A. This application is based on a modified version of the classification scheme of this thesis, and shows therefore the potential of the methods presented here when applied in a different context.

Color pictures are figures are grouped in Appendix B.

Chapter 2

Remote sensing imagery, reference, training and test data

2.1 Introduction

The principal remote sensing data-set adopted in that research is the South America SAR mosaic generated by JPL in the framework of the Global Rain Forest Mapping (GRFM) project, with the data acquired during September-November 1995 by Japanese satellite JERS-1.

The GRFM dataset extends over the area latitude 14º S to 12º N and Longitude 50º W to 80º W. The area coverage was acquired two times during September-November 1995 and again in May-June 1996 respectively. The first acquisition coincides with annual low water mark of the Amazon River. The second acquisition corresponds to the high peak and includes also the Pantanal wetland in Mato Grosso Brazilian state, the North West part of South America up to the Atlantic Cost (Venezuela, Guyana, Suriname, and French Guyana) and Central America. The low-water mosaic, used for this research, is mainly centered on the Brazilian State of Amazonia, Mato Grosso and Parà. Along the East Cost, the Amapà State is comprised. On the North side, French Guyana, Suriname and Guyana are also included, while the Venezuela is partially covered along the south boundary with the Roraima Brazilian State. The coverage of South America West Coast comprises South Colombia, Equador and Peru. North Bolivia and Mato Grosso without the Pantanal area delineate the south border of the data set. The SAR mosaic geographical coverage can be seen in the figure 2.1.

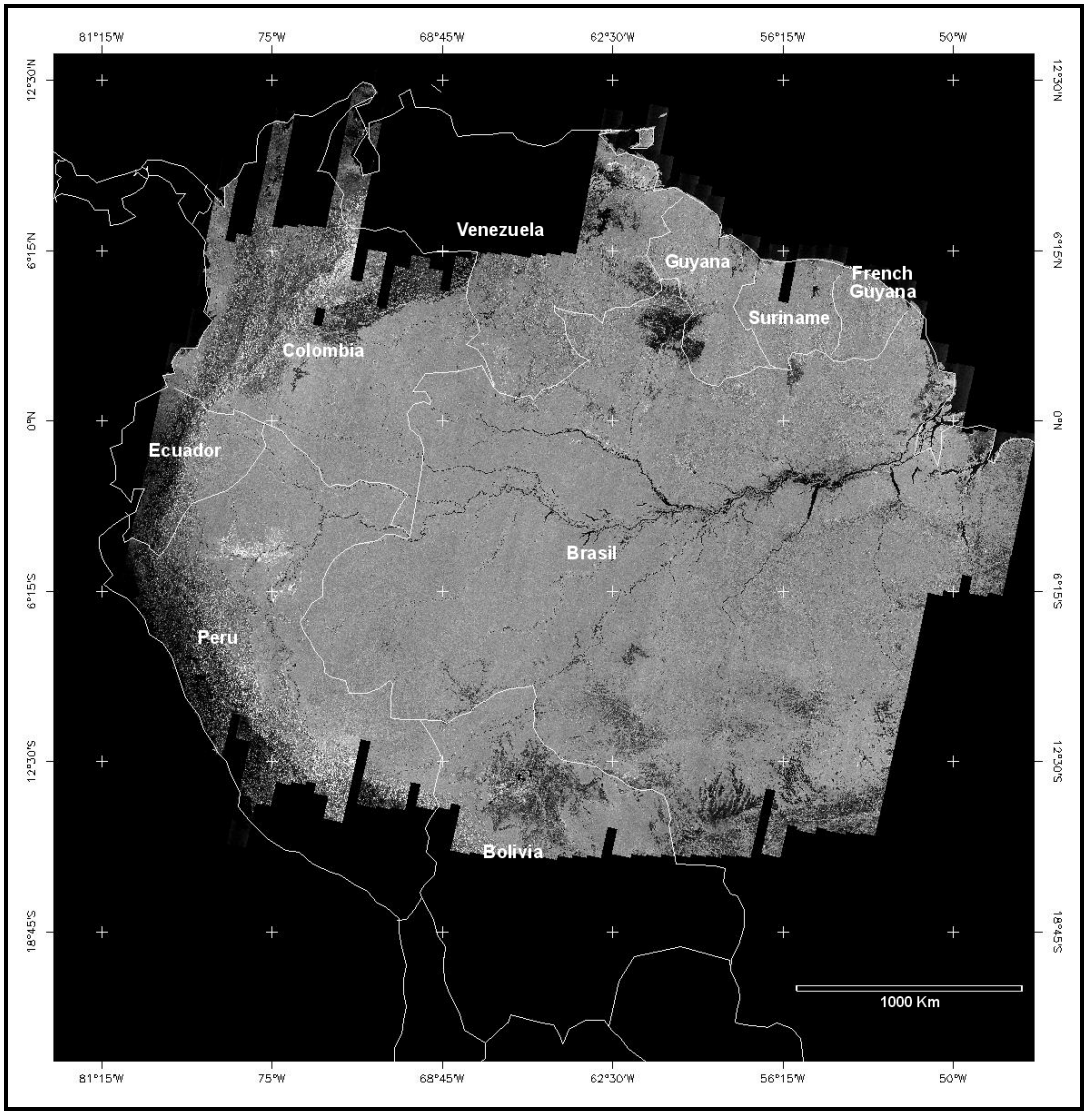

Figure 2.1 GRFM low-water dataset extends over the area latitude 14º S to 12º N and Longitude 50º W to 80º W, approximately 8 million km^2 (35000 x 41000 pixels).

Amazon rainforest is the dominant vegetation of the Amazon Basin. Several types of forest varying in term of structure, biomass, phenology, and floristic characteristics are included in the area covered by the GRFM data set (see Chapter 3).

According to the TREES map (Eva *et al.,* 1999), five main forest types can be identified: lowland dense moist forest, submontane forest, montane forest, mangroves-coastal swamp forest, and dry forest (interface with savanna). Anthropogenic disturbances in the forest domain due for example to ranching, shifting cultivation or more generally colonization can be spatially distributed in linear, diffuse or massive pattern of deforestation. Although closest forest is the dominant vegetation of the Amazon basin, some types of savanna are conspicuous on the mosaics owning to their low backscatter. The two largest savannas on the mosaic are situated at the northern (the Roraima-Rupunumi savannas) and southern (the Llanos de Mojos of northern Bolivia) bounders of the basin.

The method adopted to evaluate the maps derived from SAR data is based on the comparison with high-resolution optical Landsat Thematic Mapper (TM) data, traditionally used for deforestation mapping at high resolution at local scale.

Landsat TM optical imagery and derived maps, produced by the Tropical Rain Forest Information Center (TRFIC-NASA's Earth Science Information Partnership program) and FAO's Forest Resource Assessment Programs (FAO, 1996), are then adopted as reference data. The comparison with Landsat TM optical raw data and derived maps is done at 2 dates (92 and 95) with an interval in time that allows monitoring anthropic changes during the 90'.

The comparison methodology can be sub-divided in two steps:

1) comparison of single date images for area estimation.
2) comparison of two dates images for change detection.

The first step consists in the comparison between a single date TM image with the corresponding single date L-band mosaic in order to assess:

1) the spectral differences of the SAR data with respect to the optical data; where are the errors of commission and omissions when making independent classifications?

2) the spatial limitations; how do area estimates of forest areas from the SAR (100 m pixel size) derived classifications compare to those from reference Landsat TM (30m pixel size) derived classifications?
3) How do the errors relate to the spatial fragmentation of the landscape (hence to the land-use practices)? What are the implications for regional monitoring?

The second step will consist in the comparison between two dates TM images with the corresponding two dates SAR data in order to assess:

1) the feasibility of change detection with radar data;
2) the errors associated with change detection when using the JERS radar mosaics.

In this thesis we mainly focus on the comparison of single date images for area estimation providing some indications for a future monitoring system based on for change detection (Rignot and Chellappa, 1992; Rignot and van Zyl, 1993). The general scheme the methodology is reported in figure 2.2.

Acquisition frequency and geographical coverage of the optical reference data are dependent from cloud coverage. Consequently we can derive training estimate and the associated errors at local scale, selecting three sites within the entire mosaic representative of the different forest cover pattern and deforestation dynamics in the Amazon basin. One additional testing site of interest is selected to assess the generalization ability of the adopted classifier over a fourth independent site.

In order to overlap in time with the 92 optical data set, we locally replicate the processing chain from 92 JERS-1 PRI data to generate small mosaics over the three training sites.

Details on the South America SAR mosaic generated by JPL in the framework of the GRFM project are given in section 2.2. The criteria for the training and testing site selection are detail in section 2.3. Details on training and testing data set compilation is given in section 2.4; generation of ‘small’ SAR mosaic for 92-93 period is described in section 2.4.1; problems of geographical reference of the optical dataset

according with the GRFM are detail in section 2.4.2. Conclusions are reported in section 2.5.

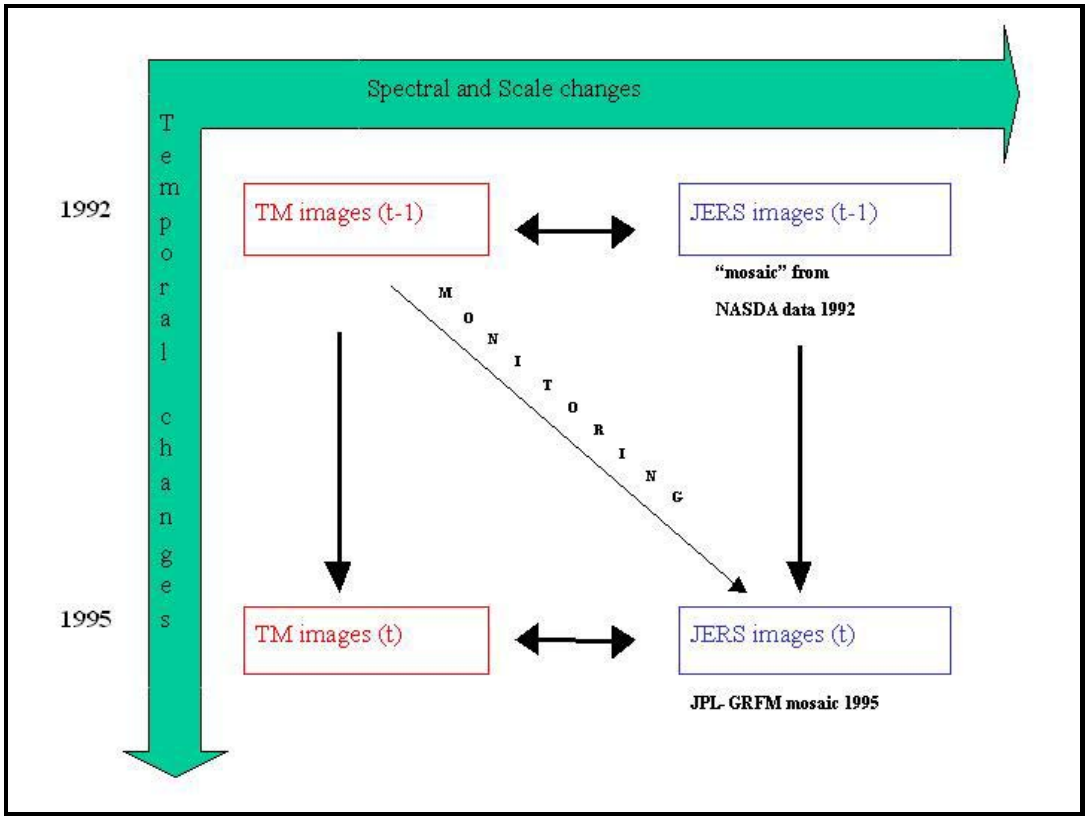

Figure 2.2: Conceptual scheme of the methodology for the comparison between forests estimates from SAR data and high-resolution optical Landsat TM data at local scale.

2.2 GRFM South America mosaic

During September-November 1995, and again in May-June 1996, high-resolution L-band HH-polarized SAR imageries of the entire Amazon basin are acquired by NASDA's JERS-1 satellite, as part of NASDA's GRFM project. *In a cooperative effort between NASDA and Alaska SAR facility (ASF), the approximately 2500 scene for each date are processed and NASA's JPL mosaics them into two digital datasets with 3 arc-second (approximately 100 m) resolution*.

JERS-1 satellite, launched by NASDA and Japanese Ministry of International Trade and Industry (MITI) in February 1992, operated until October 1998 an L-band SAR (23.5 cm/1275 MHz) with horizontal (HH) co-polarization, 35 look angle and a recurrence cycle of 44 days. NASDA performed the data acquisition schedule for the GRFM project and the recorded data (same 13,000 scene) are down-linked either at the NASDA Earth Observation Center (EOC) in Japan or at the ASF to be processed to full resolution (12.5 m ground resolution at three looks) ground range amplitude 16-bit 'Level 2.1' product from NASDA (Shimada, 1996) and 8-bit high resolution product from the ASF respectively (Bicknell, 1992).

The raw data for South America Mosaic NASA JPL Mosaic are (mostly) processed by the Alaska SAR Facility (ASF) in Fairbanks, Alaska. According with the ASF processor the conversion of *DN* values to Sigma $_0$ is:

$$\text{Sigma}_0 = 20*\log_{10}(DN)+F \qquad (2.1)$$

where *DN* is the *DN* value of each pixel (between 0 and 255), and F is the calibration factor. For the South American data, the calibration factor F = -48.54. The result will be in dB. The noise equivalent sigma 0 is about -18 dB.

Description of the *relevant parameter of the JERS-1 data used for the South America GRFM low-water mosaic generation by JPL* are reported in Table 2.1.

Table 2.1: The relevant parameter of the JERS-1 data used for the South America GRFM low- water mosaic generated by JPL.

Frequency	L-band (1275 MHz, 23.5 cm)
Polarization	HH
Incident angle	35 +/- 2.7 degrees
Single scene dimension (max)	1024 x 1024 100 m pixels
Number of looks (theoretical)	64 x (3 looks per 12.5 m pixel)
Orbit and processing specifics	57 orbits, one orbit per day, 1583 scenes, 15 km cross track overlap and 20 km along track overlap between scenes
Collection period	September - December 1995

Next steps in the GRFM processing chain - down-sampling of the full-resolution scene from 12.5 m pixel spacing to 100 m pixel size, validation of images radiometry and geometry, additional calibration an the 100 m resolution framelets, mosaic generation and CD-ROM generation - are separately developed at NASDA, JPL and JRC according to the project division into three geographical regions: South and Central America (JPL), Central and Western Africa (JRC), South East Asia and Northern Australia (NASDA, ERSDAC). These image mosaicking procedures developed and utilized at NASDA, JPL and JRC vary in several steps (Rauste *et al.*, 1999a, b).

As far as our research is concerned, the work is focused on the South America GRFM mosaic generated by JPL.

The full resolution scenes are down-sampled from 12.5 m full resolution to 100 m-pixel size by block averaging in power domains within 8x8 pixels window.

Image mosaicking is preformed by means of block adjustment using the 100m framelets. The iterative block adjustment is applied to data from one season only and the second season coverage rectified scene-by-scene to the first 'master' mosaic. In the adjustment procedure relative scene displacements, calculated by image correlation in the overlapping area between scenes, are used as observations and ground control points, derived from existing maps or from the World Vector Shoreline data set, are added as additional observation for absolute geo-location (Siqueira *et al.,* 2000).

The GRFM data-set over South America comprises three layers: low-water amplitude, high-water amplitude, and low-water texture calculated as variance on mean ratio within 8x8 pixels used for the down-sampling from 12.5 m full resolution to final resolution of about 100 m. The final characteristics of the South America JPL output are 3 arcseconds pixel spacing in latitude and longitude (approximately 89-93 meters) amplitude and texture mosaics on an equiangular latitude/longitude grid.

For the objectives of this research we focus only on information extraction from the low-water amplitude data set. We want to extract a high-resolution forest-non-forest map using only 1 radar-band posing the basis for replicating in the future the coverage with radar mosaics adequately distributed in time to monitor anthropic changes.

In any case thematic information that can be extracted from low water amplitude and texture combined with high water mosaic is much higher than what we need for our simple thematic definition as we demonstrate in Appendix A.

2.3 Training and testing sites set selection

The location of the three training sites for this study are chosen taking as guidelines the Tropical Forest Ecosystem Environments monitoring by Satellites (TREES) (Malingreau *et al.,* 1995) stratification of the tropical forests into "hot spots" and "cool spots" of deforestation (Achard *et al.,* 1998). The three training sites cover different forest and savannah ecosystems along with different land uses. These land use types reflect the major forms of anthropogenic activity within the Amazon basin (large scale ranching, selective logging, shifting cultivation, organized colonization projects and mining) (Peralta and Mather, 2000). The Amazon basin is under anthropogenic pressure from two main areas. From the region of dynamic forest change, along the Brazilian sates of Para and Mato Grosso, the first front has been extended into the forest domain by the construction of roads, both along the north of Para state up into Roraima and from the south of Mato Grosso through Rondonia to Acre.

Two of the selected sites are respectively located in Mato Grosso and Rondonia as representative of this front of deforestation. The third site is in Colombia where the second front of deforestation is formed by migrant's incursions into the Amazon basin at its western end. For clarity, we will indicate each site with the Landsat TM path and row codes – Mato Grosso site: 226-69, Rondonia site: 230-69, Florencia-Napo site: 8-59. The fourth study area, located in the North Rondonia state of Brazil, is identified as testing site 231-68.

Training and testing site geographical position and the relative hot spot area are shown in figure 2.3;

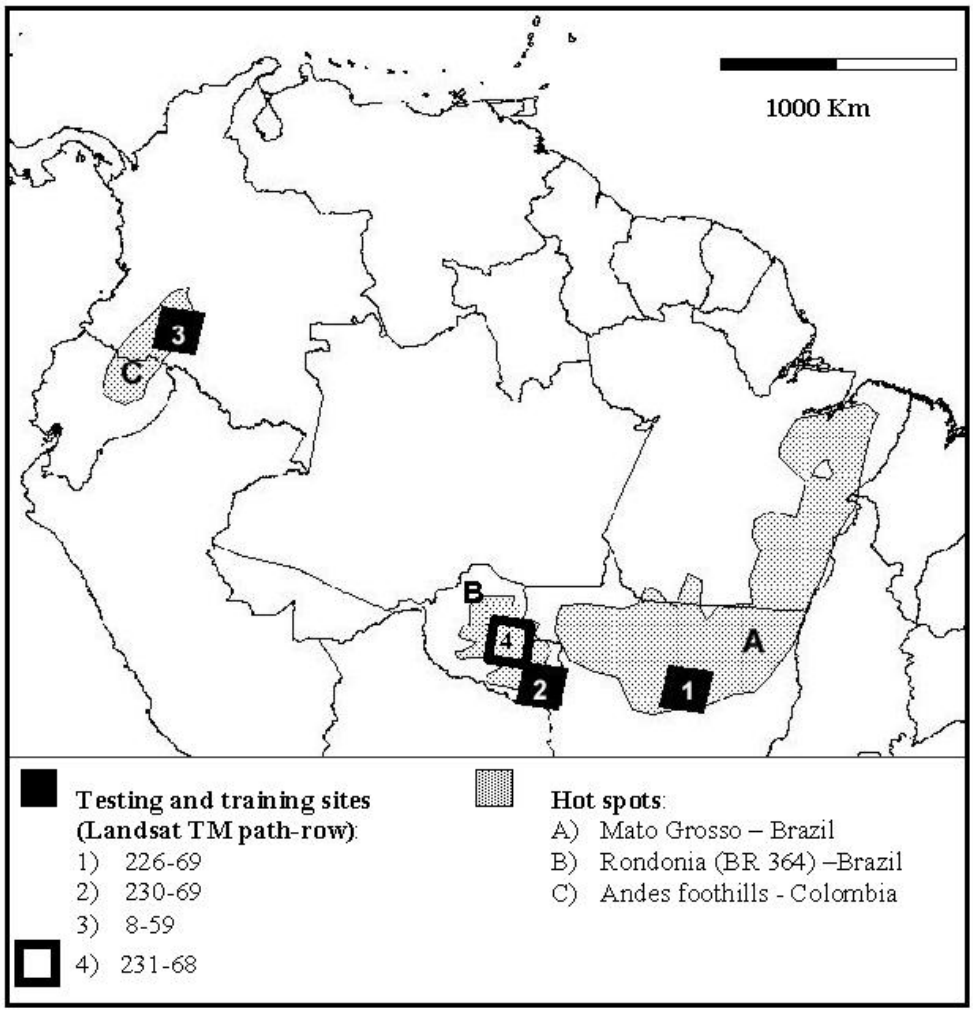

Figure 2.3: Training site (1, 2, 3) and testing site (4) geographical position and the relative hot spot area (A, B, C).

Figures 2.4 a, b, c show the SAR L-band 100 m and the corresponding Landsat TM data for each training site. The location, vegetation type, deforestation pattern, deforestation causes, initiator and driving forces are given as descriptive parameters of those sites.

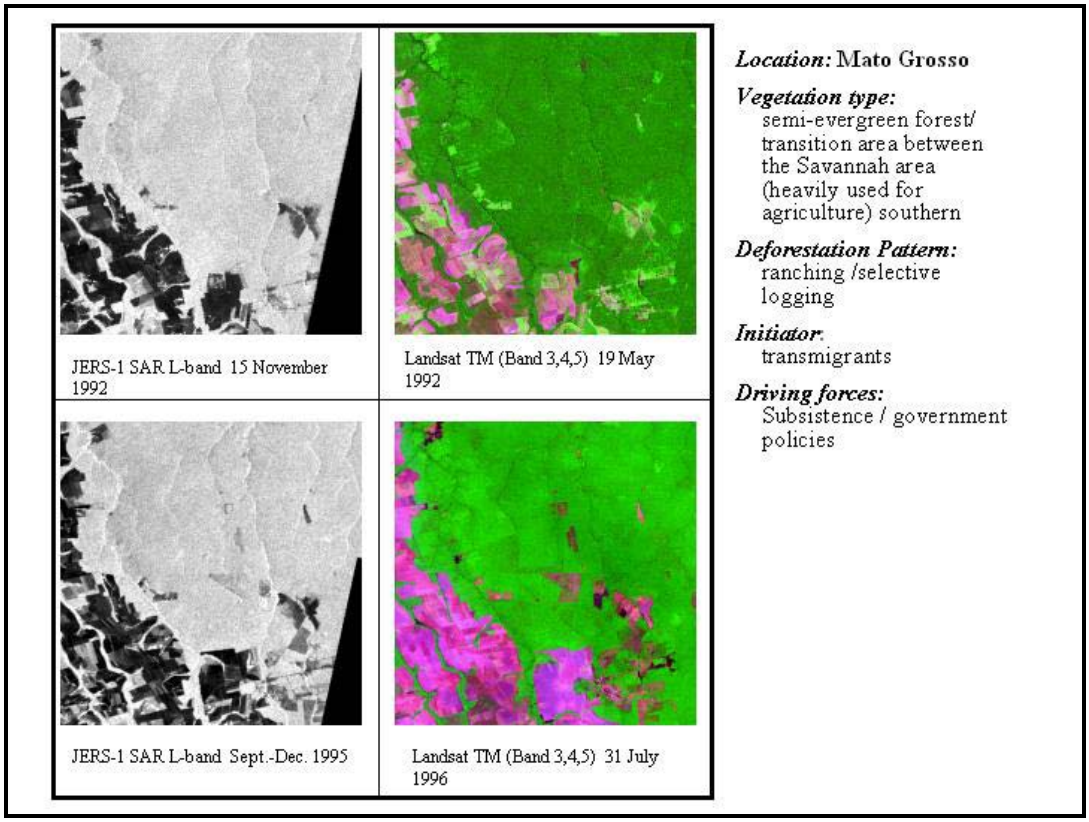

Figure 2.4 a: SAR L-band 100 m and the corresponding Landsat TM over Mato Grosso site. Descriptive parameters of this site are also reported (see color Figure B.3 - Appendix B, pp. 202).

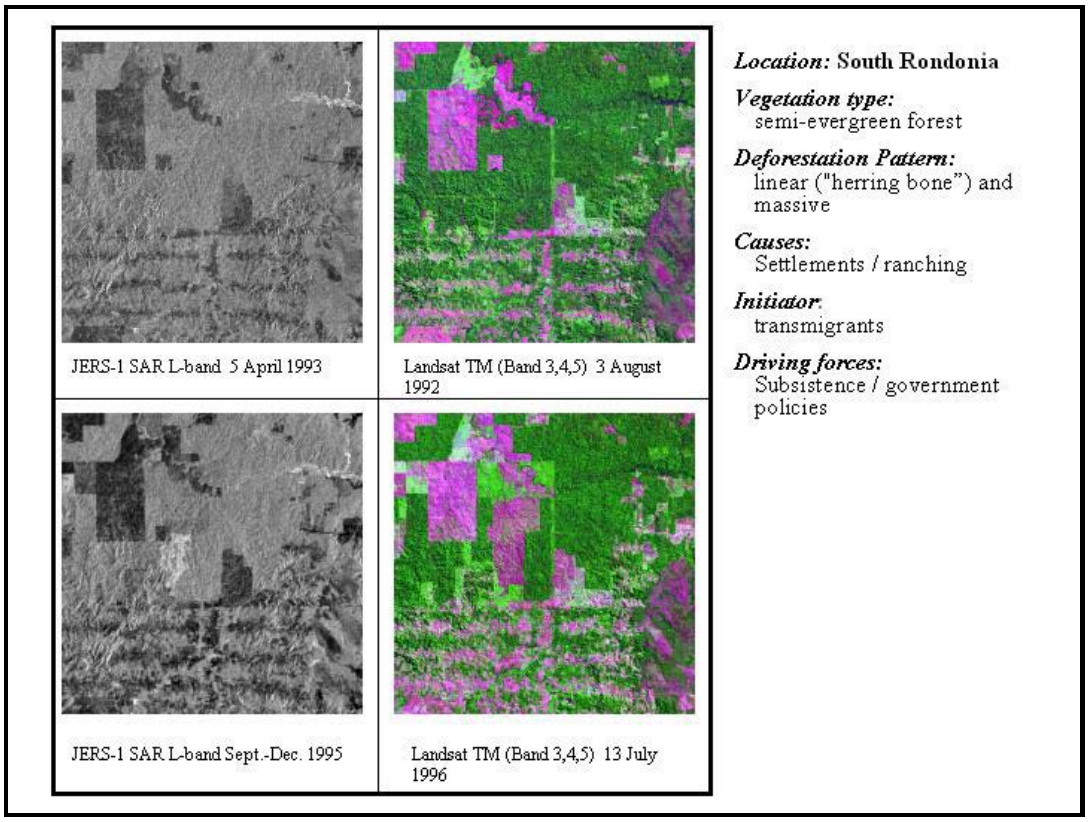

Figure 2.4 b: SAR L-band 100 m and the corresponding Landsat TM over Rondonia site. Descriptive parameters of this site are also reported (see color Figure B.4 - Appendix B, pp. 203).

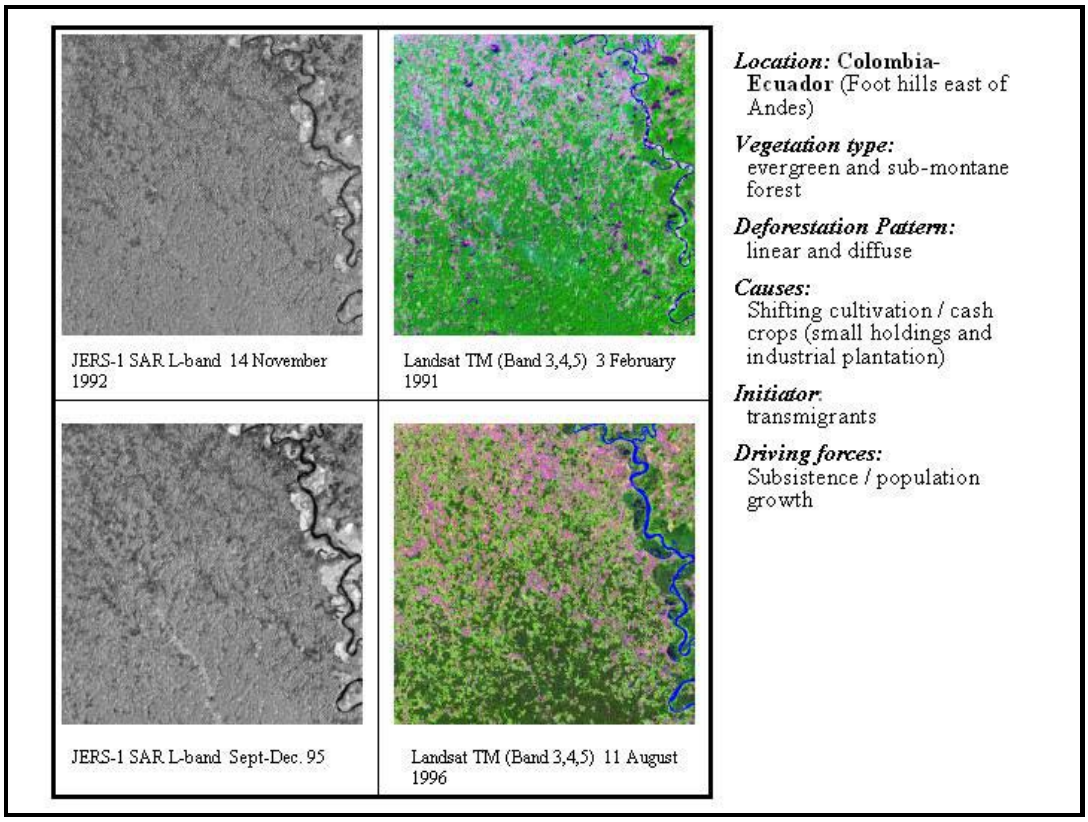

Figure 2.4 c: SAR L-band 100 m and the corresponding Landsat TM over Florencia-Napo site. Descriptive parameters of this site are also reported (see color Figure B.5 - Appendix B, pp. 204).

2.4 Training and testing data sets compilation

2.4.1 Generation of 'small' JERS-1 L-band mosaic for 92-93 period

The area covered by a Landsat TM images is 185 km * 185 km, while the area covered by JERS-1 L-band (Level 2.1) images is 75 km * 75 km so about 9 JERS-1 images are necessary to cover adequately a Landsat TM image. In order to have an adequate coverage with JERS-1 L-band data in correspondence of Landsat TM optical images for 92-93 period we build three small mosaics with JERS-1 L-band images.

To build a data set of JERS-1 comparable with TM images, in terms of area covered we follows the next steps:

1) Selection from NASDA archive of JERS-1 L-band images in 1992-93 in correspondence of TM 1992-93 images
2) Wavelets Multi-resolution Decomposition from 12.5 to 100 m
3) Mosaic generation.

1) The available scenes in NASDA archive in 92/93 partially cover the Landsat TM scene and the relative NASA – JPL Mosaic samples coverage.

The relative position between the 92/93 JERS-1 L-band images and the Landsat TM image coverage for each training site are schematically shown in the figure 2.5.

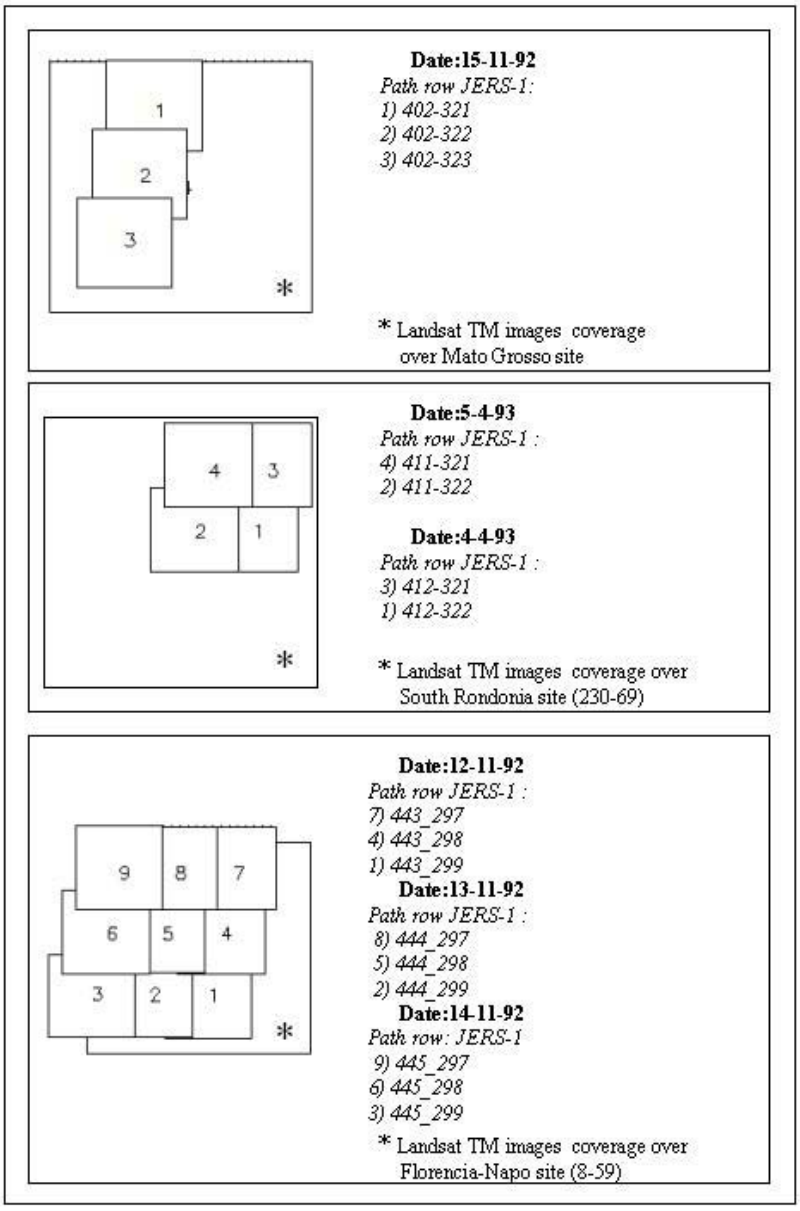

Figure 2.5: Schematic representation of the relative position between the 92/93 JERS-1 L-band images and the Landsat TM image coverage for each training site. Radar image acquisition dates and path/row numbers are also reported.

2) Wavelets Multi-resolution Decomposition

In that phase of the work mosaic post processing tools developed by the Radar Remote Sensing Team of the Global Monitoring Vegetation (GVM) to generate the GRFM Project Africa mosaics are used. To maintain high radiometric resolution, the down sampling from 12.5 meter pixel spacing to lower resolution is performed by wavelet decomposition - in effect a low pass filtering process resulting in more than 100 looks per pixel. This processing product may consist of calibrated SAR scene at 100 m pixel spacing to be mosaicked. The calibration of most space-borne SAR sensors is based on the use of the tropical forest as a calibration target. Usually the antenna pattern, determined on the ground before the launch of the satellite, is revised based on the fact that the backscattering coefficient of the tropical forest is constant over a wide range of incidence angles. The revised antenna pattern is then used in connection with SAR processing to produce calibrated SAR products. This approach works well if all the necessary spacecraft (such as platform altitude, angles) and processing parameters remain constant or are known with the required accuracy. Uncontrolled drift in these parameters may cause changes in the SAR range pattern and degrade the (relative) calibration accuracy.

The NASDA archive scenes, used for the three “small” mosaics generation, are processed (NASDA level 2.1) at different times and probably with different processor version. This can explain the fact that in some scenes the range pattern shows an anomalous behavior whereby the average amplitude decreases from near range to far range (see the histograms reported in figure 2.6). This anomalous backscatter behavior could be due under-correction of the antenna pattern and it generates a striping effect between one path and the other.

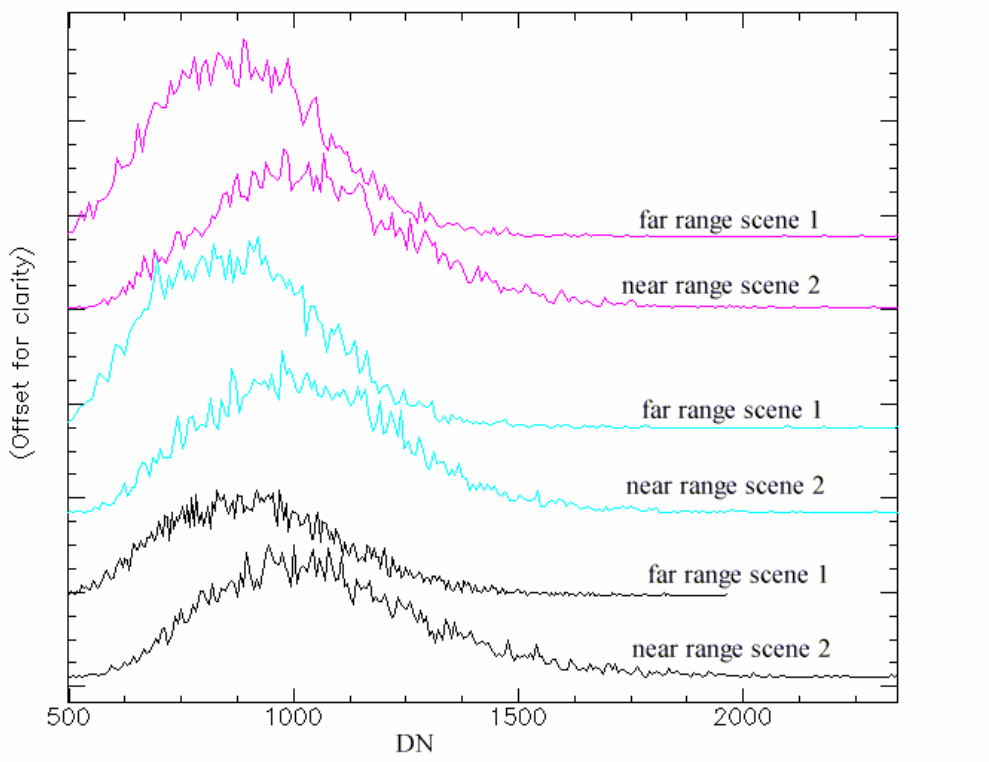

Figure 2.6: Histogram comparison between 3 overlapping sample selected on the far range of a frame and on the near range of the adjacent path and on the same row frame.

A calibration constant value (2.2) as function of the pixel range location is applied for the unbalanced scenes reducing the far range near-range unbalance (see figure 2.7):

$$F = \frac{1}{k}\frac{\sin\alpha_i}{\sin\alpha_{ref}} \tag{2.2}$$

where calibration constant , α_i distributed target incident angle and α_{ref} reference incident angle.

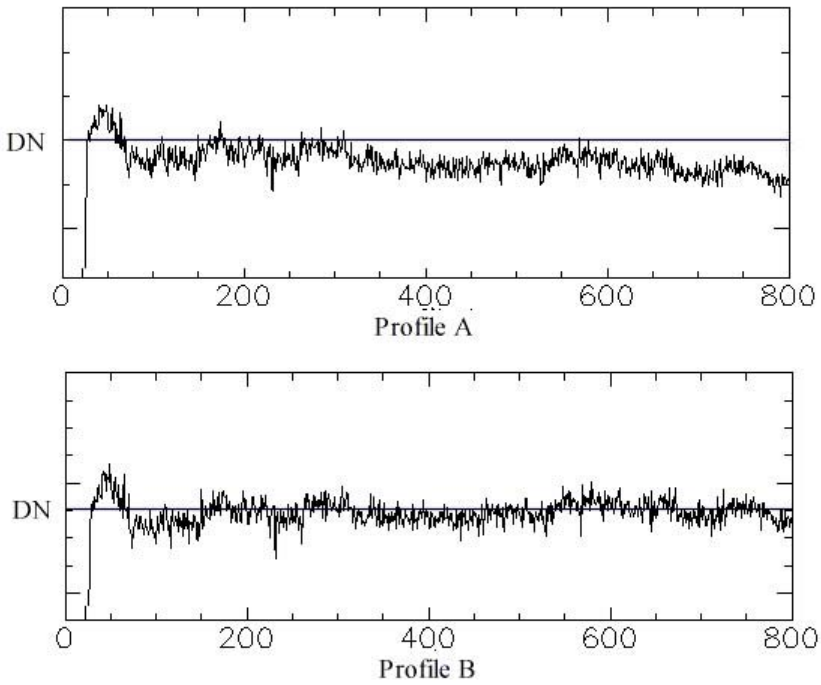

Figure 2.7: Frame means profiles from far range to near range: profile A - before calibration, profile B - after calibration

The effect to the of this calibration is principally visible in stripe effect reduction (see figure 2.8 a and b)

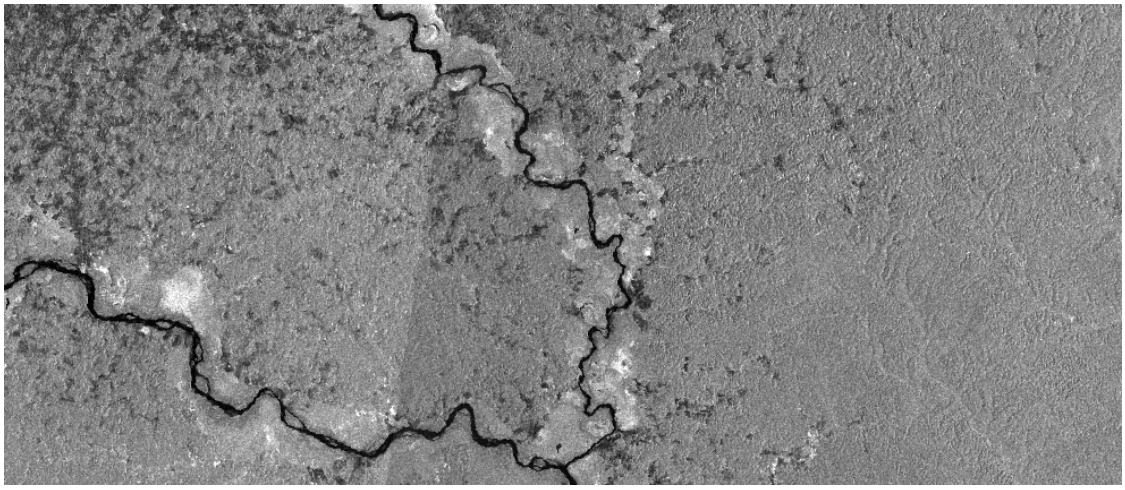

Figure 2.8 a: Stripe effect between two frames of different paths

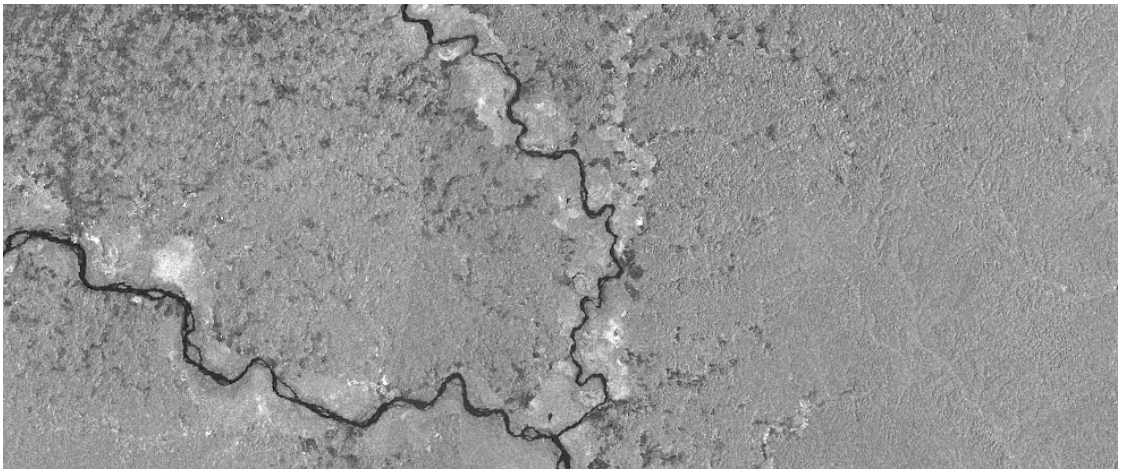

Figure 2.8 b: Calibration effect in stripe problem reduction

3) Mosaic generation.

In order to generate the three “small” mosaics, the low-water JPL mosaic is used as geographical reference. Each frame is manually co-registered respect the mosaic and then mosaicked with the neighboring frame.

The final mosaic results are shown in Figure 2.9 a-c.

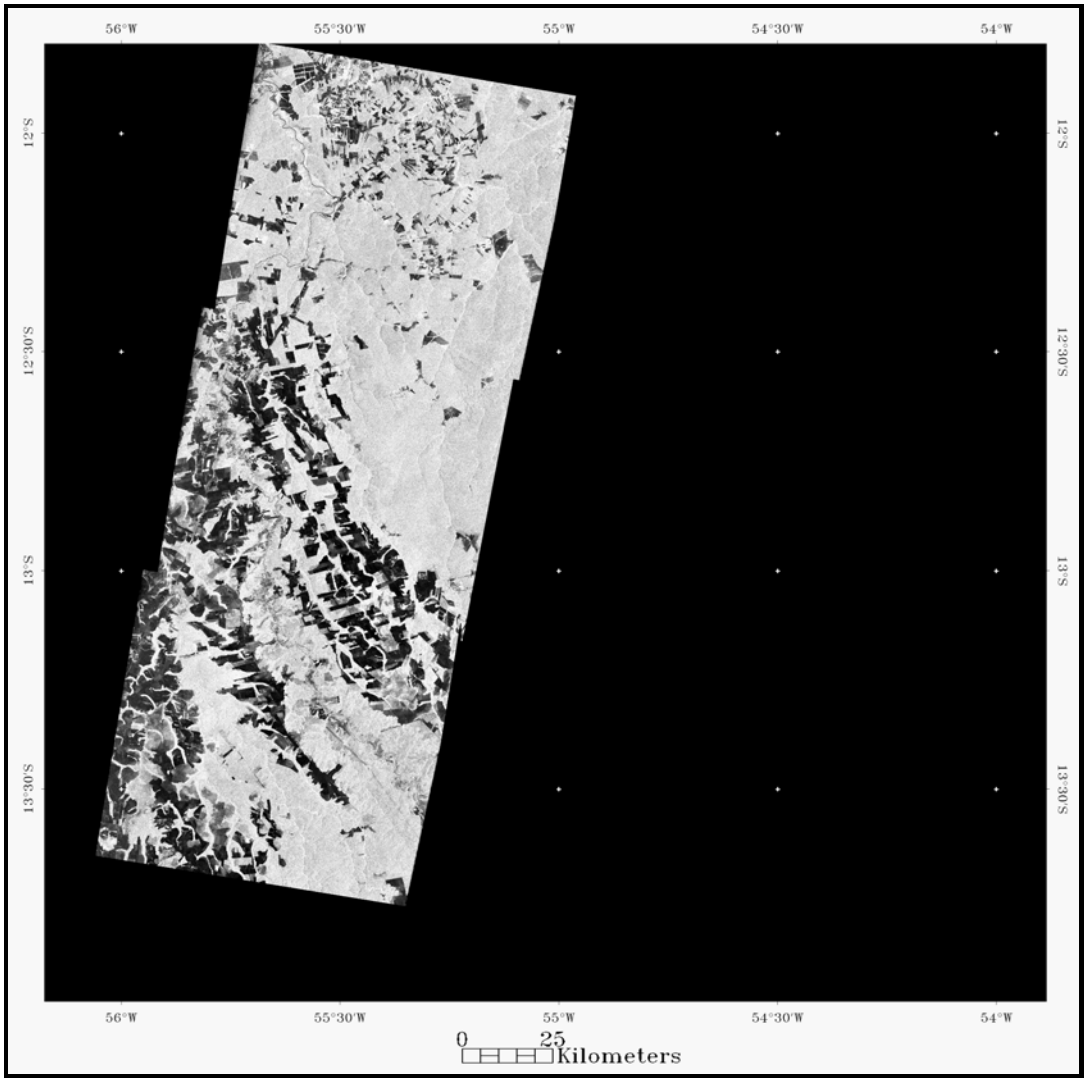

Figure 2.9 a: JERS-1 SAR 92/93 “small mosaic”: Mato Grosso training site.

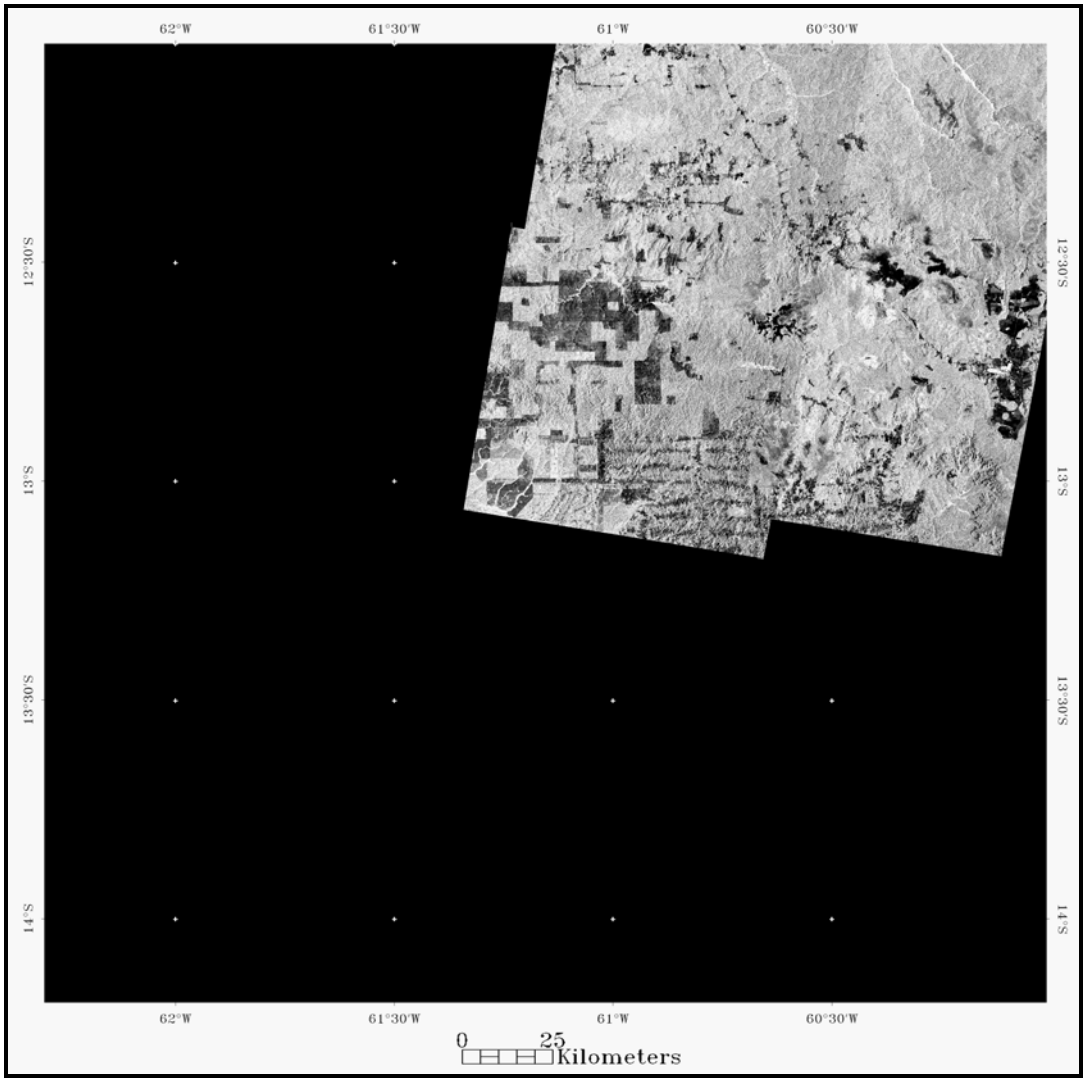

Figure 2.9 b: JERS-1 SAR 92/93 “small mosaic”: South Rondonia training site.

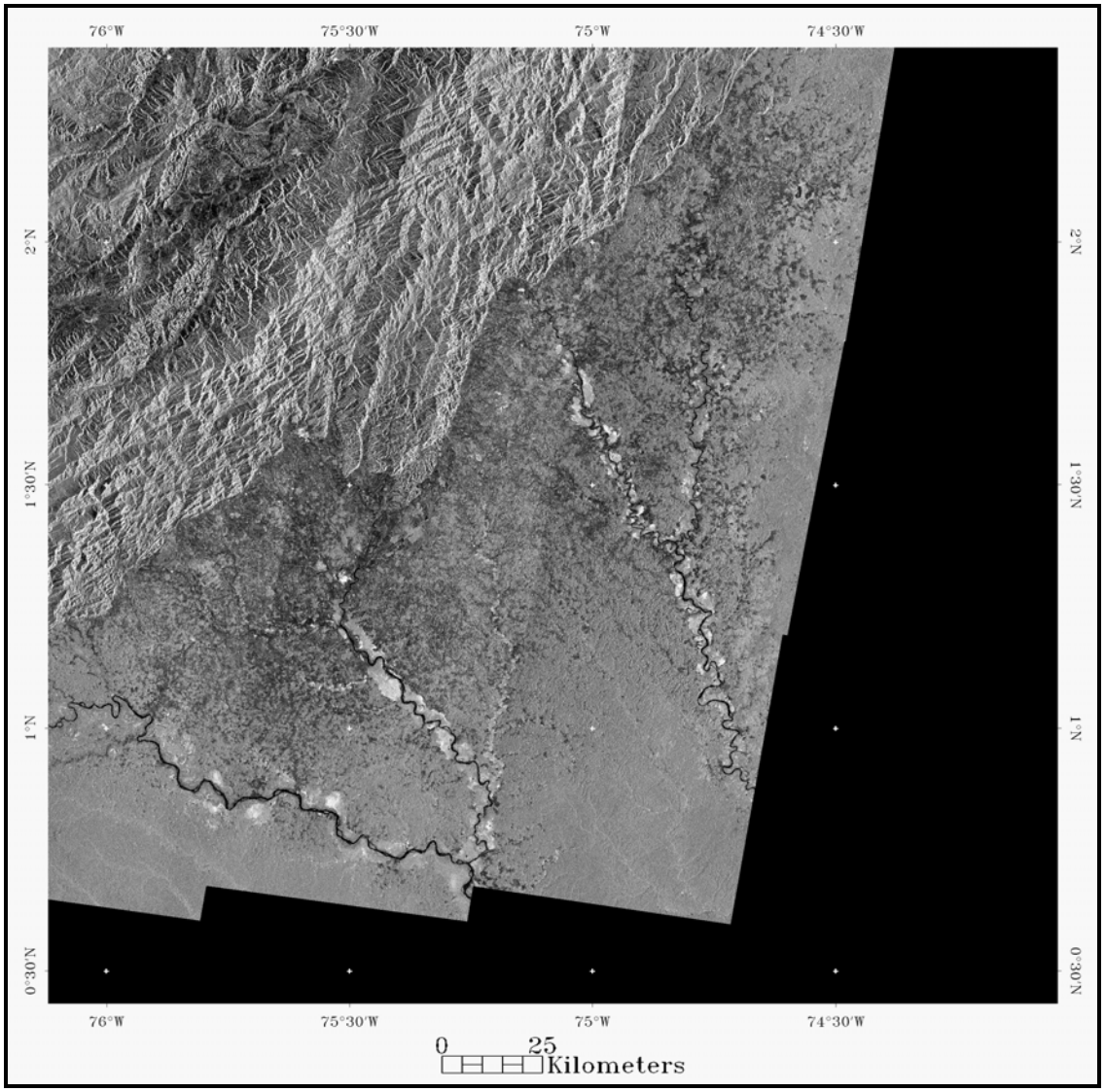

Figure 2.9 c: JERS-1 SAR 92/93 “small mosaic”: Colombia-Equador training site.

Finally we want to underlain that we generate this second data set for 1992/93 because even though at local scale it was acquired with a temporal interval respect to the GRFM low water mosaic that is sufficient for capturing the changes due to deforestation phenomena distributed. On the contrary the low water and high-water GRFM mosaic are too close in time for these purposes and less representative of the anthropic changes during the 90' in the Amazon Basin.

2.4.2 Optical data set compilation: raw data, maps

According to the method adopted for SAR map evaluation, optical Landsat Thematic Mapper (TM) data and derived map are collected. Landsat TM maps, produced by the Tropical Rain Forest Information Center (TRFIC-NASA's Earth Science Information Partnership program) and FAO's Forest Resource Assessment Programs (FAO, 1996) are assumed as validated reference. Nevertheless also Landsat TM raw data are collect for a direct comparison with SAR data in order to evaluate spectral and spatial differences between the two imaging systems.

For the Mato Grosso (226-69) and South Rondonia (230-69) sites, TRFIC maps are adopted. For the Florencia-Napo site (8-59) a forest map is derived from Landsat TM raw data through a classification scheme called hierarchical NMP (HNMP) (De Grandi, 2001b). For this training site FAO's maps are used as reference for class labeling. For the North Rondonia site (231-68), a TRFIC is available (for detail on reference map see chapter 4).

A summary of optical raw data and the optical maps is presented in table 2.1.

Table 2.1: Summary of optical raw data and the optical adopted as reference data set.

Site (Landsat TM path-row)	**Landsat TM raw data**	**Landsat TM reference map**
226-69 Mato Grosso (training)	Landsat TM (Band 3,4,5) 19 May 1992	TRFIC TM 19 May 92
	Landsat TM (Band 3,4,5) 31 July 1996	TRFIC TM 31 July 96
230-69 South Rondonia (training)	Landsat TM (Band 3,4,5) 3 August 1992	TRFIC TM 15 May 92
	Landsat TM (Band 3,4,5) 13 July 1996	TRFIC TM 13 July 96
8-59 Florencia Napo (training)	Landsat TM (Band 3,4,5) 3 February 1991	FAO 1990
	Landsat TM (Band 3,4,5) 11 August 1996	FAO 96
231-68 North Rondonia (testing)	-	TRFIC TM 13 July 96

2.4.3 Images calibration

Calibration is the process of quantitatively defining the system response to known, controlled signal inputs. Calibration increases in importance if the intent is to obtain geophysical or biophysical information about the surface of the Earth. Calibration becomes critical when we consider analyses that require multiple images. For example the basic premise in using optical remote sensing data for change detection is that changes in land cover result in changes in radiance values and changes in radiance due to land cover change are large with respect to radiance changes caused by other factors (Singh, 1987). Some authors carried out comparative studies of change detection techniques and found that post-classification comparison was less effective than enhancement procedures (Singh, 1989). Other authors found that post-classification comparison is the most accurate procedure and present the advantage of indicating the nature of the changes (Mas, 1999).

In this thesis we mainly focus on the comparison of single date images for forest assessment. Some indications for a future monitoring system are based on the comparison between forest maps at different time (see section 2.1). Moreover same calibration problems problem are found both for optical and SAR data, as detailed afterward.

For these reasons in this research work post-classification comparison is adopted.

Landsat TM calibration problems

In the optical data set compilation (section 2.4.2), satellite images acquired by Landsat-5 TM system, are collected.

Investigators have founds that the top-of-the-atmosphere (TOA) reflectance is getting too low over time to allow a proper atmospheric correction. Before the lunch

of Landsat-7 on April 15, 1999, there was not official update to the Landsat TM calibration and the latest article on Landsat TM absolute radiometric calibration was by Thome (Thome *et al.,* 1994). With the success of Landsat 7, renewed efforts are underway to ensure radiometric calibration across the Landsat series of sensors. The Landsat Project Science Office (LPSO) has developed an analysis plan that establishes a framework for cross-calibration between Landsat-7 ETM+ and Landsat 5 TM (Teillet *et al.,* 1999). For more information see: http://www.ccrs.nrcan.gc.ca/ccrs/

Being the process on going, we will applied post-classification comparison between temporal different scenes is applied, not to introduce wrong factors with an incorrect calibration.

JERS-1 SAR calibration problems

When we talk of SAR calibration we must be distinguish between absolute or relative calibration. If the proper calibration steps are taken (range-spread loss, antenna pattern removal, and effective ground scattering area correction) and the proper absolute calibration is used, it would be possible to estimate the radar backscattering coefficient within the intrinsic calibration uncertainties.

The conversion of *DN* values could be written as in (2.1).

The Amazon data acquired for South America Mosaic NASA JPL Mosaic are (mostly) processed by the Alaska SAR Facility (ASF) in Fairbanks, Alaska. NASDA EOC processed the NASDA archive JERS-1 frames selected in correspondence of TM 1992-93 images. Using the calibration factor for the two processors the formula become respectively:

NASDA EOC processing $\sigma_0 = 20 \cdot \log_{10}(DN) - 60.20$ (2.3)

ASF processing $\sigma_0 = 20 \cdot \log_{10}(DN) - 48.54$ (2.4)

A radiometric relative balancing could therefore done assuming a system model whereby the radiometric imbalance is due to a gain factor *a* and an offset *b* in the transfer function. Selecting homogeneous targets in same areas, assuming the normality in the statistical distribution of the target, the problem is reduced to the liner transformation of normal random variable.

By the following equation system, the gain *a* and bias *b* could be computed from the mean and standard deviation in the two overlapping area (*x,y*):

$$mean_y = a \cdot mean_x + b \tag{2.5}$$

$$stdev_y = a \cdot stdev_x \tag{2.6}$$

Then the linear transformation could be applied to the whole image.

Because of calibration problems, for the optical date post-classification comparison is used. The same methodology is coherently used for SAR data; the forest mapping classification was therefore applied on *DN* values.

2.4.4 SAR and optical data co-registration

In order to compare different data set, images co-registration is required. The purpose of the co-registration process is to have a imagery data set (optical and SAR raw data, optical and SAR thematic map) in the same map reference system (U.S. Geological Survey, 1993). The low-water JPL mosaic is used as geographical reference in this co-registration process.

The JPL mosaic projection is a standard geographic equiangular projection, in which each pixel is a fixed angular number of degrees. The datum of the mosaics is

WGS-84. The mosaic pixel spacing is nominally 3 arcseconds. The longitudinal ground pixel spacing changes with Latitude. At the equator, 3 arcseconds corresponds to 93 meters in Latitude and Longitude. Moving away from the equator, the pixel spacing in meters - in Longitude - decreases with Latitude. At 15 degrees North or South of the equator, the pixel spacing corresponding to 3 arcseconds is 89 meters. To convert the Longitude angular pixel spacing (in decimal degrees) to meters, the angular value must be multiply by 111,319.5, and by the cosine of the Latitude. For the Latitude angular pixel spacing, must be multiply by 111,319.5.

The imagery registration to the reference mosaic requires to estimates the parameter of a geometrical transformation. The transformation parameters can be estimates through a manual selection of homologous points between the two images if the transformation can be assimilates to a roto-translation with scale variation; the identification of a large number of homologous point is required if the orbital geometry and geographical projection parameters must be estimates.

To reduce the manual point selection, Landsat TM orbits information is used to convert raw data to an equiangular projection referred to Clarke Ellipsoid.

Given $X=($TM image matrix along along-scan and across-scan satellite direction) and known from the orbital geometry model (Mather, 1987):

- M_1= scale change
- M_2=Earth rotation correction
- M_3=Skew correction

The raw data can be transformed through 2.2

$$X^I = M_1 * M_2 * M_3 * X \tag{2.2}$$

From the knowledge of the orbit characteristic of the satellite platform, the coordinates of the image center can be derived according to UTM (Universal Transversal Mercator) or SOM (Space Oblique Mercator). Through this first approximate co-registration, the position differences between images are reduced to a plane translation and a note scale variation. (Landsat TM: 0.003*0.003 deg. ($d\lambda$, $d\varphi$), SAR JPL Mosaic: 0.000833*0.000833 ($d\lambda$, $d\varphi$)). The refined registration is performed by the manual selection of homologous point between SAR end optical images. The optical map is registered to the JPL mosaic according to the same transformations.

The JPL mosaic is used as geographical reference also for the 92/93 JERS-1 mosaics, as detailed in section 2.4.1.

2.5 Summary and conclusions

Compilation of remote sensing data set adopted in this research work is described in this chapter. Criteria for data selection and data characteristics – satellite sensor, geographical coverage, and imagery format - of the satellite imagery data set are detailed.

The South America GRFM SAR mosaic generated by JPL with the data acquired during September-November 1995 by JERS-1 satellite is used as principal data-set to derived forest map.

Landsat Thematic Mapper (TM) optical imagery and derived maps, produced by the Tropical Rain Forest Information Center (TRFIC-NASA's Earth Science Information Partnership program) and FAO's Forest Resource Assessment Programs (FAO, 1996), are adopted as reference data to evaluate the maps derived from JERS-1. Within the entire SAR mosaic three training sites, which cover different forest and savannah ecosystems along with different land uses, are selected:

1) to apply classification training phase, as prerequisite for up scaling to whole Amazon data set.
2) to provide classification accuracy in comparison with Landsat TM optical maps which are locally available respect to the mosaic geographical coverage.

One additional testing site of interest is selected to assess the generalization ability of the adopted classifier over a fourth independent site.

Landsat TM data are available at 2 dates (1992 and 1995) distributed in time to monitor anthropic changes during the 90'. The GRFM data-set overlaps in time with the 1995 data; to compare optical and SAR data at the 2 dates, small SAR mosaics from 1992 JERS-1 PRI data over the three training sites are also generated.

For the data-set compilation the GRFM mosaic is revealed to be as semi-continental geographical reference for:

1) 1992 small SAR mosaics,
2) optical raw data (Landsat TM),
3) thematic maps.

The compilation of a remote sensing data set requires to define the criteria for data selection and to establish a common reference system to compare the satellite imagery. The low water GRFM mosaic generated by JPL over South America used as principal data-set to derived forest map, is reveal to be geographical reference systems for the optical and SAR imagery and for the derived thematic maps used in this research. The SAR mosaic for the continuous coverage, the geographical consistencies, and higher resolution comparing with other semi-continental data set, is reveal to be a useful geographical reference for the comparison of different imagery data-set and it can be adopted as base reference for future remote sensing research.

Chapter 3

The classification problem: methods and thematic class definition

3.1 Introduction

3.1.1 Fundamentals of the image classification process

In remote sensing literature "image classification" refers to the process of creating thematic maps from satellite imagery. The general term classification describes the entire process from the raw image up to the assignment of a label to each portion of an image resulting in a thematic map. A thematic map is an informational representation of an image which shows the spatial distribution of a particular theme.

In the image analyses and pattern recognition literature classification methods are usually identified as image-labeling algorithms specifying. The image-labeling algorithms are part of more complex processes generally called image analysis (Gonzales and Richard, 1992). The image analysis process can be divided the three basic conceptual areas:

1) Low-level processing,
2) Intermediate-level processing,
3) High-level processing.

Figure 3.1 illustrates these concepts; the overlapping dashed lines indicating that clear-cut boundaries between processes do not exist and the techniques adopted can involve different blocks. For example, image threshold may be viewed as a pre-

processing step (low-level processing) or a used for segmentation (intermediate-level processing).

Image acquisition and pre-processing require less basic knowledge on the thematic context and more about image signal characteristic and are considered as low-level processing. Intermediate-level processing (segmentation and clustering) deals with the task of extracting and characterizing regions in an image resulting from a low-level process. Finally, high level-processing (labeling) involves recognition and interpretation. The process requires strong knowledge about the images' thematic context.

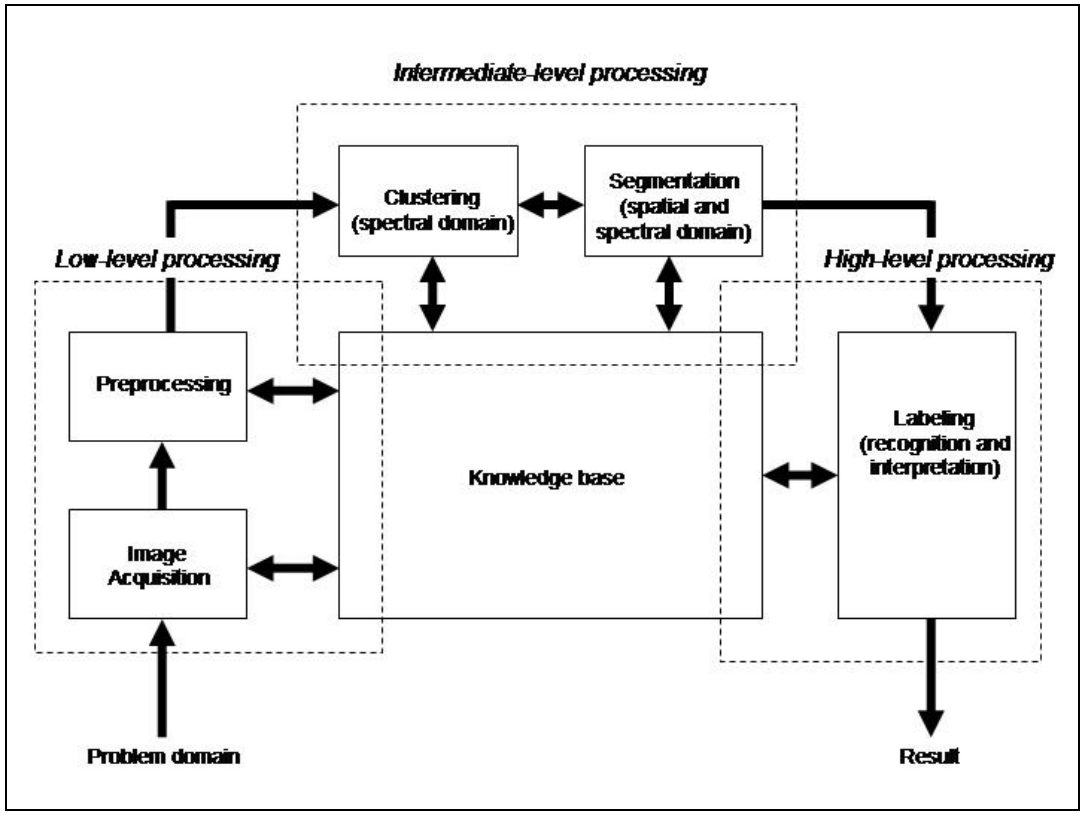

Figure 3.1: Image analysis process scheme divided in three basic conceptual areas: Low-level processing, Intermediate-level processing, High-level processing.

From the methodological point of view, classification processes are generally distinguished in:

1) Unsupervised: In an unsupervised classification, the objective is to group single or multi-band spectral response patterns into clusters that are statistically separable (features are separated solely on their spectral properties); or partitioning an image into homogeneous regions (segmentation) without ground information regarding segment properties.
2) Supervised: In a supervised classification we use some prior or acquired knowledge of the classes in a scene in setting up training sites to estimate and identify the spectral and spatial characteristics of each class.

Entering in the detail of the image analysis process, image labeling algorithms, which can be ascribed both to the intermediate-level and high-level processing, can be subdivided into three principal categories:

1) Clustering: A process in the spectral domain only that groups pixels with comparable spectral properties (in statistical sense) into categories. A region of the spectral space that belongs to a category is called a cluster. Clustering is therefore based only on spectral information.
2) Segmentation: partition of an image in the space domain into sets of connected neighboring pixels with comparable spectral properties (e.g. belonging to the same category). Segmentation is therefore based on topological and spectral information.
3) Labeling: the process of assigning a semantic meaning (e.g. a land-cover type) to a category.

Clustering and segmentation algorithm can moreover be classified in:

1) Parametric and Non-parametric
2) Non contextual (per pixel), contextual

Parametric algorithms make assumptions of the functional form and the parameters of the PDF for the classes to establish decision boundaries between them. As a consequence, it provides a way to estimate the error of the classification process itself. It is commonly divided in two steps. Non parametric algorithm any assumption on the PDF for the classes (i.e. Level-Slice Classifier, K Nearest-Neighbors Classifier)

Contextual algorithms are capable of exploiting spatial (contextual) information around the single image pixel, while non-contextual algorithm analyse behaviour o the single pixel (per pixel).

A further distinction can be done in the final labelling step. The way of assigning a semantic meaning to the image class can be:

1) 'Hard' or 'Crisp'
2) Fuzzy

One important limitation of classification of statistical approaches to land cover mapping is that the output derived consists only of the code of allocated class. This type of output is often referred to as being 'hard' or 'crisp' and is wasteful of information of the strength of class membership generated in the classification. An alternative to the 'hard' classification representation of land cover is therefore often required and should allow for partial and multiple class membership (Wang, 1990). This could be achieved by softening the output of a 'hard' classification. For instance, measure of the strength of class membership, may be output. Thus, for example, with a probability based classification a probability vector containing the probability of membership a pixel has to each defined class could be output. In this probability distribution the partitioning of the class membership probabilities between the classes would, ideally, refer to some extent the land cover composition of a mixed pixel. This type of output may be considered to be fuzzy, as an imprecise allocation may be made and a pixel can display membership to all classes

Many image-labeling techniques according with the previous definition scheme belong to one of several categories briefly described next.

Per-pixel (non-contextual) parametric (e.g., Gaussian maximum likelihood) or non-parametric classifiers (e.g., the k-nearest neighbor classification rule), followed by a post-processing low-pass filtering stage, capable of regularizing the classification solution (i.e., capable of reducing salt-and-pepper classification noise effects), based on some heuristics or empirical criteria. Although inadequate to detect fine image details when spectral classes overlap in feature space, this approach is widely adopted by the remote sensing community (e.g., in commercial image processing software toolboxes) owing to its conceptual and computational simplicity.

Neural networks that employ, in the image domain, sliding windows or banks of filters. On the one hand, neural networks are non-parametric classifiers featuring important functional properties. They are: i) distribution-free, i.e., they do not require the data to conform to a statistical distribution known a priori; and ii) importance-free, i.e., they do not need information on confidence level of each data source, which are reflected in the weights of the network after training. On the other hand, the dependence of results on the shape and size of the processing window (which are usually fixed by the user on a priori basis) is a well-known problem.

Bayesian contextual image labeling systems where Maximum A Posteriori (MAP) global optimization is pursued by means of local computations (Jhung and Swain, 1996). Because of the local statistical dependence (autocorrelation) of images, there has been an increasing emphasis on using statistical techniques based on Markov Random Fields (MRFs) to model image features such as textures, edges and region labels. In MRFs, each point is statistically dependent only on its neighbors. Thus, an MRF model is often imposed on the prior probability term to enforce spatial continuity in label assignment (inter-pixel class dependency) (Krishnamachari and Chellappa, 1997). Among the Bayesian contextual image

labeling systems we cite the Modified Adaptive Pappas Clustering (MPAC), recently published in the image processing literature. This method is also proposed in this research work as a valuable tool for forest degradation monitoring using Landsat TM imagery (see chapter 6). In (Pappas, 1992), after speculating that an MRF model of the labeling process is not very useful unless it is combined with a good model for class-conditional densities, Pappas presents a contextual clustering technique, where a novel context-sensitive (i.e. locally adaptive) spectral model for class-conditional densities is proposed. This algorithm is hereafter referred to as the Pappas Adaptive Clustering (PAC) algorithm. Starting from the PAC architecture, the MPAC algorithm employs both local and global (image-wide) spectral statistics in the class-conditional model plus contextual information in the MRF-based regularization term to smooth the solution while preserving genuine but small regions (Baraldi *et al.,* 2000).

In recent years there has been a great development of new methods for image-labeling algorithms. Unfortunately, owning to their functional, operational, and computational limitations, many labeling techniques, both supervised and unsupervised, have had a minor impact on their potential field of application (Zamperoni, 1996; Jain and Binford, 1991; Kunt, 1991). Related to remote sensing applications, like the one described in this research work, we can make the following considerations:

1) Improved adaptability and data-driven learning capabilities would make image-labeling algorithm easier to use and more effective when little prior ground truth knowledge is available.
2) Computationally efficient algorithms and architectures should be made available when training and processing time may still considered a burden, e.g. in classification tasks at regional or continental scale.

3) Preserving fine structures, especially man-made objects, would increase the impact of labeling methods in cartography or analyses of agricultural sites.

In the next section image-labeling adopted in this research particularly for GRFM SAR mosaic will be detailed.

3.1.2 Overview of a special purpose classification process for the GRFM SAR mosaic

Automatic extraction of thematic information from the high-resolution GRFM SAR mosaics calls for suitable image processing techniques. In general, issues to be considered are related to: i) the nature of the SAR signal (speckle): ii) sensitivity of the signal to the geophysical parameters, iii) the scaling properties of the phenomena of interest, iv) the computational load due to the size of the data sets.

In our specific thematic context the goal is to obtain unsupervised image classification into a limited set of classes (e.g. forest, non-forest, and degraded forest). The image-labeling techniques must take into account the following characteristics of the radar imagery:

1) the SAR signal is affected by multiplicative noise
2) some classes of interest (e.g. forest) correspond to highly textured regions.

First attempts to extract thematic information on the vegetation cover either by visual inspection or by automatic classification has already proved that the GRFM mosaics can provide a new and important characterization of some geophysical parameters related to tropical forests (see Chapter 1 for details). However, quantitative validation and error analysis of regional-scale estimation, even for a simple thematic definition the forest cover assessment and forest cover changes, still need to be worked out and consolidated (Mayaux *et al.,* 2002; Saatchi *et al.,* 1999; Simard *et al.,* 1997 and 1999).

Conventional per-pixel (i.e. non-contextual) clustering techniques, e.g., ISODATA (Tou and Gonzalez, 1974), that employ a distance criterion in the measurement (feature) space, as well as contextual clustering algorithms, like the MPAC that work in the joint spatial/spectral image domain based on a piecewise constant signal model eventually affected by an additive white Gaussian noise field independent of the scene, are incapable of dealing with texture (correlation) and/or multiplicative noise, i.e. they are affected by salt-and-pepper classification noise effects (over-segmentation) when dealing with radar images.

Bayesian contextual image-labeling systems, where a MAP global optimization is pursued by means of local computations, may employ Markov MRFs to model image features such as textures, edges and region labels (Smits and Dellepiane, 1997). Unfortunately, GMRFs are good at describing a variety of smooth textures, but perform poorly when sharp edges or small isolated features are to be preserved.

Other texture classifiers may consist of neural networks employing, in the spatial image domain, sliding windows or multi-resolution filter banks. On the other hand, the dependence of results on the shape and size of the processing window (which are usually fixed by the user on a priori basis, i.e. these parameters are neither data-driven nor adaptive) is a well-known problem and further investigation is needed in this context.

The image labeling algorithm to be designed would take into due account multiplicative noise, and still would solve the problem of textured classes.

We propose here a new classification scheme for producing a high-resolution regional scale forest map of the Amazon. The main components of the scheme are shown in Fig. 3.2 and are summarized next.

The GRFM data-set volume (1.3 Gb) calls for processing smaller (660*660) partially overlapping tiles extracted from the mosaic (see figure 3.2, block 1). The

overlapping area prevents border effects when the output map is generated from the mosaic of single tiles.

A novel wavelet multi-resolution decomposition/reconstruction technique is employed to generate an edge-preserving piecewise constant radar image (see figure 3.2, block 2). The radiometric characteristics of the reconstructed signal are at this stage a closer approximation to the piece-wise constant model required by segmentation algorithms (Simard *et al.,* 1998b).

Two image-labeling techniques are proposed for thematic information extraction from each tile (see figure 3.2, block 3a, 3b):

1) Region growing technique
2) Two-stage Nearest Multiple Prototype (NMP) classifier.

The regional scale map is finally obtained mosaicking together each labeled tile (see figure 3.2, block 4).

The first image-labeling technique, henceforth be dubbed *region-growing technique*, is based on a region-growing algorithm. The wavelet decomposition supplies additional information on the edge chains and this fact suggests that the combined radiometric and structural information should be exploited in the segmentation phase. This is achieved by the region-growing algorithm that incorporates boundaries defined by the first order statistic of the amplitude data and by the edge maps. Each segment is merged into segments categories based on a Jeffries-Matusita pairwise minimum distance criteria.

The second image-labeling technique is a *two-stage Nearest Multiple Prototype* (NMP) classifier. The NMP first stage employs a near-optimal vector quantization algorithm called Enhanced Linde-Buzo-Gray (ELBG). At the second stage of NMP, vector prototypes are combined into land cover classes of interest with the help of expert photo interpreters. In the pattern recognition phase, each pixel is labeled according to the nearest labeled prototype. This second technique will henceforth be

dubbed "per pixel two-stage hybrid classifier" (*per pixel* indicates that the classifier does not use spatial contextual information, *hybrid* indicates that, after an unsupervised learning phase, supervised many-to-one relationships are established for the final labeling).

A summary of the image processing techniques adopted in this research both for SAR and optical data classification is summarized in Table 3.1.; the algorithm adopted in the different processing steps (preprocessing, segmentation or clustering, labeling) are reported.

Table 3.1: General overview on image processing techniques adopted in this research both for SAR and optical data classification

<table>
<tr><th></th><th colspan="3">SAR</th><th>Landsat TM</th></tr>
<tr><td>Preprocessing</td><td></td><td colspan="2">Wavelet multi-resolution decomposition/reconstruction</td><td>IHS color transformation</td></tr>
<tr><td rowspan="2">Segmentation or Clustering</td><td rowspan="2">ISODATA</td><td>Region growing</td><td rowspan="2">ELBG</td><td rowspan="2">ELBG</td></tr>
<tr><td>Jeffries-Matusita pairwise minimum distance criteria</td></tr>
<tr><td>Labeling</td><td>Unsupervised photo-interpretation</td><td>Unsupervised photo-interpretation</td><td>Unsupervised photo-interpretation</td><td>MPAC</td></tr>
</table>

An overview of the wavelet multi-resolution decomposition/reconstruction technique, together with the extension of the technique developed specifically for the present application, is presented in section 3.4. The image-labeling techniques are described in section 3.5. The thematic class definition and characterization is reported in section 3.6. Conclusions are given in section 3.7.

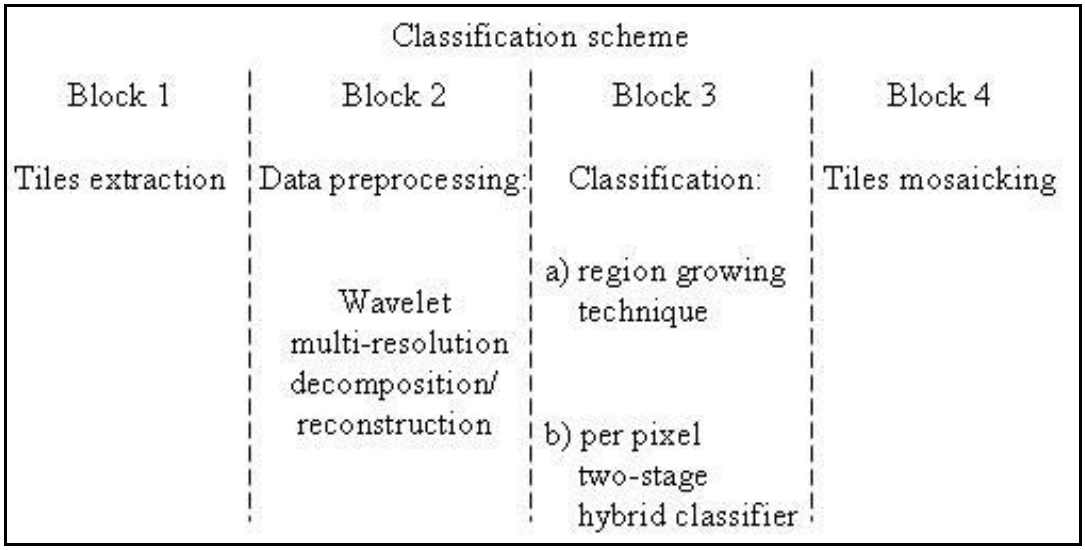

Figure 3.2: Flow chart of the 4 building blocks of the classification scheme for producing a high-resolution regional scale forest map of the Amazon. Block 1: partially overlapping tile (660*660 pixels) extraction from the mosaic. Block 2: wavelet multi-resolution decomposition/reconstruction technique to generate an edge-preserving piecewise constant radar image. Block 3: region growing technique and per pixel two-stage hybrid classifier proposed for thematic information extraction from each tile. Block 4: labeled tiles mosaicking.

3.2 A wavelet algorithm for edge-preserving smooth approximation of SAR imagery

Wavelets have been applied to radar image analysis and understanding in recent years (Simard *et al.,* 98a; Stewart *et al,* 93; Fukuda *et al.* 98 and 99a, b; Niedermeier *et al,* 2000; Ferretti *et al.,* 99; De Grandi *et al.,* 99a, 2000c, 2001a). De Grandi *et al.* have proposed in (De Grandi *et al.,* 2001a) a wavelet based edge-preserving

smoothing algorithm for SAR images. This algorithm is at the core of the pre-processing step of our classification scheme. Although the algorithm is not strictly part of the developments which are the objective of this thesis, an overview is given in this section to set the ground for understanding the overall classification approach. The basic wavelet algorithm was extended to take into account the problem of smoothing within-class textural edges. This original work is documented in section 3.4.5.

As an example of the algorithm in action, a subset of the original GRFM data and the corresponding reconstructed smoothed image are shown in Fig. 3.3 a) and (b).

3.2.1 Underlying theory

The proposed smooth image approximation strategy is inspired by several works by Mallat in which a particular mother wavelet acts as a multi-scale differential operator (Mallat, 1989, Mallat, 1999, Mallat and Zhong, 1992, Mallat and Hwang, 1992).The starting point in Mallat's derivation is the definition in the space L^2 (square integrable functions) of a mother wavelet ψ which is the derivative of a smoothing function θ. A smoothing function is any function that is differentiable, whose integral equals 1, and that converges to 0 at infinity. A mother wavelet defined in this way satisfies automatically the admissibility condition because its integral equals 0.

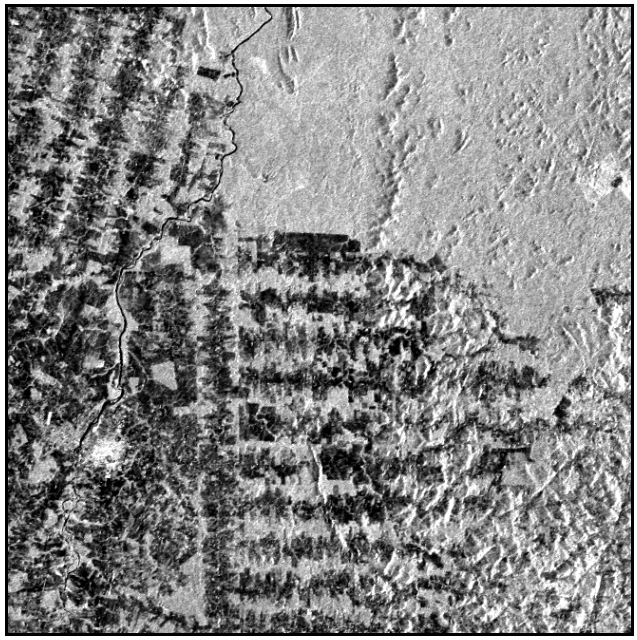

(a)

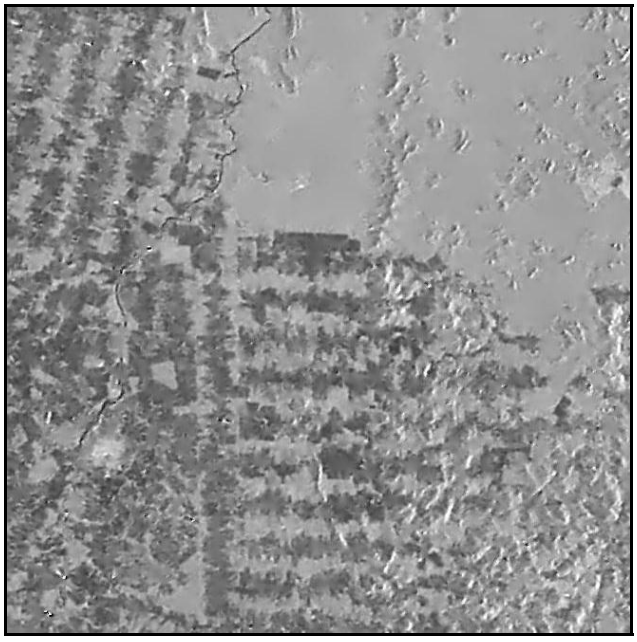

(b)

Figure 3.3: A tile extracted from the GRFM SAR data mosaic (a). Imaged area is 66x66 km^2. The corresponding smooth image generated by the wavelet reconstruction algorithm is shown in (b).

The continuous wavelet transform of a function $f(x)$ at scale s and position x is defined as:

$$W_{\psi} f(x,s) = f(x) \otimes \frac{1}{s} \psi(x/s) \tag{3.1}$$

where $\otimes$ is the linear convolution operator.

An important consequence of the mother wavelet's definition is that the wavelet transform at scale s is proportional to the derivative of the signal smoothed by the scaling function at scale s:

$$W(x,s) = s \cdot \frac{d}{dx}\left(f(x) \otimes \frac{1}{s} \cdot \theta\left(\frac{x}{s}\right) \right) \tag{3.2}$$

A discrete dyadic wavelet providing a complete and stable signal representation based on the continuous transform (1) is also introduced in (Mallat, 1999), together with a fast numerical algorithm based on a filter bank. This algorithm uses separable convolutions (rows and columns) with discrete filters h and g (corresponding to the scaling function and the mother wavelet) whose impulse responses are dilated at each dyadic scale 2^j, $j \in \{Z\}$, by inserting $2^j - 1$ zeros between each coefficient of the filter. The algorithm is dubbed "algorythme a` trous" in French, because the inserted zeros create holes in the filter. Wavelet coefficients at dyadic scales 2^j are computed by cascading convolutions with the dilated filters (see figure 3.13). Numerical values of the high- and low-pass filter coefficients are given in (Mallat and Hwang, 1992). This discrete wavelet transform is over-sampled (i.e. there is no decimation between successive stages); therefore the low-pass filtered images S_{2^j} and wavelet coefficient images $W^x_{2^j}$ and $W^y_{2^j}$ have the same size at all scales.

Since the discrete dyadic wavelet transform provides a stable representation, inversion is possible through the definition of a dual dyadic wavelet. The 2-D signal

(image) S_{2^j} at dyadic scale 2j can be reconstructed given the smooth approximation $S_{2^{j+1}}$ and wavelet coefficients $W^x_{2^{j+1}}$ and $W^y_{2^{j+1}}$ at dyadic scale 2^{j+1} using a fast filter bank algorithm with dual filters $\tilde{h}, k, l$ (Mallat and Hwang, 1992).

Let us identify with M_{2^j} the gradient modulus image, $M_{2^j} = \sqrt{(W^x_{2^j})^2 + (W^y_{2^j})^2}$, and $\alpha_{2^j} = \arctan\left(W^y_{2^j} / W^x_{2^j}\right)$ the image holding the local direction of the gradient at scale 2^j. It is demonstrated in (Mallat and Zhong, 1992) that local maxima of the gradient modulus defined along the direction of the gradient and their evolution with scale can be used to detect sharp image transitions and characterize their regularity.

Mathematically the regularity of a function at one point can be characterized by the Lipschitz condition (Davis, 1975). In turn the Lipschitz condition can be estimated by the trajectories in space-scale of the wavelet modula maxima.

The pointwise Lipschitz condition is:

$$\left\| f(x_1) - f(x_0) \right\| \le \lambda \left\| x_1 - x_0 \right\|^{\alpha} \tag{3.3}$$

Basically one considers increments of a function in the neighborhood of a point x_0, and tries to understand whether the function is bounded and at which order α in the increment (notice that the order can be non-integer). Nearly full reconstruction or approximation (de-noising) of the signal is possible taking into account only the information carried by the wavelet modulus maxima (Mallat and Zhong, 1992). These properties of the wavelet representation are exploited by our de-noising method which is outlined below. A block diagram of the algorithm is shown in Fig. 3.4 and 3.5.

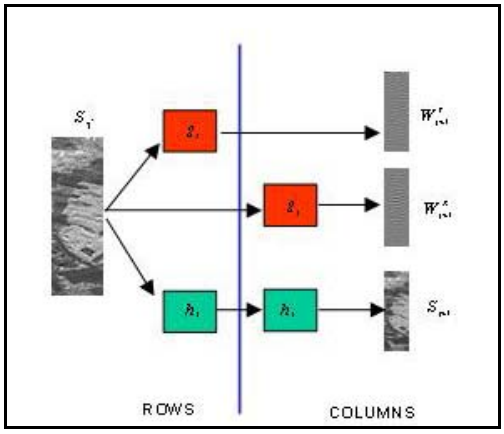

Figure 3.4: Block diagram of the direct 2D discrete wavelet transform**.** S_j is the smooth image at scale 2^j. W_{j+1}^x, W_{j+1}^y are the wavelet transform components along respectively the row and column directions and at scale 2^{j+1}. h_j and g_j are the low pass and high pass filters dilated by inserting $(2^j - 1)$ zeros between each coefficient.

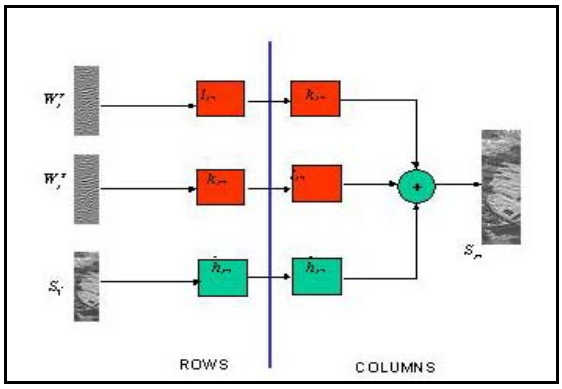

Figure 3.5: Block diagram of the inverse discrete wavelet transform. S_j is the smooth image at scale 2^j. W_j^x W_j^y are the wavelet transform components along respectively the row and column directions and at scale 2^j. $\tilde{h}_j$, k_j and l_j are the low pass and high pass filters associated to the dual mother wavelet and dilated by inserting $(2^j - 1)$ zeros between each coefficient.

3.2.2 Image model

Our radar image model takes into account how the radar backscatter changes with scale for: i) homogeneous areas featuring stationary texture and speckle statistics, and ii) non-stationary image structures like image contours, lines and point targets (De Grandi *et al.,* 1999b).

Let us consider the smooth approximation of a radar image generated by the low-pass branch of the decomposition filter bank. At fine spatial resolution (small scale) sharp transitions of the signal may occur due to speckle in homogeneous constant reflectivity areas, across contours between adjacent homogeneous areas featuring different constant reflectivity, across textured areas (texture edges), and in correspondence of point targets. As the spatial resolution decreases (scale increases), texture and noise are progressively wiped out and the smoothed signal tends to become piecewise constant or slowly varying. Also weak transitions associated with fine features (genuine but small regions) tend to disappear or fall under the noise threshold. On the other hand strong transitions associated with contours between homogeneous or textured areas tend to persist across increasing spatial scales. In other words, starting from a suitably coarse resolution, strong signal transitions (i.e. transitions that persist through increasing spatial scales) may be identified by tracking their positions while moving from coarser to finer resolution levels. The choice of the coarse resolution level from which image synthesis (reconstruction) starts depends on the signal characteristics (e.g., how much texture one wants to wipe out), from the noise model, and from the type of discontinuities to be preserved. For example, fine resolution levels are suitable as starting points for the reconstruction of fine features, while coarse resolution levels are suitable for the reconstruction of large homogeneous areas.

An example of wavelet modulo dependency with the scale related to a signal profile extracted in correspondence of a "strong" edge (forest, non-forest) is presented in figure 3.6.

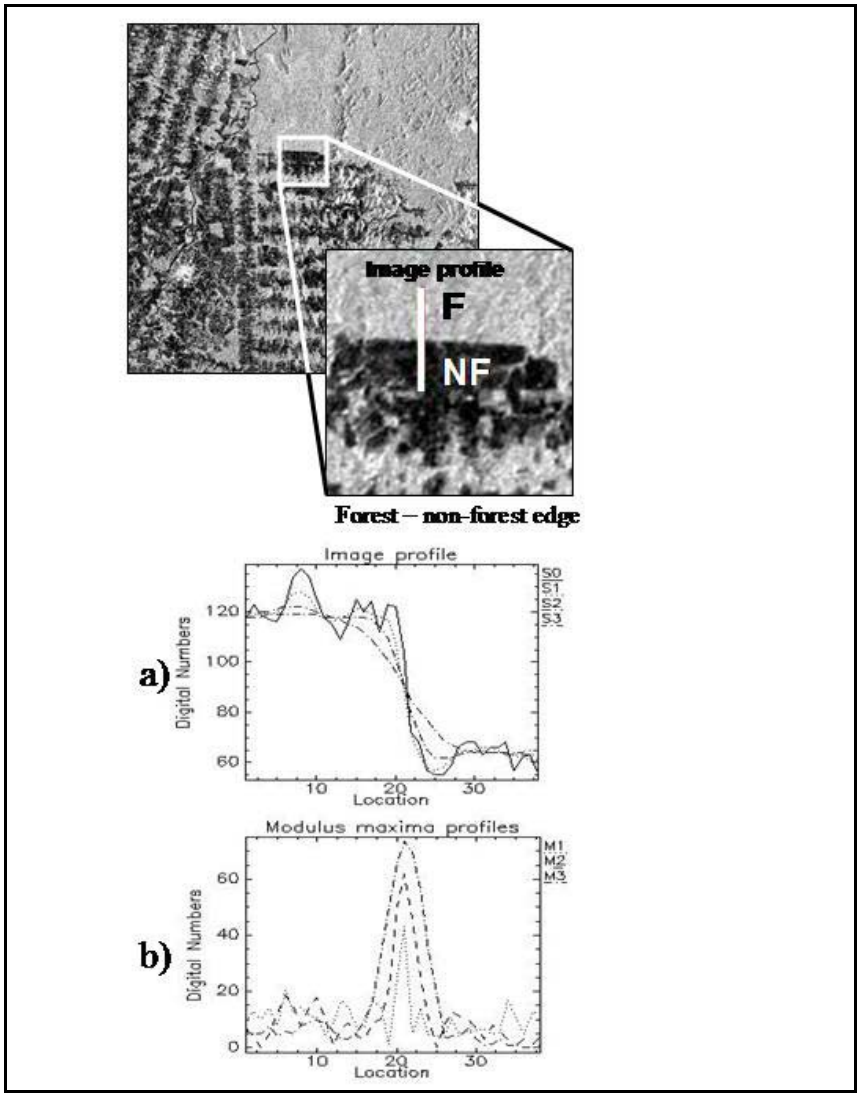

Figure 3.6: Strong edge delimiting a non-forest (clear cut) area from a forest area. In the three signal profiles: a) Original signal (S^0) and smoothed signal S^j on scales 2^1,2^2,2^3.; b) Gradient modula (*M1, M2, M3*) on scales 2^1,2^2, 2^3.

3.2.3 Wavelet modulus maxima tracking

Tracking positions and values of the wavelet modulus maxima through spatial scales is the fundamental mechanism underpinning the edge-preserving smoothing algorithm by image synthesis (reconstruction).

To illustrate the issue concerning the properties of wavelet modulus maxima, it is instructive to consider the case of simple isolated singularities in a mono-dimensional continuous space. Using (1), that is convolving the dilated mother wavelet with the function representing the singularity, and estimating the Lipshitz exponent by (3) one can demonstrate that:

1) The Lipschitz exponent of the Dirac δ distribution is equal to –1. The modulus of the wavelet transform decays as *1/s*, and the maxima (approximating δ) are shifted in position proportionally to scale *s*.
2) The Lipschitz exponent of the Heaviside unit step function is equal to 0. The wavelet modulus maximum does not decay with scale and is not shifted in position.
3) A smooth step with n continuous derivatives has positive Lipschitz exponent. The wavelet modulus maximum increases with scale and its position does not change.

These simple cases suggest that the evolution in position and value of the gradient modulus maxima with scale carries information about: i) the regularity of the function, and ii) the Lipschitz exponent of the signal discontinuity. In other words, this information may be employed to categorize signal discontinuities and estimate the Lipschitz exponent associated with a signal discontinuity.

In the discrete case, discontinuities can be only approximated at the finite resolution of the smallest scale (i.e. at the finest resolution level). The discrete cases corresponding to the continuous functions discussed above are shown in figure 3.7a (Dirac), 3.7b (step), 3.7c (smooth edge). In 3.7d**,** a rectangular pulse smoothed by a Gaussian function is shown. In this case the wavelet modulus maxima evolution with

scale is not monotonic: it starts increasing with the first few dyadic scales, and then decreases because, at a certain scale, the support of the analyzing wavelet becomes larger than the width of the smoothed signal. Therefore the true steepness of the rising (or falling) front cannot be sensed.

Note that, up to this point, isolated discontinuities have been considered exclusively. At the scale where the spatial separation of neighboring discontinuities becomes smaller than the resolution of the analyzing wavelet, wavelet modulus maxima merge together (see 3.7 e).

The maxima follower operation can be summarized as follows. First, persistent maxima at the coarse scale of choice are searched. The maxima location problem is reduced to a one-dimensional problem by intersecting the gradient with a plane in the direction of the gradient.

Once the modula maxima are detected at coarse scale, they need to be tracked in position and value at the finer scales. Maxima positions can change with scale according to the type of discontinuities (e.g. relative to the size of the support of the scaling function).

One more problem is that the wavelet coefficients become increasingly noisy towards finer scales. At scale 2^1 the coefficients are too noisy to be useful. The wavelet coefficients at this critical scale are therefore reconstructed by extrapolation from the selected maxima at scale 2^2 using the Lipshitz exponent estimated by the maxima trajectories with scale.

Summarizing, the wavelet maxima follower algorithm produces information on the position and amplitude at each scale of the wavelet modula maxima that define contours of areas of interest. This information is used for de-noising the fine scale wavelet coefficients, to refine the maxima thresholding of small features using a comparison between two scales and for the reconstruction algorithm.

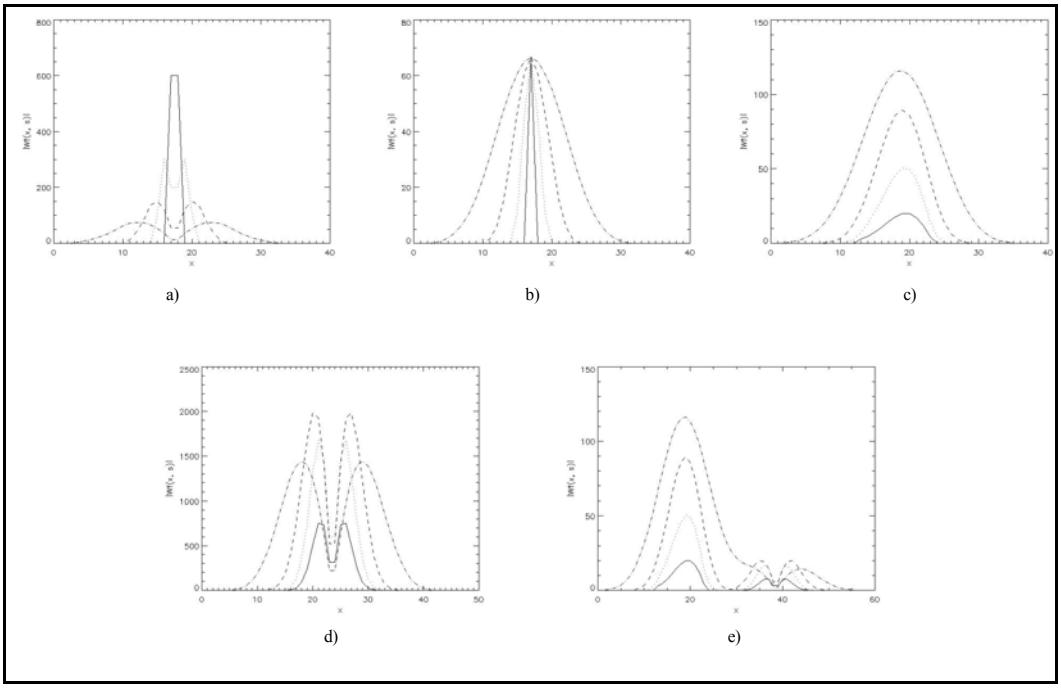

Figure 3.7: Wavelet modula decay with scale for different type of discontinuities and in case of a discrete signal. Frame a) shows the case of a one pixel wide pulse that approximates a Dirac δ . Frame b) a step edge that approximates a Heaviside function. Frame c) a smoothed step edge. Frame d) a Gaussian function that approximates an impulse. Frame e) two non-isolated discontinuities (a step edge and an impulse). The solid line corresponds to scale 2^1. The dotted line to scale 2^2. The dashed line to scale 2^3 . The dash dotted line to scale 2^4 .

3.2.4 Reconstruction from regularized neighborhoods of selected wavelet modulus maxima

The second step in the de-noising method aims at reconstructing, while moving from coarser to finer resolution, an edge-preserving smoothed signal. The reconstruction is achieved by means of an inverse wavelet transform and exploiting the evolution with scale of wavelet modulus local maxima detected by the tracking

algorithm. Algorithms for the reconstruction of a signal from the extrema of its wavelet transform have been proposed in (Carmona, 1995; Mallat and Zhong, 1992). In these works, starting from values and positions of modulus local maxima, the wavelet transform is estimated at all points to be used as input to the inverse wavelet transform for signal reconstruction. In our setting the wavelet transform is already known at all points; thus a simpler and computationally efficient signal reconstruction algorithm can be adopted.

In one dimension, the reconstruction algorithm proposed here searches right and left neighborhoods of the retained gradient modulus maxima characterized by a monotonic derivative. A regularized version of the wavelet modulus is used for the estimation of the two neighborhoods to avoid non-monotonicity due to noise. Wavelet coefficients are retained in these neighborhoods and set to zero everywhere else (trimmed coefficients).

In the two dimensional case (image), the left and right neighborhoods are searched along the cross section of the regularized gradient modulus (2D) in the direction defined by the gradient angle. The values of the gradient modulus and angle within the neighborhoods are then used to compute the wavelet coefficients.

Finally missing coefficients among the trimmed ones are reconstructed by interpolation from the nearest neighbors.

Image reconstruction at scale 2^0 is obtained by the inverse wavelet transform using the smoothed image at scale 2^S and the trimmed and interpolated wavelet coefficients at scales 2^S *to* 2^1.

The second step in the de-noising method aims at reconstructing, while moving from coarser to finer resolution, an edge-preserving smoothed signal by means of an inverse wavelet transform exploiting the evolution with scale of wavelet modulus local maxima detected by the tracking algorithm. Algorithms for the reconstruction of a signal from the extrema of its wavelet transform have been proposed in (Mallat,

1999; Mallat and Hwang, 1992). In these works, starting from values and positions of modulus local maxima, the wavelet transform is estimated at all points to be used as input to the inverse wavelet transform for signal reconstruction. In our setting the wavelet transform is already known at all points; thus a simpler and computationally efficient signal reconstruction algorithm can be adopted.

In one dimension, our reconstruction algorithm searches right and left neighborhoods of the retained gradient modulus maxima characterized by a monotonic derivative. A regularized version of the wavelet modulus is used for the estimation of the two neighborhoods to avoid non-monotonicity due to noise. Wavelet modulus regularization is obtained by applying smoothing spline filters as described in (Unser *et al*., 1993). Wavelet coefficients are retained in these neighborhoods and set to zero everywhere else (trimmed coefficients).

In the two dimensional case (image), the left and right neighborhoods are searched along the cross section of the regularized gradient modulus (2D) in the direction defined by gradient angle. The values of the gradient modulus and angle within the neighborhoods are then used to compute the wavelet coefficients.

Finally missing coefficients among the trimmed ones are reconstructed by interpolation from the nearest neighbors.

To summarize, identifying as 2^{ns} the application-dependent coarsest resolution level where wavelet analysis (decomposition) is conducted, image reconstruction at scale 2^0 is obtained by the inverse wavelet transform employing the smoothed image at scale 2^{ns} plus the trimmed and interpolated wavelet coefficients computed at scales 2^{ns} to 2^1.

3.2.5 Wavelet thresholding for de-noising and texture smoothing

Multiplicative speckle noise in radar imagery poses a number of problems in the reconstruction of an edge-preserving smoothed signal. In homogeneous areas at fine

resolution, speckle generates strong gradients proportional to the mean value of the signal. If speckle is white then it tends to behave like a series of δ distributions; therefore, the amplitude of wavelet modulus maxima decays with scale. If speckle is correlated, it tends to behave like a series of pulse functions. In this case the amplitude of gradient modulus maxima increases with scale up to the point where the wavelet support becomes comparable to the correlation length, and then its starts decreasing. However since singularities created by speckle noise are not isolated, wavelet modulus maxima tend to merge so that their tracking from coarser resolution to finer resolution becomes difficult. Therefore, de-speckling criteria based exclusively on the Lipschitz condition have to be ruled out.

If the strength of speckle at the scale chosen as starting point for the reconstruction is relevant, then wavelet coefficients must be suitably threshold to filter out noise effects. Because of the multiplicative nature of speckle, wavelet coefficient thresholding must be spatially adaptive. For instance a technique proposed in (Simard *et al.,* 1998b) calls for normalizing the gradient modulus at scale s by the smooth image at the same scale.

In our application the GRFM data set at 100 m pixel size is generated from high resolution JERS-1 imagery by low pass filtering and down-sampling, and the equivalent number of looks is approximately equal to 59. Therefore most of the effects related to speckle are only relevant at scale 2^1 and the gradient does not need to be normalized.

To summarize, on the one hand wavelet coefficients at scale 2^1 bear important information related to image sharp transitions. On the other hand these coefficients are likely to be affected by noise. Thus, special care must be taken in dealing with wavelet coefficients at scale 2^1. Filtering or regularizing these coefficients induces blurring of the image. In our image reconstruction strategy, the position of meaningful singularities at scale 2^1 are estimated in correspondence of the gradient

modulus local maxima detected at scale 2^2 while their values are extrapolated from the Lipschitz exponents estimated by the evolution with scale of the corresponding gradient local maxima.

With regard to texture smoothing, strong texture edges due to within-class variance (i.e. within-class texture edges) also propagate through scales and can persist up to the scale chosen as starting point for signal reconstruction. If a slowly varying signal is required over texturally uniform image areas, then wavelet coefficients relative to textural edges must be adaptively threshold based on their context. For example, in our application, within-forest class texture contours may persist at scale 2^3, which is the one chosen to initiate image reconstruction.

Therefore a novel application-specific rule-based mechanism was developed to distinguish between gradient modulus local maxima related to forest/non-forest inter-class transitions (to be preserved), from those related to forest within-class texture variations (to be removed) (see figure 3.8). For each gradient modulus local maximum detected in M_{2^3} along the direction of gradient α_{2^3} at scale 2^3, two pairs of mean and standard deviation values extracted from the smoothed signal S_{2^3} are estimated along an image profile. This image profile is: i) centered on the position of the gradient local maximum, ii) oriented along the direction of the gradient, iii) up to 10 pixel-long, and iv) shorter than 10 pixel if it intersects another gradient local maximum. Pairs of signal mean and standard deviation values extracted from S_{2^3} along the right and left side of such a profile are identified as data pairs (m_1, m_2) and (SD_1, SD_2) respectively. Reference forest statistics (m_{F_i}, SD_{F_i}), $i=1,..,N$, are collected off-line from a set of N low-textured forest area samples extracted from S_{2^3}. Three hierarchical rules are adopted to filter out within-class forest edges (see Table 3.2), i.e. edges featuring class forest on both sides, given a pixel where a gradient local maximum is localized at scale 2^3:

Table 3.2: Three hierarchical rules adopted to filter out within-class forest edges

Rule I. Preservation of non-forest inter-class transitions

Wavelet maximum identified by $((SD_1 < SD_{F_i})$ and $(SD_2 < SD_{F_i}))$, for all *i=1..N,* is not threshold because it correspond to an edge pixel which is not involved with class forest on both sides (i.e. this is not a within-forest class edge).

ELSE

Rule II. Comparison between backscatter mean values in the right and left wavelet maximum neighborhoods

At least one neighborhood (right or left) is representative of class forest then backscatter mean values in the right and left neighborhoods are comparable if:

$((m_1 - 2 \cdot SD_1) < m_2 < (m_1 + 2 \cdot SD_1))$ AND $(SD_1 < SD_2))$ or

$((m_2 - 2 \cdot SD_2) < m_1 < (m_2 + 2 \cdot SD_2))$ AND $(SD_1 > SD_2))$

THEN

Rule III. Forest intra-class wavelet modulus local maximum threshold

According to rule II this is a within-class type of edge. If the mean backscatter is near the prior forest class:

$((m_{F_i} - 2 \cdot SD_{F_i}) < \frac{(m_1 + m_2)}{2} < (m_{F_i} + 2 \cdot SD_{F_i}))$, for all *i=1,..,N*

this wavelet modulus local maximum is removed because it belongs to a within-forest class contour.

(m_1, m_2) = pairs of signal mean values extracted from S_{2^3} along the right and left side of a profile

(SD_1, SD_2)= pairs of signal standard deviation values extracted from S_{2^3} along the right and left side of a profile respectively.

$((m_{F_i}, SD_{F_i})$, *i=1,..,N* $)$ =reference forest statistics.

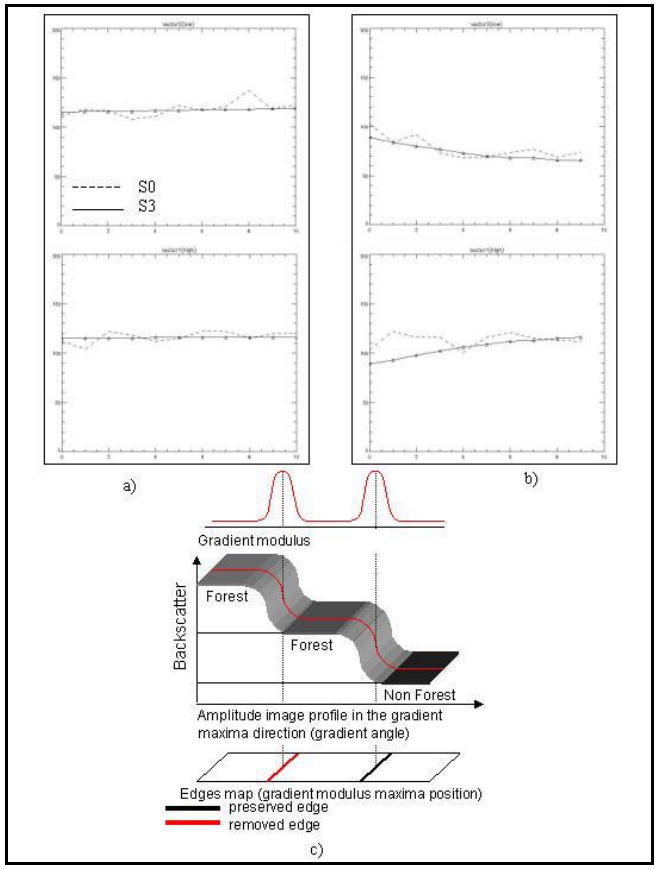

Figure 3.8: a) and b) signal statistics (mean, standard deviation) collected along the profile from the local maxima position up to the closest local maxima are indicated by triangles. c) Diagram illustrating the principle of the rule-based mechanism used to distinguish between gradient modulus local maxima related to forest/non-forest inter-class transitions (to be preserved), from those related to forest within-class texture variations (to be removed).Statistics from profile a) correspond to intra-class signal variation (forest signal textural variations) and the related modula maxima will be not considered for the image reconstruction. b) Correspond to inter-class signal variation (forest – non-forest signal textural variations) and the related modula maxima will be considered for the image reconstruction (see color Figure B.6 - Appendix B, pp. 205).

3.3 GRFM specific classification techniques

3.3.1 Region growing technique

This image-labeling technique - dubbed region-*growing* -, consist of 2 steps:

1) An application-dependent region growing algorithm for image segmentation.
2) A segment-based two-stage hybrid learning classifier.

First a region-growing algorithm is used to build a segmentation map from the piece-wise smooth reconstructed image and the edge map generated by the wavelet decomposition. In support to the segmentation step at first connections are created between neighboring maxima along a path where the gradient has similar properties (modulus and angle) with respect to the maxima. This closure operation allows for a better definition of the contours; also a vector representation of the contours can be generated. The algorithm for maxima linkage uses a growing window to explore the neighborhood of each maximum. The window is grown until either at least one more maximum is included or a prefixed size is reached. If no more maxima are included, the maximum under consideration is considered to be either an isolated singularity or the terminal point of the current chain. Otherwise the nearest maximum is analyzed, and is included in the chain if two conditions are satisfied: 1) the gradient angles (extrapolated from scale 2^3) are aligned within a tolerance; 2) the relative magnitudes of the modula are comparable within prefixed bounds. Each chain is represented by a linked list. When all maxima have been examined, a second pass is performed to check maxima labeled as terminal nodes of the chains, and to connect them if their gradient values satisfy the criteria mentioned above.

The region-growing algorithm for image segmentation works as follows.
We call a stitch a point belonging to the maxima linked lists (see previous definition). From a random position a seed region is grown including recursively all neighboring pixels that do not include a stitch. In our case 49 pixels are counted in for obtaining a

sufficient statistics. The local statistic of the seed point is computed; the sample variance is used as the point estimate of the variance; an interval estimate of the variance based on the assumption of normality of the data is derived. Also given the sample mean, the theoretical variance for a homogeneous area is computed assuming multiplicative noise in the data. The signal model in our case foresees Raleigh distributed correlated speckle amplitude data**,** the statistical properties of which are modified by a series of low pass filters in the wavelet decomposition. If the lower bound of the interval estimate of the local variance is greater than the theoretical variance of a homogeneous area then the seed point is discarded since its local statistic is not representative of a homogeneous area. The seed point is also flagged as a non-classified point, while the points that were included in the region are still kept as candidates for future assignments. If the local variance is compatible with the theoretical variance, pixels in the seed region are assigned to a new segment and the region is grown further, always recursively-assigning neighbors that do not belong to stitches. Each new candidate pixel is compared with the local statistic and is accepted in the segment if its value falls between two standard deviations from the segment mean. While the segment is grown also the local statistic (mean and variance) are updated until they reach asymptotic values. Each assigned pixel is flagged as processed and assigned a progressive segment number in the output segment map. The growth process is stopped when no more neighbors can be accepted; then a new seed position is chosen as the nearest not yet processed pixel on the bisected distance of the original seed to the image origin. The overall segmentation process is stopped when all pixels have been flagged as processed. Three snapshots of different stages of the region growing process are shown in Fig. 3.9.

As second step a segment-based two-stage hybrid learning classifier is adopted. Each segment is represented by a two-dimensional feature vector consisting of the per-segment mean and standard deviation of backscattered power. The unsupervised

learning first stage of the classifier iteratively gathers segments into segment categories based on a Jeffries-Matusita pairwise minimum distance criterion until a user-defined number of segment categories is reached. In the supervised learning second stage, unsupervised segment categories are gathered into supervised classes of interest according to expert photo-interpreters.

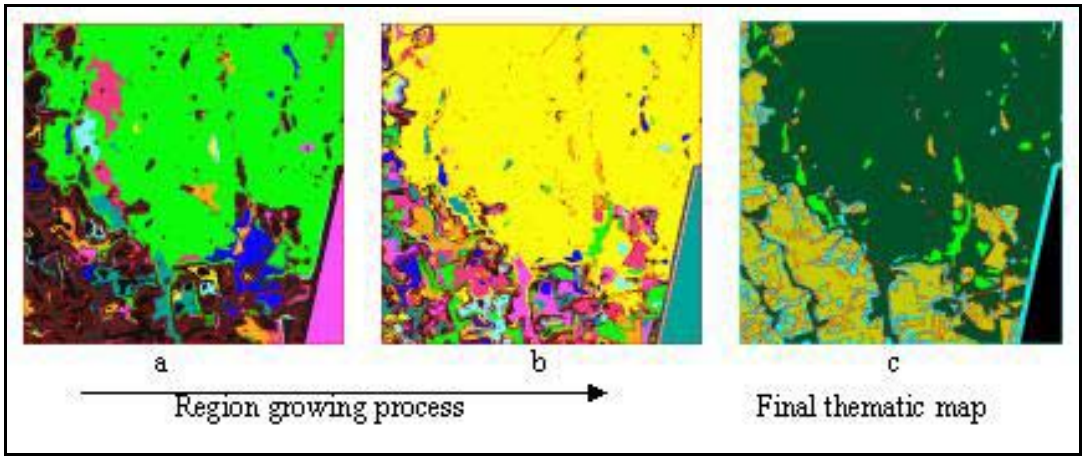

Figure 3.9: representation of 2 steps in the region growing processes (a, b) up to the final thematic map (c) (see color Figure B.7 - Appendix B, pp. 206).

3.3.2 Per pixel two-stage hybrid classifier

The second image-labeling technique consists of a two-stage Nearest Multiple Prototype (NMP) classifier. The NMP first stage employs ELBG near-optimal vector quantization algorithm. At the second stage of NMP, the vector prototypes are combined into land cover classes of interest with the help of expert photo interpreters.

To combine high classification accuracy with low processing time, a computationally efficient per-pixel (i.e. non-contextual) clustering algorithm is input with a smoothed approximation of the radar data at full resolution computed by the pre-processing block proposed in section 3.4.

A synoptic view of the main building blocks is given in figure 3.10. The first unsupervised learning stage consists of ELBG (see figure 3.10, block1). ELBG is a vector quantization algorithm recently proposed in the pattern recognition literature as an improvement over the well-known LBG (i.e. hard c-means) vector quantization algorithm (Patane` and Russo, 2000, 2001, 2002). It is a batch non-constructive vector quantizer, i.e. it tries to minimize a distortion error, or mean square error (MSE), with a fixed number of codewords which is user-defined. The original contribution of ELBG is to employ local optimization criteria, which may require codewords to move across non-contiguous Voronoi regions, to reduce the global distortion (quantization) error. It has been shown that ELBG (Patane` and Russo, 2001)**:**

1) Is near-optimal and stable, i.e. its output results are virtually independent of the initial position of templates;
2) In terms of quantization error minimization, performs better than several clustering techniques found in the literature;
3) Is fast to reach convergence;
4) Features low computation overhead (<10%) with respect to the traditional LBG.

At the second stage of the NMP classifier, template vectors are labeled, i.e. many-to-one relationships between unsupervised template vectors (codewords) and land cover classes of interest are defined with the help of expert photo-interpreter. In the pattern recognition phase, each pixel is labeled according to the minimum-distance-to-prototype criterion (see figure 3.10, block2).

As an alternative to the labeling method proposed here, the non-contextual ELBG clustering step may be followed in cascade by the contextual Modified Pappas Adaptive Clustering (MPAC) algorithm. This algorithm segments image data in a joint spatial/spectral image domain. The drawback of this approach is a greater

computational overhead while the advantage is that no additional user supervision is required by the system to run. Owing to its Bayesian maximum a posteriori contextual adaptive multi-resolution labeling scheme, MPAC is considered superior to several alternative labeling algorithms, including ELBG, in terms of image detail detection capability and robustness to changes in the user-defined number of input clusters.

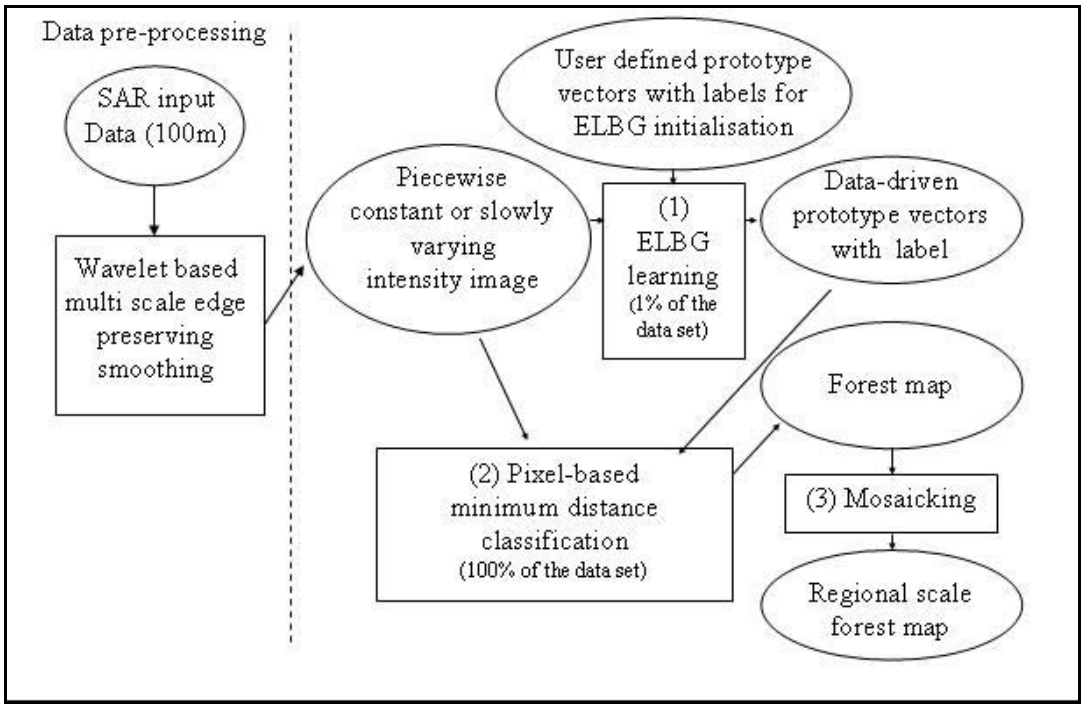

Figure 3.10: Main building blocks of the per pixel two-stage hybrid classifier

3.4 Definition and characterization of thematic classes

Out of the wide amount of ecological and geographical information content of the GRFM South America mosaic, our attention is focused on a simple thematic context comprising the following land-cover classes: forest (F), degraded forest (DF), non-forest (NF) and water (W).

Our thematic goal here is here is to produce a land-cover map, where classes are defined in connection with what overlays or currently covers the ground. It is reminded that a land-use map refers on the other hand to the predominant purpose for which an area is employed (USDA Forest Service, 1989).

Synoptic description and radiometric characterization of the selected land cover thematic classes are reported in figure 3.11. Homogeneous clusters for the classes *forest, non-forest and degraded forest* are extracted in the learning phase of the classification process. The statistical properties of the clusters (mean and standard deviation) are shown in the graph at the center of the figure. The graph is surrounded by a number of images (icons) that depict the radar view of the thematic classes. In the forest class (first icon, top-left) we include open and dense forest, without phenological distinction or distinction of species.

Figure 3.12 shows pictorially the difference between evergreen forest in alluvium plains with a homogeneous and dense canopy (high backscatter, *DN= 110*, σ^0 = -7.71; area 1) and evergreen up-land forest with dryer and open canopy (low backscatter, *DN=106,* σ^0 *=-8.03;* area 2) in the Mato Grosso state of Brazil.

Figure 3.13 shows the difference between lowland floodplain forest (*DN=130,* σ^0 *=-6.26*; area1) and mangrove forest (*DN=105,* σ^0 *=-8.11*; area2) in the coastal area of Guyana. The presence of different species and phonological diversity explain the radiometric variability within the same thematic class.

The flooded forest is characterized by high digital number as can be seen in figure 3.14 (*DN=255,* σ^0 *=-0.41*; area1).

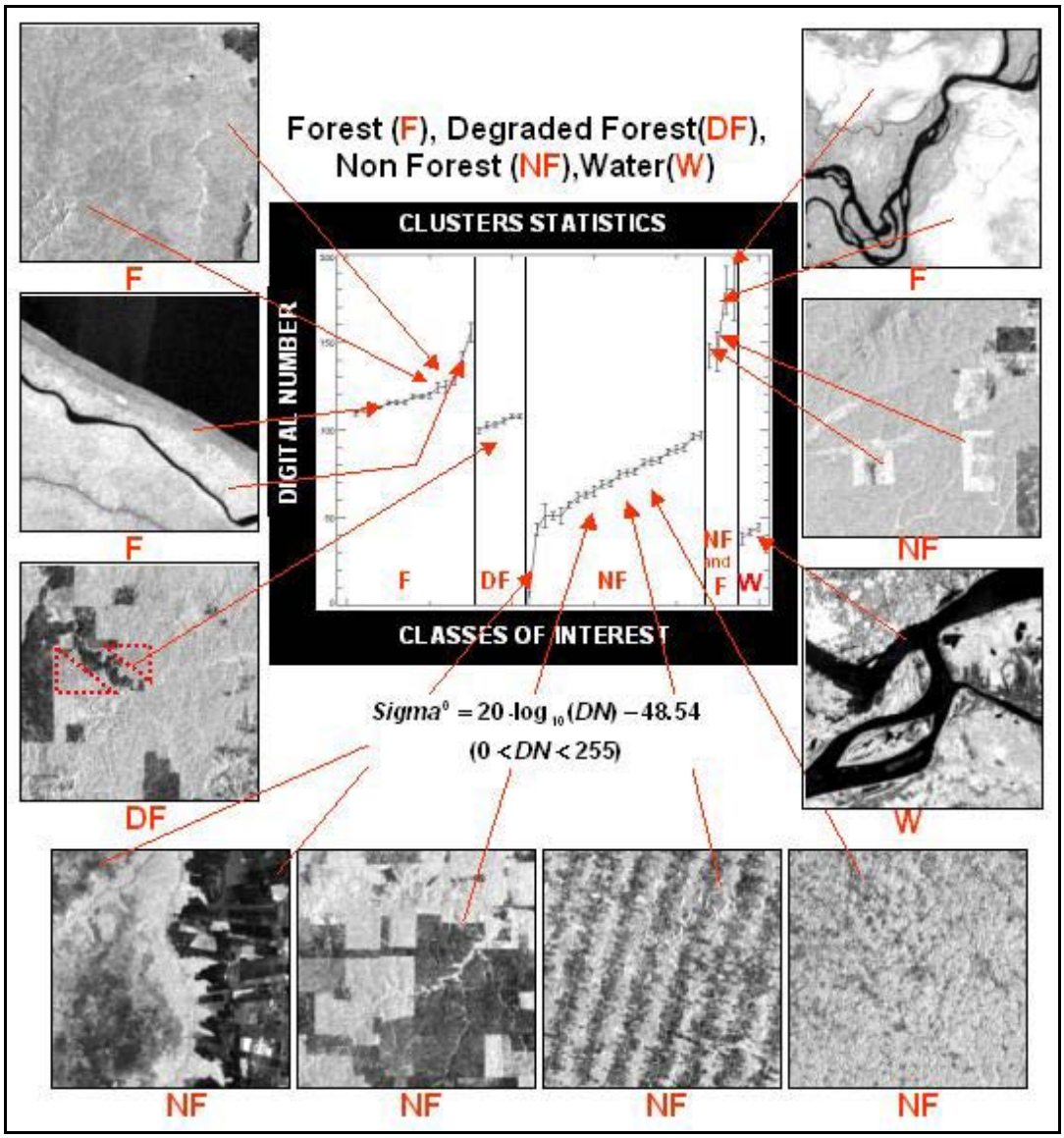

Figure 3.11: Synoptic description and radiometric characterization of the selected land cover thematic.

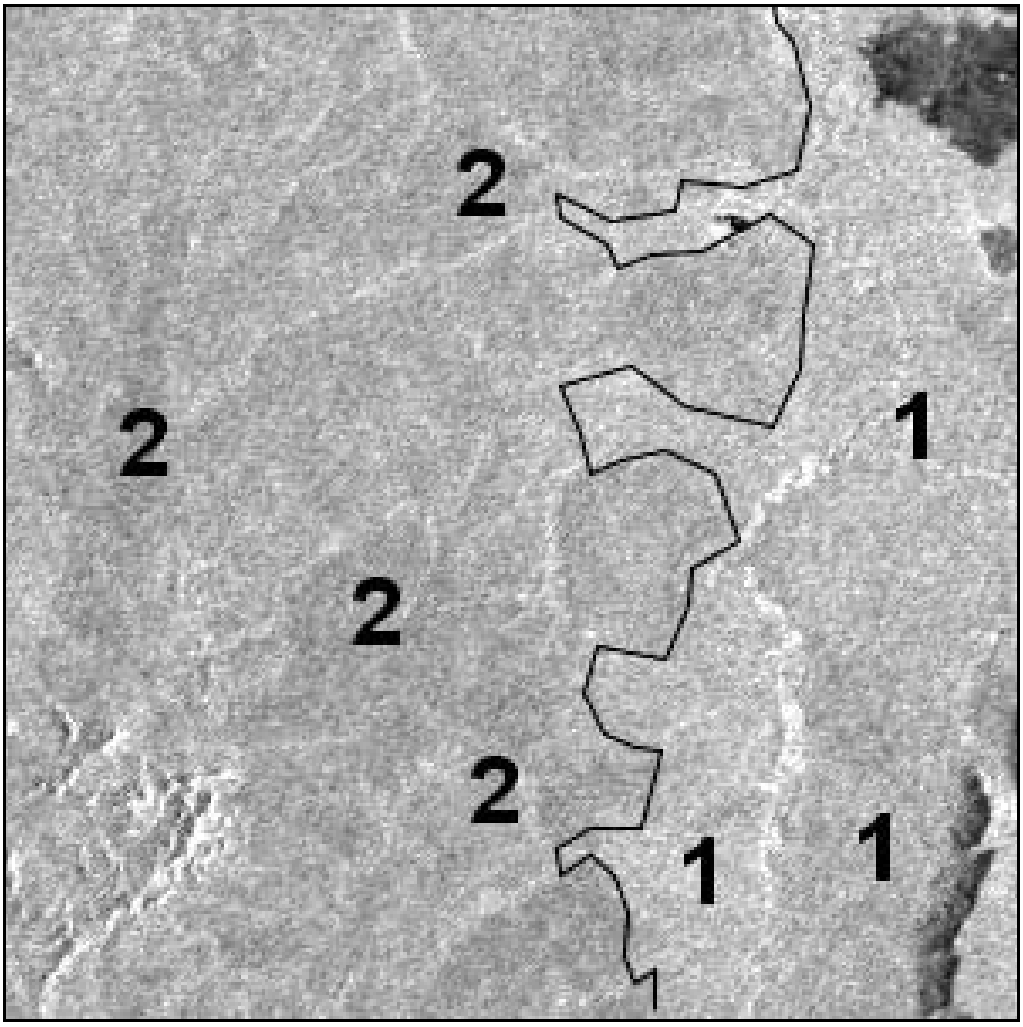

Figure 3.12: Forest class: evergreen forest in alluvium plains with a homogeneous and dense canopy (*DN*=110, σ^0 =-7.71; area 1) and evergreen up-land forest with dryer and open canopy (*DN*=106, σ^0 =–8.03; area 2). Image area: 30x30 km^2.

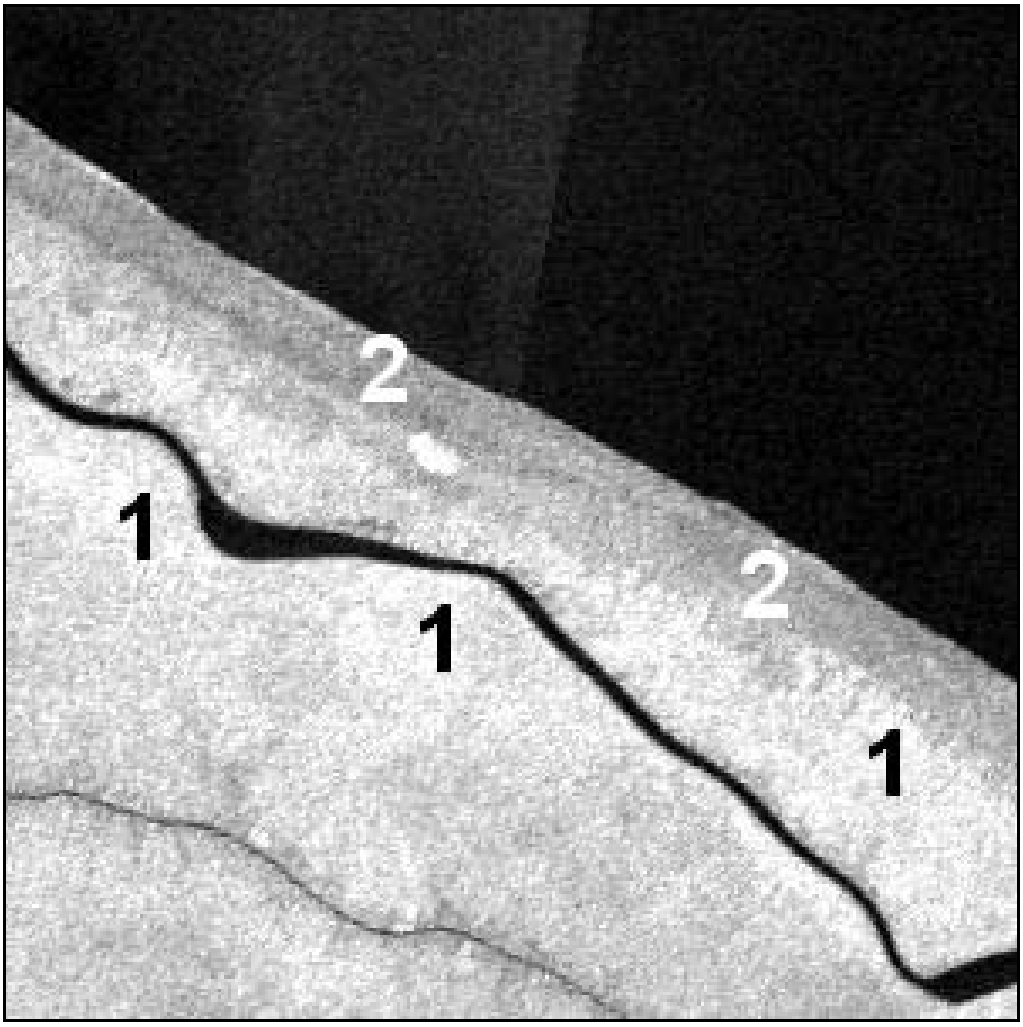

Figure 3.13: Forest class: lowland floodplain forest (*DN*=130, σ^0 =–6.26; area 1) and mangrove forest (*DN*=105, σ^0 =–8.11; area 2). Image area: 30x30 km^2.

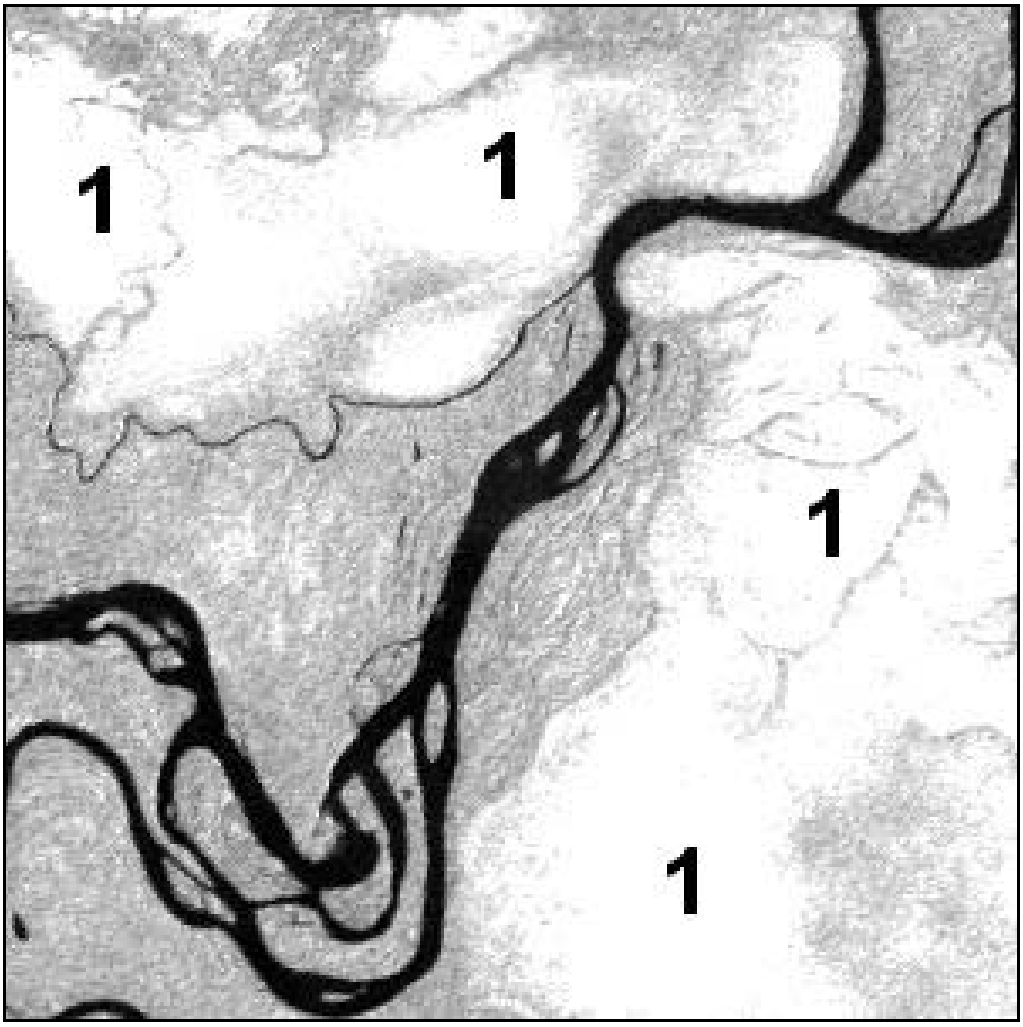

Figure 3.14: Forest class: flooded forest (*DN*=255, σ^0=-0.41; area 1). Image area: 30x30 km^2.

All the anthropogenic disturbances in the forest domain (owning to ranching, shifting cultivation, selective logging) fall into the classes *non-forest and degraded forest*. We use the action term "degraded forest" to describe any intermediate state from forest class to deforestation. Degraded forest can also be a mosaic of isolated forest patches within non-forest regions or vice versa isolated bare-soil regions

surrounded by a forest area (see the schematic representation indicated as “original data” in figure 3.15).

It is worth while noticing that this type of degradation may be identified as a homogeneous class using the wavelet multi scale edge preserving smoothing (section 3.4). The wavelet-based zooming procedure progressively dilates the receptive field until these ‘mosaic’ regions tend to become piece-wise constant and surrounded by sharp transitions that we will call intra-class edges. The adaptive wavelet coefficient threshold applied at this scale is capable of distinguishing these intra-class edges from the so-called inter-class transitions (textural edges). In the reconstructed signal these mixed classes will be perceived as a piece-wise region with a radiometric intermediate behavior from forest class to deforestation (see the schematic representation indicated as “reconstructed data” in fig 3.15).

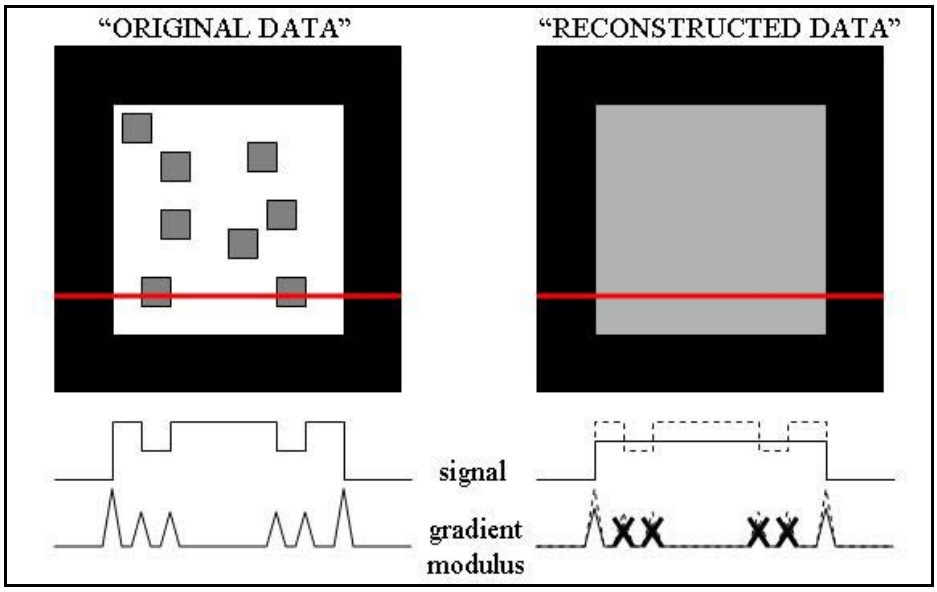

Figure 3.15: Schematic representation of degraded forest class (i.e. mosaic of isolated forest region surrounded by a forest area). In the reconstructed signal these mixed classes will be perceived as a piece-wise region (see color Figure B.8 - Appendix B, pp. 206).

With a single-date classification, changes from forest to clear-cut degradation cannot be discriminated from an area of partial re-growth like the abandoned pasture framed by the 2 red boxes of figure 3.16 (*DN=100,* σ^0 *=-8.54*).

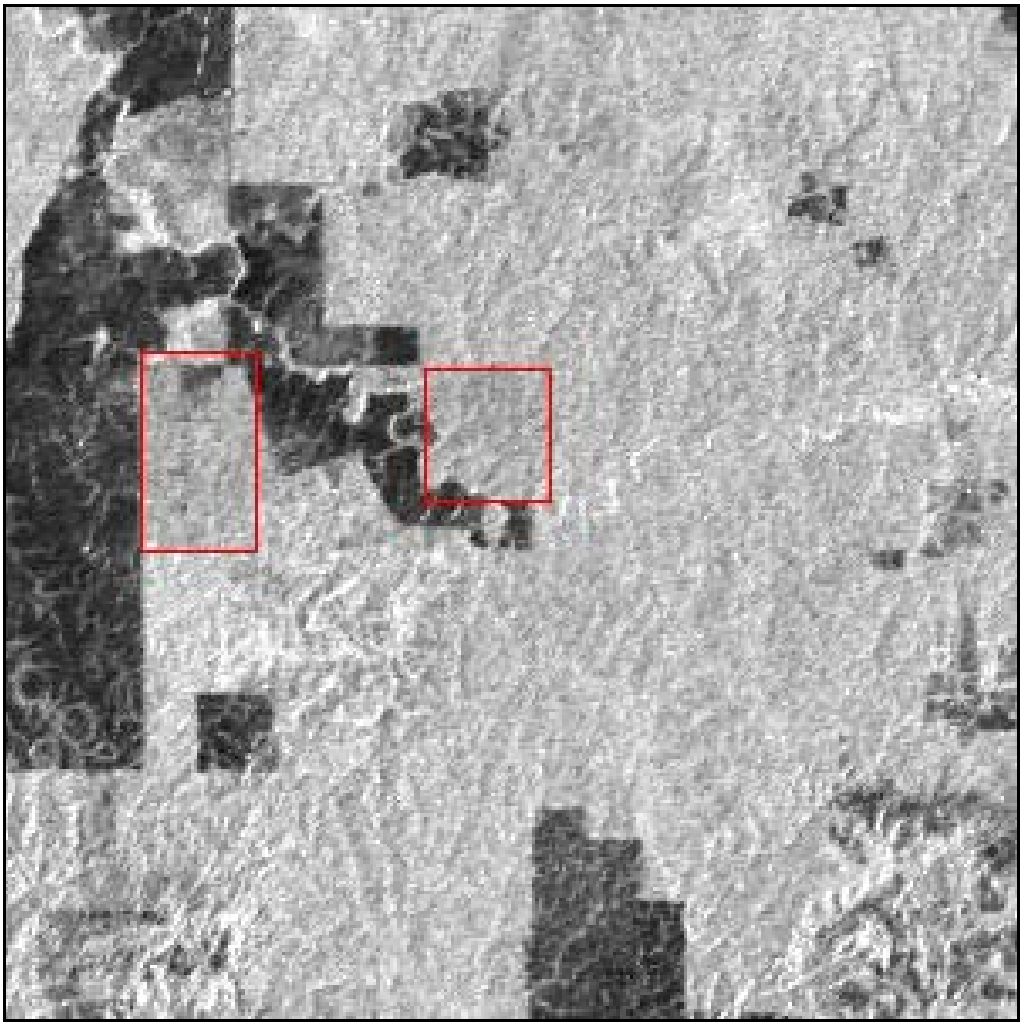

Figure 3.16: Degraded forest class: abandoned pasture with partial re-growth forest in the 2 red boxes (*DN*=100, σ^0 =-8.54). Image area: 30x30 km^2 (see color Figure B.9 - Appendix B, pp. 207).

The different spatial arrangement of deforestation included in the non-forest classes and characterized by low backscatter clusters (*105<DN<130, -8.11<* σ^0 *<-6.26*) are shown in figure 3.17a, b, c that refer to areas in Mato Grosso, Rondonia, and Colombia respectively.

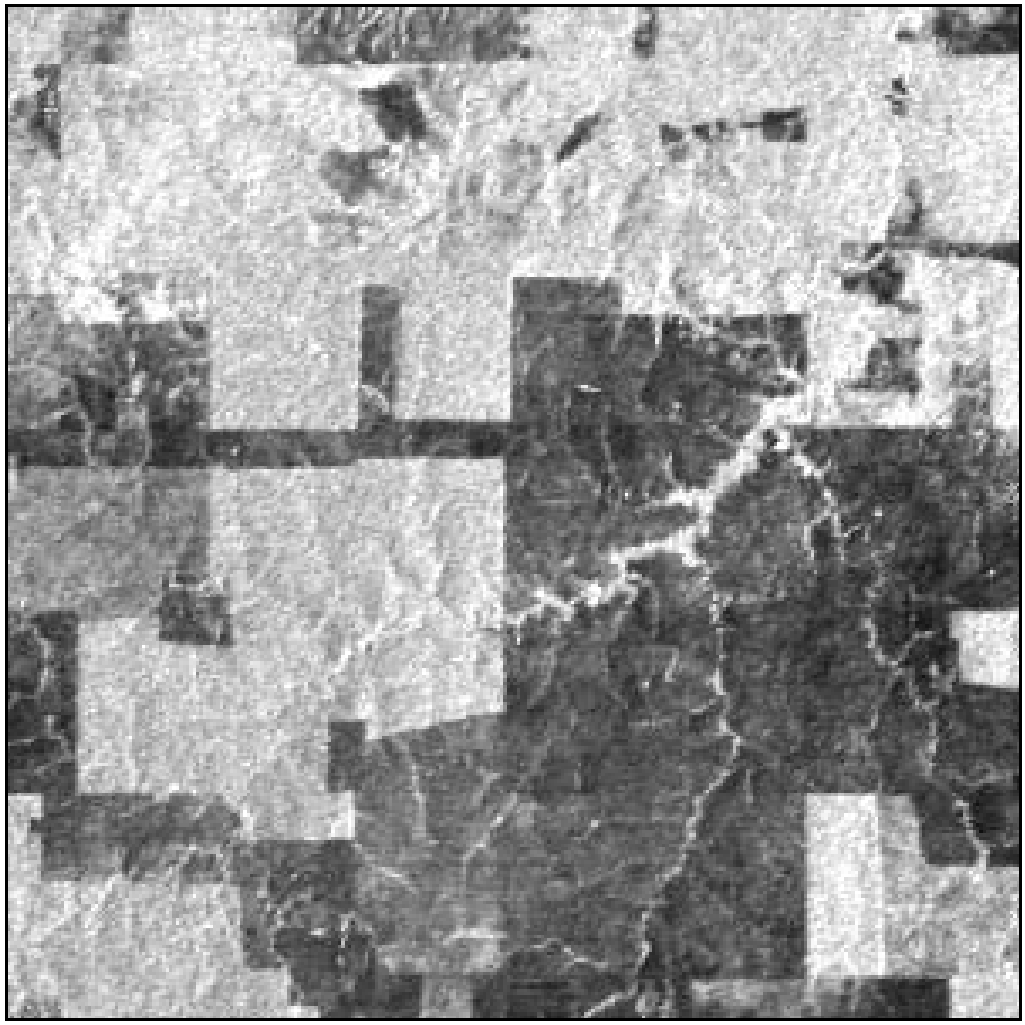

Figure 3.17 a: Non-forest class: different spatial arrangement of deforestation: big ranches in Mato Grosso (Brazil), (105<*DN*<130, -8.11< σ^0 <-6.26). Image area: 30x30 km^2.

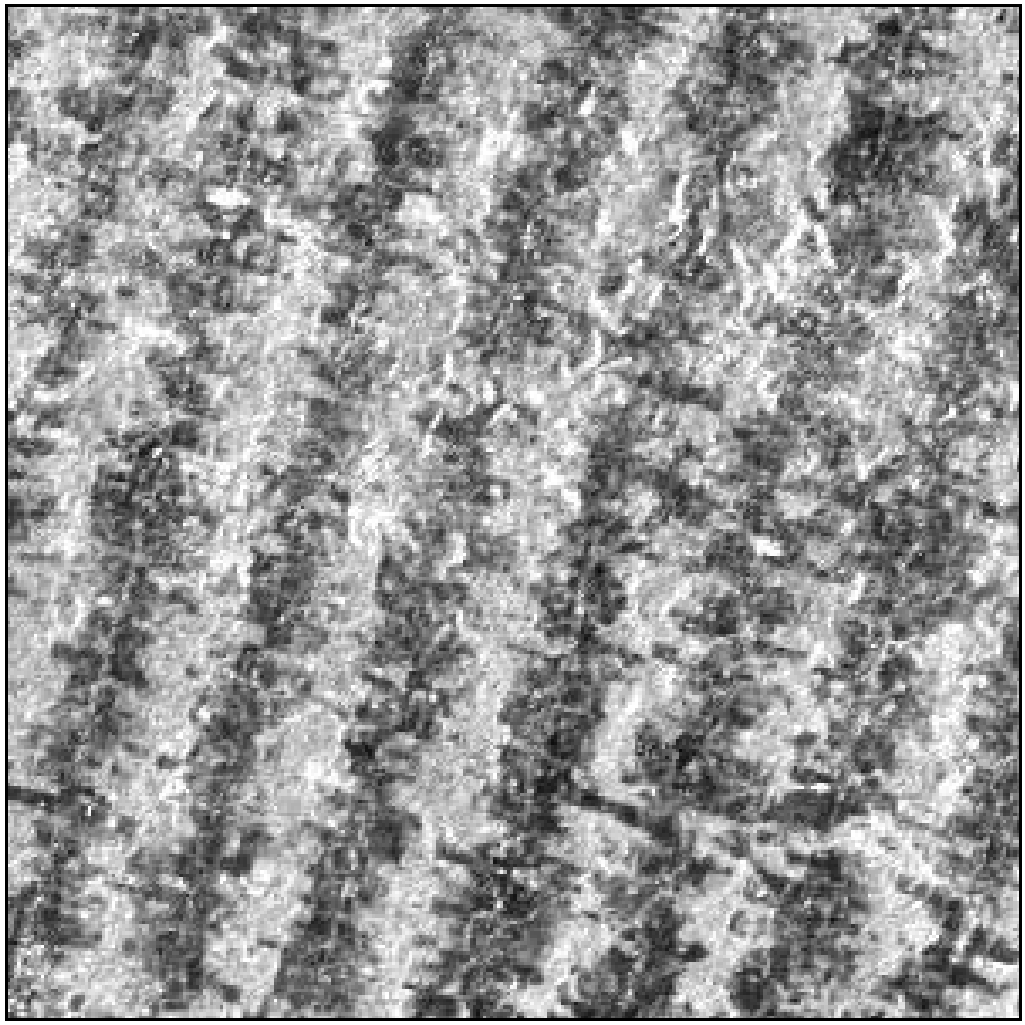

Figure 3.17 b: "Herring bone" patterns in Rondonia (Brazil), (105<*DN*<130, -8.11<σ^0<-6.26). Image area: 30x30 km^2.

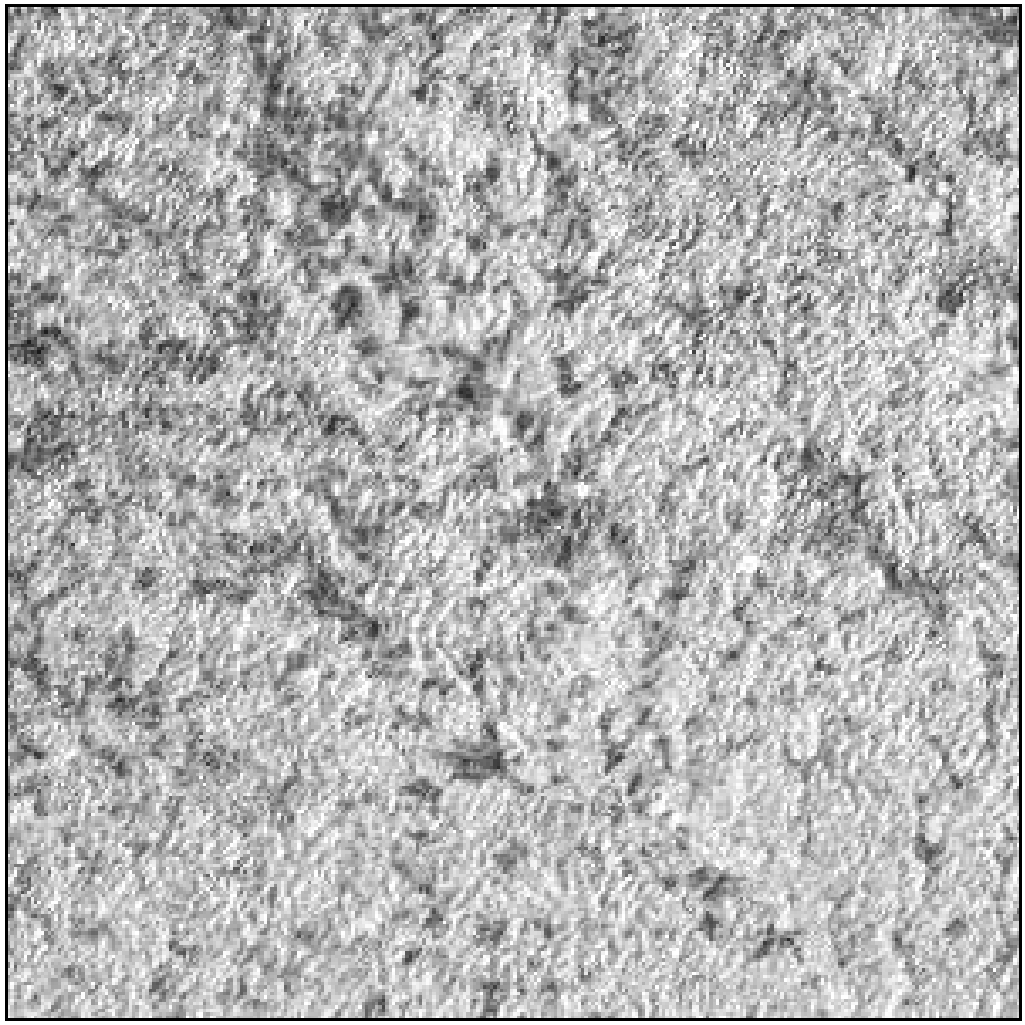

Figure 3.17 c: Non-forest class: different spatial arrangement of deforestation: widespread and small forest cuts in Colombia ($105<DN<130$, $-8.11<\sigma^0<-6.26$). Image area: 30x30 km^2.

The non-forest class includes also natural areas not covered by forest like natural or cultivated savanna (see figure 3.18; $30<DN<90$, $-18.99<\sigma^0<-9.45$).

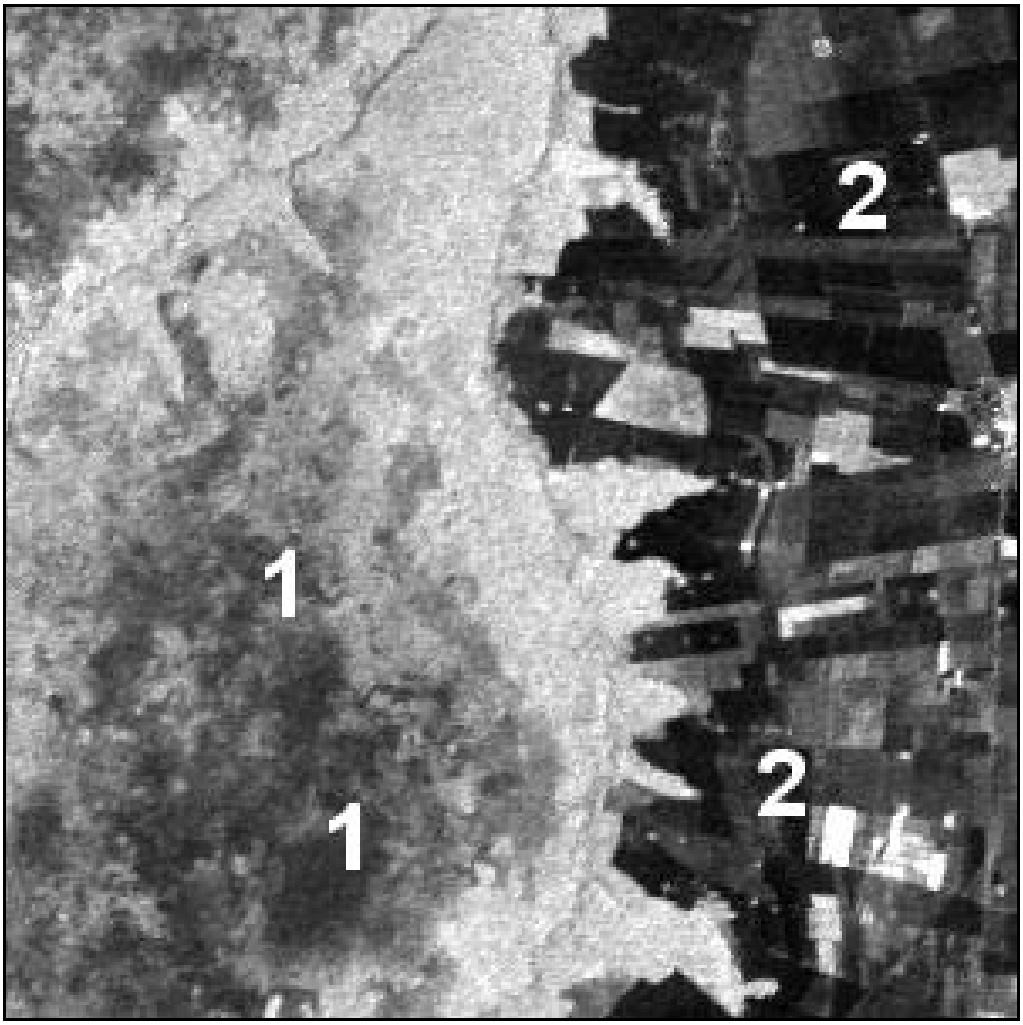

Figure 3.18: Non-forest class: natural savanna (area 1) and cultivated savanna (area 2), ($30<DN<90$, $-18.99<\sigma^0<-9.45$). Image area: 30x30 km^2.

The water class including lakes and rivers is characterized by low backscattering values (*DN=30,* σ^0 *=-18.99*) sometimes comparable with bare-soil backscatter (see figure 3.19).

The seawater bodies can be both high and low backscatter depending on wind effects.

Figure 3.19: Non-forest class: Rio Negro (north) and Rio Solimoes (south) becoming Amazon rivers and characterized by low backscattering values (*DN*=30, σ^0 =-18.99). Image area: 30x30 km^2.

New clear cuts can be characterized by high-backscatter (*DN=235,* σ^0 *=-1.11*) when partial logging occurred or the stems are still lying on the ground. Radar signals penetrate the more open canopy and the cut trunks on the ground increase the double-

bounce backscatter. In that case the geometric shapes of these areas help in the distinction from natural high backscatter targets (figure 3.20).

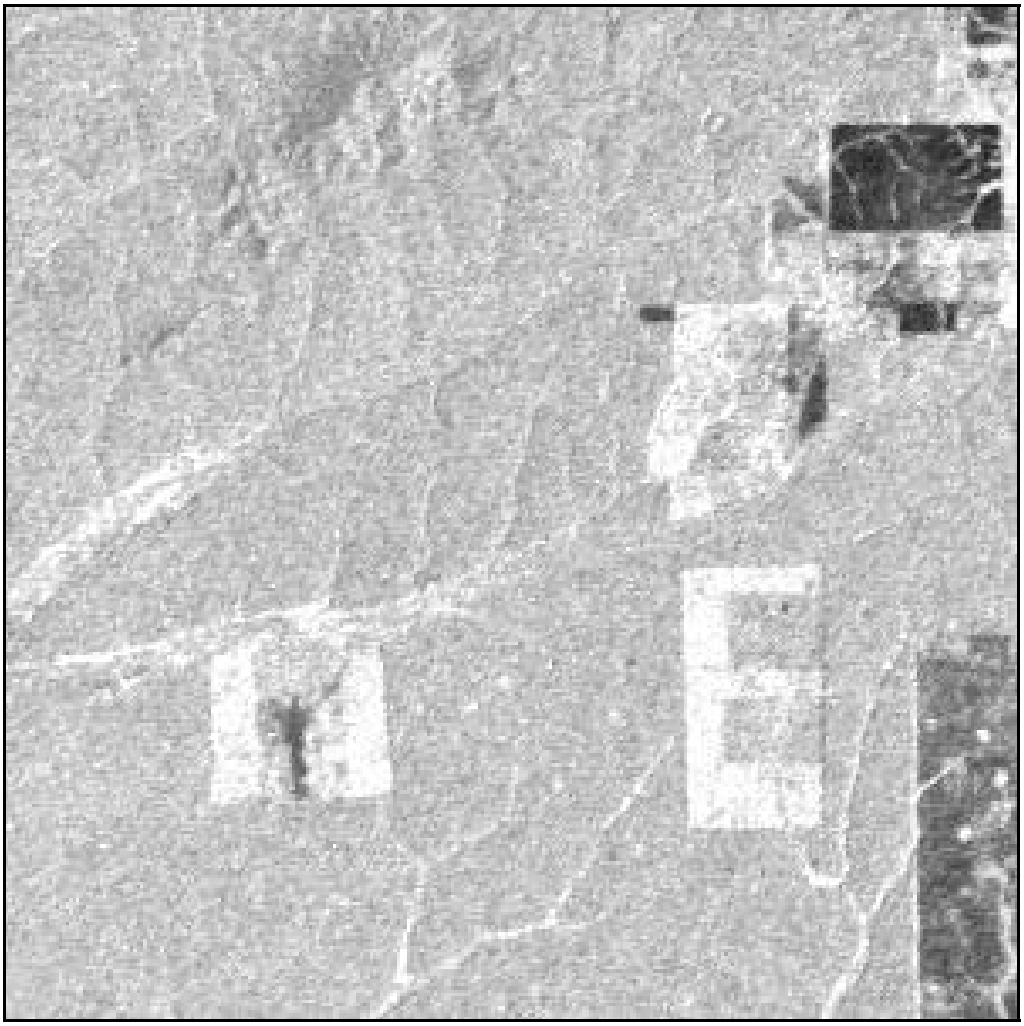

Figure 3.20: Non-forest class: new clear cuts where the trees have not been completely cut and the cut trunks lain on the ground increase the double-bounce backscatter (*DN*=235, σ^0=-1.11). Image area: 30x30 km^2.

3.5 Summary and conclusions

In this chapter operational classification scheme suitable for processing large coverage radar data sets, such as the GRFM South America mosaics, is presented and detail from the technical and operational point of view. The proposed classification approach consists of: i) wavelet multi-resolution decomposition/reconstruction pre-processing technique capable of backtracking the value and position of image singularities from coarse to fine resolution levels of analysis, and ii) two per-pixel image-labeling techniques for thematic information extraction. The first image-labeling technique, dubbed *region-growing technique,* is based on an application-dependent region growing algorithm. Then the classifier iteratively gathers segments into segment categories based on a Jeffries-Matusita pairwise distance. As second image clustering technique a *two-stage NMP classifier* is proposed. The NMP first stage employs ELBG near-optimal vector quantization algorithm. At the second stage of NMP, the vector prototypes are combined into land cover classes of interest with the help of expert photo interpreters.

Both the techniques are easy to use, requiring minor user interaction, but the per pixel two-stage hybrid classifier runs faster.

Two major issues have to be tackled for extracting thematic information from the GRFM mosaics: i) high variance of the radar signal in high backscattering homogeneous areas or in non-homogeneous textured areas reduces the clusters separability and tends to produce over-segmentation, ii) large data volume (1.3 Gb).

Due to the first problem, conventional clustering techniques (ISODATA) are ill suited (see the results in Chapter 4). The proposed wavelet multi-resolution decomposition/reconstruction technique is capable of generating an edge-preserving piecewise constant radar image with radiometric characteristics of the reconstructed signal closer to the piece-wise constant model required by a certain class of image-labeling algorithms. The designed image-labeling technique takes into due account

multiplicative noise and contemporary solves the problem of some classes of interest (e.g. forest) corresponding to highly textured regions.

A special purpose processing chain that works on partially overlapping tiles extracted from the mosaic had to be developed to solve the second problem.

Two clustering techniques are proposed for thematic information extraction (region-growing algorithm, per pixel two-stage hybrid classifier). Classification results, performance characterization and validation of the techniques are reported in Chapter 5.

Chapter 4
Validation of the classification maps and error analysis

4.1 Introduction

In chapter 3 we proposed a new classification scheme for producing a high-resolution regional scale forest map of the Amazon. A novel wavelet multi-resolution decomposition/reconstruction technique was employed to generate an edge-preserving piecewise constant SAR image and two image-labeling techniques were proposed for thematic information extraction.

Quantitative validation and error analysis of the regional area deforestation estimates are presented in this section. In this application field, Landsat TM is widely employed as a valuable data source (INPE, 1996; FAO, 1990 and 1996; TRFIC; Stone and Lefebvre, 1998). Therefore it was decided to use maps derived from Landsat TM as reference data for our assessment. The TM maps were produced by the Tropical Rain Forest Information Center (TRFIC) – a NASA's Earth Science Information Partnership program - and by the FAO's Forest Resource Assessment Programs (FAO, 1996).

In our context the purpose of forest mapping and in particular of deforestation estimation is to evaluate the anthropogenic disturbance on the forest domain. However the disturbance - transition from forest to non-forest - is sensed in different ways by different instruments (in our case Landsat TM and JERS-1 SAR), because each instrument is sensible to different scattering mechanisms. It is therefore difficult to define a unique measurable quantity that can be used to compare results derived

from the two instruments. We assume that Landsat TM maps are the validated reference data but we keep into account possible spectral and spatial differences between these two imaging systems during the comparison analyses.

The reference data are described in section 4.2, methods and tools adopted for results validation are presented in section 4.3. Results of classification accuracy analysis are presented in section 4.4. First the overall accuracy of vegetation maps (SAR and optical reference data) is reported (section 4.4.1). Second, analysis by test site of the confusion maps is presented (section 4.4.2). Conclusions are reported in section 4.5.

4.2 Available reference data

For validation of the results and error analysis, three training areas and one testing site have been selected. The three training site locations are: the Mato Grosso State, and the South Rondonia State in Brazil, the Florencia-Napo region in Colombia. The sites are identified respectively as sites 226-69, 230-69 and 8-59 according to the Landsat TM path-row codes of the related images. They include different forest and savannah ecosystems and present different land use types reflecting the major forms of anthropogenic activity within the Amazon basin (see Chapter 2). The generalization ability of the per-pixel two-stage hybrid classifier is assessed over a fourth independent site in North Rondonia State (identified as testing site 231-68).

Forest classification maps from SAR data, acquired in 1992/93 and 1995/96 over the three sites, are derived using the two proposed image-labeling techniques (see chapter 3). The region growing technique is applied to the JERS-1 1992/93 data sets available from the NASDA archive. The hybrid classifier is applied to the 1995 JERS-1 data set extracted from the GRFM South America low water mosaic. Sites

226-69, 230-69, and 8-59 are used for ELBG training; site 231-68 is used for the testing phase.

For each acquisition epoch (1992/93 and 1995), two Landsat TM thematic maps of the Mato Grosso and South Rondonia sites are taken as reference data sets. These maps were produced by the NASA Tropical Rain Forest Information Centre (TRFIC). A third independent classification of Landsat TM data for the Florencia-Napo site is used. A TRFIC Landsat TM thematic map was available over the North Rondonia site (231-68) for the testing phase of the hybrid classifier. Maximum time difference between the acquisition dates of SAR data and optical data is less than one year (Salvador and Pons, 1998).

TRFIC validated the accuracy of their classifications through a field-based accuracy assessment program. The map pixel spacing is 30 m and the geographic localization error is rated as 500 m. The classes in the TRFIC thematic product are: *Forest, Deforested, Regrowing Forest, Water, Cloud, Cloud Shadow, Cerrado*. To compare the SAR maps with the TRFIC thematic maps, we combine these seven classes as indicated in table 4.1

Table 4.1: Class correspondence between the TRFIC thematic maps and the SAR maps.

TRIFIC thematic classes	**SAR thematic classes**
5. Cloud	0. No correspondence
6. Cloud Shadow	
4. Water	1. Water
1. Forest	2. Forest
3. Re-growing Forest	3. Degraded forest
2. Deforested 7. Cerrado	4. Non-forest

A map at 30 m pixel spacing of the Florencia-Napo site (8-59) was derived from a third independent classification of Landsat TM imagery acquired in 1991 and 1996,

and using a classification scheme called hierarchical NMP (HNMP) (De Grandi, IGARSS 2001). This scheme comprises 2 stages. At the first stage – unsupervised learning – a vector quantization algorithm is used (Patane` and Russo, 2000 and 2001). At the second stage template vectors are labeled, i.e. many-to-one relationships between unsupervised template vectors and land cover classes of interest are established. Two maps produced by the FAO's Forest Resource Assessment (FAO, 1996) are used as reference for class labeling. The FAO data consist of a forest classification derived from the visual interpretation of 1990 and 1996 Landsat TM scenes adopting a minimum mapping unit of 100 hectares. To retain the same spatial location and scale in the comparison, the optical maps are co-registered with SAR maps and scaled from 30 m to 100 m . Manually selected tie points are used for registration to avoid spatial relative errors in the comparison.

A summary of the reference and SAR maps used in the validation step and in a performance comparison of the methods is presented in Table 4.2

Table 4.2: Reference maps and SAR maps used in the validation phase and for the performance comparison of the methods. In the column "Optical maps": TRFIC indicates thematic maps produced by the NASA Tropical Rain Forest Information Centre; HNMP indicates an independent classification of Landsat TM data.

Site (Landsat TM path-row)	SAR maps			Optical maps
	ISODATA	**Region growing classifier**	**two-stage hybrid classifier**	
226-69 Mato Grosso (training)	JERS-1 Ampl. 15 Nov. 92	JERS-1 Ampl. 15 Nov. 92	_	TRFIC TM 19 May 92
	_	_	GRFM Ampl. Sept.-Dec.95	TRFIC TM 31 July 96
230-69 South Rondonia (training)	JERS-1 Ampl. 5 April 93	JERS-1 Ampl. 5 April 93	_	TRFIC TM 15 May 92
	_	_	GRFM Ampl. Sept.-Dec.95	TRFIC TM 13 July 96
8-59 Florencia Napo (training)	JERS-1 Ampl. 14 Nov. 92	JERS-1 Ampl. 14 Nov. 92	_	HNMP TM 2 March 91
	_	_	GRFM Ampl. Sept.-Dec.95	HNMP TM 11 Aug. 96
231-68 North Rondonia (testing)	_	_	GRFM Ampl. Sept.-Dec.95	TRFIC TM 1996

4.3 Methods and tools

To examine the mapping accuracy, confusion matrices between SAR and Landsat TM maps are computed. Moreover we present the confusion matrix information in a form termed confusion map. In this representation we color code those image pixels that represent commission and omission errors in the matrix (see (Congalton and Green, 1999) for a definition of commission and omission errors).

In accordance with the mathematical representation of the error matrix given in table 4.3, the overall accuracy is defined as:

$$A = \frac{\sum_{i=1}^{k} n_{ii}}{n} \tag{4.1}$$

Where n_{ii} denote the number of samples classified in the same category *i* in the two classifications and n is the total number of samples. The overall accuracy is a measurement of the degree of discrepancy between SAR and reference maps.

In the agreements and disagreements budget, the following causes must be taken into account together with the classification errors (Arbia and Haiming, 1993):

1) Real changes of the vegetation between the SAR and the TM acquisition dates. Those changes could have a natural (phenology) or an anthropic cause.
2) Differences of the imaging systems and wave scattering mechanisms.
3) Co-registration problems.

It is difficult to establish a unique parameter that could define how the forest/non-forest transition is measured by optical and SAR instruments; therefore we expect high discrepancies between maps derived by the two instruments for the *degraded forest* class and in the boundary regions between *cerrado* (natural savanna) and the humid forest ecosystem.

The confusion map shows spatially where these discrepancies occur, facilitating the analysis of the problem.

The confusion matrix layout and codes are reported in table 4.3. The confusion matrix columns represent the reference data, while the rows indicate the remote sensing classification. For example the matrix element 23 is an area classified as non-forest in the reference map and forest by the maps to be assessed. The pixel percentage content in matrix element 23 is given by n_{35} in the confusion matrix.

Matrix elements 0 to 4 – *Unclassified, Water, Forest, Degraded Forest, and Non-forest* - are the ones that feature comparable accuracy in the two classifications. Matrix elements from 5 to 24 are the discrepancies between the two maps.

Table 4.3: The confusion matrix layout and codes for confusion maps.

	unclassified		**water**		**forest**		**deg-forest**		**non-forest**		
unclassified	0	n_{11}	9	n_{12}	13	n_{13}	17	n_{14}	21	n_{15}	n_{1+}
water	5	n_{21}	1	n_{22}	14	n_{23}	18	n_{24}	22	n_{25}	n_{2+}
forest	6	n_{31}	10	n_{32}	2	n_{33}	19	n_{34}	23	n_{35}	n_{3+}
deg-forest	7	n_{41}	11	n_{42}	14	n_{43}	3	n_{44}	24	n_{45}	n_{4+}
non-forest	8	n_{51}	12	n_{52}	16	n_{53}	20	n_{54}	5	n_{55}	n_{5+}
		n_{+1}		n_{+2}		n_{+3}		n_{+4}		n_{+5}	
	C	**M**	**C**	**M**	**C**	**M**	**C**	**M**	**C**	**M**	

C = class identifiers used in the confusion maps
M= confusion matrix values

The relationship between discrepancies in the remote sensing maps and the deforestation pattern was investigated. Visual inspection of the satellite images collected for the study over three different sites reveals the different ways human intervention can carve deforestation patterns into the forest landscape. A variety of measurements can be performed to numerically describe these different spatial patterns. In our analysis we used the average perimeter-over-area-ratio "PA" (Johnston, 1998), defined by (4.2).

$$PA = \frac{1}{m}\sum_{k=1}^{m}\frac{P_k}{A_k} \tag{4.2}$$

Where m=total number of patches, $P_k\left(k = 1....m\right)$ = perimeter of single patches, $A_k\left(k = 1....m\right)$ = area of the single patches.

In a labeled image, segments are defined as connected image areas featuring the same label type. Intuitively, a labeled segment (e.g., class *forest*) is: i) compact where it features low PA values; and ii) fragmented (patchy) where PA values tend to increase (see figure 4.1).

Figure 4.1: Examples of compactness characterization using the Perimeter-over-Area (PA) measure.

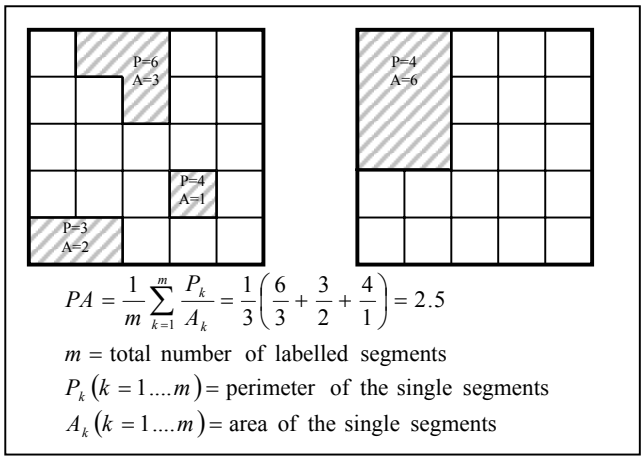

4.4 Results

4.4.1 Overall accuracy

For the three sites (226-69, 230-69, 8-59) we calculate the overall accuracy between optical reference data and radar maps. The radar maps are derived using two classifiers (region growing and hybrid classifier). The degree of agreement between optical and radar data is higher using the former.

In Table 4.4 the overall accuracy is reported when only the class sub-set *forest – non forest* is considered.

The 1992 and 1996 TRFIC maps and the radar maps for the Mato Grosso site are shown figure 4.1 for visual comparison.

Table 4.4: Overall accuracy for class set forest/non-forest. Results obtained using 1992 and 1995 data sets.

Site (Landsat path-row)	**SAR region growing - Reference maps** (1992 data set)	**SAR hybrid classifier - Reference maps** (1995 data set)
226-69	91%	92%
230-69	73%	84%
8-59	57%	82%

Overall training accuracies of the hybrid classifier over Mato-Grosso (226-69), South Rondonia (230-69) and Florencia-Napo (8-59) sites are compared with the overall testing accuracy for the North Rondonia (231-68) site in table 4.5. Note that in this table, elements (row, column) 2, 3 and 2, 4 are empty because class cerrado is not detected either in the Florencia-Napo training site or in the North Rondonia test site.

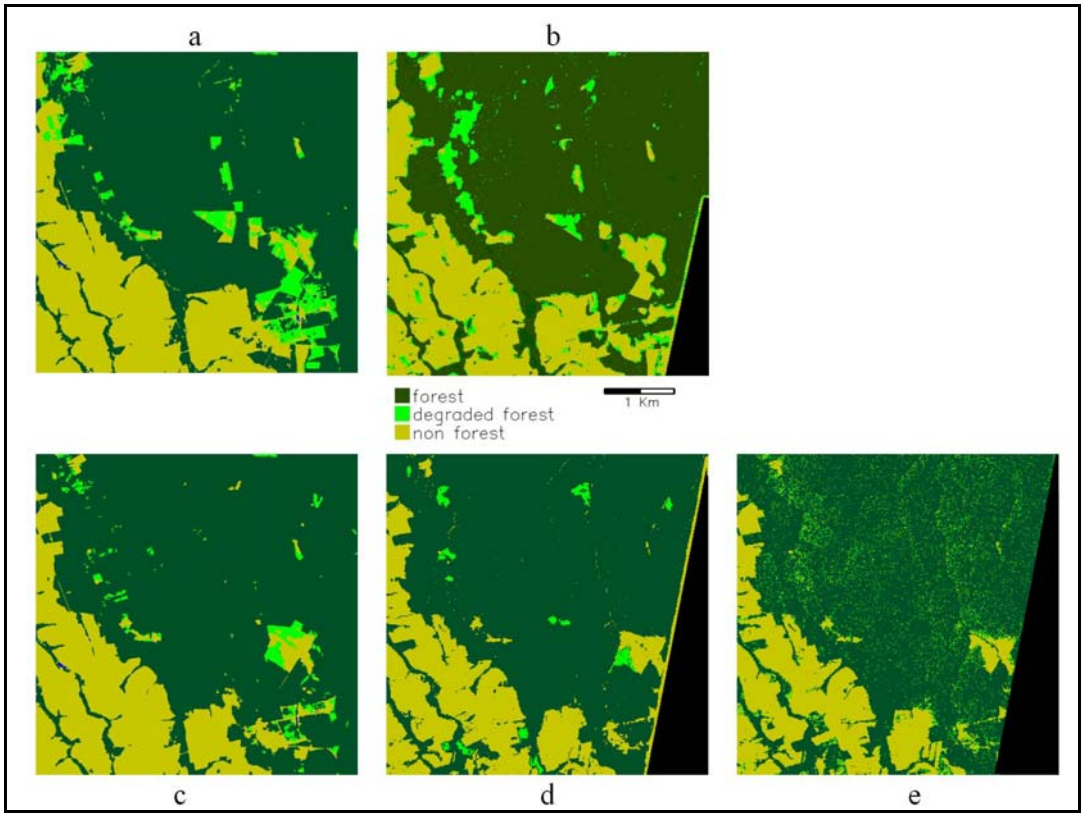

Figure 4.1: 1996 and 1992 TRFIC maps for the Mato Grosso site (a, c.). Hybrid classifier map (1995 data set) (b). ISODATA and region growing (1992/93 data set) (d, e) (see color Figure B.10 - Appendix B, pp. 208).

Table 4.5 shows that, when class set A (water, forest, degraded-forest, non-forest) is involved, the testing accuracy (77%) is: i) better than that obtained in related works (Sgrenzaroli, 2001) and ii) in line with training accuracies. The major source of misclassification is identified in the *degraded forest* class. If this class is removed, the average testing accuracy increases to 87%.

These experimental results are consistent with theoretical expectations: low backscattering values of the *degraded forest* class (due to partially logging or forest regrowth) are comparable to those of the *cerrado* class and/or *open canopy forest*

class. This effect is documented by row B of table 4.5, where accuracy results are reported for the case when the *cerrado* class is omitted from classification. On the other hand high backscattering values of class *degraded forest* (due to recently cut trunks still lying on the ground and causing double-bounce effects) may overlap those of class *flooded forest*.

SAR maps derived by the hybrid classifier and the reference map over the three training sites (226-69, 230-69, and 8-59) are shown for visual comparison in figure 4.2.

The capability of the hybrid classifier to generalize over the entire data set is documented in figure 4.3. Here the SAR map over the testing site (231-68), the SAR map over the South Rondonia site (230-69), the corresponding TRFIC map over the same testing site are shown.

Table 4.5: Overall training accuracy of the hybrid classifier over Mato-Grosso (226-69), South Rondonia (230-69) and Florencia-Napo (8-59) compared with the overall testing accuracy for the North Rondonia (231-68) test site (results obtained with 1995 data set).

	Training (1995 data set)				**Testing** (1995 data set)
	230-69	226-69	8-59		231-68
A	83%	72%	58%		77%
B	86%	75%			
C	92%	84%	82%		87%
A: water, forest, deg. forest, non-forest B: water, forest, deg. forest, non-forest excluding cerrado C: forest, non-forest					230-69 Mato Grosso 226-69 South Rondonia 8-59 Florencia-Napo 231-68 North Rondonia

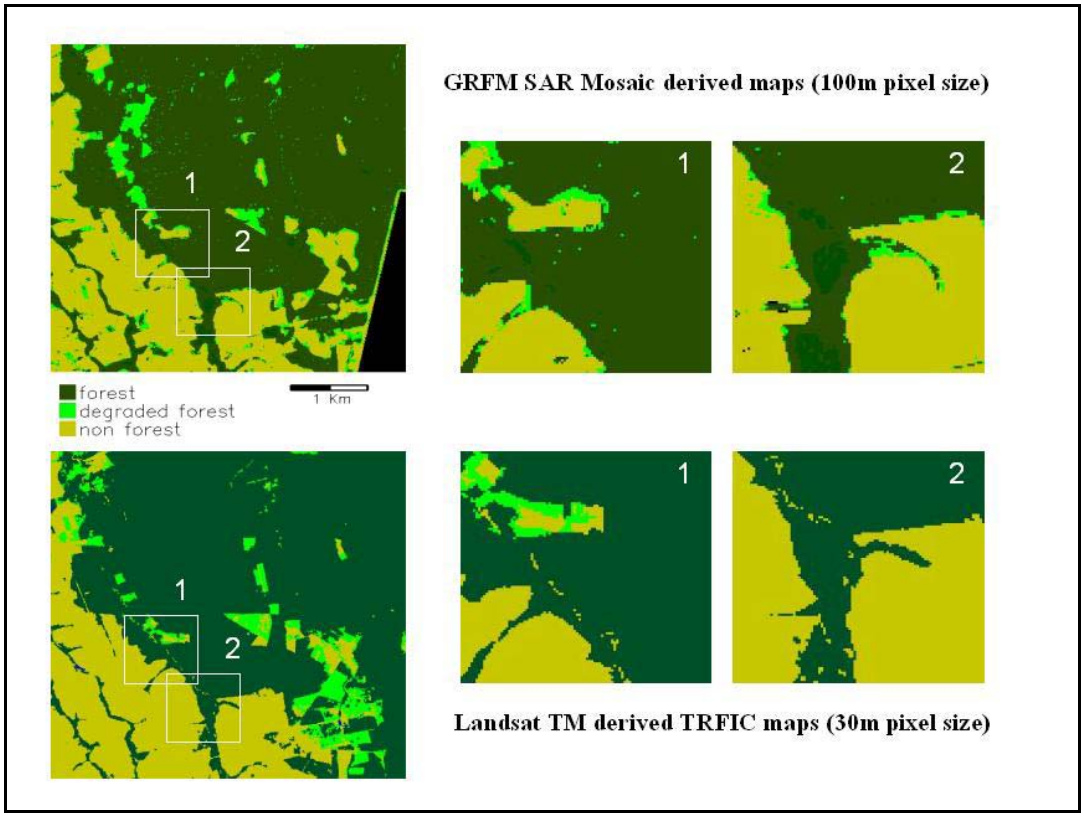

Figure 4.2 a: Comparison between the SAR map using the hybrid classifier and the TRFIC reference map of the Mato Grosso training site (226-69) This site is characterized by ranching and selective logging (see color Figure B.11 - Appendix B, pp. 209).

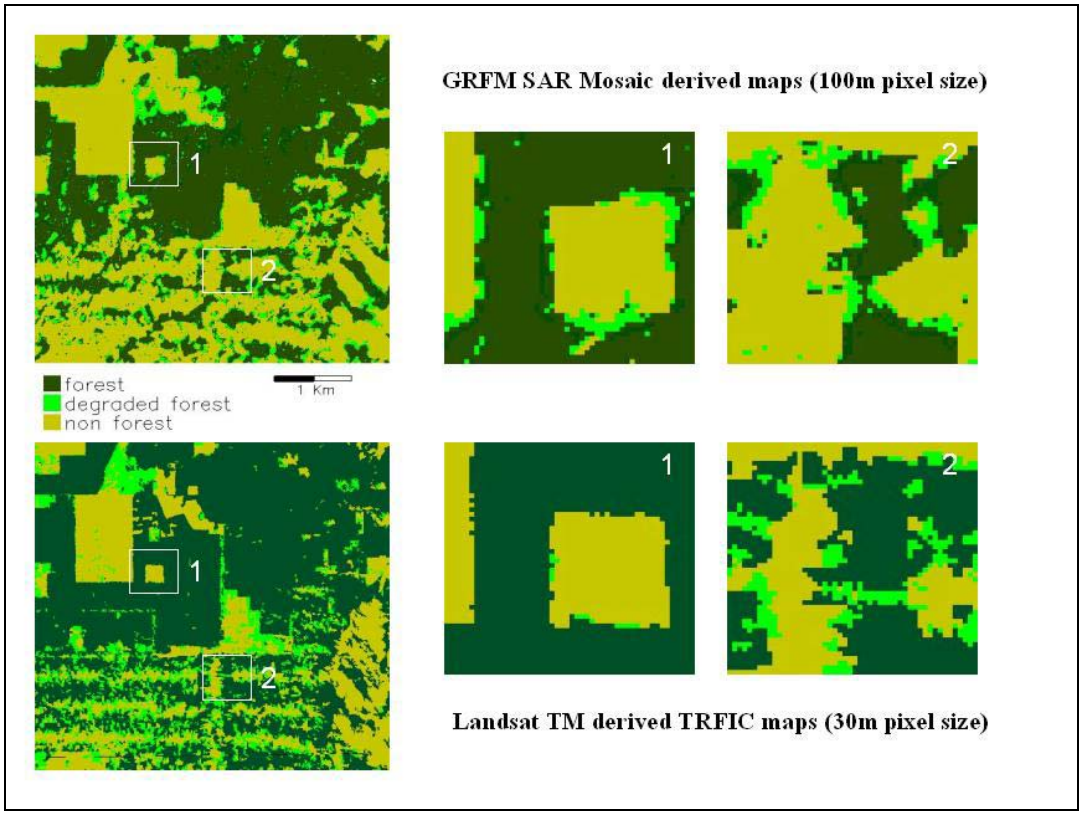

Figure 4.2 b: Comparison between the SAR maps derived using the two-stage hybrid classifier and the TRFIC reference map of the South Rondonia training site (230-69). This site is characterized by linear ("herring bone") and massive deforestation (see color Figure B.12 - Appendix B, pp. 210).

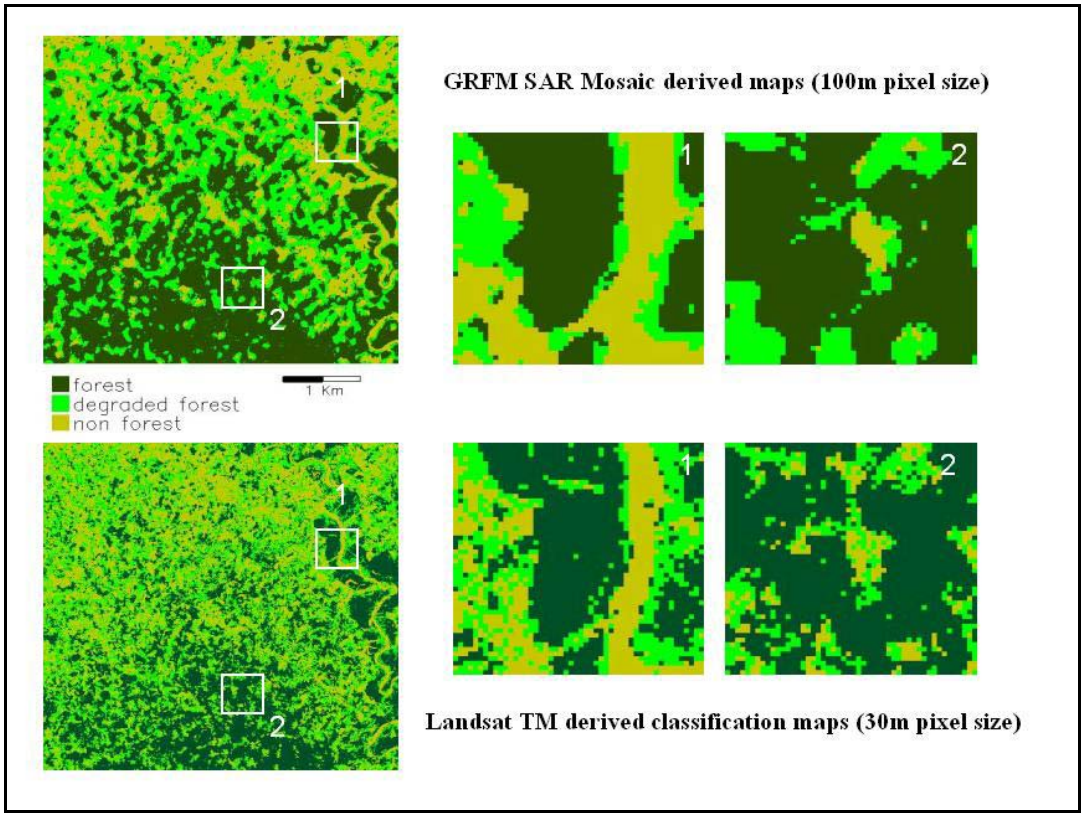

Figure 4.2 c: Comparison between the SAR maps derived using the two-stage hybrid classifier and the Landsat TM classification of the Florencia-Napo training site (8-59). This site is characterized by linear and widespread deforestation (see color Figure B.13 - Appendix B, pp. 211).

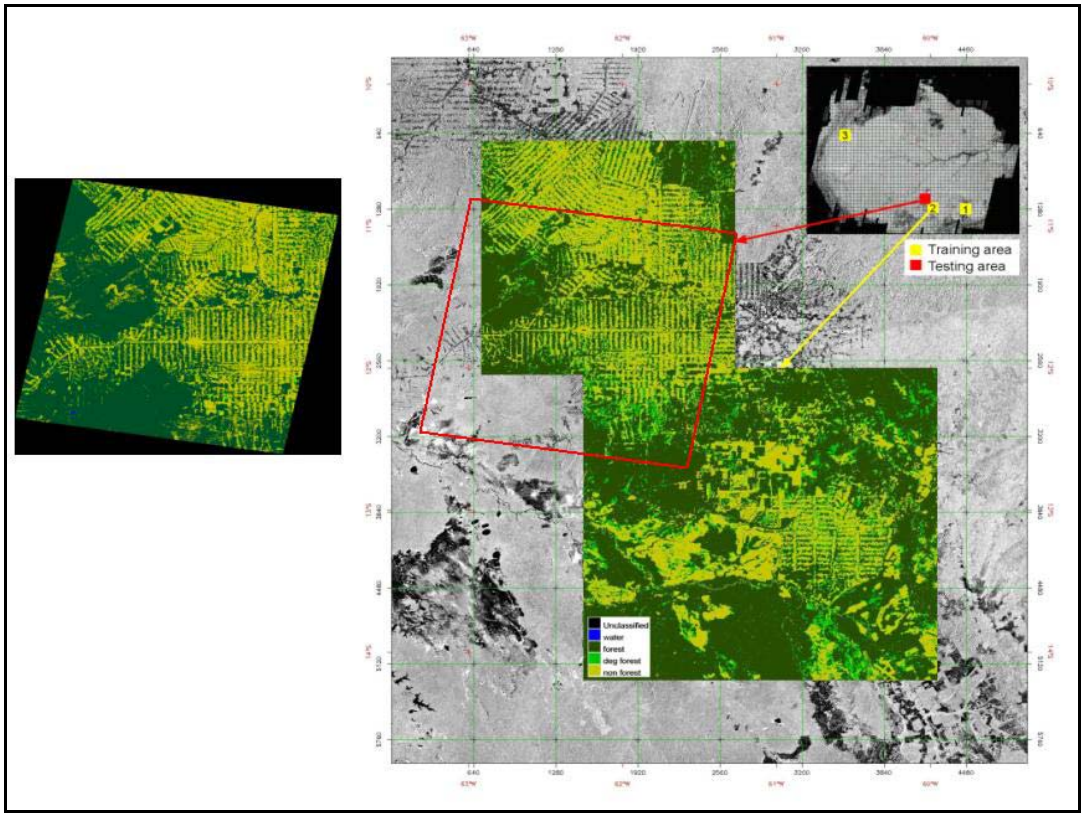

Figure 4.3: The SAR map of the testing site (231-68) and the SAR map of the South Rondonia site (230-69). The two maps are overlaid to a sub-set of GRFM SA mosaic in the inset on the left. The SAR map of the testing site (231-68) is compared with the corresponding TRFIC map of the same testing site (the location on the GRFM data set is framed by a red box). Training sites (1. Mato Grosso, 2. South Rondonia, 3. Florencia-Napo) and testing site (North Rondonia) are highlighted in the inset showing the entire GRFM SA mosaic (see color Figure B.14 - Appendix B, pp. 212).

To investigate whether our test results hold true for the entire mosaic, the hybrid classifier is applied to the entire South America data set down-sampled at 1200 m pixel spacing. In this case, ELBG is run with 32 prototype vectors using the down-sampled GRFM South America data set, while the wavelet-based data pre-processing is not used. The classification at 1.2 km resolution is qualitatively consistent with the forest map produced by the Tropical Forest Ecosystem Environments monitoring by Satellites (TREES) project (Malingreau *et al.,* 95; Eva *et al.,* 95). This product was derived from 300 ERS ATSR-2 optical images acquired between 1998 and 2000. The TREES map and the map derived from the GRFM mosaic are shown in Figure 4.4. The thematic classes in the TREES map are: *Water, evergreen forest, dry forest, mangrove, open/fragmented forest, plantation, non-forest, and semi-evergreen forest/shrubs ('Chaco').* To facilitate the visual comparison we have combined and color-coded *evergreen forest, dry forest*, and *mangrove* as class *forest*, *open/fragmented forest* as class *degraded forest*. Classes *plantation, non-forest, and semi-evergreen forest/shrubs* ('Chaco') as class *non-forest*.

Yet another important issue that we have investigated (using the 100 m products) is the dependency of the classification discrepancies on different deforestation patterns. The discrepancy increases with the degree of deforestation pattern complexity as measured by PA. Possible explanations are:

1) Differences in spatial sampling between the SAR data (100 m) and the Landsat TM data (30 m).
2) Increase of co-registration errors with the landscape complexity.
3) Higher dynamics of change in highly fragmented zones (mainly due to changes in the natural target between two acquisition dates)

Table 4.6 confirms that the discrepancy between SAR and reference maps increases with the PA values. The PA is computed for class *forest* in the reference map.

Table 4.6: Overall accuracy of the SAR maps as a function of different landscape patterns as measured by PA for class forest. Reference maps are both the TRFIC maps (226-69, 230-69) and the independent classification of Landsat TM raw data (8-59). (Results obtained using the 1992/93 data set).

Site (Landsat path-row)	**SAR map Accuracy**	**PA**
226-69	91%	0.057
230-69	73%	0.144
8-59	57%	1.037

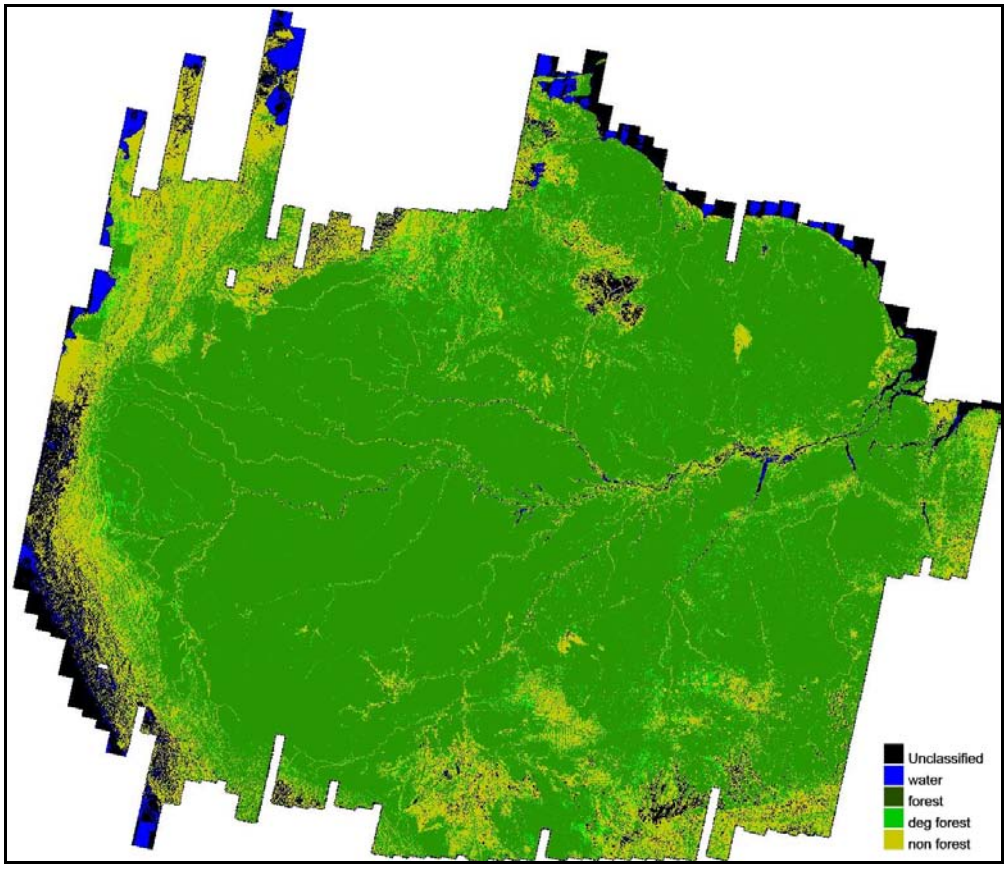

Figure 4.4a: Forest map (1.2 km pixel spacing) derived from the whole GRFM SAR South America mosaic (see color Figure B.15 - Appendix B, pp. 213).

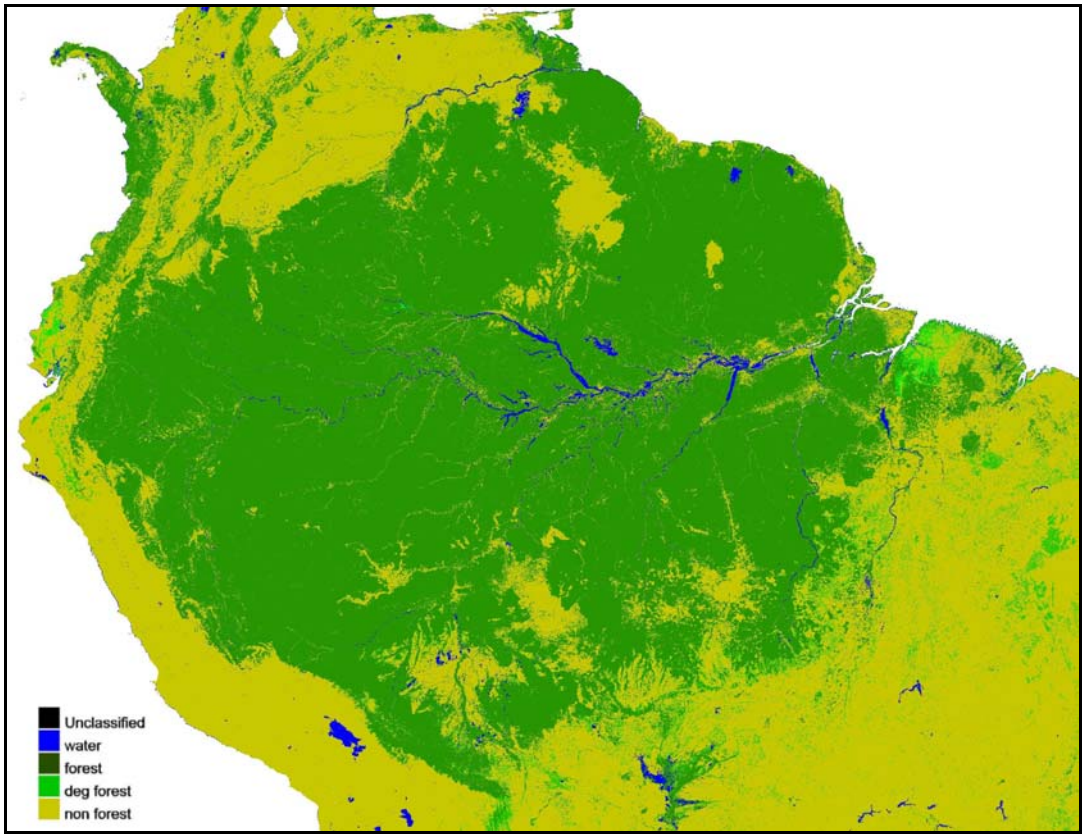

Figure 4.4b: The TREES project South America forest map. This product was derived from 300 ERS ATSR-2 optical images acquired between 1998 and 2000 (see color Figure B.16 - Appendix B, pp. 214).

4.4.2 Analysis by site

In this section confusion matrices are presented in a form termed confusion map to show where errors occur in space. The confusion maps between reference maps (TRFIC maps and independent classification of Landsat TM data) and SAR maps (region growing) are analyzed by site. This analysis refers to data acquired in 1992/93, regarding SAR maps, is conducted using the region growing classifications and helps to detail and localize the discrepancies and similarities between the two thematic products.

Confusion maps and the related confusion matrices are presented for three sites: Mato Grosso, South Rondonia and Florencia-Napo. Results are presented in decreasing order of overall accuracy and starting from the matrix element characterized by a higher percentage of coverage. In the confusion matrix the columns refer to the reference map and the rows to the SAR map. In addition we report the commission and omission errors for classes' *forest, degraded forest* and *non-forest*. The *unclassified* class for the SAR classification refers to the criteria expounded in chapter 3 section 3.5. If, during the growing process the lower bound of the interval estimate of the local variance is greater than the theoretical variance of a homogeneous area then the seed point is discarded and flagged as a non-classified point. For the TRIFIC map the unclassified class corresponds to the *Cloud, Cloud Shadow* classes, where there no correspondence with SAR map, according to table 4.1.

Mato Grosso (226-69) site

Table 4.7: The confusion matrix for the site Mato Grosso 226-69. The TRFIC map and the SAR map obtained by the region growing classification are considered.

	unclassified		water 1		forest 2		deg forest 3		non-forest 4		Total
unclassified	*0*	**0.000**	*9*	**0.000**	*13*	**0.274**	*17*	**0.003**	*21*	**0.011**	0.288
water 1	*5*	**0.000**	*1*	**0.000**	*14*	**0.000**	*18*	**0.000**	*22*	**0.000**	0.000
forest 2	*6*	**0.000**	*10*	**0.014**	*2*	**68.524**	*19*	**1.503**	*23*	**4.824**	74.865
deg forest 3	*7*	**0.000**	*11*	**0.000**	*15*	**0.922**	*3*	**0.284**	*24*	**0.104**	1.310
non forest 4	*8*	**0.000**	*12*	**0.026**	*16*	**0.859**	*20*	**0.316**	*4*	**22.334**	23.535
Total		0.000		0.041		70.580		2.107		27.273	100.00

Class	Commission (%)	Omission (%)	Accuracy (%)
forest 2	8.985	2.912	97.088
deg forest 3	48.708	86.505	13.495
non forest 4	4.406	18.109	81.891

The confusion map for the Mato Grosso site is reported in figure 4.5 on the left. The related confusion matrix is reported in Table 4.7. The matrix element 23 exhibits the highest confusion. The matrix element 23 – SAR classification: 4.824%-

corresponds spatially to an area of shrub-land coverage, at the boundary between the cerrado (savanna) and the humid forest ecosystems. This suggests that the transition from closed forest to agricultural land, predominantly ranching, is discriminated differently by the SAR and by the optical sensor. In those areas vegetation coverage is often determined by a fluctuating water table that is very high between the rainy and the dry seasons (Furley *et al.,* 1992).

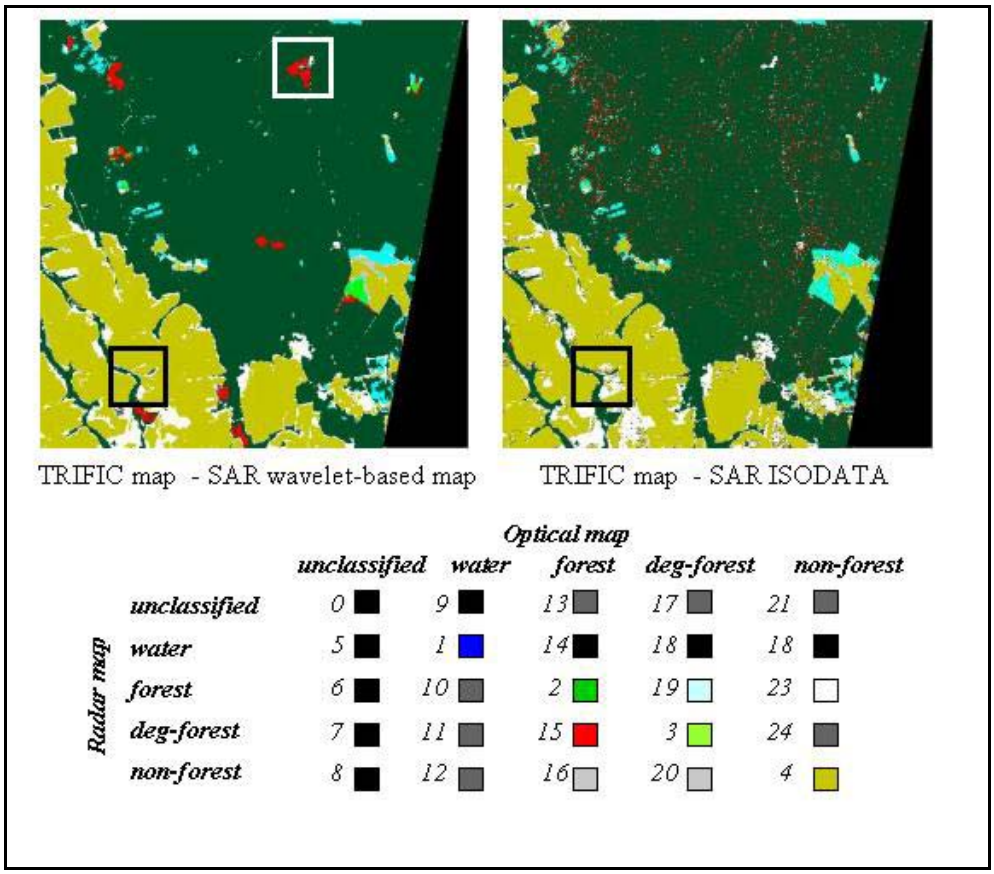

Figure 4.5: Two confusion maps of Mato Grosso site (226-69) between reference maps and SAR maps: Region growing on the left, ISODATA classifications on the right (see chapter 5). The area enlarged in figure 4.6 is framed by a white box. The area enlarged in figure 4.7 is framed by a black box (see color Figure B.17 - Appendix B, pp. 215).

The SAR sensor is particularly sensitive to soil conditions and therefore the main source of discrepancy in this case is due to natural changes that occur between the Landsat TM and SAR acquisition dates. It must be noted that the region growing classification technique is able to distinguish at least partially these areas classifying them as *degraded forest*.

The degraded areas - detected by the optical sensor and not by SAR - are grouped in small patches. The scale of the disturbed area and the canopy coverage are most likely different at the two dates when the SAR and the optical data were acquired. This fact could explain the low accuracy reported in matrix element 19 (SAR classification accuracy: 1.503%).

The same analysis applies to matrix element 15: (SAR classification accuracy: 0.922%). Here however the class *forest* is detected in the optical maps and class *degraded forest* in the SAR maps. The confusion matrix element 15 is present in 8 spots in the forest domain of the related confusion map when using the region growing classifier. Visual inspection of the full resolution Landsat TM scene reveals a canopy coverage discontinuity in those spots. The regular spatial arrangements of these spots suggest anthropogenic disturbances. We can infer that the discrepancies described by the confusion matrix element 15, are due to a misclassification of the optical data (see the zoomed-in area in figure 4.6).

The radar backscatter statistics of those areas with regular spatial patterns are compared with samples corresponding to *forest* and *non-forest* classes. The mean backscatter of the textured areas with regular spatial patterns is near the value of the nominal backscatter for the *forest* class.

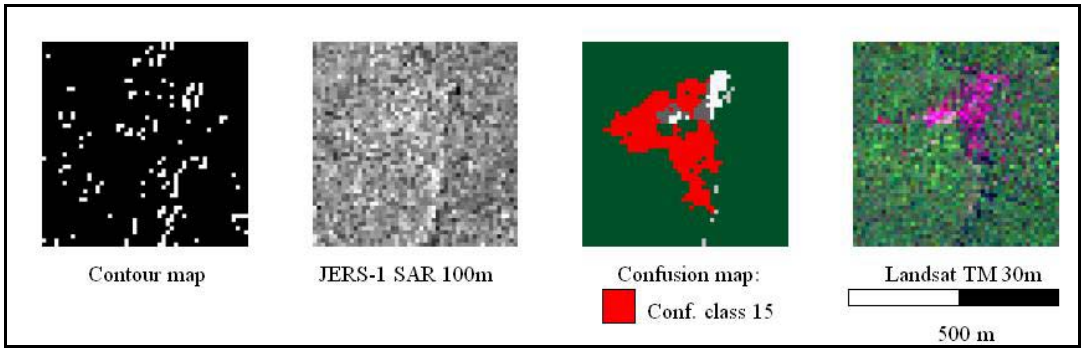

Figure 4.6: The zoomed-in area in the TM image shows spatial arrangements that are suggestive of anthropogenic disturbances. However these patterns are not included in the TRFIC map. In the region growing map he same area is classified as degraded forest while in the TRFIC map it is classified as forest. In this case the discrepancy, relative to confusion matrix elements 15, is due to a misclassification of the optical data (see color Figure B.18 - Appendix B, pp. 216).

Despite the radiometric proximity, the region growing technique is able to detect those transition areas. This is due to the fact that in the region growing process the presence of edges and small radiometric variations around the considered seed position is taken into account.

A synoptic description of data flow in the generation of the thematic maps when using the region growing classifier and ISODATA is given in figure 4.7. The images in the inset at top right (SAR classification) and the inset at bottom right (TRIFIC map) are suggestive of the relative agreement for the class *forest* between the two maps when the region growing classifier is used.

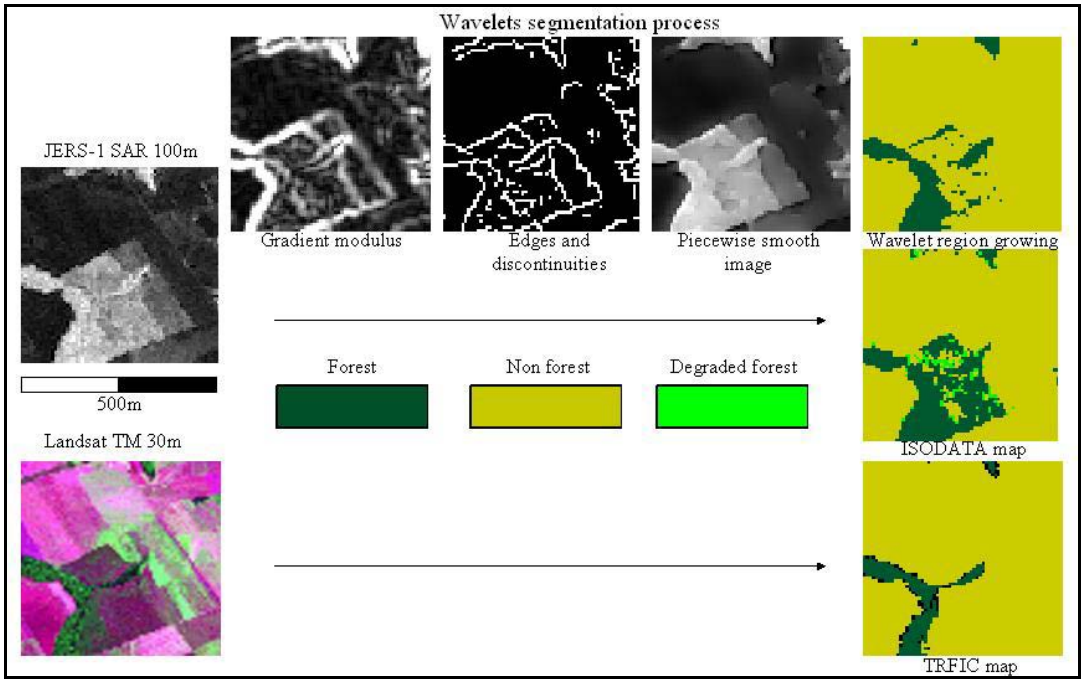

Figure 4.7: Synoptic description of data flow in the generation of the thematic maps and for the different classification methods.

Pictures at the right of the figure show the relative agreement for the class forest between the SAR map derived by wavelet–based region growing – first inset top right - and the reference TRFIC –last inset bottom right.

In the center right inset the SAR map derived by ISODATA technique is shown (see section 4.6) (see color Figure B.19 - Appendix B, pp. 217).

Rondonia (230-69) site

Table 4.8: The confusion matrix for site 230-69: TRFIC map, SAR wavelet-based region growing classification.

	unclassified		water 1		forest 2		deg forest 3		non-forest 4		Total
unclassified	*0*	**0.000**	*9*	**0.000**	*13*	**0.000**	*17*	**0.000**	*21*	**0.000**	0.000
water 1	*5*	**0.000**	*1*	**0.000**	*14*	**0.000**	*18*	**0.000**	*22*	**0.000**	0.000
forest 2	*6*	**0.030**	*10*	**0.000**	*2*	**55.033**	*19*	**5.884**	*23*	**5.227**	66.174
deg forest 3	*7*	**0.006**	*11*	**0.000**	*15*	**4.110**	*3*	**1.319**	*24*	**1.828**	7.263
non forest 4	*8*	**0.040**	*12*	**0.000**	*16*	**5.001**	*20*	**4.521**	*4*	**17.000**	26.562
Total		0.077		0.000		64.144		11.724		24.054	100.00

Class	Commission (%)	Omission (%)	Accuracy (%)
forest 2	17.369	14.205	85.795
deg forest 3	50.703	88.750	11.250
non forest 4	39.756	29.329	70.671

The Rondonia site is partially characterized by the transition between cerrado and forest vegetation. At the margin between forest and cerrado the difference between acquisition dates plays a predominant role in explaining the matrix element 23 with highest confusion– SAR classification: 5.227%.

Spatially this element is localized in the transition zone. Soil moisture conditions are relevant in this type of interface area where the low canopy density allows the SAR signal to penetrate. In any case this analysis shows that the wavelet-based method can differentiate the interface areas because of the higher sensitivity to local signal variations.

Matrix element 19 - SAR classification: 5.884%- is mostly localized in two zones: areas characterized by herringbone deforestation patterns, and areas affected by micro-topographic effects. In the first case the rapid changes of strongly degraded areas and the scale of the changes are causes of discrepancies. It is therefore difficult to differentiate classification errors from real land cover changes that have occurred between the optical and SAR acquisition dates. The errors increase in areas with

micro-topography: in this case a visual interpretation is required to highlight variation due to topography from deforestation patterns.

For matrix element 16 it is difficult to distinguish recent clear-cuts detected by SAR from misclassification errors – SAR classification 5.001%. Areas with regular spatial arrangement, observed in a Landsat TM scene acquired later than the TRFIC map, confirm the presence of clear-cuts. Changes, ascribed to new clear-cuts using Landsat TM acquired on May 15, 92 and the Landsat TM scene acquired on August 3, 92, are around 0.6%.

Matrix element 15 is mostly localized in areas with regular spatial arrangement in the wavelet segmentation map (35% of matrix element 15). Classified as forest in the May 12, 1992 TM scene, after three months these areas present new clear-cuts that are visible in a TM image acquired on August 3, 1992. The region growing classification seems to be able to detect degradation due to new clear cuts (i.e. selective logging).

Colombia (8-59) site

Table 4.9: The confusion matrix for site 8-59: TRFIC map, SAR wavelet-based region growing classification.

	unclassified	water 1	forest 2	deg forest 3	non-forest 4	Total
unclassified	***0*** **0.000**	***9*** **0.000**	***13*** **0.000**	***17*** **0.000**	***21*** **0.000**	0.000
water 1	***5*** **0.000**	***1*** **0.636**	***14*** **0.544**	***18*** **0.610**	***22*** **3.260**	5.050
forest 2	***6*** **0.000**	***10*** **0.228**	***2*** **43.890**	***19*** **11.689**	***23*** **15.458**	71.265
deg forest 3	***7*** **0.000**	***11*** **0.000**	***15*** **0.000**	***3*** **0.000**	***24*** **0.000**	0.000
non forest 4	***8*** **0.000**	***12*** **0.180**	***16*** **5.525**	***20*** **4.745**	***4*** **13.234**	23.684
Total	0.000	1.044	49.960	17.044	31.952	100.00

Class	Commission (%)	Omission (%)	Accuracy (%)
forest 2	9.678	8.041	8.041
deg forest 3	54.794	12.149	12.149
non forest 4	32.705	58.582	58.582

In this area the available FAO visual interpretation of the Landsat TM scene has a coarse minimum mapping unit (100 ha). Consequently comparison with the SAR

results was performed using the map generated by an independent classification of the 1991 Landsat TM scene (see section 4.2). The FAO visual interpretation was used only as a guideline for class identification and combination. The lack of a high-resolution visual interpretation must be taken into account in the evaluation of the discrepancies between SAR and optical data

The region growing classification does not detect the *degraded forest* class. Many factors conspire to create difficulties in distinguishing *degraded fores*t from *forest* class: the nature of the terrain, the micro-topography associated with small-scale drainage networks and small dimension of each deforested patch. The intermediate state of degradation, between forest and clear-cuts, is consequently confused with natural features. For these reasons we have decided to label the classes only as *forest* or *non-forest*. As a consequence there are many off diagonal cell zero values in the confusion matrix (tables 4.9). The matrix element 23 with the higher confusion incorporates all these sources of errors - SAR classification: 15.458%.

Besides this widespread pattern, deforestation is also characterized by rapid changes from clear-cut to abandoned and partially re-grown patches. Therefore real changes between optical and SAR scenes are an important source of the high discrepancies and are difficult to quantify. Changes from clear-cut to partially re-grown forest can explain the matrix element 19 - SAR classification: 11.689% - where a high percentage of pixels is labeled as degraded in the 1991 Landsat TM and as forest in the 1992 SAR maps.

The rapid changes from forest to non-forest are revealed by the comparison with a Landsat TM scene acquired 2 years before - from 26.142% of non-forest area in 1989 to 31.952% in 1991. This rapid decrease of forest area is a possible explanation for the matrix elements 16 - SAR classification: 5.525%.

Finally the poor agreement between optical and SAR maps can be due to coregistration errors that become relevant when the frequency of spatial variations within each class is high.

4.5 Summary and conclusions

Quantitative validation of the classification maps and error analysis of the deforestation estimates are addressed in this chapter.

Maps derived from Landsat Thematic Mapper (TM) are used as reference data to evaluate the maps derived from JERS-1 data. This comparison allows us to highlight spectral and spatial differences between these two imaging systems, which are sensible to different wave scattering mechanisms. Confusion matrices between maps derived from SAR and Landsat TM are used to examine the mapping accuracy. Confusion matrix information is presented in a form termed confusion map to show where errors occur in space.

Specific analyses by site allow us to draw the following conclusions:

1. Major source of misclassification is attributed to the *degraded-forest* class.
2. Discrepancies with respect to reference data increase with the degree of deforestation pattern complexity.

A first result of the validation process is that the wavelet-based classifier provides a classification accuracy of 87% in forest/non-forest mapping. The high performance of the wavelet-based algorithms can be ascribed to several factors**.** The zooming capability of the wavelet transform makes it possible to generate by inversion a synthetic image with a better signal to noise ratio in areas corresponding to the thematic classes of interest. The adaptive wavelet coefficient thresholding is the core component of the algorithm; it enables the distinction of the local maxima, related to the transitions between classes of interest we want to separate, from

"textural" edges. The thresholding is applied at that scale where the wavelet coefficients carry predominantly information on strong persistent edges and the noise influence has decayed significantly. This adaptive system improves for example the detection of fragmented areas with anthropogenic disturbances.

The performance of a region-growing algorithm and a per-pixel two-stage hybrid classifier was compared. Both approaches rely on the wavelet pre-processing. The hybrid classifier is computationally more efficient. The degree of agreement between optical and radar data is higher using the hybrid classifier technique than the region growing technique.

Therefore the hybrid classifier was selected for mapping the entire GRFM South America dataset. The capability of this classifier to generalize over the entire data set was demonstrated.

A further confirmation that our test results hold true when the entire mosaic is considered comes from the comparison of the map extracted from the entire GRFM South America SAR data set classification and the TREES map that was derived from 300 ERS ATSR-2 optical-images.

In the analysis by site, a cartographic representation of the confusion matrix was used that results is a powerful technique for quantifying and locating spatially points of agreement and disagreement between SAR and Landsat TM maps.

Comparison of the results derived from the SAR imagery with reference optical data reveal a number of factors that influence this quantitative assessment.

1. A high percentage of discrepancies between the two sources of information (SAR, optical) are due to real changes, which occurred between the two acquisition dates. This suggests that the rapid dynamic of the selected "hot spot" areas must be taken into due account.
2. SAR and optical observations are driven by different scattering mechanisms that arise in the landscape evolution during the deforestation process. This fact is

particularly evident at the interface area between forest and clear-cuts, where it is more difficult to establish a unique descriptor of the intermediate deforestation steps (degraded forest, partial re-growth). The canopy density and soil conditions (roughness, moisture) play important roles in the radar backscatter from those interface areas.

3. A spatial pattern measurement (perimeter over area) indicates a dependency between the deforestation pattern complexity and the degree of agreement between SAR and TM derived maps. The decrease of agreement with the increase of landscape complexity can be mainly attributed to under-sampling of the spatial fragmentation in degraded forest areas at 100 m resolution.

The discrepancy between optical and radar derived maps for the *degraded forest* class requires a deeper analysis in order to asses whether these discrepancies can be ascribed to errors in the radar derived maps or to omissions in the maps derived by optical instruments.

Chapter 5

Relative performances of a wavelet-based segmentation technique and ISODATA clustering

5.1 Methods and tools for comparison of estimates

Kappa statistic (Congalton and Green, 1999) is adopted to measure the significance of the difference in accuracy between the wavelet-based region growing classifications and those derived by a conventional ISODATA clustering technique. An error matrix is created by sampling 300 points per category of interest – forest, degraded forest, non-forest. Stratified random samples extracted from the 1992/93 data sets are used.

Let $\hat{K}_{Seg}$ and $\hat{K}_{Iso}$ denote the estimate of Kappa for the error matrix [SAR wavelet-based region growing -TM map] and [SAR ISODATA -TM map] respectively. Let also $\hat{var}(\hat{K}_{Seg})$ and $\hat{var}(\hat{K}_{Iso})$ be the corresponding estimates of the variance computed using the Delta method (Congalton and Green, 1999). For testing the significance of a single error matrix we use (5.1), while (5.2) is used to test if the two independent error matrices are statistically significantly different.

$$Z_{Seg} = \frac{\hat{K}_{Seg}}{\sqrt{\hat{var}(\hat{K}_{Seg})}} \tag{5.1}$$

$$Z_{Seg-Iso} = \frac{\left|\hat{K}_{Seg} - \hat{K}_{Iso}\right|}{\sqrt{\hat{var}(\hat{K}_{Seg}) + \hat{var}(\hat{K}_{Iso})}} \tag{5.2}$$

where Z is standardized and normally distributed (Congalton and Green, 1999).

5.2 Results

In the inter-comparison, both ISODATA clustering and the wavelet segmentation are applied to 1992/93 SAR data sets.

For a visual comparison between classifications derived by the two techniques for the Mato Grosso site see figure 4.1 in chapter 4.

Overall accuracy of the vegetation maps derived from SAR is calculated with respect to maps derived from optical data for class set forest – non-forest. Table 5.1 shows that maps generated by the wavelet segmentation have higher accuracy than the ones derived by ISODATA for each site.

Table 5.1: Overall accuracy of the vegetation map from SAR using ISODATA and wavelet-based region growing techniques with respect to optical reference data for class set forest – non-forest (results obtained using 1992 data sets).

Site **(Landsat path-row)**	**ISODATA (SAR) - Reference Map (optical data)** (1992 data set)	**wavelet-based region growing (SAR) - Reference Map (optical data)** (1992 data set)
226-69	86%	91%
230-69	66%	73%
8-59	55%	57%

The relative performance of the two classification techniques is assessed through the Kappa analysis. Table 5.2 presents, for the three sites (226-69, 230-69, and 8-59), the results of the analysis of the error matrices related to the wavelet segmentation and ISODATA clustering. The ranges of Kappa are ranked as strong

agreement $\left(\hat{K} > 0.8\right)$, moderate agreement $\left(0.4 < \hat{K} < 0.8\right)$, and poor agreement $\left(\hat{K} < 0.4\right)$ (Landis *et al.,* 1977). Wavelet segmentation maps reach moderate agreement for both Mato Grosso (226-69) and Rondonia (230-69) sites. Only the ISODATA map of the Mato Grosso site exceeds the poor agreement threshold.

Table 5.2 also presents the variance of Kappa and Z statistic. The Z critical value for determining if a classification is significantly better than random results is 1.96 at 95% confidence level. The Z statistic values are greater then 1.96 for all the classifications.

Results in table 5.3 indicate whether the two classification techniques are significantly different. The test $Z_{\text{Wave-ISO}}$ shows that the wavelet-based region growing technique is significantly more accurate than the ISODATA technique. We have earlier assessed that the overall training accuracies the two stage hybrid classifier over the Mato Grosso (226-69), South Rondonia (230-69), and Florencia-Napo (8-59) sites are higher than the ones related to the wavelet-based region growing technique (see section 4.4.1, table 4.4); we can therefore conclude that the hybrid classifier is significantly more accurate than the ISODATA technique.

Table 5.3: Results of Kappa analyses, variance of $\hat{Z}$, Z statistic and of $Z_{\text{Wave-ISO}}$ for the wavelet-based region growing and the ISODATA classification methods.

Site (Landsat path row)	Classification method	KHAT	Var. KHAT	Z statistic	Delta Z
226-69	Wavelet r. g.	0.605	0.000457	28.30	27.43
	ISODATA	0.603	0.000482	27.47	
230-69	Wavelet r. g.	0.407	0.000557	17.24	200.50
	ISODATA	0.265	0.000681	10.18	
8-59	Wavelet r. g.	0.303	0.000780	10.86	101.67
	ISODATA	0.205	0.000967	6.61	
Wavelet r. g. = wavelets-based per pixel two stage hybrid classifier					

The overall accuracy takes into account only the diagonal elements of the error matrix while the Kappa accuracy includes information on the off-diagonal elements. An analysis by site of the off-diagonal classes using confusion maps (see figure 4.5 in chapter 4) helps to detail and localize the factors that conspire to the discrepancy between maps derived by the two classification methods (for details see: Sgrenzaroli *et al.,* 2002).

From the analysis by site of the off-diagonal classes using confusion maps, we derive the following conclusions:

1) The spatial arrangement of the off-diagonal classes reveals high discrepancy between wavelet region-growing and ISODATA classifications.
2) Differences between the wavelet-based region growing and ISODATA classifications are mostly localized in areas with regular spatial arrangement. The so-called salt-and-pepper classification effect, which is typical of per-pixel (non-contextual) classifiers, affects ISODATA classifications.

3) Speckle is probably the principal cause of discrepancy: the wavelet-based technique uses a reconstructed signal, where the speckle strength is further reduced but the spatial resolution is maintained, while the ISODATA is applied to the original 100 m imagery.

The data flow in the generation of the thematic maps using the wavelet-based region growing and ISODATA techniques is presented in figure 4.7 in chapter 4.

5.3 Summary and conclusions

The relative performances between a wavelet-based region growing segmentation technique and a conventional clustering technique (ISODATA) are assessed in this chapter. The Kappa statistic measures the significance of the differences between results obtained by the two approaches when applied to SAR imagery.

Outcome of the test shows that the wavelet-based technique provides better accuracy and is capable of generalizing over the entire data set.

Results of the error analysis with respect to maps derived from Landsat TM show higher agreement for the two wavelet-based techniques rather than the ISODATA classification. This classification is based only on a distance criterion in the radiometric domain. The results are confirmed by confusion matrices, overall accuracy, visual comparison of the derived maps, and from estimates for the Kappa statistic.

Chapter 6
Extension of the thematic problem to include the degraded forest class

6.1 Introduction

A recent work (Nepstad *et al.,* 1999) has pointed out that forest disturbances (forest degradation phenomena) that reduce tree cover but do not eliminate it, such as surface fires in standing forest or selective logging, are not included in deforestation mapping programs. To assess deforestation phenomena in the Amazon basin crisp and binary forest / non-forest classification may be incapable of describing the variety of land use types corresponding to the major forms of anthropogenic activities within the Amazon basin.

The results reported in chapter 4 show that the discrepancy between maps derived from SAR and optical instruments increases when the class degraded forest is taken into account.

To assess whether these discrepancies can be ascribed to the SAR-derived maps or to omissions in the Landsat maps (TRFIC, classification using FAO's maps as reference), the problem of forest degradation monitoring is investigated using both optical and SAR imagery. A forest degradation monitoring technique using Landsat TM imagery is proposed in section 6.2. Forest degradation monitoring using multi-temporal high resolution SAR imagery is described in section 6.3. Conclusions are given in section 6.4.

6.2 Forest degradation monitoring using Landsat TM imagery

As a first step, we identify two forest degradation types by visual inspection in the Landsat TM raw images covering the Mato Grosso site and a test site in the Brazilian Parà State.

The first type of forest degradation consists of small isolated bare soil regions, which may be due to the beginning of forest colonization or selective logging, surrounded by the forest area. As shown in figure 6.1, the regular spatial distribution of this phenomenon reinforces the hypothesis that some anthropogenic activity has taken place in the forest area. This first type of forest degradation phenomena is identified as the Vegetation-Bare Soil class (VB) to indicate the presence of small regions of bare soil within the forest area. VB bare soil is spectrally different from bare soil outside the forest domain (i.e. clear cuts). These small regions are probably partially covered from vegetation under-story that is left when the trees are felled during selecting logging and this should explain the spectral behavior.

The second type of forest disturbance consists of clear-cut regions that are abandoned and where forest re-growth takes place. These are wide areas with a regular shape, known as “capoeira”, that have a spectral behavior quite similar to the forest one (see figure 6.2). Such second type of forest degradation phenomena is identified as Vegetation-Forest class (VF) to indicate its spectral similarity to the Forest class (F).

Both VB and VF are separate independent spectral classes that can be discriminated from forest and bare soil.

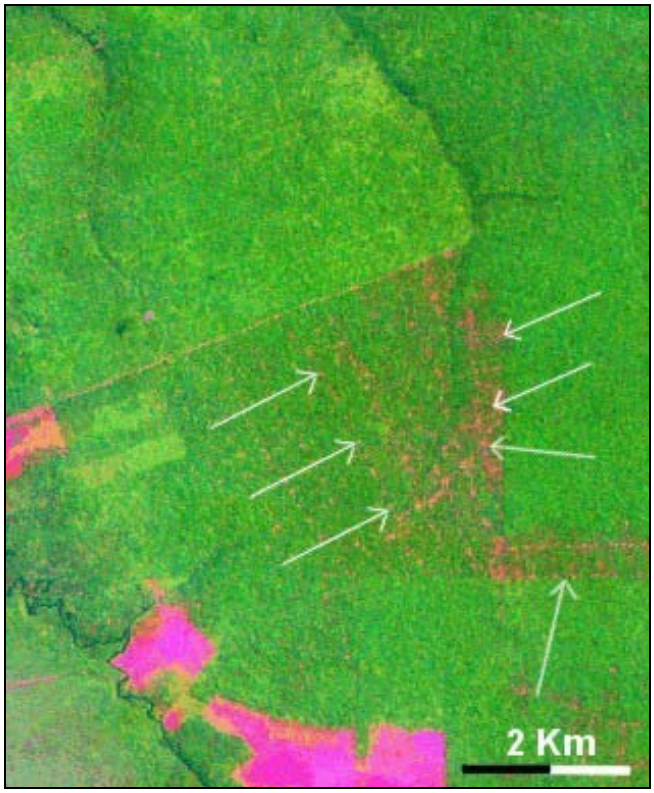

Figure 6.1: A first type of forest disturbance (marked by white arrows). It consists of isolated bare soil patches surrounded by the forest domain. The patches are readily visible in the Landsat TM 226-69 (1992) image (R: Band5, G: Band4, B: Band3). This forest degradation phenomenon is identified as Vegetation-Bare Soil class (VB) (see color Figure B.20 - Appendix B, pp. 218).

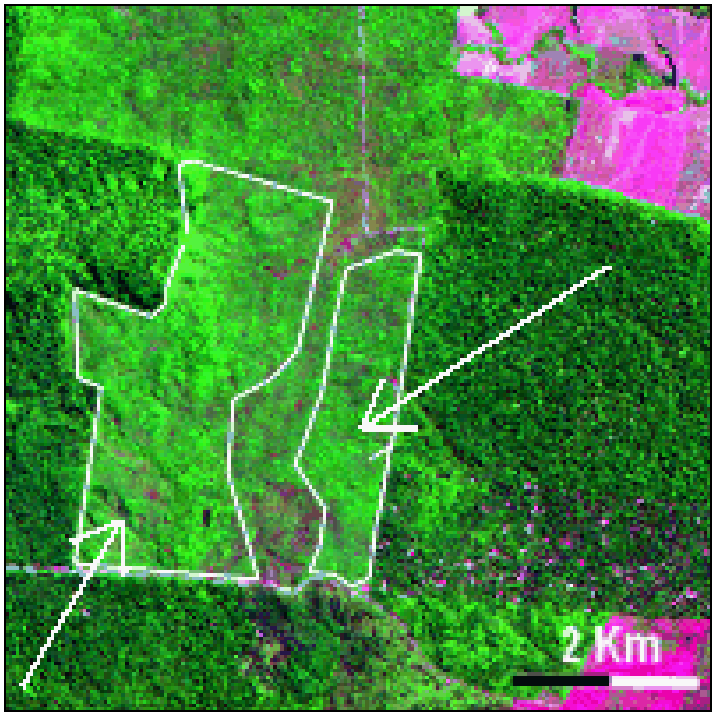

Figure 6.2: A second type of forest disturbance is visible in the Landsat TM 222-62 (1999) image (R: Band5, G: Band3, B: Band3). White contours indicate two large regions of forest degradation featuring a regular shape and a spectral signature quite similar to that of the forest class. This second forest degradation phenomenon is identified as Vegetation-Forest class (VF) (see color Figure B.21 - Appendix B, pp. 219).

To provide a complete partition of our Landsat TM test scenes we select the following land cover classes:

1. Water (W).
2. Forest, close canopy (F)
3. Bare soil and agricultural areas (BA).
4. Degraded forest DF=VB+VF.

Bare soil and agricultural areas (BA) coincide with the non-forest class adopted in the classification legend of chapter 4; Vegetation-Bare Soil (VB) and Vegetation Forest (VF) are included in the degraded forest class that was previously defined.

The design of a classification system, capable of automatically detecting classes VB and VF, is driven by a set of requirements derived from the pictorial attributes of the degraded areas that are visually detected in Landsat TM images (see figure 6.1 and 6.2). These requirements are listed next:

1) To detect forest degradation phenomena of type VB, the labeling algorithm should be able to detect small but genuine regions by working at high spatial resolution. In other words, our minimum mapping unit should be equal to the pixel size.
2) To degradation phenomena of type VF, the labeling algorithm should be sensitive to local spectral variations, i.e., capable of detecting weak spectral boundaries between slowly varying or piecewise constant image intensity areas (such as between VF and F image areas).
3) To avoid image over-segmentation, the labeling algorithm should be insensitive to natural within-class spectral variance, i.e., to local spectral variations due to shadows or micro-topographic effects. In other words, our labeling scheme should be provided with a class-conditional noise model. By avoiding over-segmentation, i.e., the so-called salt-and-pepper classification effect which is typical of per-pixel (non-contextual) classifiers, labeled output can be obtained that features cartographic quality.
4) In terms of user interaction, the labeling algorithm should be intuitive and easy to use, i.e., user-defined parameters should be as few as possible and with an intuitive physical meaning.

A novel three-stage classification method is proposed to comply with these requirements. The first classification stage is a pre-processing module consisting of

an Intensity-Hue-Saturation (IHS) color transformation (Daily, 1983) that emphasizes quantitative (spectral) and qualitative (visual) separability of the two forest degradation phenomena of interest (VB and VF). The second stage consists of a contextual clustering algorithm for image labeling. The third stage is the output module providing a many-to-one relationship between second stage output categories (clusters) and desired output classes.

The second classification stage, which is the core of the classification procedure, is the Modified Pappas Adaptive Clustering (MPAC) which is a Bayesian, maximum-a-posteriori, spectral (applies only to images with little textural information), iterative (sub-optimal), hierarchical (coarse-to-fine), contextual and adaptive optimization process for image labeling. MPAC: i) easy to use (i.e., it employs few and intuitive user-defined parameters); ii) robust to changes in initial conditions; and iii) capable of providing smooth output maps while preserving genuine but small regions**.**

To test the robustness of our classifier and accuracy of the derived maps we select two contiguous Landsat TM scenes acquired in 1999 during the same satellite pass (Path-Row: 222-62, 222-63) over the Pará site. Digital photos were collected along a transect in this area (Setzer, personal communication, 1999). The data collection was part of an aerial survey organized by the Brazilian Space Research Agency (INPE) in 1999. We use these digital photos for validation of our classification map.

The Pará site is well representative for degradation forest phenomena. The predominant vegetation is evergreen terre firme forest with above ground biomass of 250-300 t/ha (tons/hectares). Timber extraction has become a major industry over the last 15 years, centered on Paragominas, leading to a landscape of logged and "superlogged" forests (see below), along with pasture (Uhl and Vieira, 1989). The cycle of exploitation begins with selective logging for the most valuable species. These regions are later revisited for less lucrative timber and become a fragmented,

open canopy forest, termed “super-logged forest”, which is increasingly prone to fire (Cochrane *et al.,* 1999). In the final phase the remnant forest is cleared for pasture.

From the selected TM scenes of the Pará test site we extract three sub-images (test1, test2, and test3), 450 x 450 pixels in size to be compared with aerial images (see figure 6.3).

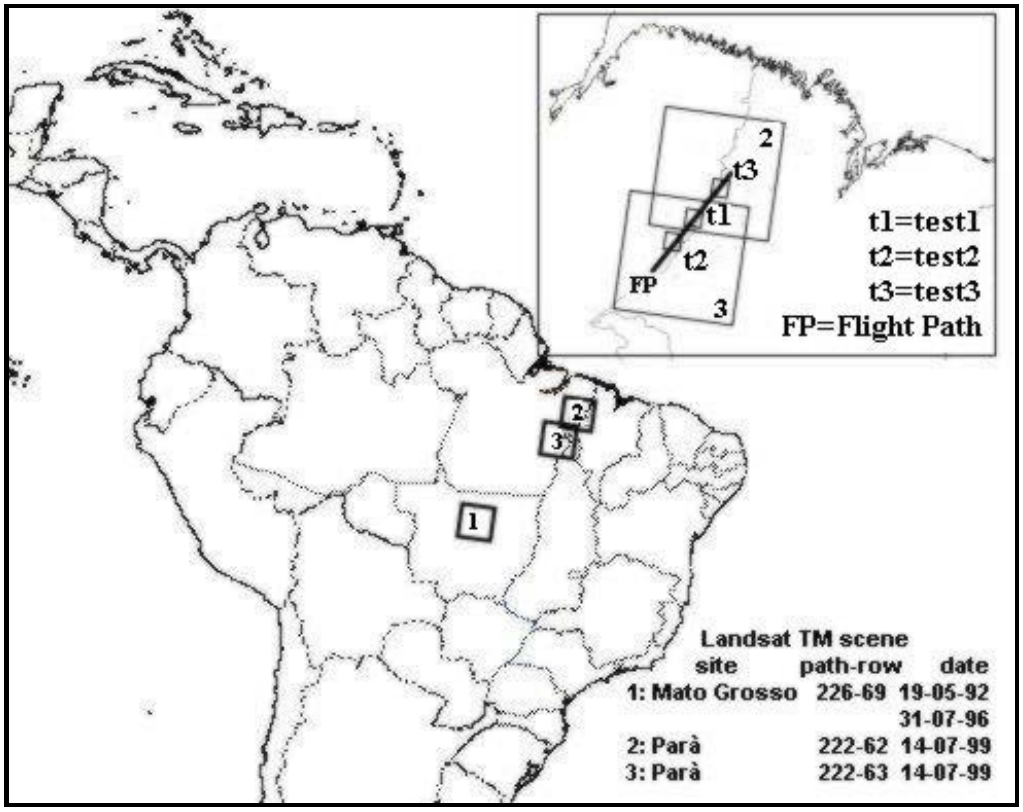

Figure 6.3: Three Landsat TM scenes cover the Pará and Mato Grosso test sites in the Amazon basin. Three TM sub-images (identified as test1, test2, and test3) are extracted from this data set in correspondence to the flight path followed during an aerial photo campaign.

Over the Mato Grosso site (226-69) the two Landsat TM raw images available (1992 and 1995) coincide with the TRFIC maps (see table 4.2, chapter 4), and a FAO

classification (derived from 1996 Landsat TM – path/row 226-69). Relevant omissions in the TRFIC and FAO maps are assessed by comparison of our Landsat TM classification and TRFIC or FAO maps.

The validation procedure analyzes in particular those parts of the TM sub-maps (corresponding to raw sub-images test1 to test3, see figure 6.3) that overlap with aerial photos and are characterized by VB and VF forest degradation type (se figure 6.4 and 6.5 respectively).

According to an expert photo-interpreter the degree of match between visually detected degradation phenomena in aerial photos and automatically detected VB pixels in TM images is satisfactory. This statement is reinforced by considering that areas with label VB in the TM image become areas labeled as new clear-cuts in aerial photos acquired about two months later. This is consistent with the fact that the degraded forest type VB is expected to be involved in rapid and strong changes in the forest cover (figure 6.6).

For more details on of the classification methodology and a quantitative assessment see (Sgrenzaroli *et al.,* 2002a)

In the Mato Grosso test site, the two selected multi-temporal TM scenes, 1245x1245 pixels in size, cover an area of approx. 139,502 ha (the geographical location is indicated in figure 6.3). In the two TM maps, the VF class extension is approx. 9,141 ha (6.5%) in 1992 and 13,175 ha (9.4%) in 1996. Extension of class VB is approx. 17,612 ha (12.6%) in 1992 and. 8,922 ha (6.4%) in 1996.

To compare the 1992 TM map with the TRFIC deforestation map, first, the TRFIC classes are reduced to label types *water, forest, degraded forest and non-forest* (see table 4.1, chapter 4). Second, cover types of the TM classification map are reduced to classes *water, forest and non-forest*, by aggregating classes VF, VB, and BA into the *non-forest* metaclass.

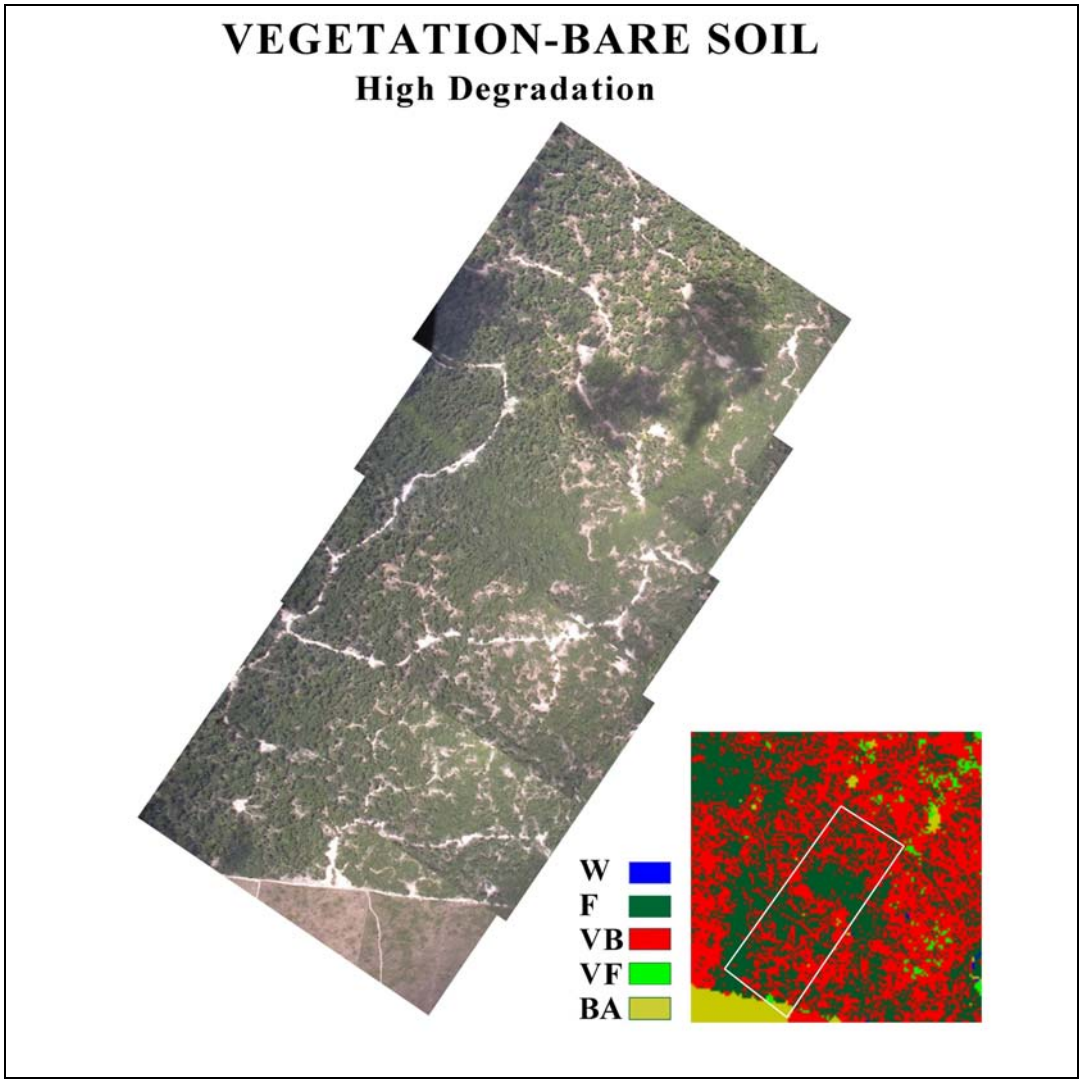

Figure 6.4: Comparison between aerial photos and a TM thematic map (see the white outline at the bottom right) in which the density of the VB degradation class is considered “high” (see color Figure B.22 - Appendix B, pp. 220).

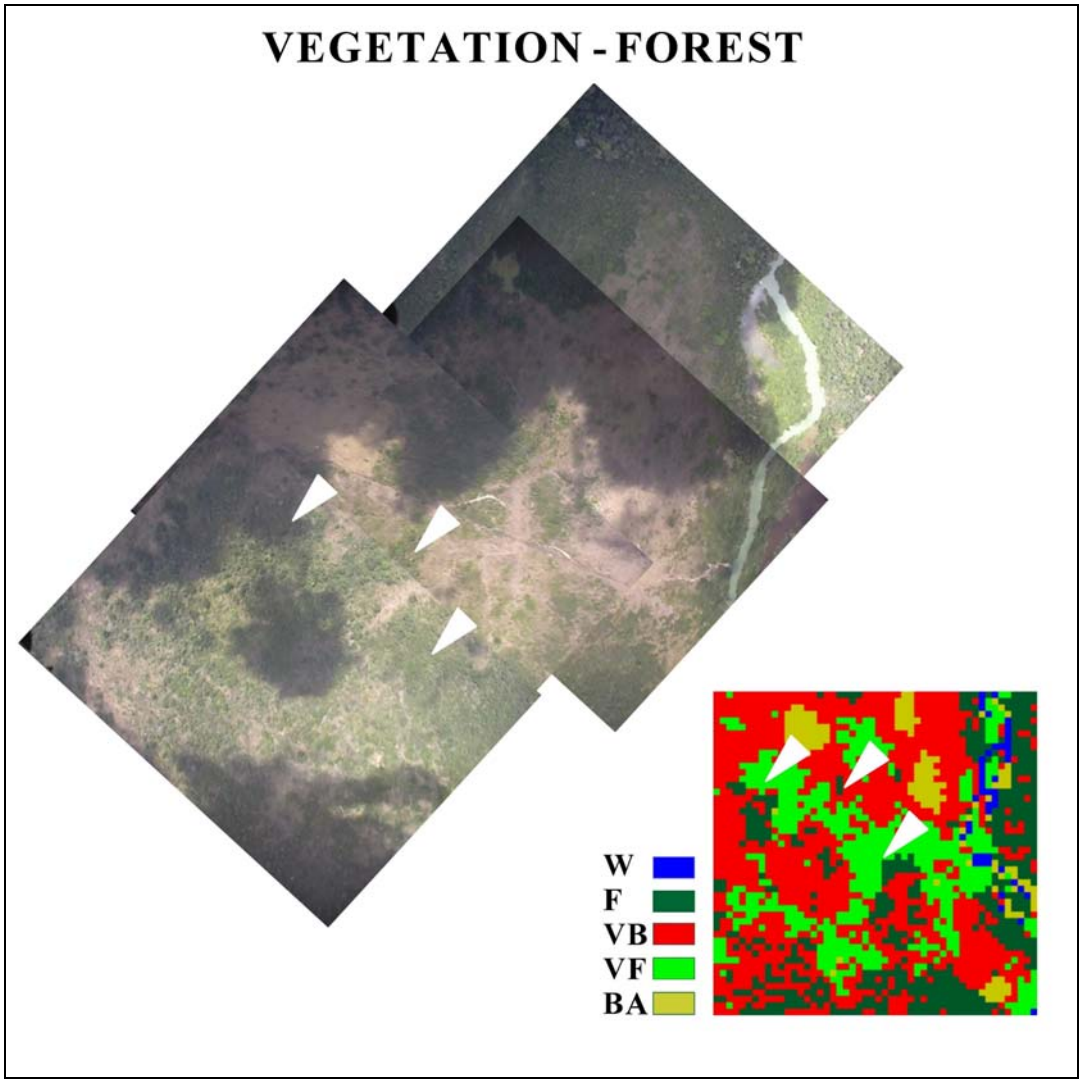

Figure 6.5: Comparison between aerial photos and a TM thematic map where Vegetation-Forest (VF) degradation phenomena are detected (see color Figure B.23 - Appendix B, pp. 221).

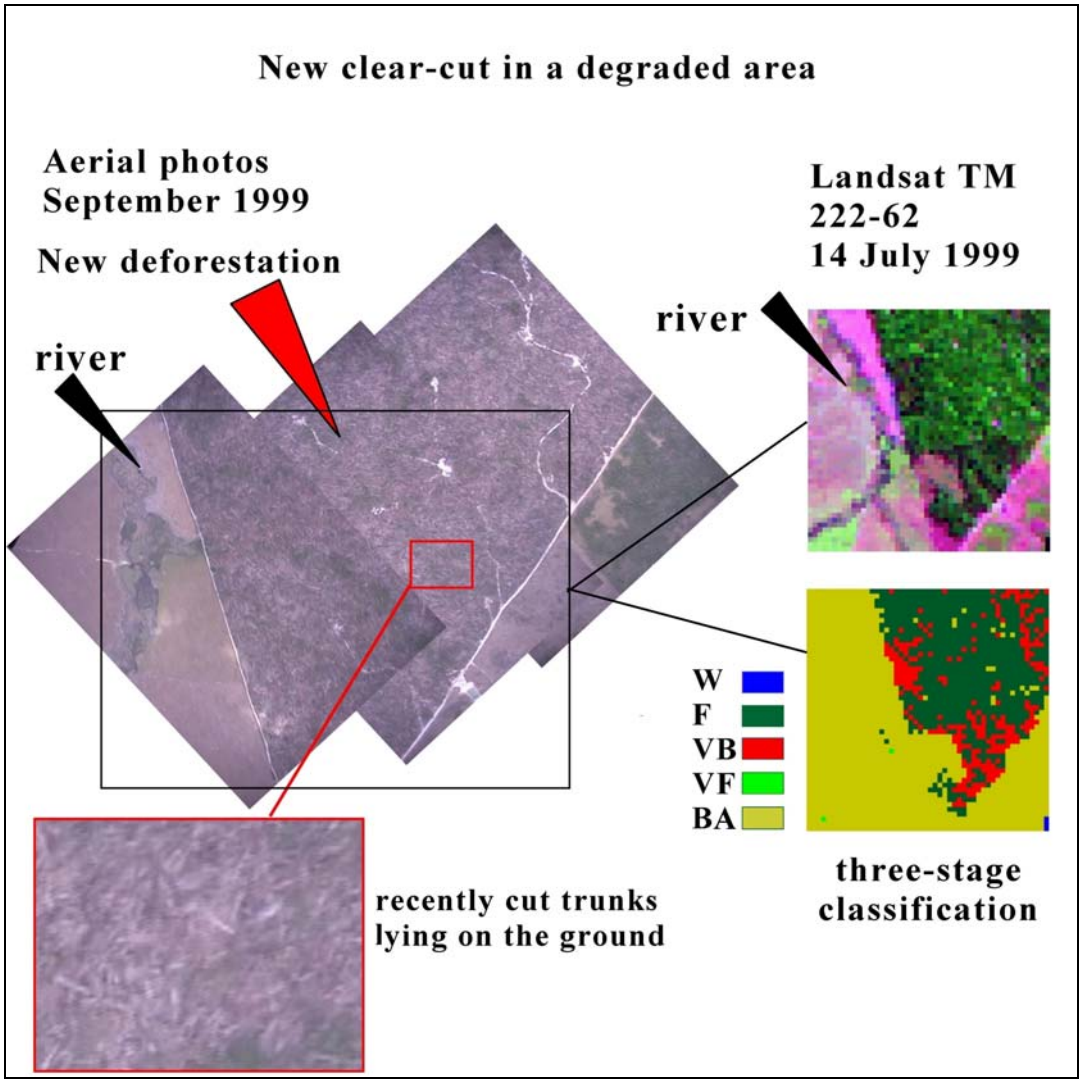

Figure 6.6: High dynamics of change in areas affected by forest degradation phenomena. Class Vegetation-Bare soil (VB) detected in the Landsat TM image becomes new clear- cuts in aerial photos taken about two months later, where recently cut stems are still lying on the ground (position of the river can be used to localize the aerial photo with respect to the TM image and the corresponding thematic map) (see color Figure B.24 - Appendix B, pp. 222).

Finally, from these two re-aggregated maps, classification statistics of the *water, forest and non-forest* classes are computed as shown in table 6.1. This table points out that, overall, the three-stage classifier assigns to the forest class 13.0% fewer pixels than the TRFIC map. Conversely, the three-stage classification system assigns to the non-forest metaclass 12.8% more pixels than the TRFIC map.

Table 6.1: Comparison between the TRFIC classification and the MPAC-based classification. Water, forest, and non-forest classes are considered for comparison.

	TRFIC classification (%)	**Three-stage classifier (%)**
Water	0.03	0.15
Forest	72.85	59.88
Non-forest	27.12	39.97
Total	100.00	100.00

The related confusion matrix is reported in table 6.2, where the percentage of non-forest pixels detected by the three-stage classifier is presented according to its class components BA, VB, and VF. This table shows that, respectively, 18.2% (= 12.0% + 6.2%) of the TRFIC forest metaclass and 21.6% (= 14.2% + 7.4%) of the TRFIC non-forest metaclass overlap with TM forest degradation areas. These percentages are equivalent to a ground coverage of 26,723 ha (= 18,525 ha + 8197 ha), corresponding to 19.1% (= 100 x 26,723 ha / 139502 ha) of the total surface coverage. Note that 55% of the TRFIC water class (equivalent to 30 ha) overlaps with forest degradation types VB and VF.

Concerning the 1996 FAO classifications map of the Mato Grosso test site, a direct comparison with the 1996 TM data map is difficult because: i) the FAO land use/land cover legend is quite different from land cover classes detected by the three-stage classifier; and ii) the two output maps employ different minimum mapping

units. The FAO map mapping unit is equal to 100 hectares; the derived maps have a pixel size of 100 m; the TM thematic map is derived from the 1996 TM raw data with a pixel size equal to 30 m.

Table 6.2: Confusion matrix between the TRFIC classification and the three-stage classifier. Pixels belonging to the non-forest metaclass detected by the MPAC-based classifier are divided into elementary classes BA, VB and VF.

Overall accuracy=85%		**TRFIC classification (%)**			
		Water	**Forest**	**Non forest**	**Total**
Three-stage classifier (%)	**Water**	25.82	0.17	0.06	0.15
	Forest	2.47	80.99	3.21	59.88
	Non-forest	71.71	18.84	96.73	39.97
	Total	100.00	100.00	100.00	100.00
	BA	16.28	0.61	75.04	20.79
	VB	54.93	11.99	14.25	12.62
	VF	0.50	6.24	7.43	6.55
	Total	71.71	18.84	96.73	39.97

For the sake of comparing results, the following strategy has been adopted. First, the TM classification map is sub-sampled at the pixel size of 100 m. Next, the sub-sampled TM data map, the FAO map and the corresponding Landsat TM 226-69 (1996) image are visually compared by an expert photo-interpreter as shown in figure 6.7.

This qualitative inspection confirms that the *closed canopy forest* class defined by FAO includes forest degradation phenomena detected in TM data (no *open canopy forest* as defined by FAO is present in this area of interest). Quantitatively, the FAO *closed canopy forest* class exceeds class *forest* detected by the three-stage classifier by approximately 10%. In particular, class VF appears to be the first cause of discrepancies between the two maps. Sometimes the VF class overlaps with the FAO

mosaic forest-shrubs class, although it is generally included in the FAO *closed canopy forest* class. The VB forest degradation class overlaps with the FAO class *short/long fallow, closed canopy forest, other land covers and shrubs* in decreasing order.

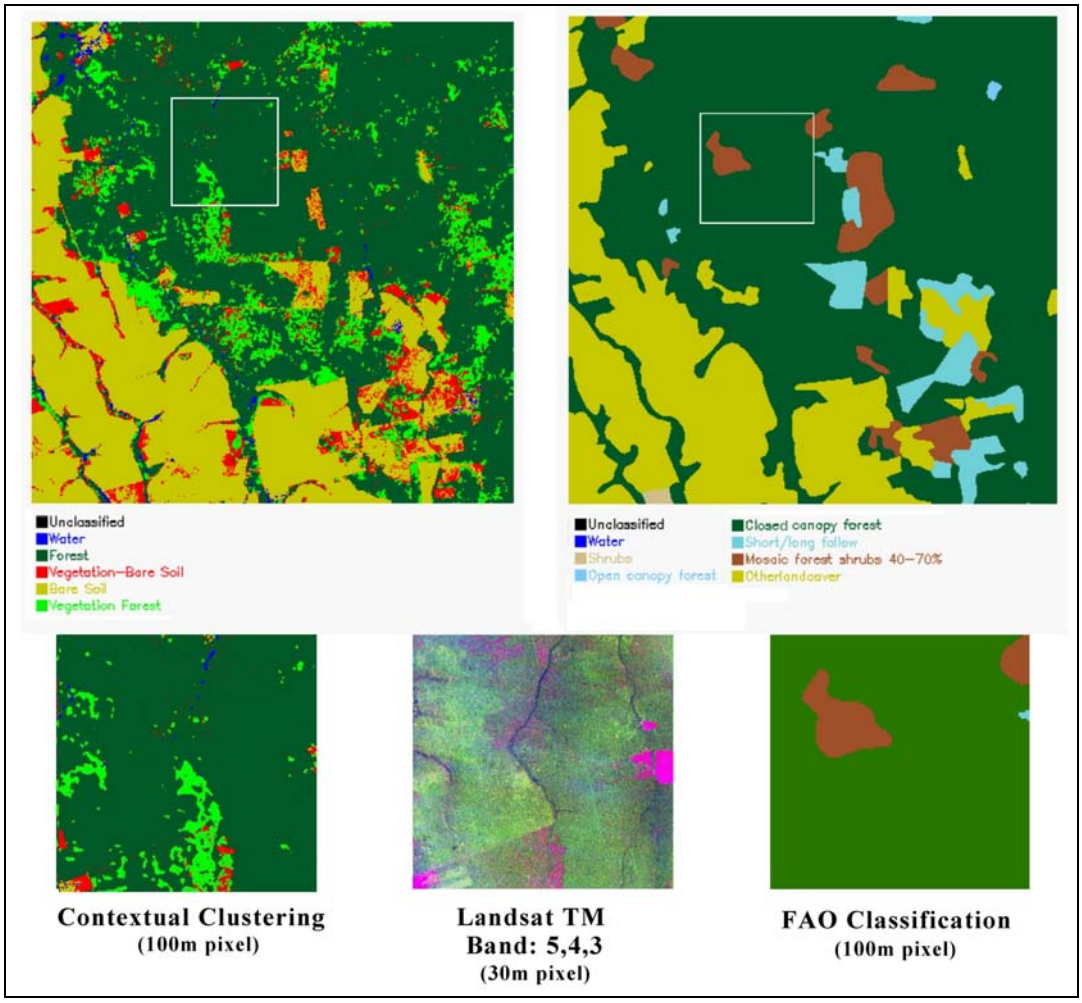

Figure 6.7: Comparison between a subset a Landsat TM 226-69 (1996) image, the corresponding TM thematic map (down-sampled at 100 m), and the FAO map (see color Figure B.25 - Appendix B, pp. 223).

This investigation shows that, in the three 1999 Landsat TM Parà sub-maps, forest degradation phenomena account for 13% up to 45% of the ground coverage. This result is in line with the work of Stone and Lefevbre who estimated a forest alteration of 12% due to selective logging in the Brazilian State of Pará from the year 1988 to 1991 (Stone and Lefevbre, 1998).

In the Mato Grosso test site, two maps, generated from 1992 and 1996 TM scenes, reveal that forest degradation areas: i) account for, respectively, 19% and 16% of the ground coverage; and ii) overlap with 10% and 18% of the *forest* class detected by the FAO and TRFIC deforestation mapping programs in 1992 and 1996 respectively. This result is in agreement with the work by Nepstad *et al*. who speculate that present estimates of annual deforestation for the Brazilian Amazon capture less than half of the forest area that is impoverished each year (Nepstad *et al.,* 1999).

Finally these results confirm the hypothesis that some discrepancies related to class *degraded forest* between maps derived from optical and radar instruments can be ascribed to omissions in the maps derived from optical data (TRFIC, Landsat TM classification using FAO's maps as reference) and point to the need for proper classification techniques to monitor forest degradation phenomena.

6.3 Forest degradation monitoring using multi-temporal high resolution SAR imagery.

Accuracy assessment of the forest maps from SAR (100 m pixel size) using optical reference data (30 m-pixel size) proves that the classification accuracy of the radar maps decreases with the landscape spatial fragmentation (see section 4.2 and 4.3 in chapter 4). Moreover the major source of misclassification is identified in class *degraded forest* which can be visually perceived in high resolution Landsat TM images (30 m) as consisting of small isolated bare soil patches.

To what extent can these discrepancies be ascribed to spatial limitation of the GRFM SAR mosaic at 100 m resolution?

We'll try to give an answer considering the full resolution JERS-1 SAR images used for the GRFM mosaic generation. The radar instrument ground range resolution is 18m., while pixel spacing in the GRFM South America mosaic data is 3 arcsecond (89-93 meter). Radiometric resolution of the full-resolution JERS-1 ground range products is 3 looks. The GRFM mosaic data have approximately 200 looks due to averaging.

The main problem is to improve the signal to noise ratio of JERS-1 full resolution data (reduce the speckle strength) to achieve a better interpretation.

A set of 8 JERS-1 images, acquired over the same area in the Mato Grosso training site from 1992 to 1996 and having the same acquisition geometry (i.e. same orbit and frame number), was made available by NASDA's archive (Level 2.1 NASDA products, NASDA Hatoyama Earth Observation Center – HEOC). Acquisition dates of 8 JERS-1 images over the same area in the Mato Grosso training site are: November 15, 1992; May 23, 1993; September 19, 1993; July 24, 1994; October 20, 1994; December 03, 1994; October 7, 1995; May 14, 1996.

We co-registered the 8 images manually selecting tie- points by visual inspection of homologous features recognizable in all images. A multi-temporal speckle filtering technique (De Grandi *et al.,* 97b) was then applied to the co-registered time-series of full-resolution JERS-1 images. The filter reconstructs the underlying radar reflectivity time-evolution at the highest possible spatial resolution of the signal and for each image in the series. Therefore 8 filtered images were generated with significant improvement of the signal to noise ratio. A visual comparison of a 4-look JERS-1 image and the corresponding filtered image over a zoomed area of the Mato Grosso site (October 7, 1995) is shown in figure 6.8.

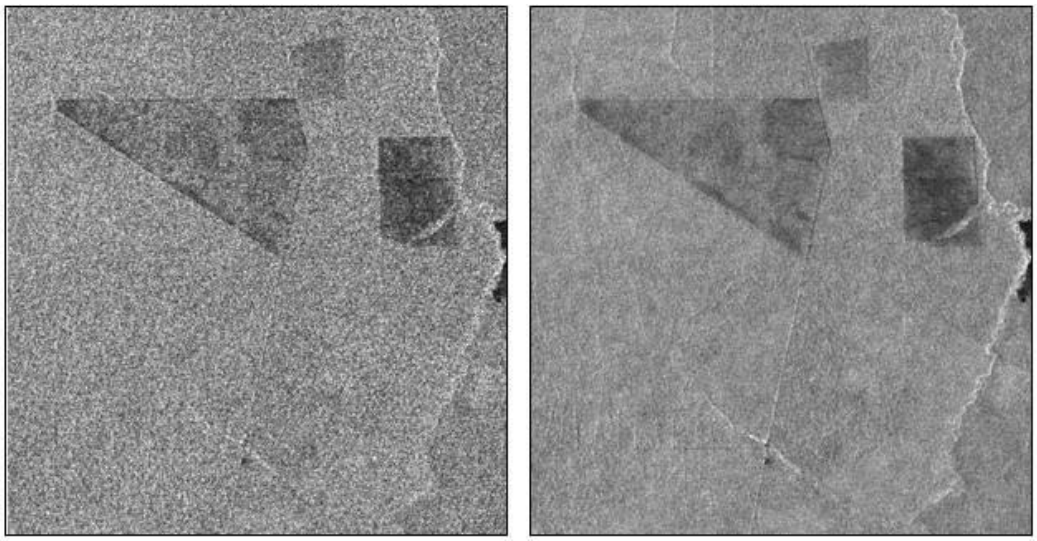

Figure 6.8: Comparison between 4-look JERS-1 image over a zoomed area of the Mato Grosso site (October 7, 1995) and the corresponding filtered image.

In a single filtered SAR image at high resolution (12.5 m) degradation phenomena are now clearly detectable. As shown in figure 6.9, small isolated and elongated bare soil regions that are distributed in a regular pattern in the forest domain (degradation phenomena due to selective logging) are detected both by

Landsat TM (30 m pixel size) and 12.5 m JERS-1 filtered image, while these phenomena are not visible in the 100m GRFM mosaic.

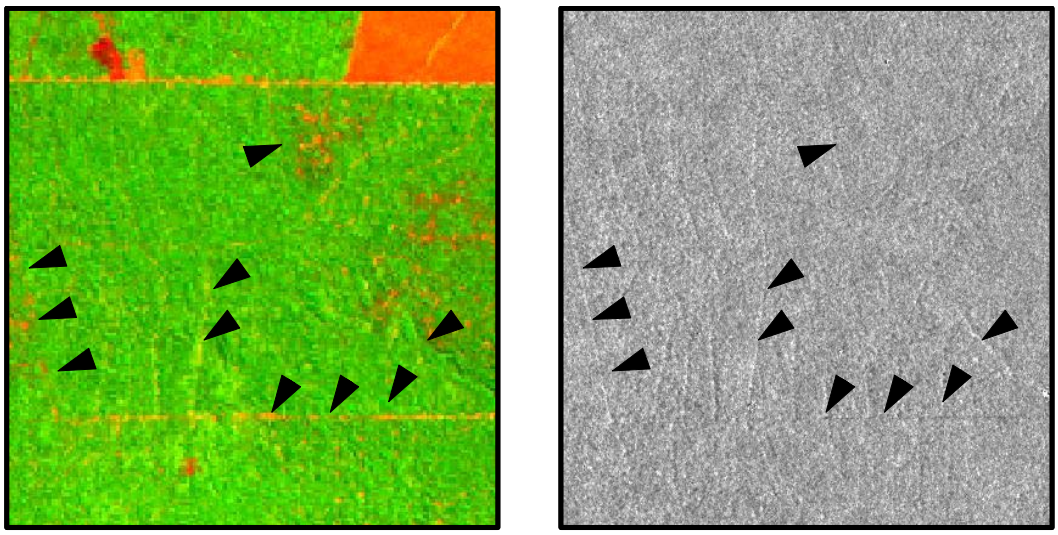

Figure 6.9: Small isolated and elongated bare soil regions distributed regularly in the forest (degradation phenomena due to selective logging) are captured (black arrows) both by Landsat TM (30 m pixel size, acquisition date: 31-07-96) (a), and 12.5 m JERS-1 filtered image (acquisition date: 07-10-95) (b) (see color Figure B.26 - Appendix B, pp. 224).

Moreover, the use of a time series of high resolution filtered images sets the ground for monitoring in time deforestation phenomena (see figures 6.10).

This short section in not exhaustive of all possibilities opened up by the use of temporal sequence of filtered high-resolution JERS-1 images and more work is needed for automatic extraction of thematic information from these multi-temporal data sets.

However**,** these preliminary considerations may be put forward:

1) By increasing the radiometric and spatial resolution of JERS-1 imagery degradation phenomena corresponding to narrow and short spatial patterns can be detected. The same features are not detectable in the maps derived from SAR imagery at 100 m resolution. This is one of the main causes of discrepancy with respect to maps derived from optical instruments with a resolution of 30 m.
2) High resolution and speckle-filtered time-series of JERS-1 images are a pre-requisite for monitoring deforestation in time.

JERS-1 data collected in the NASDA archive constitute a valuable historical data set from 1992 to 1997; the foreseen NASDA ALOS mission will assure continuity for the future in providing such multi-temporal data.

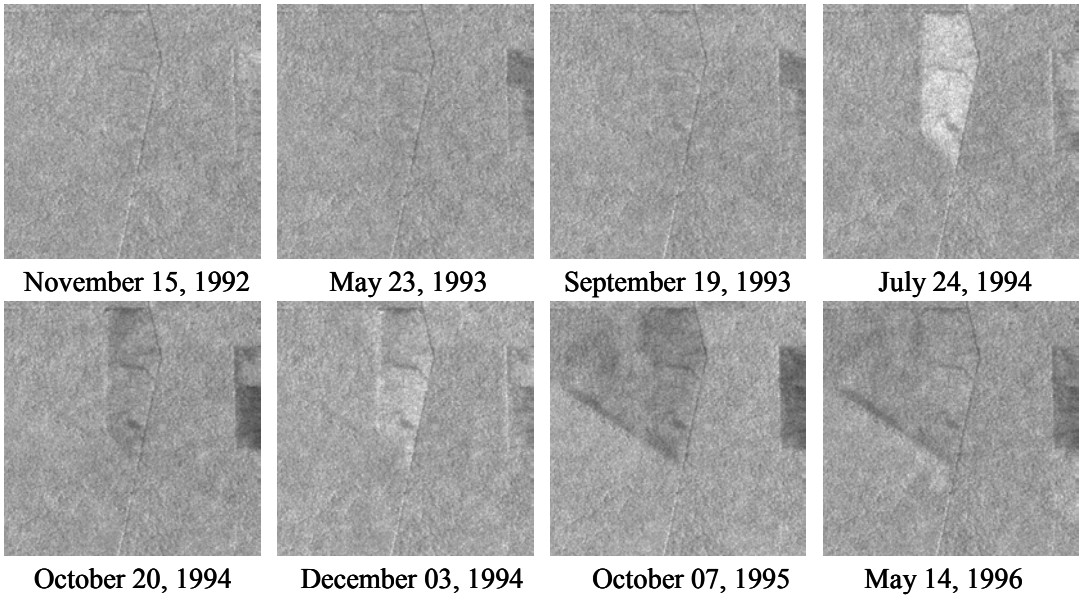

Figure 6.10: Temporal sequence of filtered images allows for monitoring in time of deforestation phenomena that becomes visible since the July 24, 1994 image.

6.4 Summary and conclusions

The issue of detecting the degraded-forest class, generally ignored by Amazonian deforestation mapping programs (INPE, 1996 and 1998; FAO, 1997; TRFIC), is attacked using data acquired by both optical and SAR instruments. To the purpose:

1) A novel three-stage classification scheme is proposed for forest degradation phenomena detection in Landsat TM images.
2) A multi-temporal speckle filtering technique is applied to a series of full-resolution JERS-1 SAR images (12.5 m pixels size). In a single high resolution filtered SAR image degradation phenomena are detectable and evolution from degradation to deforestation can be monitored through the time series of images.

A three-stage classification procedure is developed for detecting degraded forest classes in Landsat TM images. The method is tested over two areas in Mato Grosso and in the Para' Brazilian state. This classifier is capable of managing spectral information on a different scale to preserve small but genuine regions. It is easy to use and robust to changes in input conditions. In the Para' site degradation phenomena detected by the three-stage classifier are confirmed as anthropic disturbances in the forest area by visual interpretation of aerial photos. Nepstad *et al*. speculated that present estimates of annual deforestation for Brazilian Amazzonia capture less than half of the area that is impoverished every year. This statement is confirmed by our experiment. Indeed the TM thematic maps of the Mato Grosso test site reveal that forest degradation areas: i) account for 19.17% and 15.83% of the total mapped area (45 x 45 km^2) in 1992 and 1996 respectively; ii) overlap with 10% and 18% of the forest class detected by FAO and TRFIC deforestation mapping in 1992/93 and 1996. These results reinforce the hypothesis that some discrepancies

between maps derived from optical and radar instruments can be ascribed to omissions in the former.

To understand how much these discrepancies are due to spatial resolution of the GRFM SAR mosaic (100 m) we use a set of 8 JERS-1 full resolution (12.5 m) images acquired over the Mato Grosso training site from 1992 to 1996. A multi-temporal speckle filtering technique generates 8 filtered images with a significant improvement of the signal to noise ratio. In this filtered imagery small isolated and elongated bare soil regions that are regularly distributed in space are now visually detectable in a forest area. These details could not be detected in the GRFM SAR mosaic.

Automatic extraction of these features for producing a degradation forest map will be the topic of future work. In any event these first results reveal the possibility of zooming in the GRFM data set where higher spatial resolution is required using historical JERS-1 multi-temporal datasets. A mapping strategy based on multi-scale continental coverage (from 100 m down to 12.5 m) using all-weather SAR acquisitions could be supported by the foreseen NASDA ALOS mission.

Chapter 7

A model for correcting global estimates from local ones

7.1 Introduction

In chapter 4 we observed that the discrepancy between SAR maps (100 m pixel size) and Landsat TM maps (30m pixel size) increases with the degree of deforestation pattern complexity. A possible explanation can be the difference in spatial sampling between the SAR and the TM data sets. We assume that the local error estimates could be used to correct globally the SAR classification maps. To the purpose we define a parameter that depends on the fragmentation figures and is proportional to the errors measured between Landsat TM maps and the SAR maps.

A method for calibrating area estimates of tropical forest by inverting a model of the influence of the spatial forest fragmentation on the spatial aggregation bias as characterized by two nested regression models has been tested by Mayaux and Lambin (Mayaux and Lambin, 1995 and 1997). In that case the correction function was calibrated on the basis of tropical forest maps derived from AVHRR 1 km data for the entire inter-tropical belt and a random sample of 13 Landsat TM scenes distributed among the main tropical forest regions.

In our case the input data for the regression are area estimates from Landsat TM maps at 30 m pixel size and SAR maps at 100 m pixel size. The regression parameters are then applied to the GRFM SAR (100 m pixel size) mosaic to predict land-cover proportions (at 30 m resolution).

Methodology and results are given in section 7.2; conclusions are reported in section 7.3.

7.2 Methodology and results

In Chapter 4 (section 4.4.1) we showed that SAR map accuracy decreases with forest spatial fragmentation index. The index consists of a spatial measure, the perimeter-over-area (PA) ratio (see formula 4.2).

Tests for correction function estimation indicate that the PA index is sometimes not univocally defined. Indeed for certain forest patterns two different spatial fragmentation configurations result in the same PA numerical value as shown in figure 7.1. Note that these deforestation patterns were not considered in the experiment described in Chapter 5.

For the task described here we prefer to introduce the Matheron (MI) index because it presents the same trend as PA but does not suffer from ambiguity. MI is defined as:

$$\mathrm{MI} = \frac{\text{number of runs between forest and other cover type pixel}}{\sqrt{(\text{number of forest pixel})}\ \sqrt{(\text{total number of pixel})}} \tag{7.1}$$

In our test case the South America GRFM mosaic (100 m pixel size) is used as a global data source. A set of Landsat TM maps (30 m resolution) is used as local data source. More specifically, the Landsat TM maps cover three sites in Mato Grosso, South Rondonia, and Florencia-Napo that are representative of different deforestation patterns ("hot spot" areas) (see table 4.2).

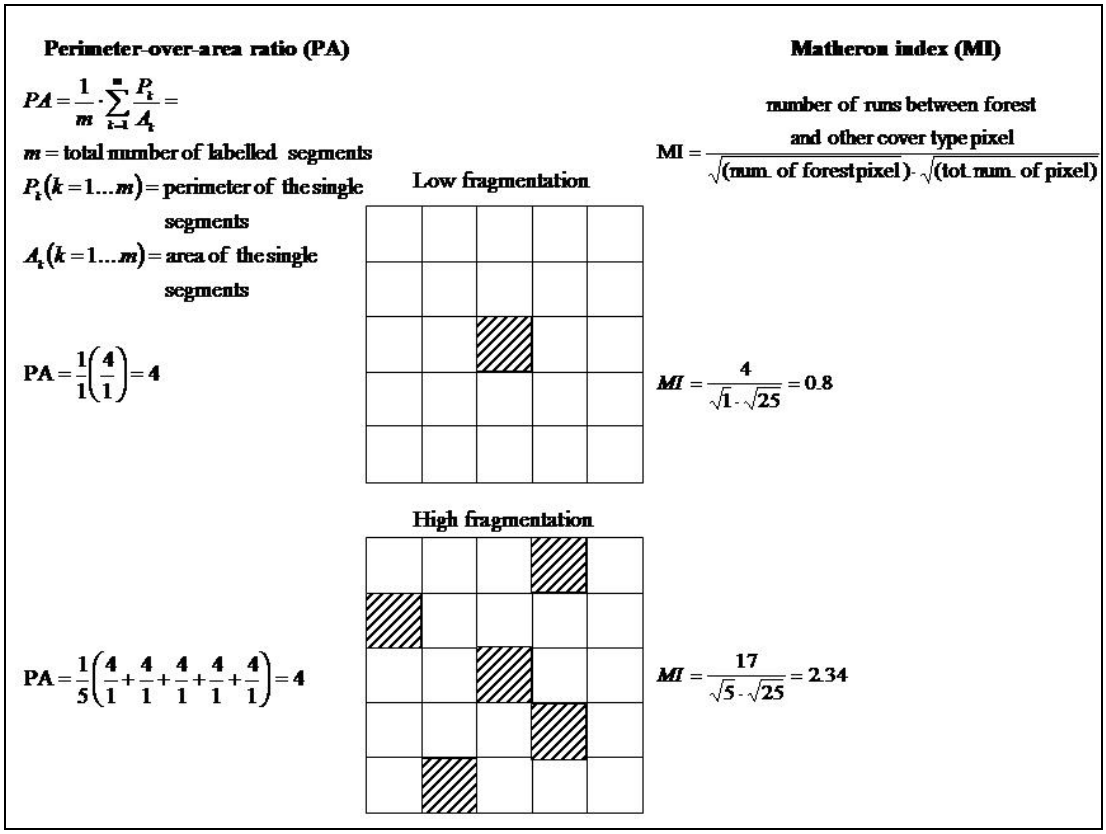

Figure 7.1: Two different fragmentation patterns – highlighted by boxes – are characterized by the same PA index; the Matheron index can discriminate the two.

The correction function for the regional-scale SAR classification is derived through the following 9 steps:

Data analysis

1) Maps derived from SAR data (100 m) and optical data (30 m) are fully partitioned into non-overlapping blocks of equal ground resolution areas.
2) Spatial measure (SM) values are computed for each block in the SAR map (these values approximately correspond to those extracted from optical data).
3) Forest percentage pairs, identified as %FH and %FL, are computed for each block at fine (TM) and coarse (SAR) resolution respectively.
4) Blocks with most similar SM values are grouped into subsets of equal cardinality. Each group of blocks is characterized by an average SM value, ASM.
5) A linear regression model is applied to each set of per-group (%FH, %FL) forest percentage pairs, i.e., each group provides one pair of linear parameters, e.g., an angular coefficient, $m_j(ASM_j)$ and an intercept value, $c_i(ASM_i)$
6) Two continuous functions (i.e. m=A+B*(ASM) and c=C+D*(ASM) in the linear case) can be fitted in least square sense from a set the liner parameter - $m_j(ASM_j)$, $c_i(ASM_i)$ - of the first liner regression process.

Data synthesis

7) The whole SAR mosaic of the Amazonian basin is classified and partitioned into non-overlapping blocks.
8) Per-block SM values and forests percentage, %FL, is computed at the resolution of the SAR mosaics (100 m).
9) Forest coverage %FH at the resolution of optical data (30 m) is estimated as %FH = m(ASM) %FL + c(ASM).

The analysis and synthesis steps are schematically represented in figure

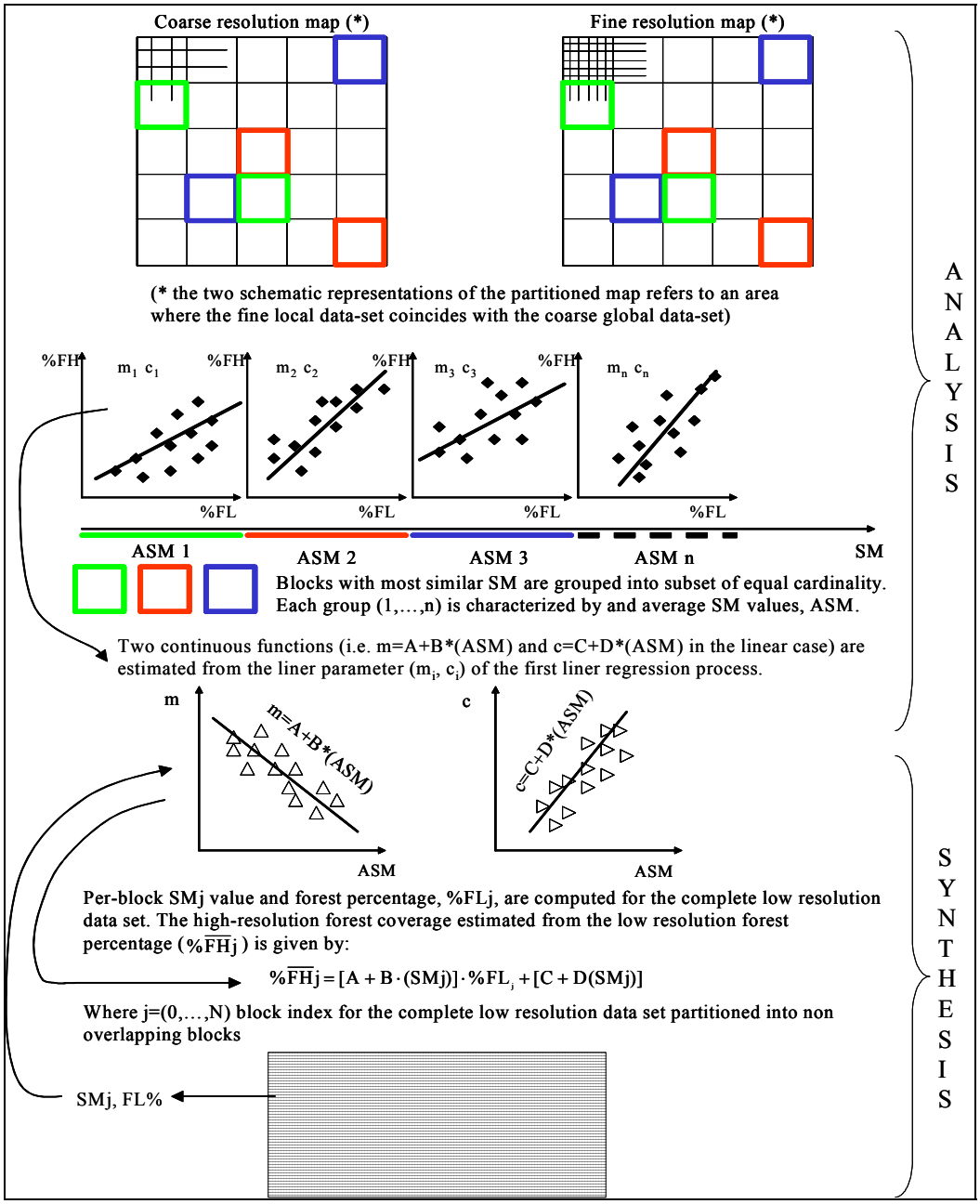

Figure 7.2: Schematic representation of analysis and synthesis steps to estimate and apply the correction function to the low resolution SAR classification (see color Figure B.27 - Appendix B, pp. 225).

The described method is applicable if the following conditions are verified:

1) The coarse resolution SM is a good proxy variable for the fine scale spatial pattern.
2) The coarse resolution SM and forest percentage, % FL, are independent variables.

Low correlation value (0.544) between SM computed from the SAR map at coarse resolution and SM computed from the TM map at fine resolution indicates that the first condition is not verified (see Figure 7.3).

Both conditions have been verified in the case that SM values at two resolutions are computed from data acquired by the same sensor. A simulation case is developed using local classifications at higher resolution derived from Landsat TM data (30 m) and the same products scaled to 100 m as lower resolution classifications. Correlation analysis between SM values computed at two resolutions (correlation=0.958) proves that the first condition is verified in this case (see Figure 7.4).

Based on this simulation we expect that the conditions underpinning the correction method will also be met when using high resolution (12.5 m) speckle filtered SAR images (see Chapter 6) as local classification estimate, and the GRFM mosaic as lower resolution global data source.

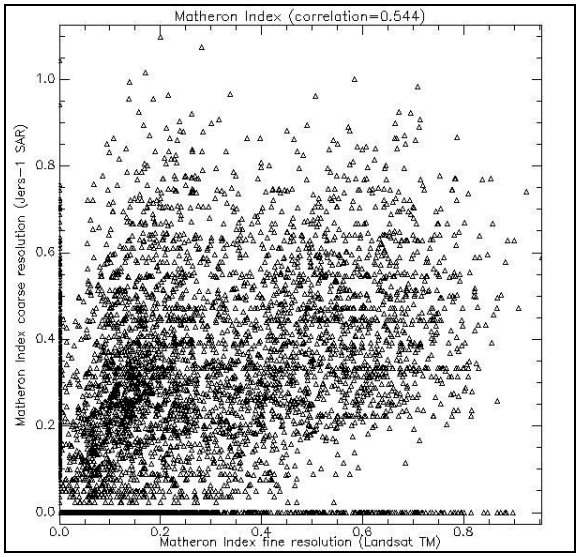

Figure 7.3: Correlation analysis between SM computed from a SAR map at coarse resolution and SM computed from a TM map at fine resolution.

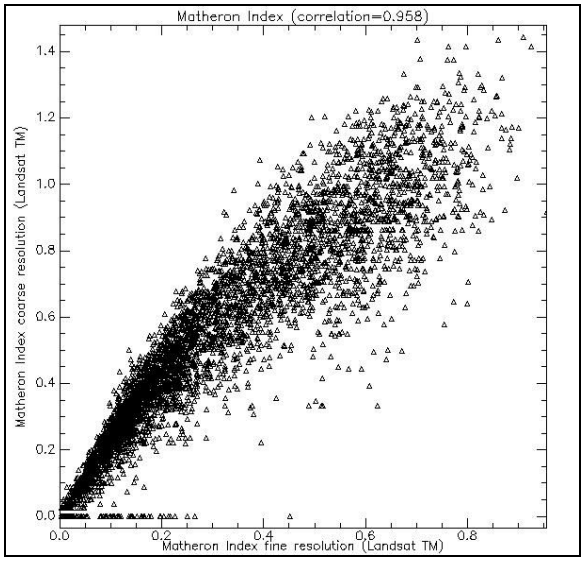

Figure 7.4: Correlation analysis between SM computed from TM map at 100m pixel size and SM computed from TM map at 30m pixel size.

7.3 Summary and conclusions

The production of global-scale thematic maps largely relies on remote sensing data at course resolution (order of several kilometres). Estimation of land-cover proportion at large scale can be affected by systematic errors. Cases in point are the discrepancies that are found between maps derived from the GRFM SAR mosaics (100 m pixel size) at regional scale and local high resolution Landsat TM maps (30 m pixel size).

An inductive learning methodology, capable of correcting vegetation map at regional-scale starting from local classification estimates at higher resolution, is proposed in this chapter. The methodology has been successfully tested in a previous work (Mayaux and Lambin , 1995 and 1997) where a coarse spatial resolution map of the entire inter-tropical belt derived from AVHRR data (1 km pixel size) is corrected using random samples of Landsat TM maps. The methodology is applicable if some assumptions are verified.

We prove that these assumptions are not verified when Landsat TM maps are used as local classifications to correct regional-scale maps derived form GRFM radar mosaics. Correction is possible when using maps at different resolution but derived from the same satellite sensor. An experiment using simulated data is set up to verify this proposition. In the experiment Landsat TM maps are used as local estimates at higher resolution for correcting the same maps scaled at a pixel size of 100 m. The simulated maps are a good proxy of regional scale coarse-resolution maps. This test suggests that GRFM regional maps could be corrected using maps derived from speckle-filtered high-resolution (12.5 m) SAR imagery.

An inductive learning methodology aimed at correcting regional-scale low-resolution classifications which are affected by errors induced by the landscape fragmentation is tested. The method is based on a linear regression between an "auxiliary" variable, which can be measured over the entire population from coarse

resolution data, and the "target" variable (land cover proportion at fine resolution), that is measured over a sample of calibration sites, is tested. The parameters of this linear regression can be estimated using samples of fine and coarse resolution data and then applied over the entire population of coarse resolution data if two conditions are verified.

By correlation analysis we prove that this correction method is not applicable using Landsat TM maps (30 m pixel size) as local estimates to correct GRFM SAR map (100 m pixel size) because the coarse resolution SM is a not good proxy variable for the fine scale spatial pattern.

A simulation exercise using Landsat TM maps at 30 m pixel size as local high resolution classification estimates and the same maps scaled at 100 m as lower resolution classification indicates that in this case the conditions underpinning the method are met.

In line with this simulation where thematic maps from the same sensor at different pixel size are used, we expect the correction method to work also in the case where maps derived from high-resolution (12.5 m) speckle filtered SAR images are used to correct regional-scale maps derived from the GRFM SAR mosaics.

Chapter 8

Overall summary and conclusions

8.1 Introduction

This final chapter gives *a summary of the main points touched upon and conclusions reached in the research work presented in this thesis*. Main theme is mapping of the tropical forest in South America at regional scale using radar mosaics derived from JERS-1 (L-Band) satellite data. Summarized items are listed following criteria of importance within the chapter organization. Advantages of forest monitoring by radar remote sensing are emphasized and future perspectives are discussed. Novel aspects and results of this research work are finally summarized and listed.

Finally some ideas are put forward which are meant to be working hypotheses for future actions and projects aimed at reducing the pressure over the tropical forest ecosystem.

8.2 Main items and conclusions in topical order

8.2.1 Remote sensing imagery, reference, training and test data

The South America GRFM SAR mosaic generated by JPL with the data acquired during September-November 1995 by NASDA's JERS-1 satellite is used as principal data-set to derive the forest map. The high-resolution L-band HH-polarized SAR imagery of the entire Amazon basin corresponds to the low-water period in the Amazon ecosystem. The approximately 2500 scene are processed and mosaiced into two digital datasets with 3 arc-second (approximately 100 m) resolution.

The GRFM mosaic offers important advantages with respect to other semi-continental optical data set such as: i) continuous coverage, ii) good geo-referencing accuracy, iii) higher spatial resolution. Due to these peculiar characteristics, the GRFM mosaics can be taken as geographical reference systems for deriving thematic maps and co-registering other remote sensing data sets and it constitutes a good baseline that can underpin future remote sensing research.

8.2.2 The classification problem: methods and thematic class definition

Tropical Forest mapping is achieved through an operational classification scheme suitable for processing large coverage radar data sets, such as the GRFM South America mosaic. The two main steps are: i) a wavelet multi-resolution decomposition/reconstruction pre-processing and ii) two image-labeling techniques: region-growing, per pixel two-stage hybrid classifier.

Two major issues have been tackled for extracting thematic information from the GRFM mosaics: i) high variance of the radar signal in high backscattering homogeneous areas or in non-homogeneous textured areas reduces the clusters separability and tends to produce over-segmentation, ii) large data volume (1.3 Gb).

For the first problem, the proposed wavelet multi-resolution decomposition/reconstruction technique is capable of generating an edge-preserving piecewise constant radar image. The radiometric characteristics of the reconstructed signal are closer to the piece-wise constant model required by a certain class of image-labeling algorithms. The proposed image-labeling techniques take into account multiplicative noise and within-class texture.

Large data volume problem was tackled by developing a special purpose processing chain that works on partially overlapping tiles extracted from the mosaic.

8.2.3 Validation of the classification maps and error analysis

Maps derived from Landsat Thematic Mapper (TM) are used as reference data to evaluate the maps derived from JERS-1 data.

The quantitative validation of the classification maps and error analysis of the deforestation estimates reveals that the classification approach, with wavelet image approximation pre-processing steps, provides a classification accuracy of 87% in forest/non-forest mapping.

The high performance of the wavelet-based algorithms can be ascribed to: i) the zooming capability of the wavelet transform which provides a better signal to noise ratio in areas corresponding to the thematic classes of interest; ii) an adaptive image approximation technique based on adaptive wavelet coefficient thresholding – a novel addition to the core algorithm – that improves the detection of fragmented areas with anthropogenic disturbances.

From the comparison between the two image-labeling techniques, it follows that the hybrid classifier results are computationally more efficient than the region-growing algorithm. The higher performance is confirmed by the degree of agreement between optical and radar data when the hybrid classifier is used.

The hybrid classifier was then selected for mapping the entire GRFM South America dataset. The comparison between the regional-scale vegetation map derived from the entire GRFM South America SAR data set and the TREES forest map - derived from 300 ERS ATSR-2 optical images - confirms the capability of the hybrid classifier to generalize over the entire GRFM data set.

A specific analysis by site allowed to highlight spectral and spatial differences with the reference data and to detect the major source of discrepancies and

misclassifications. A novel cartographic representation of the confusion matrix – dubbed confusion map – is introduced for quantifying and locating spatially points of agreement and disagreement between maps derived from different data sources.

The quantitative assessment of the mapping accuracy reveals that a high percentage of discrepancies between the two sources of information (SAR, optical data) are due to real changes of the imaged target that occurred between the two acquisition dates. This suggests that the rapid dynamic of the selected "hot spot" areas must be taken into due account.

SAR and optical observations are driven by different scattering mechanisms that arise in the landscape evolution during the deforestation process. This fact is particularly evident at the interface area between forest and clear-cuts, where it is more difficult to establish a unique descriptor of the intermediate deforestation steps (degraded forest, partial re-growth). The canopy density and soil conditions (roughness, moisture) play important roles in the radar backscatter from those interface areas.

The degree of agreement between SAR and TM derived maps depends on the deforestation pattern complexity measured by means of a spatial pattern measurement (perimeter over area). The decrease of agreement with the increase of landscape complexity can be mainly attributed to under-sampling of the spatial fragmentation in degraded forest areas at 100 m resolution.

8.2.4 Relative performances of a wavelet-based segmentation technique and ISODATA clustering

The relative performance of the wavelet-based region growing segmentation technique assessed with respect to a conventional clustering technique (ISODATA) revealed that the wavelet-based technique provides better accuracy and is capable of generalizing over the entire data set. The results are confirmed by confusion matrices,

overall accuracy, visual comparison of the derived maps, and from estimates for the Kappa statistic.

8.2.5 Extension of the thematic problem to include the degraded forest class

Discrepancy between maps derived from SAR and optical instruments turns out to increase when the class degraded forest is taken into account. The problem of forest degradation monitoring, generally ignored by Amazonian deforestation mapping programs, is investigated using both optical and SAR imagery.

For optical data, a three-stage classification procedure is developed for detecting degraded forest classes in Landsat TM images. The classifier is capable of managing spectral information on a different scale to preserve small but genuine regions. It is easy to use and robust to changes in input conditions. A test over two areas in Mato Grosso and in the Para' Brazilian state confirms Nepstad's speculation that present estimates of annual deforestation for Brazilian Amazonian capture less than half of the area that is impoverished every year.

For SAR data, a time-series of 8 JERS-1 full resolution (12.5 m) images acquired over the Mato Grosso is used to investigate the influence of spatial resolution on the thematic maps discrepancies by comparison with results obtained using the GRFM SAR mosaic (100 m). A multi-temporal speckle filtering technique is used to improve of the signal to noise ratio and obtain better estimates of the underlying SAR reflectivity for each image in the time series. In the filtered imagery small isolated and elongated bare soil regions that are regularly distributed in space are visually detectable in forest areas. These details could not be detected in the GRFM SAR mosaic. More future work is required for automatic extraction of these features but these preliminary results point to the possibility of zooming in the GRFM data set where higher spatial resolution historical JERS-1 multi-temporal datasets are

available. A mapping strategy based on multi-scale continental coverage (from 100 m down to 12.5 m) using all-weather SAR acquisitions could be supported by the forthcoming NASDA ALOS mission.

8.2.6 A model for correcting global estimates from local ones

An inductive learning methodology for correcting regional-scale low-resolution classifications which are affected by errors induced by the landscape fragmentation is tested. By correlation analysis we prove that this correction method is not applicable when Landsat TM maps (30 m pixel size) are used as local estimates to correct GRFM SAR maps (100 m pixel size). This is due to the fact that a spatial pattern measure – such as perimeter over area – at coarse resolution is not a good proxy variable for the fine scale spatial patterns.

A simulation exercise is set up using Landsat TM maps at 30 m pixel size as local high resolution classification estimates and the same maps scaled at 100m as lower resolution classifications. The trial indicates that in this case the conditions underpinning the method are met. Based on this simulation, we expect the correction method to work also in the case where maps derived from high-resolution (12.5 m) speckle filtered SAR images are used to correct regional-scale maps derived from the GRFM SAR mosaics.

8.2.7 Novel aspects and results

First novel aspect of this research work consists on the SAR dataset adopted. *The Global Rain Forest L-band JERS-1 radar mosaic over South America provides a unique and unprecedented snapshot of the humid tropical ecosystem of the Amazon Basin due to:* i) the semi-continental continuous coverage, ii) the approximately 100m resolution.

Only a few examples can be found in the literature with reference to the use of radar mosaics for global/regional scale mapping. *A new classification scheme for producing a high-resolution (100 m) regional scale forest-non-forest thematic map using the GRFM mosaic is developed in this research work.* The underpinning method is based on *a wavelet signal decomposition/reconstruction* technique. In the wavelet reconstruction algorithm, we introduce *an adaptive wavelet coefficient threshold* applied to the scale where the wavelet coefficients carry predominantly information on strong persistent edges and the noise influence has decayed significantly. In that way we can distinguish the local maxima related to the transition between classes of interest we want to separate (i.e. Forest/Non-forest transitions) from local maxima related to textural within-class variation.

Two image-labeling techniques are tested and compared: *i) region-growing algorithm* and *ii) a per-pixel two-stage hybrid classifier.* Both approaches rely on the wavelet pre-processing. The hybrid classifier is computationally more efficient.

As to regional/continental scale, the generation of thematic products from the high resolution GRFM radar mosaics poses challenging problems also with respect to *the determination of the accuracy of these estimates.* Quantitative validation and error analysis of regional area scale estimation are carried out comparing JERS-1 SAR maps with Landsat TM optical maps used as reference. A first result of the validation process is that the *wavelet-based classifier provides a classification accuracy of 87% in forest/non-forest mapping.* The analysis by site reveals that class *degraded forest is the major source of classification error.* The discrepancy between TM maps and SAR maps increases with the increment of the landscape spatial fragmentation.

A test on relative performances between the wavelet-based region growing segmentation technique and *a conventional clustering technique (ISODATA)* shows that the *wavelet-based technique provides better accuracy* and is capable of generalizing over the entire data set.

A novel three-stage classification scheme for *forest degradation phenomena detection in Landsat TM images* is proposed. Nepstad *et al.* speculated that present estimates of annual deforestation for Brazilian Amazonia capture less than half of the area that is impoverished every year. This statement is confirmed by our experiment.

The issue of detecting the degraded-forest class is attacked also using SAR data. A *multi temporal speckle filtering technique is applied to a time-series of a full-resolution JERS-1 SAR images* (12.5 m pixels size) to catch those small isolated and elongated bare soil regions regularly distributed in the forest and related to selective logging degradation. First results reveal the possibility of zooming in the GRFM data set where higher spatial resolution is required using historical JERS-1 multi-temporal datasets.

Starting from the consideration that the discrepancy between TM maps and SAR maps increases with the increment of the landscape spatial fragmentation we test an *inductive learning methodology, capable of correcting SAR regional-scale maps using local classification estimates at a higher resolution*. It is proven that the methodology is not applicable when Landsat TM maps are used as local classifications to correct regional-scale maps derived form GRFM radar mosaics. Correction is possible when using maps at different resolution but derived from the same satellite sensor. An experiment using Landsat TM maps - as local estimates at higher resolution - for correcting the same maps scaled at a pixel size of 100 m, suggests that *GRFM regional maps could be corrected using maps derived from speckle-filtered high-resolution (12.5 m) SAR imagery*.

8.3 Seed ideas on ways to reduce the pressure over the tropical forest ecosystem

8.3.1 Deforestation detection in the tropics

Earth observations by satellite provide a unique technology to acquire quantitative information on forest ecosystems at regional scale. As a case in point we propose here an approach to estimate tropical vegetation cover using as data source continental scale Synthetic Aperture Radar (SAR) mosaics at 100 m spatial resolution. Estimates provided by satellite observations constitute one input in the panoply of data needed by forest management and for the preservation process.

The *objective* of all people involved in forest management (local population, politicians, and industry executives) should be *to preserve and use this resource* with *sustainable criteria*, which means that the forest should be able to fulfill its functions now and in the future (Lammerts van Bueren and Blom, 1997). The extreme vulnerability of tropical rainforest ecosystem calls for adequate forest management techniques.

Just enclosing tropical forests in wide parks was proven to be inadequate against tropical rain forest depletion. Many examples of 'paper parks' draw the attention to two fundamental factors to be considered for tropical forest protection:

1. Forest protection must involve its human inhabitants and several contextual factors must be taken into account.
2. Tropical rainforests are mainly geographically located in developing countries for which they constitute a fundamental resource. Starvation and poverty are priority problems in many of these countries.

Many national, continental and global efforts to manage in a sustainable way and protect tropical rain forests exist. It is beyond the scope of this thesis to give an exhaustive description of these efforts. We want only to cite a particular example of

an effort to reduce the pressure over the tropical forest. This case seems particularly interesting because it offers at the same time support and resources for the local population. The example refers to the forest management methodology proposed and taught by Agricultural School "*Rainha Dos Apostolos*" in Manaus, which we had the chance to visit during a field trip in the Brazilian Tropical Forest.

8.3.2 "Agro-Forest Systems": a starting point against deforestation

Agricultural methods traditionally used for temperate climate are inadequate for tropical area. As a consequence degradation and the soil impoverishment are increased. Forest exploitation for massive ranching and pasture, typically applying complete forest clear-cuts, is the major cause of the unrecoverable soil impoverishment in South America.

The *pasture scenario*, chosen to represent deforestation in Amazonia, shows that *nutrient-poor soils and poor pasture management practices accelerate the degradation of soil and vegetation cover*, causing its abandonment after a few years of use. Soil in the undisturbed forest presents small amounts of phosphates with stable bounds with Fe and Al which guarantee low-acidity soil conditions. *Deforestation practices, based on clearing and burning, decrease the soil acidity; release cations* (positively charged ions) *and phosphates* into the soil and increase fertility for a couple of years. Thereafter, cations leaching from the system, increase of soil acidity, phosphates unavailability and the reduced buffering capacity of the dwindling supply of organic materials renders the soil structure more like a clay than a loam, as it is in the forest domain. The reduced soil fertility pushes farmers to clear new forest area starting an unsustainable cycle. (Prance and Lovejoy, 1985; Wilding *et al.,* 1983; Uhl *et al.,* 1998).

The inhabitants of the Amazonian region have been living for centuries of the products offered by the forest, *while today they are recording a remarkable decrease of these products*. Etno-botanists have observed that Kajapò Indios know the particular soil properties and they use *to leave the papaya seeds* within ashes of the fires in their villages. In that way a new plant has a higher the probability to grow.

It is therefore necessary to learn from these examples how to cultivate the forest, respecting it, and at the same time to increase productivity. However, it is not possible to leave the digging out stage and enter the production phase, failing the technical and cultural tools necessary to make a qualitative leap in the approach to environment.

The school of agriculture "*Rainha dos Apolostolos*", located 30 km from Manaus, in the heart of the Amazonian forest (see figure 8.1), is an attempt to meet this requirement. Every year the school welcomes some *300 "indios",* sons of small agricultural producers of the internal regions, to offer them a human and vocational training. *Teaching includes production and breeding techniques and methods* that may be reproduced in the places of origin, to contribute to the improvement of the living conditions of the local communities and at the same time to safeguard and maintain the Amazonian ecosystem. The school represents *a unique reality of this kind*: in the Amazonian region there are very few public or private institutes training technicians for the agricultural world, but all of them are more oriented toward work in large farming activities, rather than in the small internal realities which represent the majority. In particular the school is applying for educational purposes the so-called “Agro-Forest System” (AFS).

AFS is an agricultural technique that is adequate for an eco-sustainable usage of the tropical forest ecosystem based on the following principal criteria:

1) *The highest trees* (valued species) *are maintained in order to adequately guarantee organic soil nutrition,* to prevent sunlight to penetrate to the forest floor drying out the organics debris and to avoid soil erosion caused by rains.
2) *The free spaces in the understory is used for plantation of fruiting plants* adequately distributed on the ground and with an height profile that guarantee good sunlight penetration.

This Agricultural school was founded in 1970 for children coming form the small rural areas of the Amazon Region. Now 250 pupils follow the primary and secondary courses learning how to use the deforested area for a sustainable agriculture and pasture. During the courses they learn how to handle land-use cycling in order to reduce the soil nutrients impoverishment.

A research program with ENBRAPA / CPAA (Manaus) is *set up to assure re-growth of vegetation with the same bio-diversity present in the primary forest*. The school is sustained by Municipal Prefecture of Manaus, the International N.G.O. A.V.S.I., the European Community (C.E.E.) and Episcopal Italian Conference (C.E.I.) (de Benayon *et al.,* 1999).

Figure 8.1: Agricultural School "*Rainha Dos Apostolos*": the students can also learn aquaculture techniques (see color Figure B.28 - Appendix B, pp. 226).

Appendix A

Swamp forest map from high-water, low-water and texture GRFM mosaics

The GRFM data set over South America comprises three layers: radar backscatter acquired in the dry season (when the river staging is low, and therefore dubbed low-water mosaic), radar backscatter acquired in the wet season (when the river staging is high, and dubbed high-water mosaic), and a texture measure calculated using the high resolution backscatter data (12.5 m pixel spacing) acquired in the dry season (dubbed texture mosaic). The texture measure is the normalized standard deviation of intensity estimated by an 8x8 blocking window of the high resolution data. The color composite of high water mosaic (red channel), low water mosaic (green channel), and low water texture (blue channel) is reported in figure A1.

As explained in chapter 2, the core of the work presented in this thesis is based on the analysis of the low-water amplitude data set only, which is sufficient with respect to the stated thematic goal, namely deforestation mapping. However the thematic information that can be extracted from a combination of the low water, high water and texture mosaic is obviously much richer (Rosenqvist *et al.,* 1998 and 1999).

A similar passage from single source to multi-source data strategy can be found historically in the context of TREES project. Here a first "TREES 1" map of the humid forest of tropical South America was based on a single NOAA-AVHRR data source (Eva *et al.,* 1999). A new map was created in 2002 featuring a larger geographical region and providing a richer thematic content (Eva *et al.,* 2002). To the

purpose data sets from four instruments were used: Along Track Scanning Radiometer (ATSR-2) onboard the ERS-2 satellite, SPOT VGT onboard the SPOT 4, NASDA JERS-1 SAR, and Defense Meteorological Satellite Program (DMSP) Operational Linescan System (OLS). Each data source contributed to mapping a specific ecosystem or land cover, seasonality or water regime.

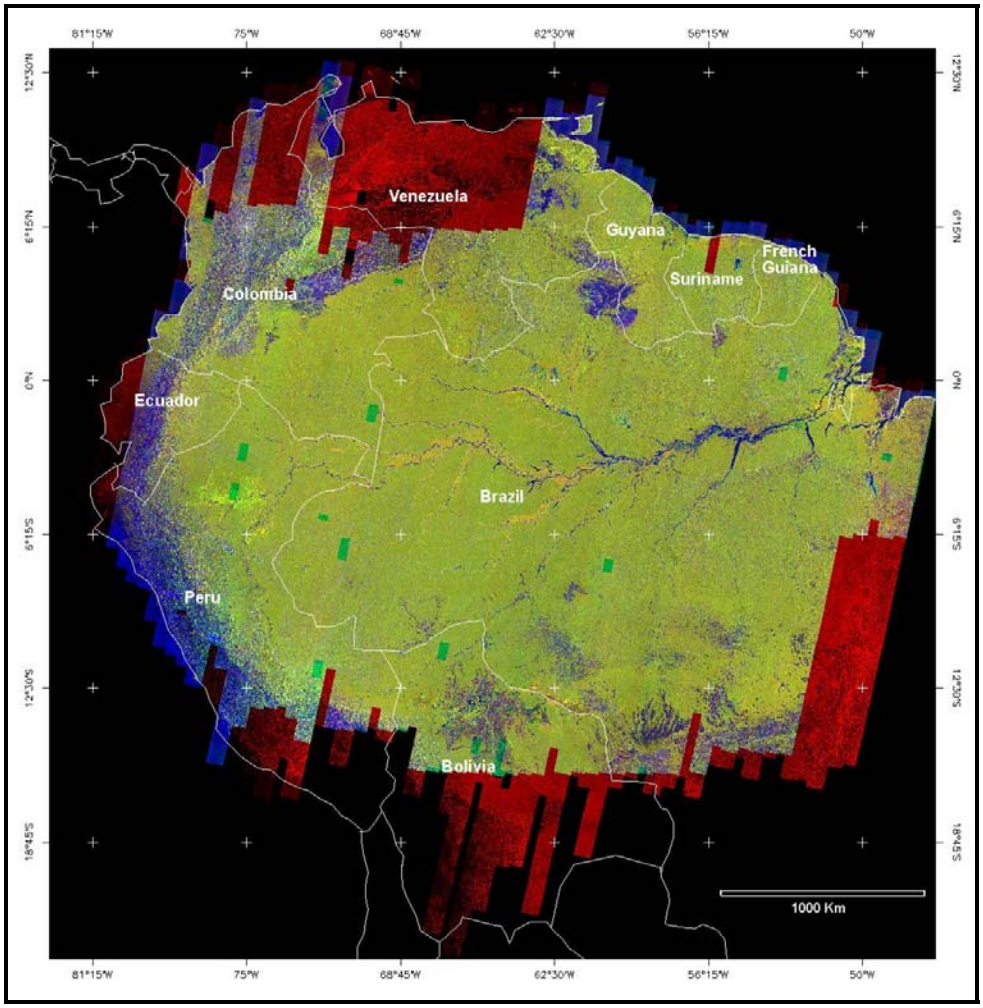

Figure A.1: Color composite of the GRFM radar mosaic layers. High water amplitude (red channel), low water amplitude (green channel), low water texture (blue channel) (see color Figure B.29 - Appendix B, pp. 227).

In particular, the GRFM mosaic layers are used to map areas of flooded forest. The new vegetation map of South America is described in this Appendix. The usefulness of a multi-sensor approach and the added thematic value offered by the GRFM mosaics are clearly demonstrated by this product. Also the possibility of adapting the classification approach proposed in this thesis to other thematic contexts is proven.

Methodological Approach

The proposed classification approach consists of: i) pre-processing stage for the generation of edge-preserving smooth approximations of the radar imagery, and ii) decision tree, ruled based, clustering technique for thematic information extraction.
The wavelet multi-resolution decomposition/reconstruction technique, described in chapter 3, is employed in the pre-processing phase to generate an edge-preserving piecewise constant low-water texture image. The radiometric characteristics of the reconstructed signal are at this stage a closer approximation to the piece-wise constant model required by the clustering algorithm.

The image labeling method consists of a decision tree clustering technique that comprises the following steps (see figure A1):

1) The piecewise constant low-water texture image is clustered according to thresholds derived from a training set. A segmented image is generated.
2) Inside each segment a threshold is applied to the low-water amplitude. A segmented image is generated.
3) Inside each segment a threshold is applied to the high-water amplitude. The final thematic map is generated.

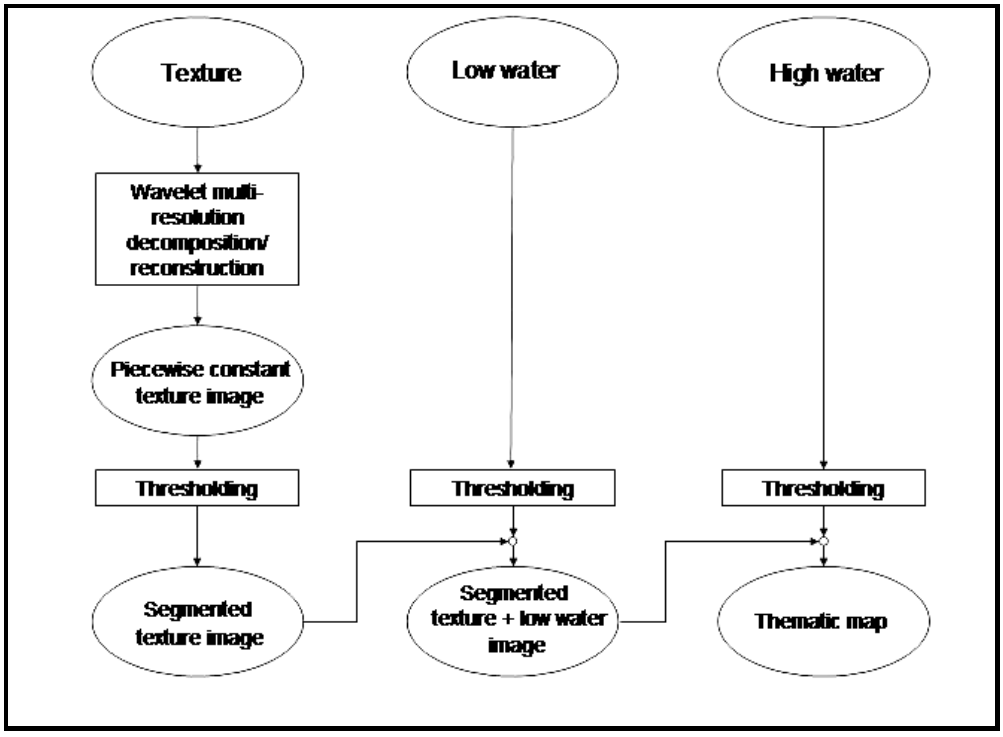

Figure A.2: Schematic view of the image labeling method

Two properties of the imagery underpin the classification method: i) the radar backscatter is enhanced by the presence of water under the forest canopy, due to double bounce scattering between the trunks and the water table, ii) in the texture image the primary rain forest features higher values than the swamp forest due to the spatial heterogeneity of the upper canopy layers of the former (micro-topography effect) (Williams, 1997; De Grandi *et al.,* 2000a).

We define the following land-cover classes (in agreement with the TREES map) and the following rules:

1) *Swamp forest- permanently flooded:* characterized by low texture values ($\leq$ 70 *DN*) and high amplitude values in both seasons (> 100 *DN*)

2) *Swamp forest- seasonally flooded:* characterized by low texture values (< 70 *DN*) and low amplitude values during one season (< 100 *DN*) and high amplitude values in the other one (> 75 *DN*).
3) *Low land forest seasonally flooded:* characterized middle low texture values (58 *DN* <Txr ≤ 70 *DN*) and low amplitude values (<100 *DN*) during one season and high amplitude values in the other one (>100 *DN*).
4) *Low land forest:* characterized middle low texture values (58 *DN* <Txr ≤ 70 *DN*) and in both the seasons amplitude values: 75< *DN* < 125
5) *Up land forest:* characterized by high texture values (70 *DN* <Txr ≤ 95 *DN*) and amplitude values: 75 < *DN* < 125.
6) *Non forest - savanna:* characterized by high or texture values (70 *DN* <Txr ≤ 95 *DN* or Txr > 96 *DN*) and low amplitude values (*DN* < 100)
7) *Non forest:* characterized by very low texture values (Txr < 50 *DN*) and variable amplitude values (<100 *DN* or > 145 *DN*)
8) *Water:* (rivers and lakes) characterized by very high texture values (Txr > 96 *DN*) and very low amplitude values.

Swamp forest differs from lowland forest mainly for the low texture value due to its different structure. Also up land forest can be discriminate from lowland forest due to its higher texture values. In this case the differences in texture values are mainly related to the terrain topography. Generally low land forest is in flat area with no topography or "micro-topography" effects, while up-land forest grows in undulated terrains where topography influences the texture values.

Nine training/testing sites were selected within the geographical GRFM mosaic coverage to be representative of the thematic context. Within the nine sites 186 regions of interest (ROI) were defined. For each site a vector map was derived from optical images (Landsat TM, SPOT). These images were made available by the

TREES project. The high water GRFM mosaic with 9 overlaid training/testing sites is shown in figure A.3.

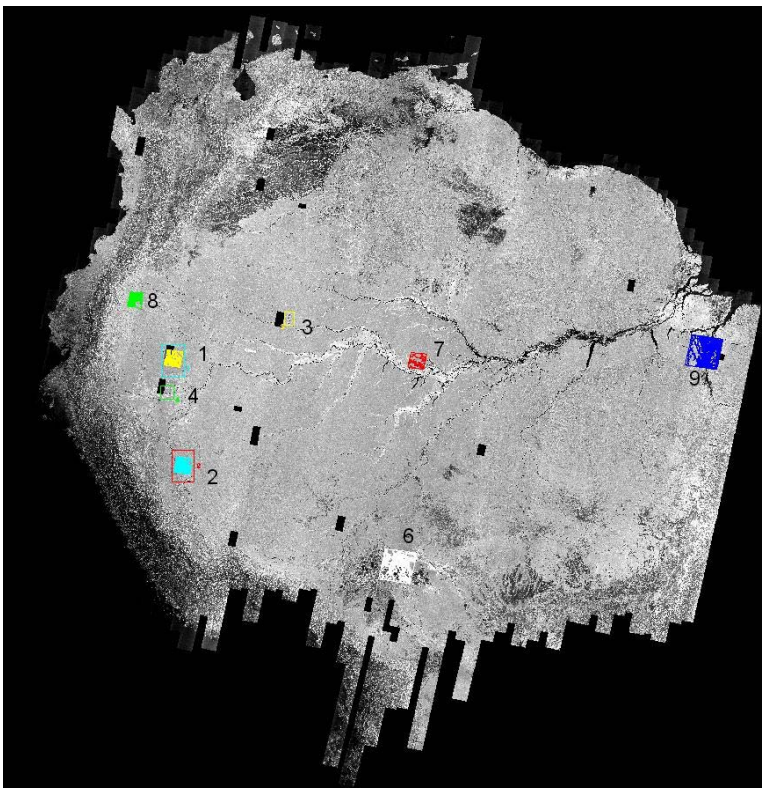

Figure A.3: The high water GRFM mosaic with 9 overlaid training/testing sites (see color Figure B.30 - Appendix B, pp. 228).

Two scatter plots (*DN* low water texture vs. *DN* low water amplitude, *DN* low water texture vs. *DN* high water amplitude) were used to establish the thresholds for the decision tree. By this process 37 classes were obtained and were combined into the 8 classes of interest. The thresholds for the decision tree and the corresponding thematic classes are reported in table A1 (where LW = GRFM low water amplitude (*DN*), HW = GRFM high water amplitude (*DN*), Txr = GRFM low water texture (*DN*).

Table A.1: Threshold values for the decision tree (*DN* values)

Txr ≤ 50	LW ≥ 100	HW ≥ 100	1 Swamp forest- permanently flooded
		HW < 100	2 Swamp forest- seasonally flooded
	LW ≤ 100	HW ≥ 100	3 Swamp forest- seasonally flooded
		HW < 100	4 Swamp forest- seasonally flooded
50<Txr ≤ 58	LW ≥ 100	HW ≥ 100	5 Low land forest
		HW < 100	6 Swamp forest- seasonally flooded
	LW ≤ 100	HW ≥ 100	7 Swamp forest- seasonally flooded
		HW < 100	8 Non classified
58<Txr ≤ 70	LW > 145	HW >1 45	9 Swamp forest- permanently flooded
	125< LW ≤ 145	HW >1 45	10 Low land forest seasonally flooded
		125< HW ≤ 145	11 Low land forest seasonally flooded
		HW ≤ 125	12 Low land forest
	100< LW ≤ 145	HW > 125	13 Low land forest
		100< HW ≤ 125	14 Low land forest
		HW ≤ 100	15 Low land forest
	75< LW ≤ 100	HW > 100	16 Swamp forest- seasonally flooded
		75< HW ≤ 100	17 Swamp forest- seasonally flooded
		HW ≤ 75	18 Swamp forest- seasonally flooded
	LW ≤ 75	HW ≤ 75	19 Non forest - savanna
70<Txr ≤ 95	LW > 145	HW >1 45	20 Non forest
	125< LW ≤ 145	HW >1 45	21 Non classified
		125< HW ≤ 145	22 Non classified
		HW ≤ 125	23 Up land forest
	100< LW ≤ 1425	HW > 125	24 Up land forest
		100< HW ≤ 125	25 Up land forest
		HW ≤ 100	26 Up land forest
	75< LW ≤ 100	HW > 100	27 Up land forest
		75< HW ≤ 100	28 Up land forest
		HW ≤ 75	29 Non forest - savanna
	LW ≤ 75	HW ≤ 75	30 Non forest - savanna
Txr > 96	LW ≥ 100	HW ≥ 100	31 Non forest - savanna
		HW < 100	32 Non forest
	LW < 100	HW ≥ 100	33 Non classified
		HW < 100	34 Non classified
	LW< 50		35 Water

A sample color composite of the high water amplitude, low water amplitude and low water texture (wavelet filtered) GRFM images of the Peru site (training/testing site number 4) is reported in figure A.4a.

The SAR mosaics can be compared with a Landsat TM auxiliary image available on the same area (figure A.4b) where sites a) and b) are indicated from ground surveyors as permanently flooded forest (*a) Pantanos del sistema botenico del Pastaza, b) Pantanos en el sistema desposicional de Ucamara*). The two scatter plots (*DN* low water texture vs. *DN* low water amplitude, *DN* low water texture vs. *DN* high water amplitude), relative to the Peru site are reported in figure A.5 a and b.

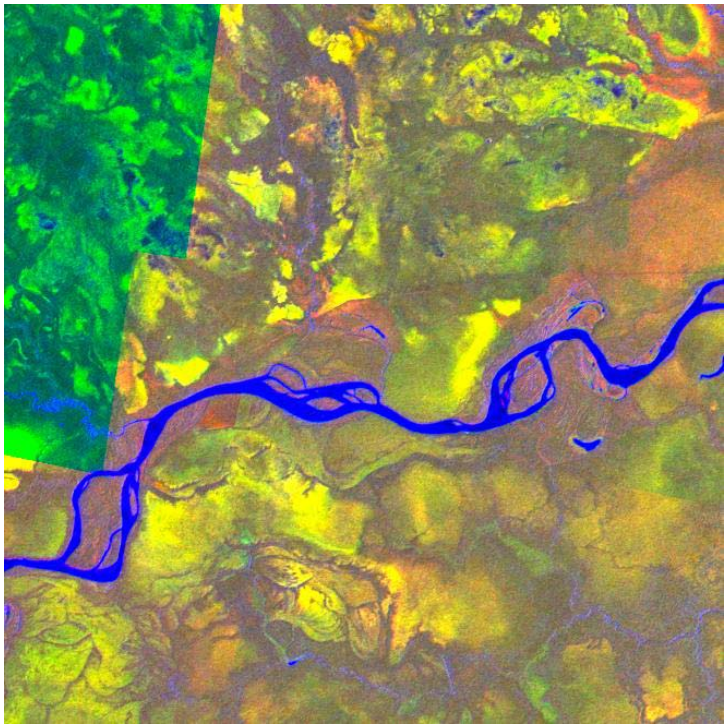

Figure A.4 a: The color composite of high water amplitude, low water amplitude and low water texture (wavelet filtered) GRFM images of the Peru site (training/testing site number 4) (see color Figure B.31 - Appendix B, pp. 229).

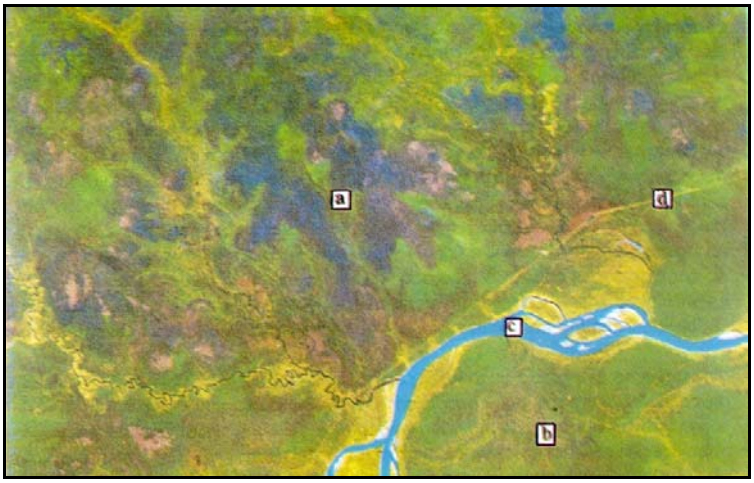

Figure A.4 b: Landsat TM auxiliary image available over the Peru site. Sites a) and b) are indicated from ground surveyors as permanently flooded forest (see color Figure B.32 - Appendix B, pp. 230).

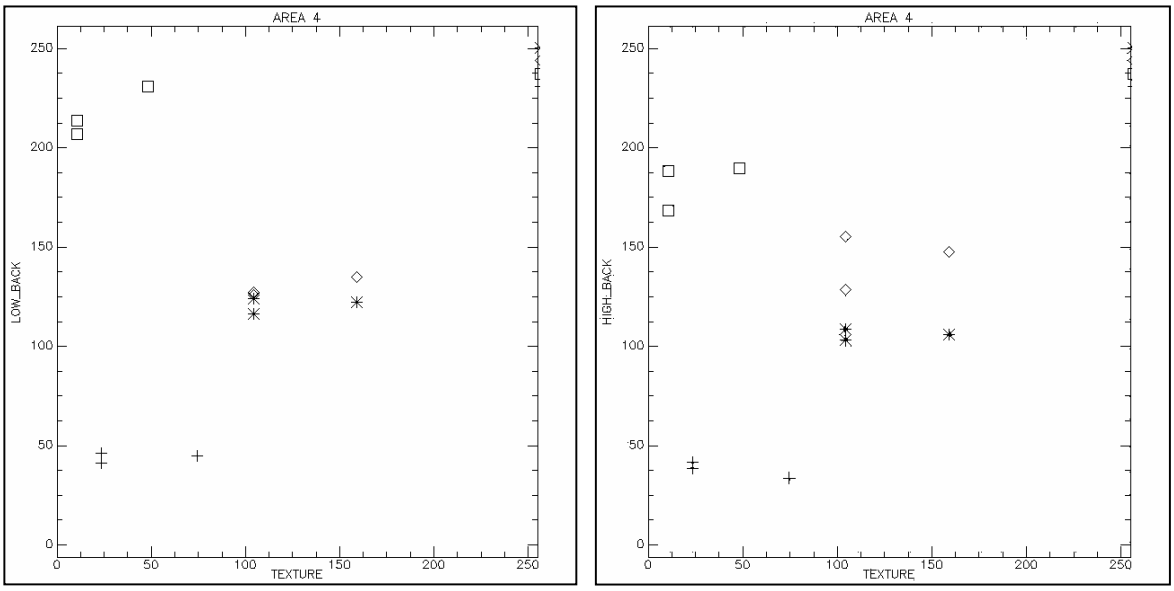

Figure A.5 a and b: The two scatter plots (*DN* low water texture vs. *DN* low water amplitude, *DN* low water texture vs. *DN* high water amplitude) relative to the Peru site.

Results

The final thematic map was obtained processing smaller (660*660) partially overlapping tiles extracted from the mosaics (see Chapter 3). The overlapping area prevents border effects when the output map is generated by assembling the classifications of the single tiles.

Some examples of the original GRFM mosaics and the derived thematic maps over four sites geographically distributed within the Amazon basin are shown in figure A.6 (delta Amazon River), figure A.7 (delta Orinoco river), figure A.8 (Rio Negro river), and figure A.9 (region in Peru). The thematic maps can be compared with the color composite of the high water amplitude, low water amplitude and low water texture images.

Several continental and country maps covering the 9 training/testing sites were used for map validation based on visual comparison by an expert photo-interpreter. A more complete validation exercise was performed on the final TREES map resulting from the combination of GRFM, ATSR-2, SPOT VGT and DMSP-OLS data sets. A list of maps consulted for the validation is reported in (Eva *et al.,* 2002). The GRFM swamp forest map is shown in figure A.10

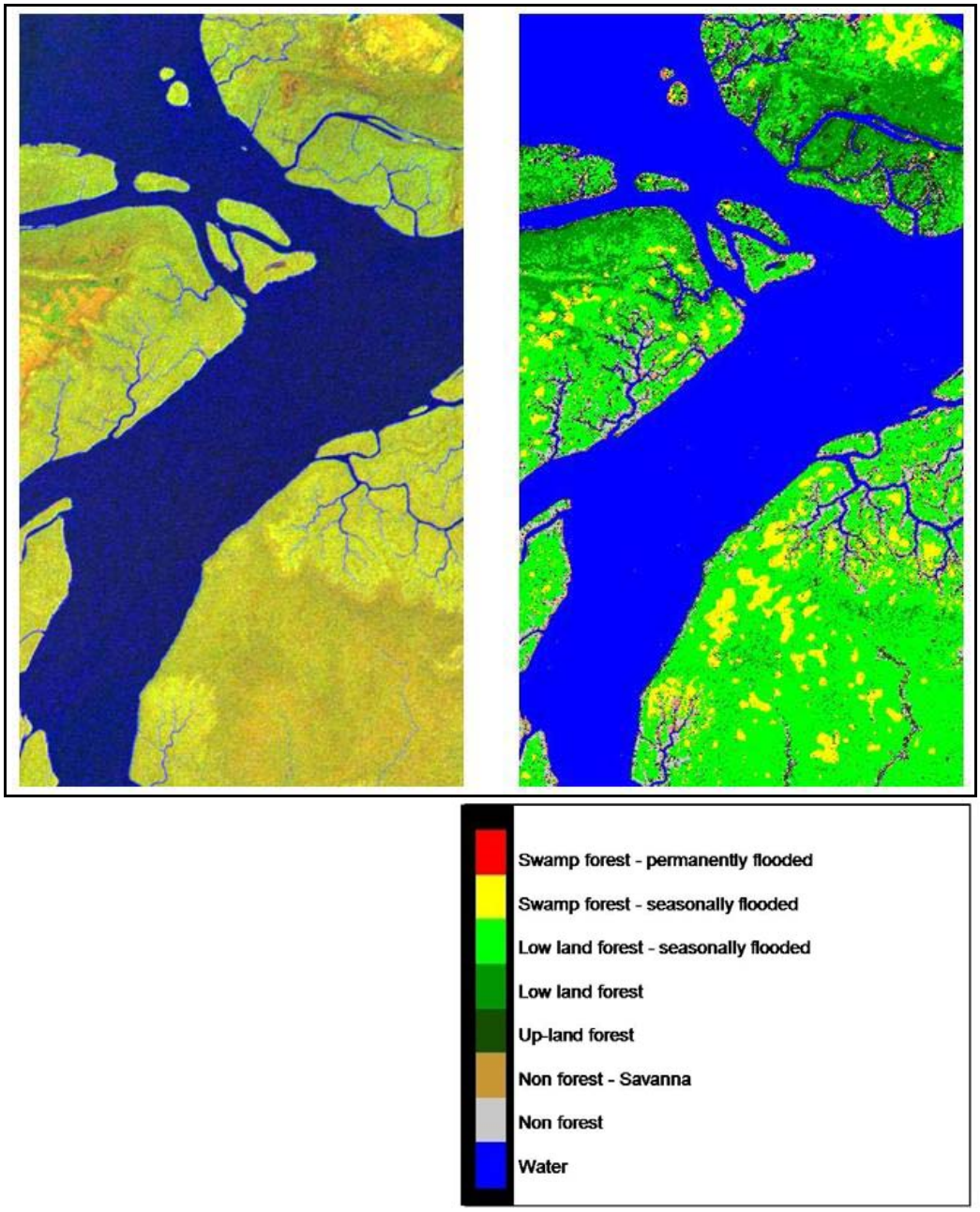

Figure A.6: GRFM color composite image and swamp forest map over the delta of the Amazon River (see color Figure B.33 - Appendix B, pp. 231).

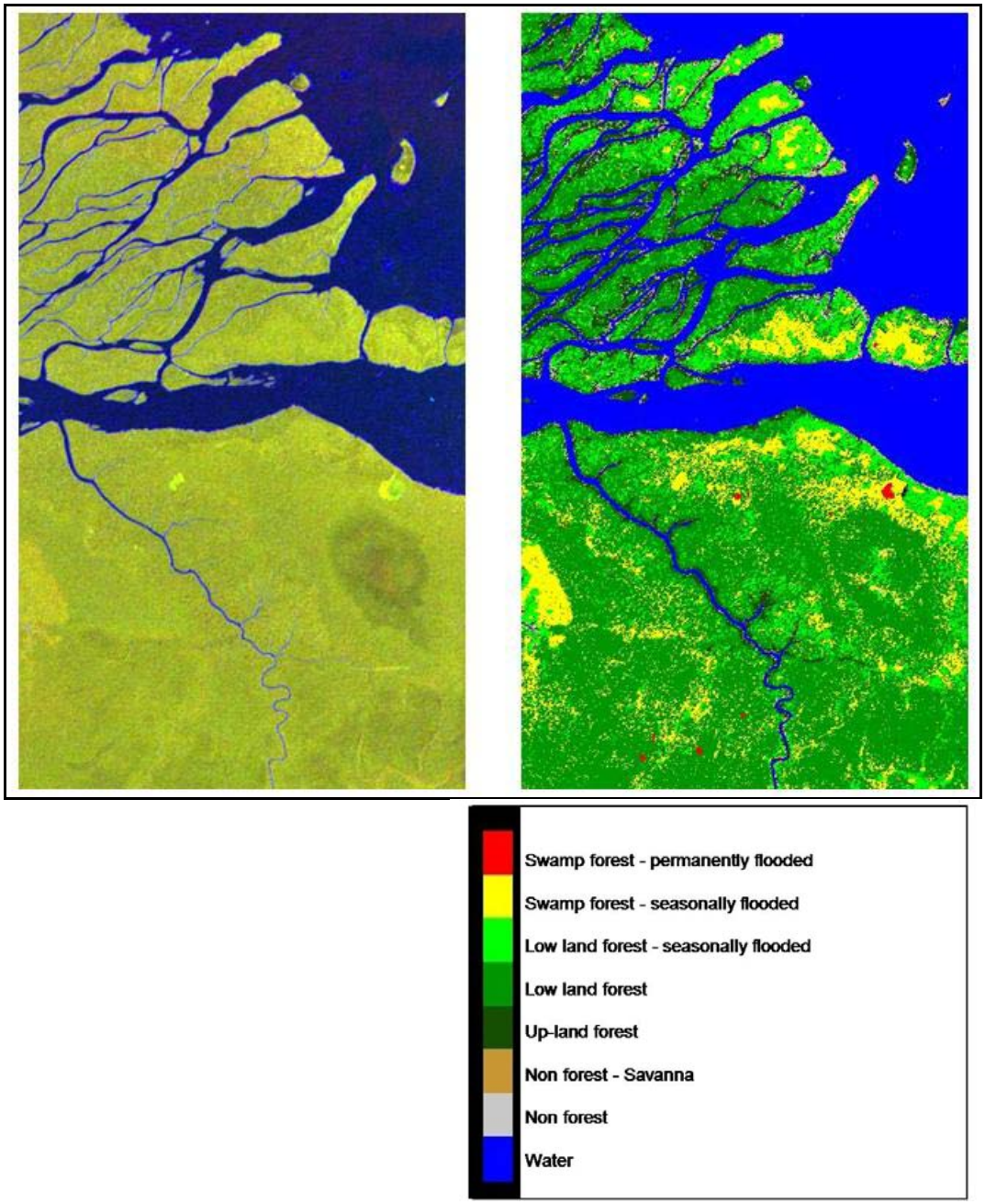

Figure A.7: GRFM color composite image and swamp forest map over the delta of the Orinoco River (see color Figure B.34 - Appendix B, pp. 232).

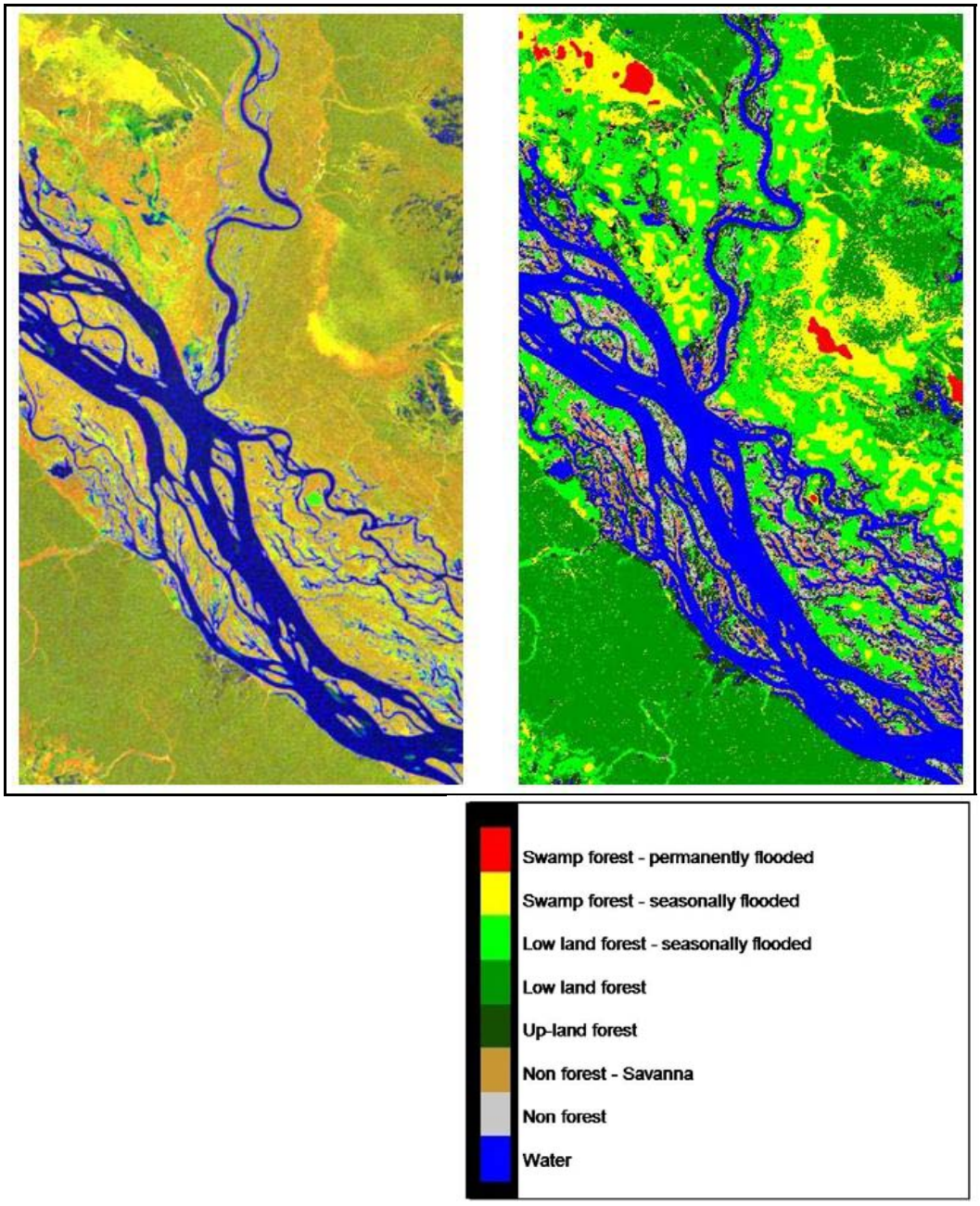

Figure A.8: GRFM color composite image and swamp forest map over an area around the Rio Negro River (see color Figure B.35 - Appendix B, pp. 233).

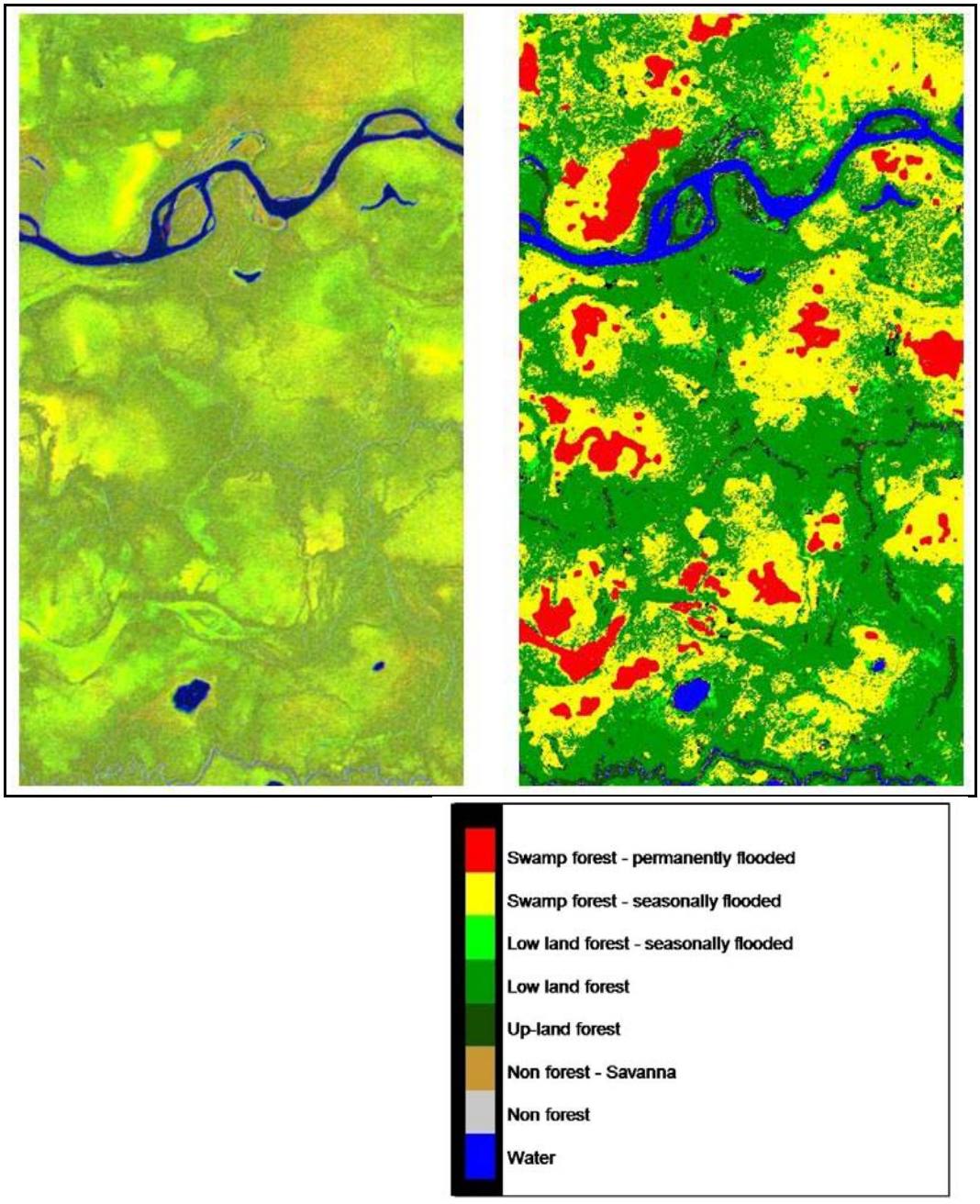

Figure A.9: GRFM color composite image and swamp forest map over a region in Peru state (see color Figure B.36 - Appendix B, pp. 234).

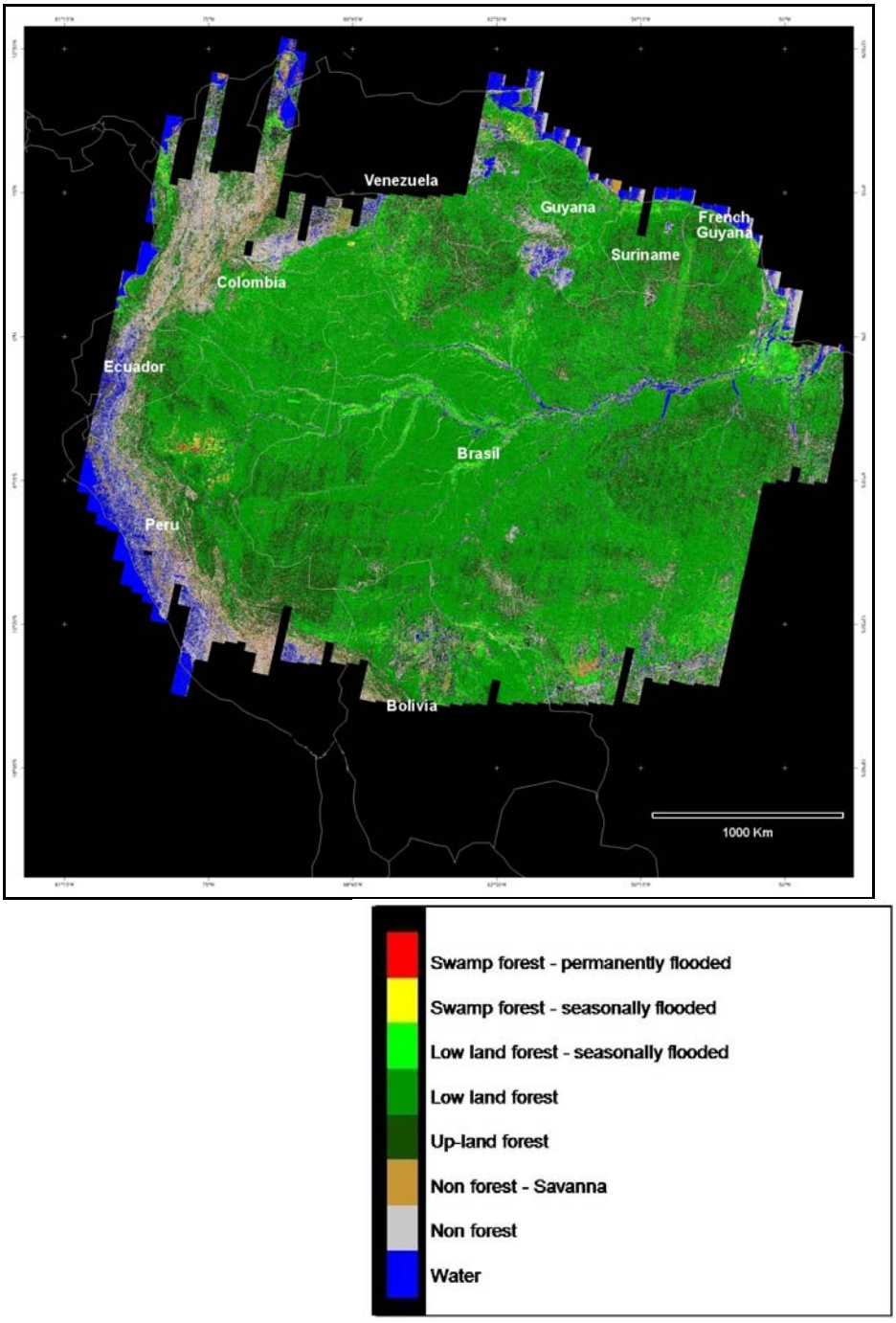

Figure A.10: The GRFM swamp forest map of South America (see color Figure B.37 - Appendix B, pp. 235).

Appendix B

Color Figures

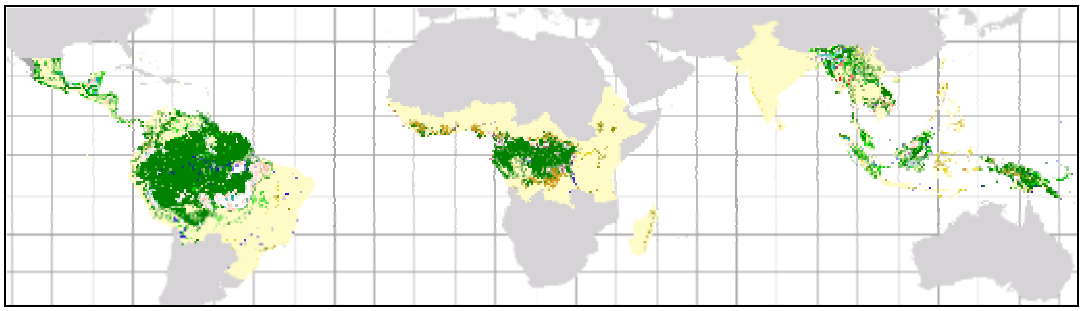

Figure B.1: Geographical location of the Tropical forest belt

Figure B.2: The photo, taken in Brazilian Amazonia, shows a deforested area where the ground was cleared by fire.

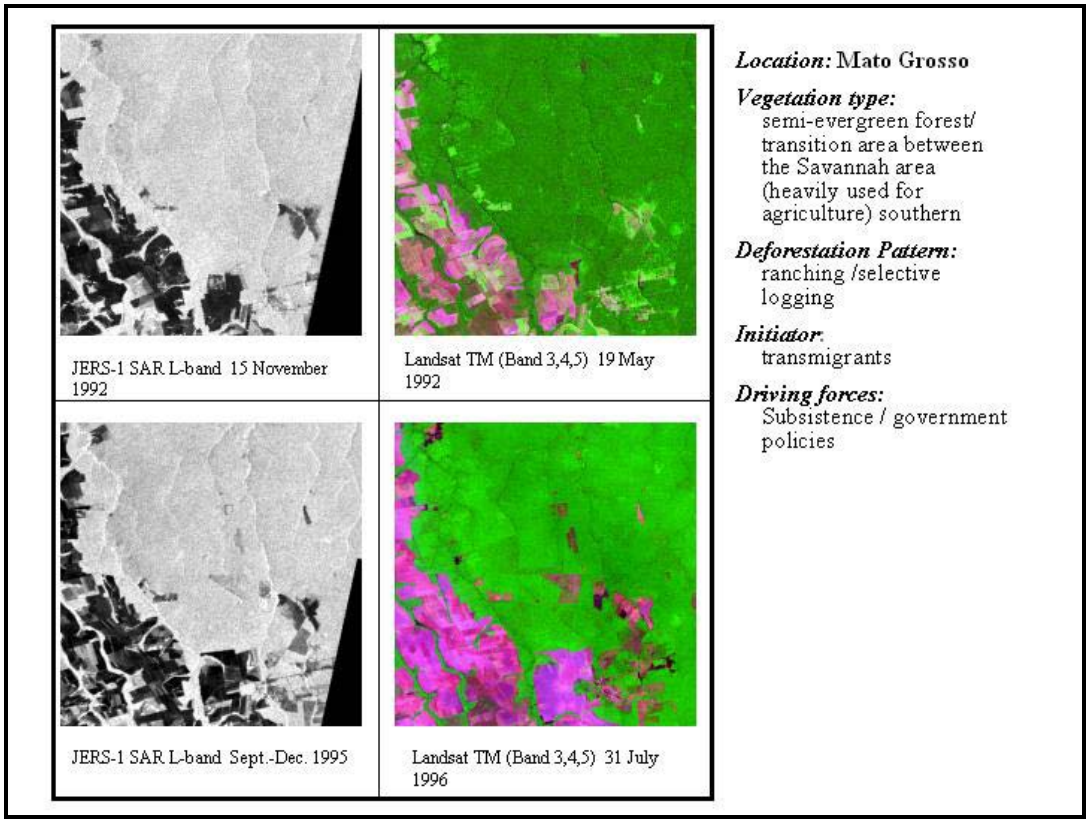

Figure B.3: SAR L-band 100 m and the corresponding Landsat TM over Mato Grosso site. Descriptive parameters of this site are also reported.

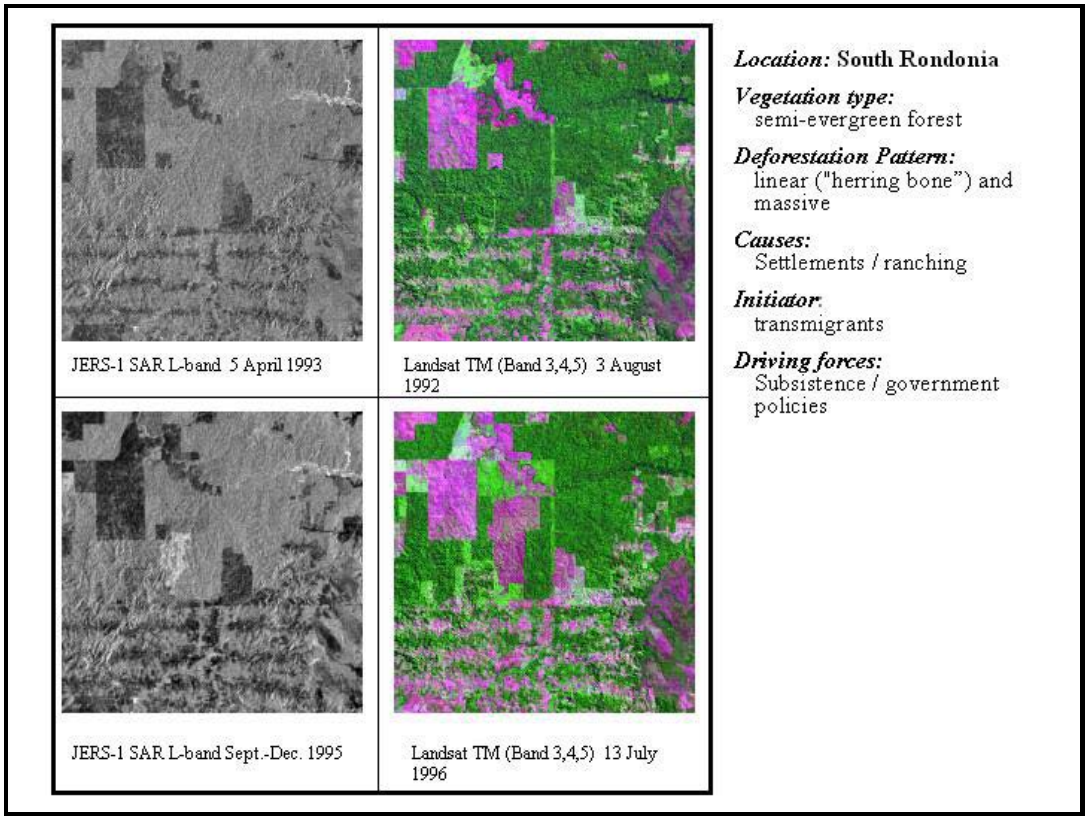

Figure B.4: SAR L-band 100 m and the corresponding Landsat TM over Rondonia site. Descriptive parameters of this site are also reported.

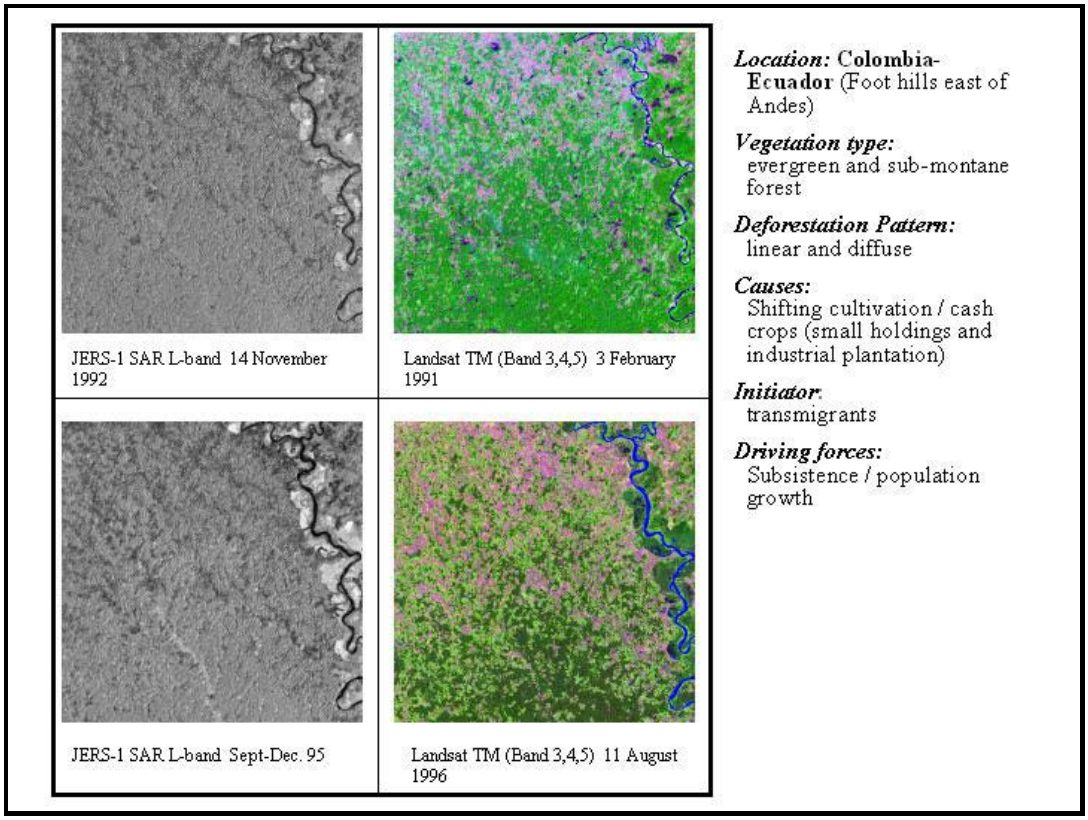

Figure B.5: SAR L-band 100 m and the corresponding Landsat TM over Florencia-Napo site. Descriptive parameters of this site are also reported.

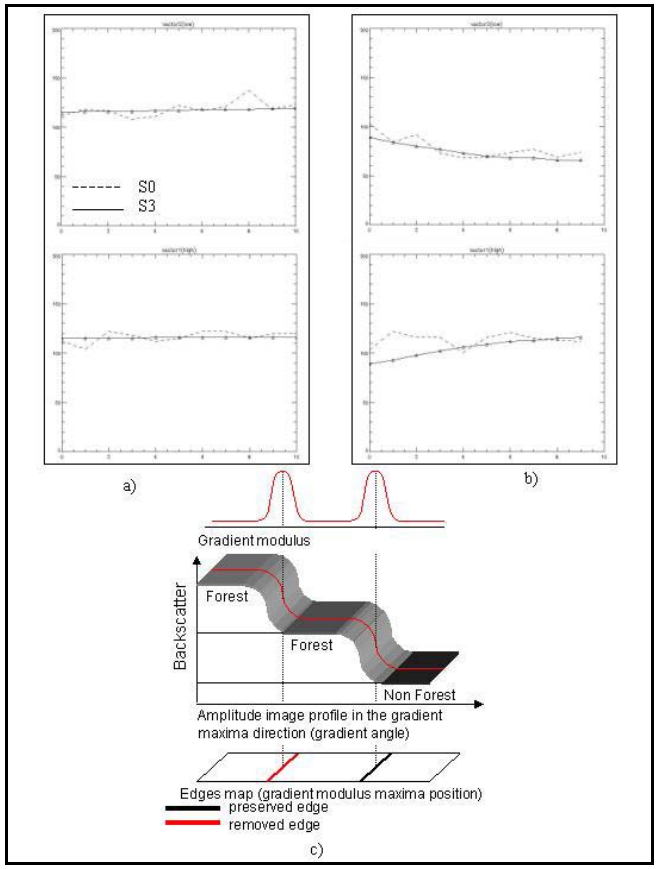

Figure B.6: a) and b) signal statistics (mean, standard deviation) collected along the profile from the local maxima position up to the closest local maxima are indicated by triangles. c) Diagram illustrating the principle of the rule-based mechanism used to distinguish between gradient modulus local maxima related to forest/non-forest inter-class transitions (to be preserved), from those related to forest within-class texture variations (to be removed).Statistics from profile a) correspond to intra-class signal variation (forest signal textural variations) and the related modula maxima will be not considered for the image reconstruction. b) Correspond to inter-class signal variation (forest – non-forest signal textural variations) and the related modula maxima will be considered for the image reconstruction.

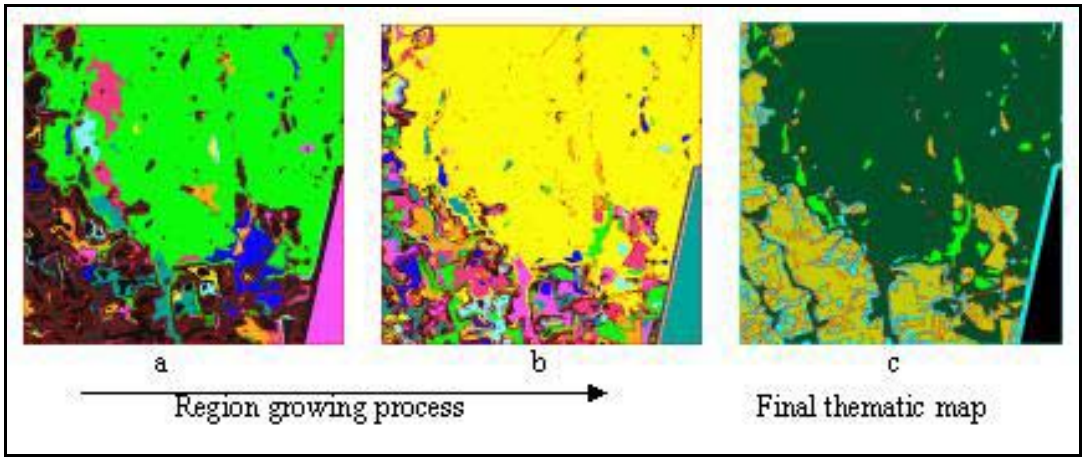

Figure B.7: Representation of 2 steps in the region growing processes (a, b) up to the final thematic map (c).

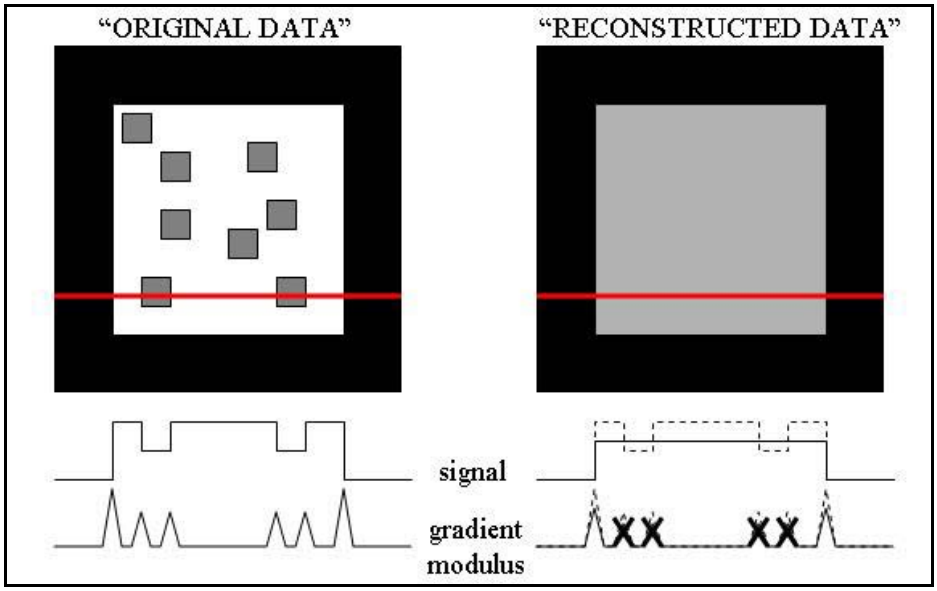

Figure B.8: Schematic representation of degraded forest class (i.e. mosaic of isolated forest region surrounded by a forest area). In the reconstructed signal these mixed classes will be perceived as a piece-wise region.

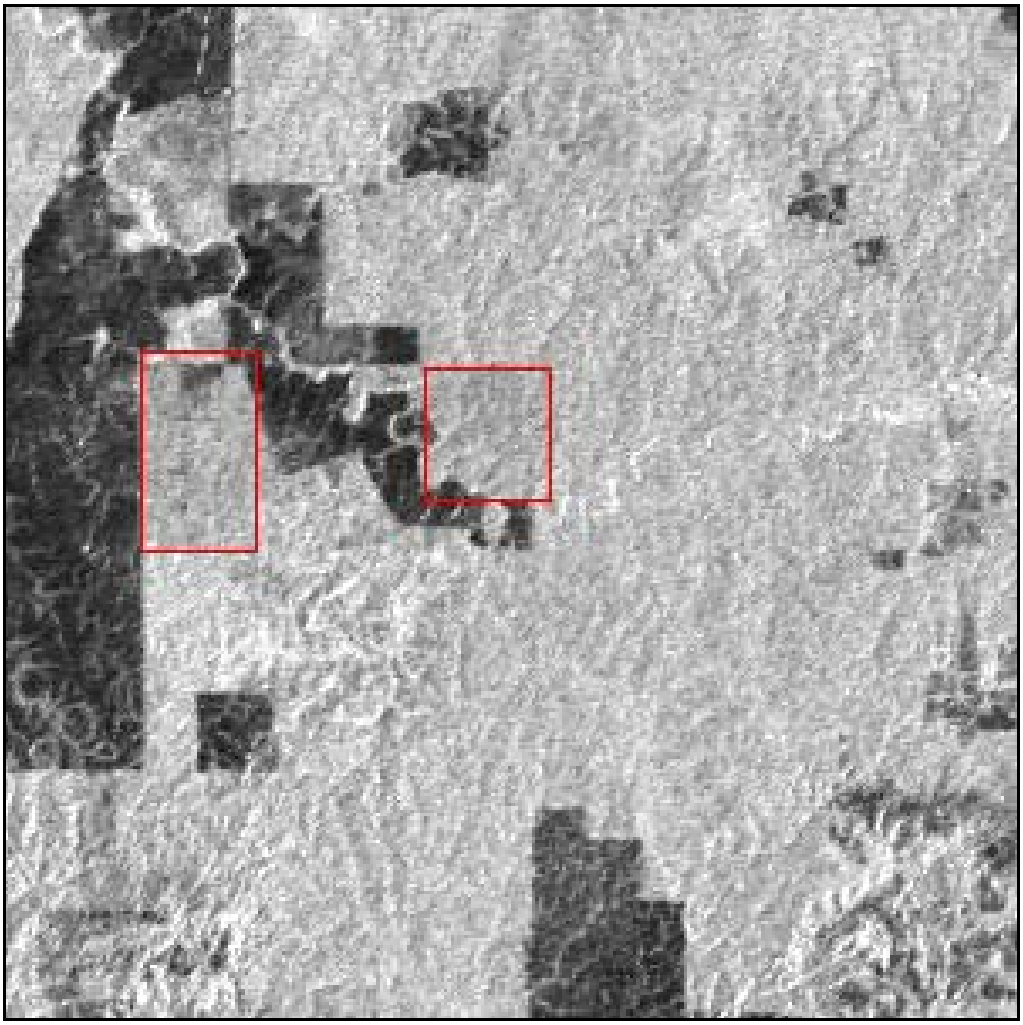

Figure B.9: Degraded forest class: abandoned pasture with partial re-growth forest in the 2 red boxes (*DN*=100, σ^0 =-8.54). Image area: 30x30 km^2.

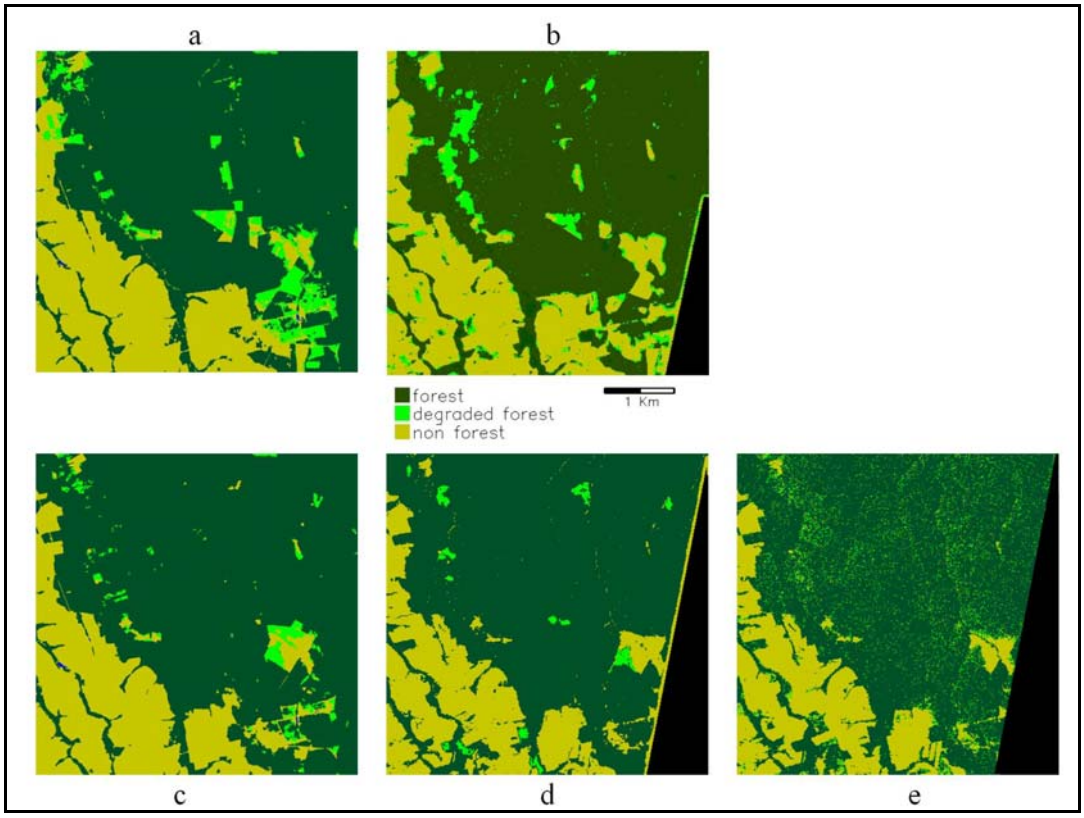

Figure B.10: 1996 and 1992 TRFIC maps for the Mato Grosso site (a, c.). Hybrid classifier map (1995 data set) (b). ISODATA and region growing (1992/93 data set) (d, e).

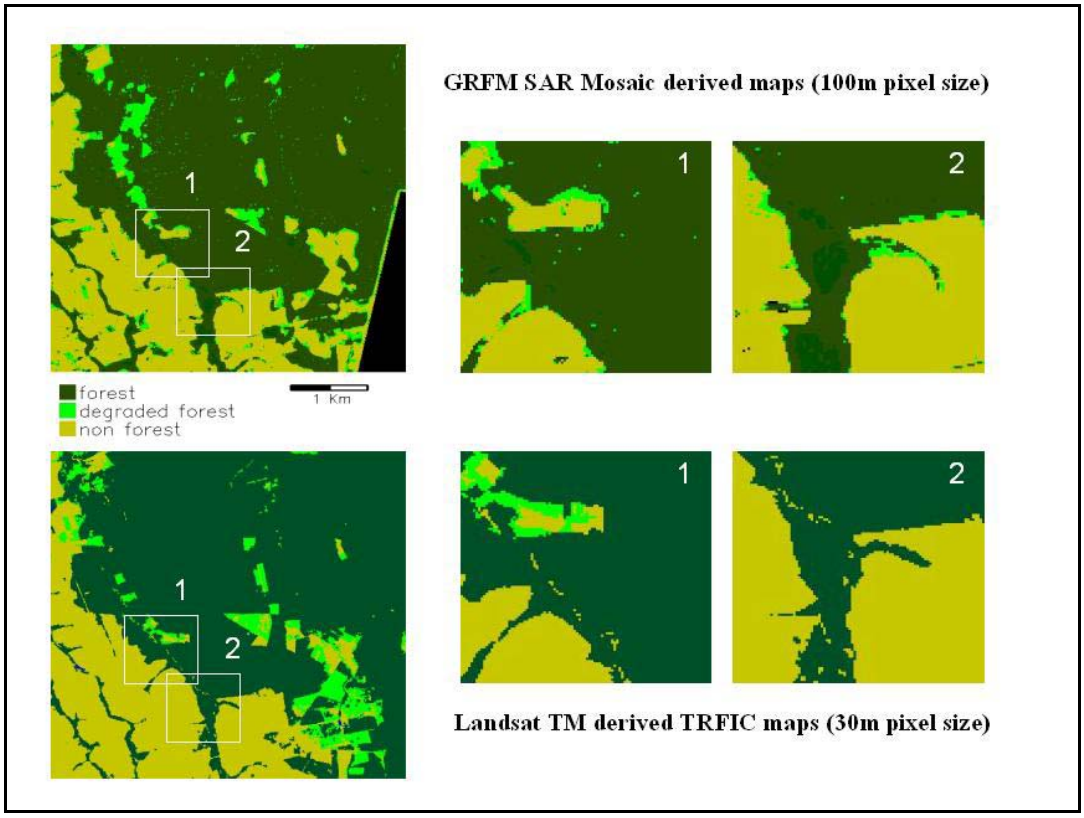

Figure B.11: Comparison between the SAR map using the hybrid classifier and the TRFIC reference map of the Mato Grosso training site (226-69). This site is characterized by ranching and selective logging.

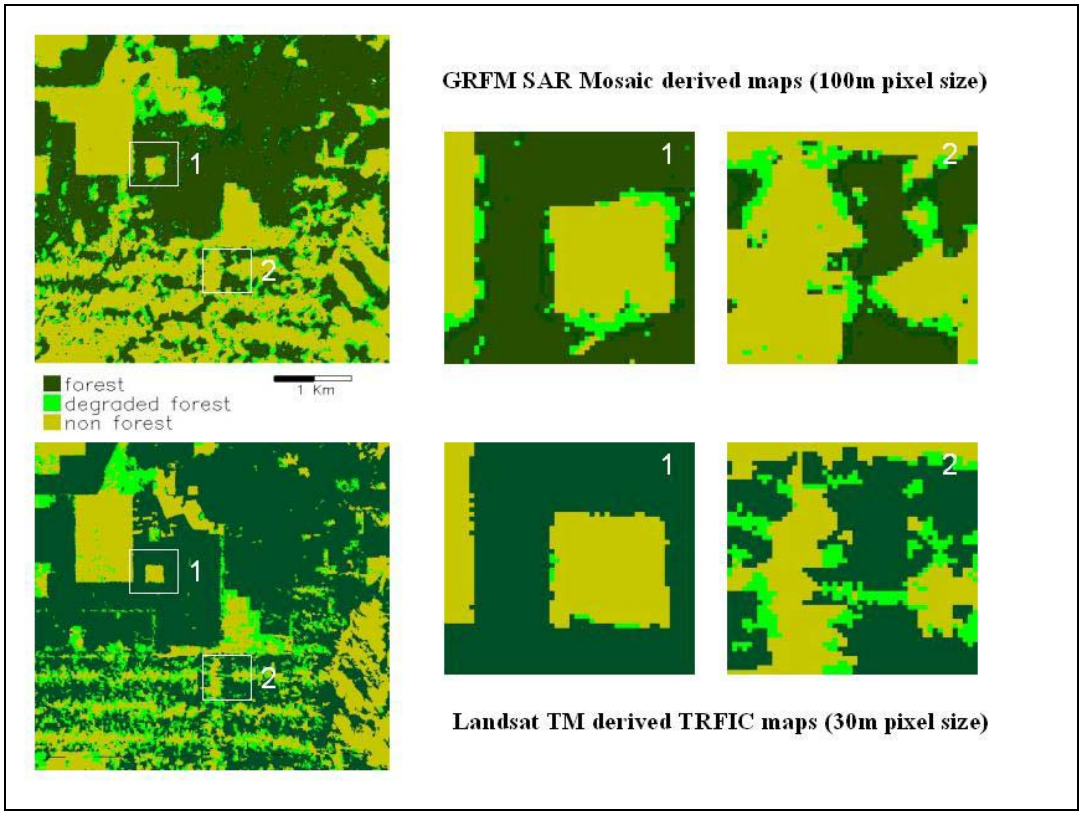

Figure B.12: Comparison between the SAR maps derived using the two-stage hybrid classifier and the TRFIC reference map of the South Rondonia training site (230-69). This site is characterized by linear ("herring bone") and massive deforestation.

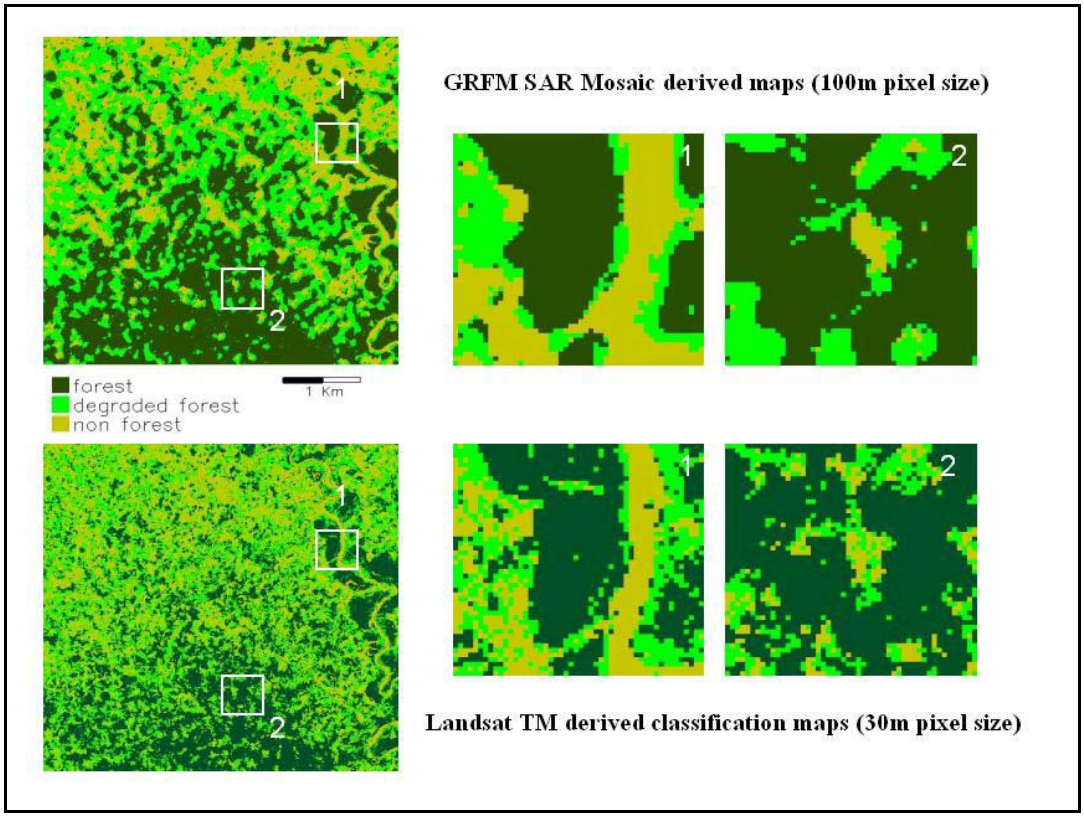

Figure B.13: Comparison between the SAR maps derived using the two-stage hybrid classifier and the Landsat TM classification of the Florencia-Napo training site (8-59). This site is characterized by linear and widespread deforestation.

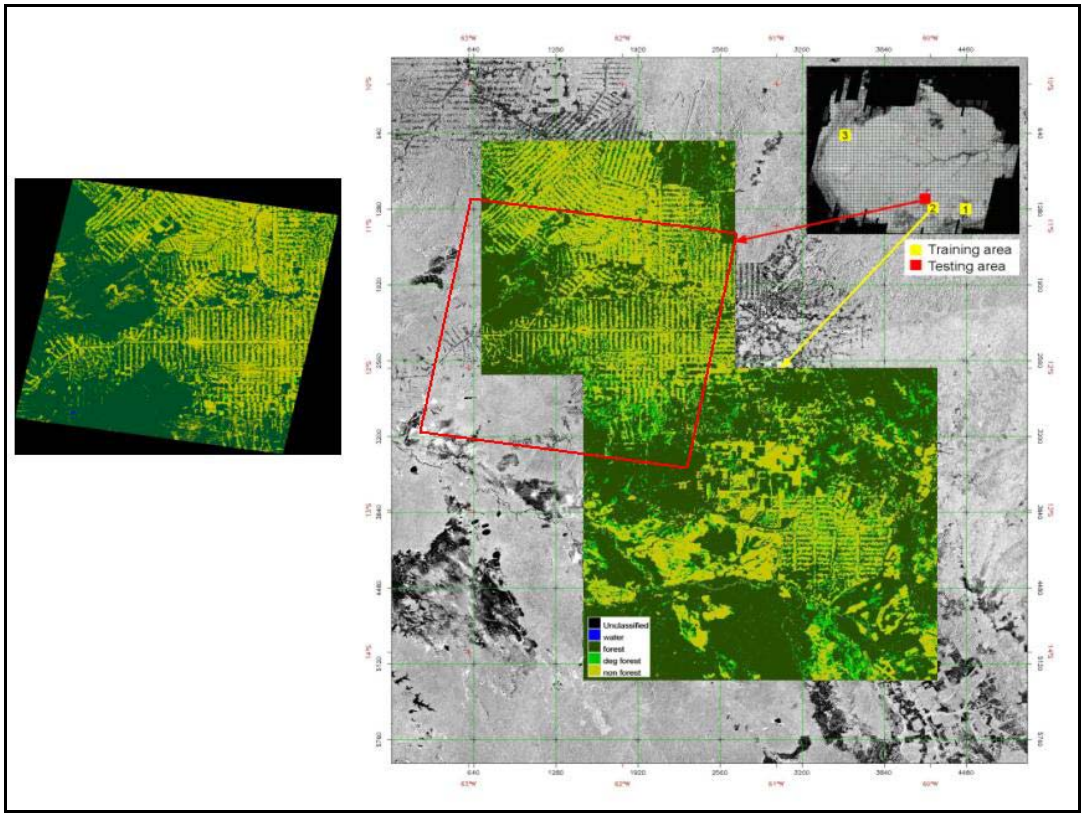

Figure B.14: The SAR map of the testing site (231-68) and the SAR map of the South Rondonia site (230-69). The two maps are overlaid to a sub-set of GRFM SA mosaic in the inset on the left. The SAR map of the testing site (231-68) is compared with the corresponding TRFIC map of the same testing site (the location on the GRFM data set is framed by a red box). Training sites (1. Mato Grosso, 2. South Rondonia, 3. Florencia-Napo) and testing site (North Rondonia) are highlighted in the inset showing the entire GRFM SA mosaic.

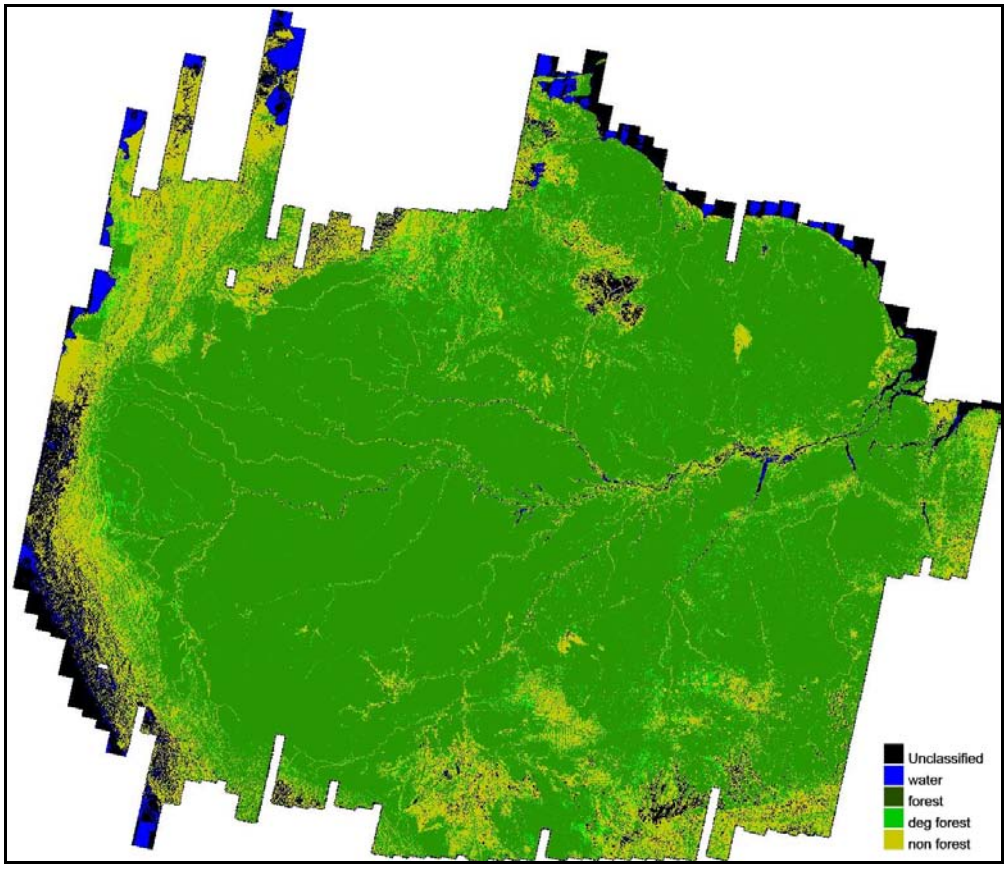

Figure B.15: Forest map (1.2 km pixel spacing) derived from the whole GRFM SAR South America mosaic.

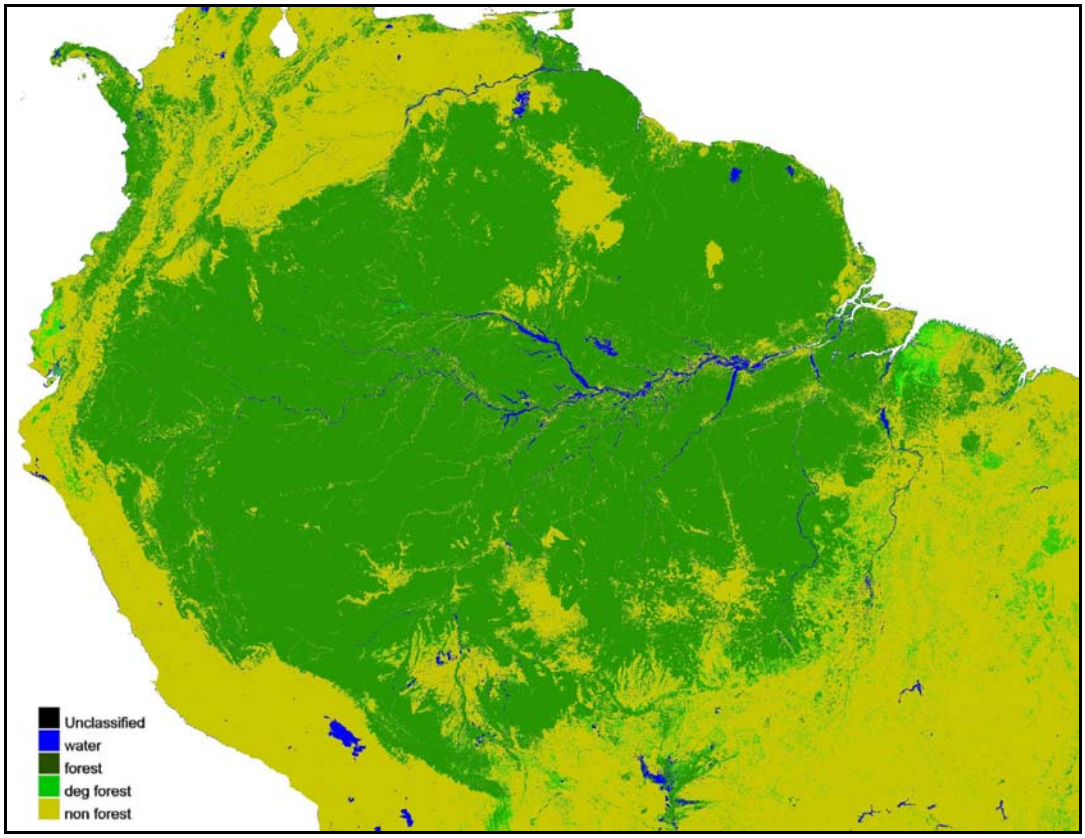

Figure B.16: The TREES project South America forest map. This product was derived from 300 ERS ATSR-2 optical images acquired between 1998 and 2000.

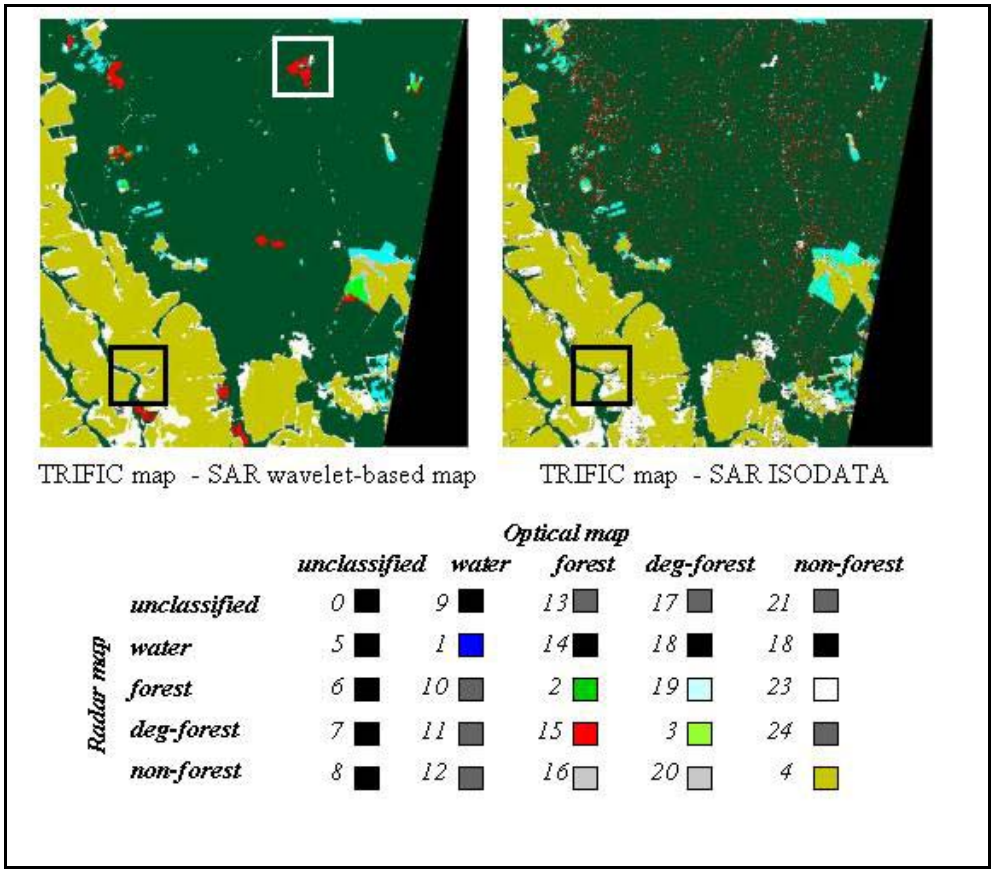

Figure B.17: Two confusion maps of Mato Grosso site (226-69) between reference maps and SAR maps: Region growing on the left, ISODATA classifications on the right (see chapter 5). The area enlarged in figure 4.6 is framed by a white box. The area enlarged in figure 4.7 is framed by a black box.

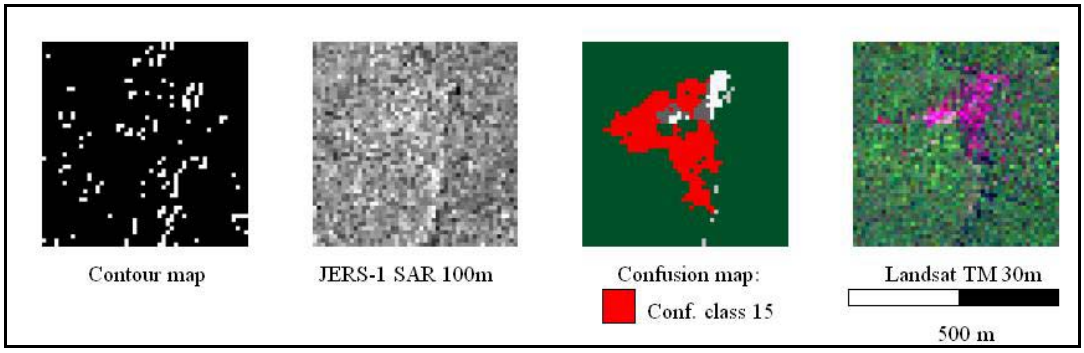

Figure B.18: The zoomed-in area in the TM image shows spatial arrangements that are suggestive of anthropogenic disturbances. However these patterns are not included in the TRFIC map. In the region growing map he same area is classified as degraded forest while in the TRFIC map it is classified as forest. In this case the discrepancy, relative to confusion matrix elements 15, is due to a misclassification of the optical data.

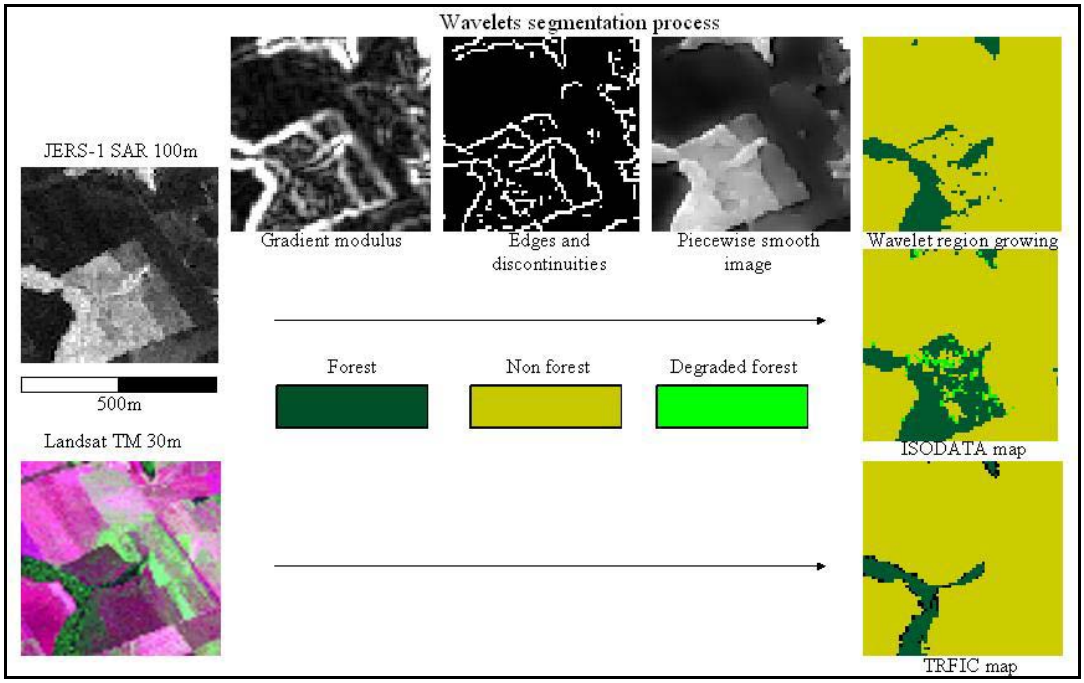

Figure B.19: Synoptic description of data flow in the generation of the thematic maps and for the different classification methods.

Pictures at the right of the figure show the relative agreement for the class forest between the SAR map derived by wavelet–based region growing – first inset top right - and the reference TRFIC –last inset bottom right.

In the center right inset the SAR map derived by ISODATA technique is shown (see section 4.6)

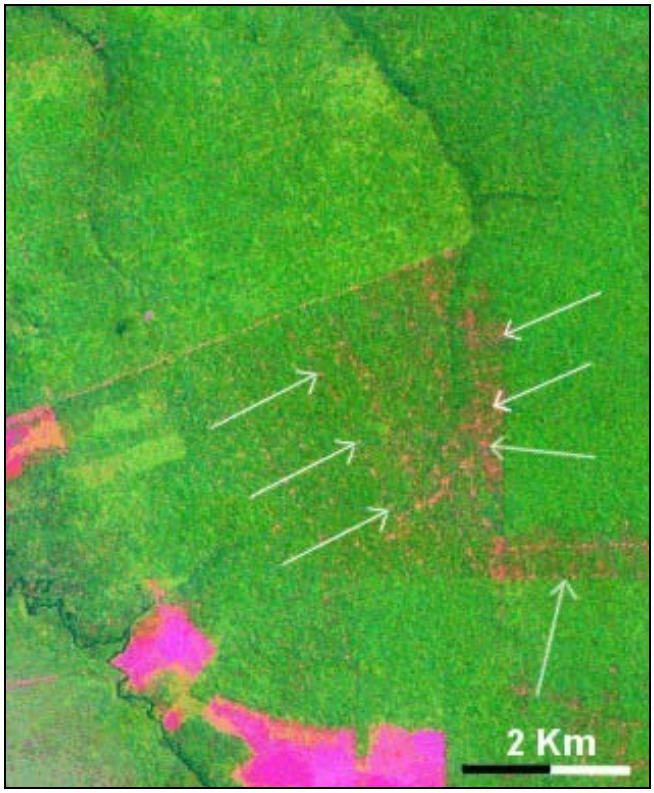

Figure B.20: A first type of forest disturbance (marked by white arrows). It consists of isolated bare soil patches surrounded by the forest domain. The patches are readily visible in the Landsat TM 226-69 (1992) image (R: Band5, G: Band4, B: Band3). This forest degradation phenomenon is identified as Vegetation-Bare Soil class (VB).

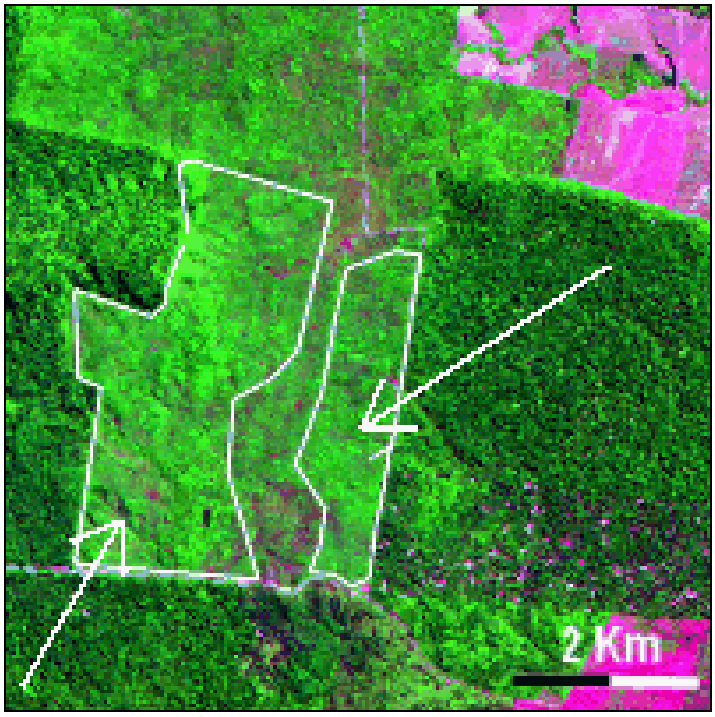

Figure B.21: A second type of forest disturbance is visible in the Landsat TM 222-62 (1999) image (R: Band5, G: Band3, B: Band3). White contours indicate two large regions of forest degradation featuring a regular shape and a spectral signature quite similar to that of the forest class. This second forest degradation phenomenon is identified **as** Vegetation-Forest class (VF).

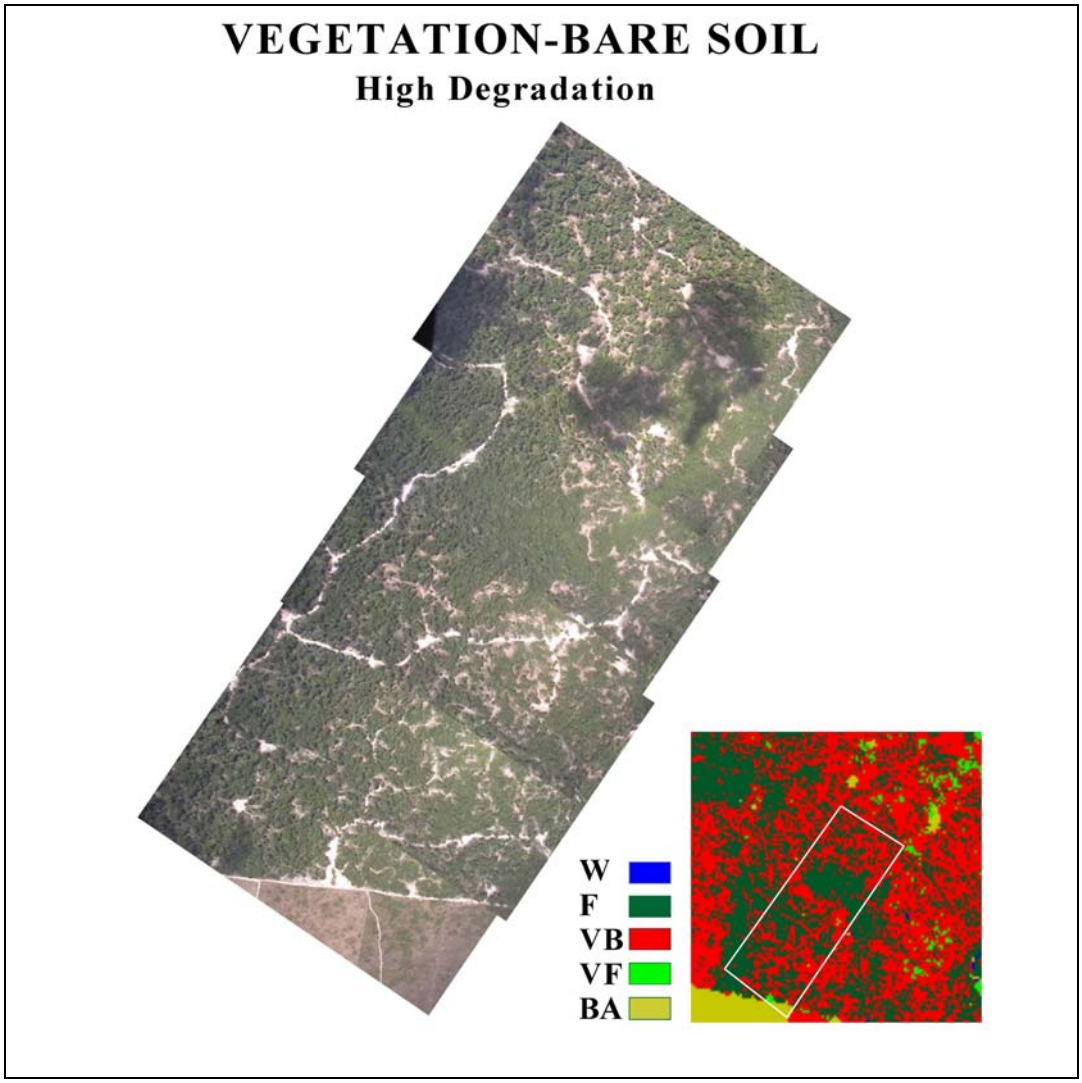

Figure B.22: Comparison between aerial photos and a TM thematic map (see the white outline at the bottom right) in which the density of the VB degradation class is considered "high."

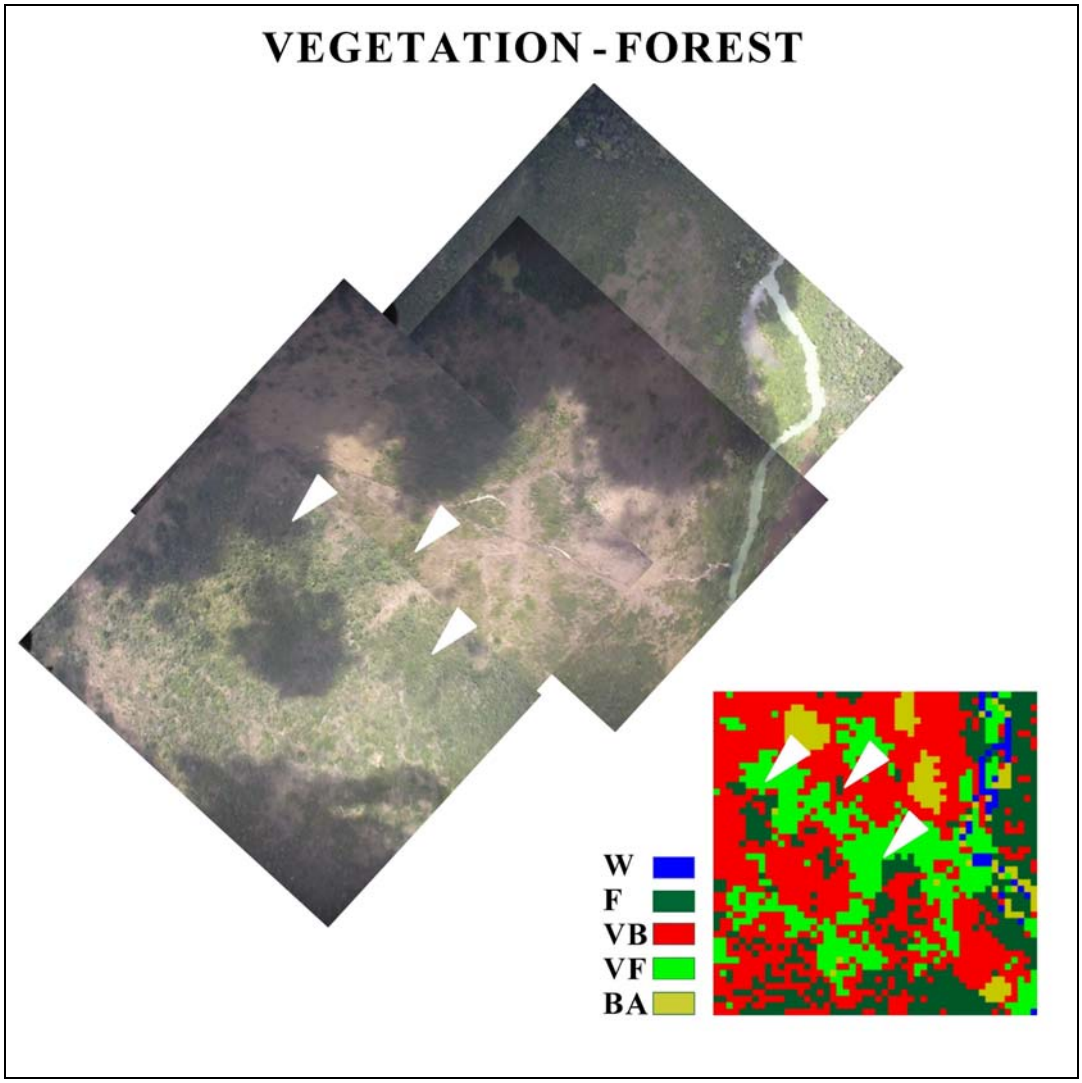

Figure B.23: Comparison between aerial photos and a TM thematic map where Vegetation-Forest (VF) degradation phenomena are detected.

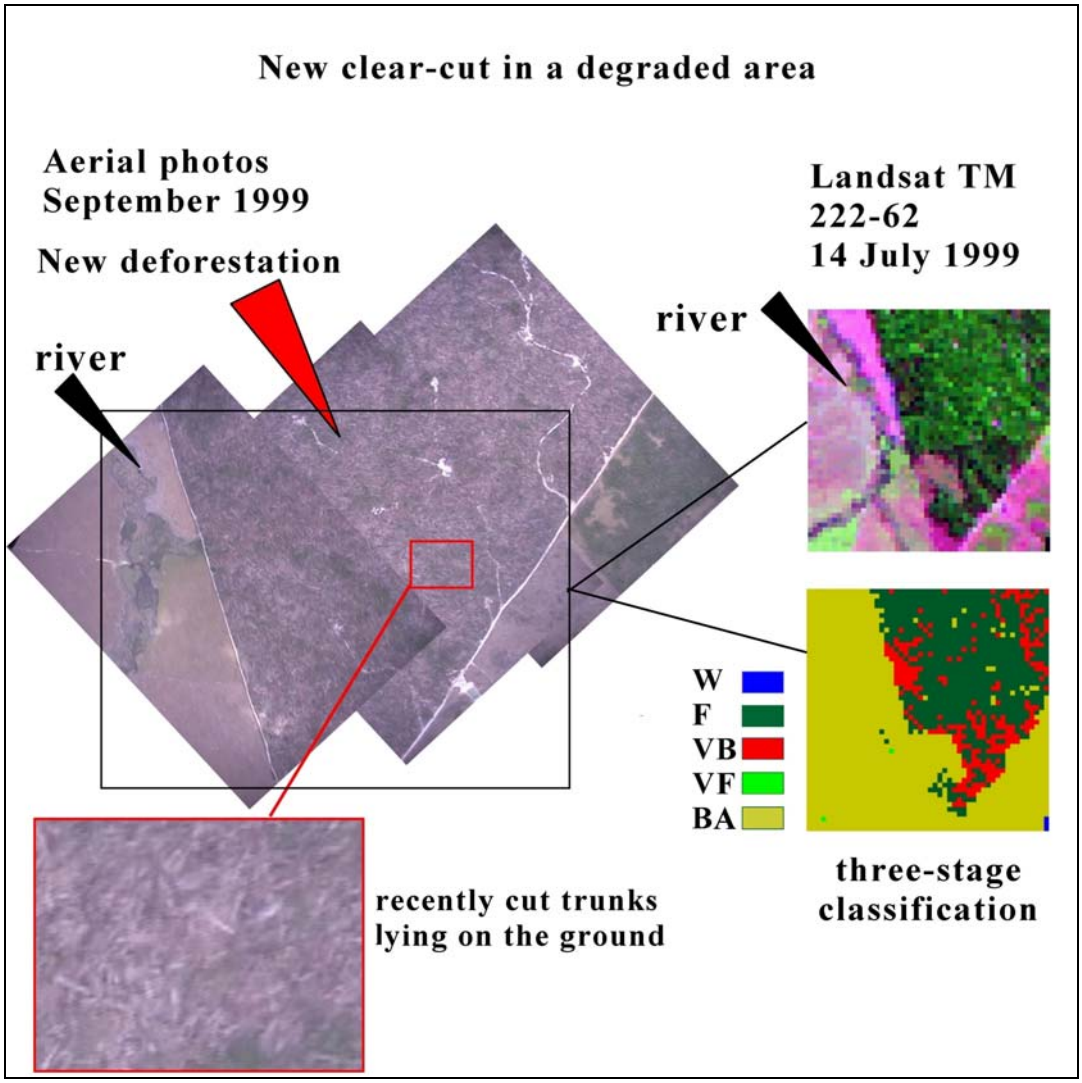

Figure B.24: High dynamics of change in areas affected by forest degradation phenomena. Class Vegetation-Bare soil (VB) detected in the Landsat TM image becomes new clear- cuts in aerial photos taken about two months later, where recently cut stems are still lying on the ground (position of the river can be used to localize the aerial photo with respect to the TM image and the corresponding thematic map).

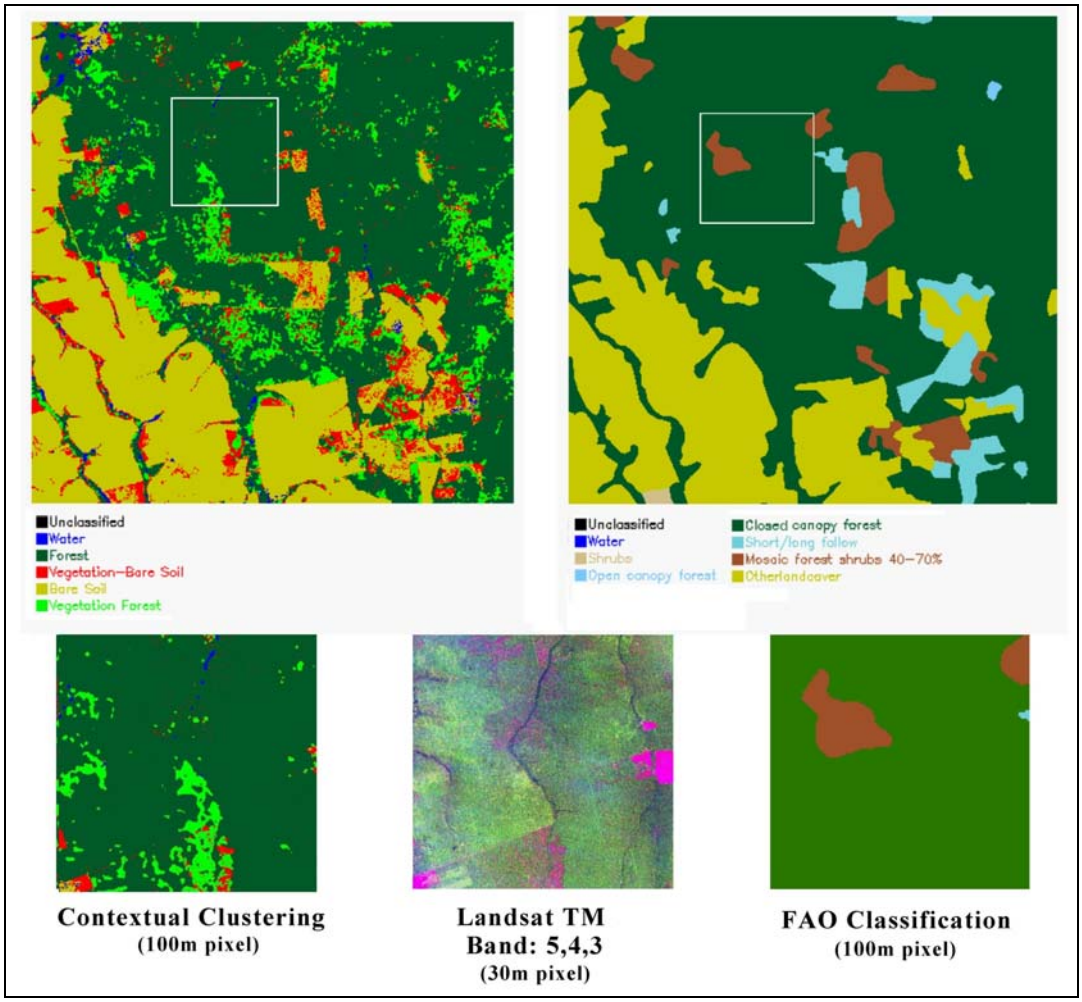

Figure B.25: Comparison between a subset a Landsat TM 226-69 (1996) image, the corresponding TM thematic map (down-sampled at 100 m), and the FAO map.

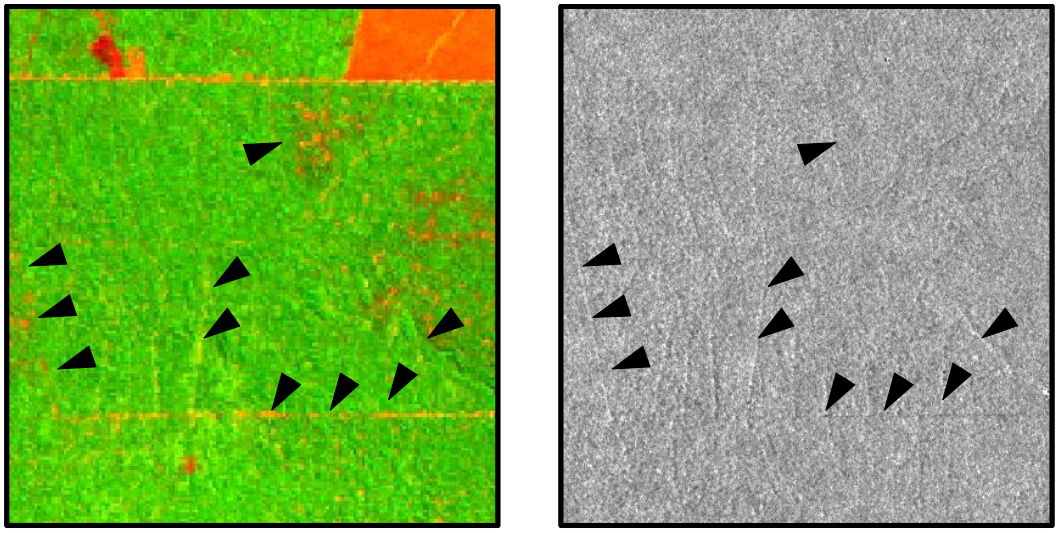

Figure B.26: Small isolated and elongated bare soil regions distributed regularly in the forest (degradation phenomena due to selective logging) are captured (black arrows) both by Landsat TM (30 m pixel size, acquisition date: 31-07-96) (a), and 12.5 m JERS-1 filtered image (acquisition date: 07-10-95) (b)

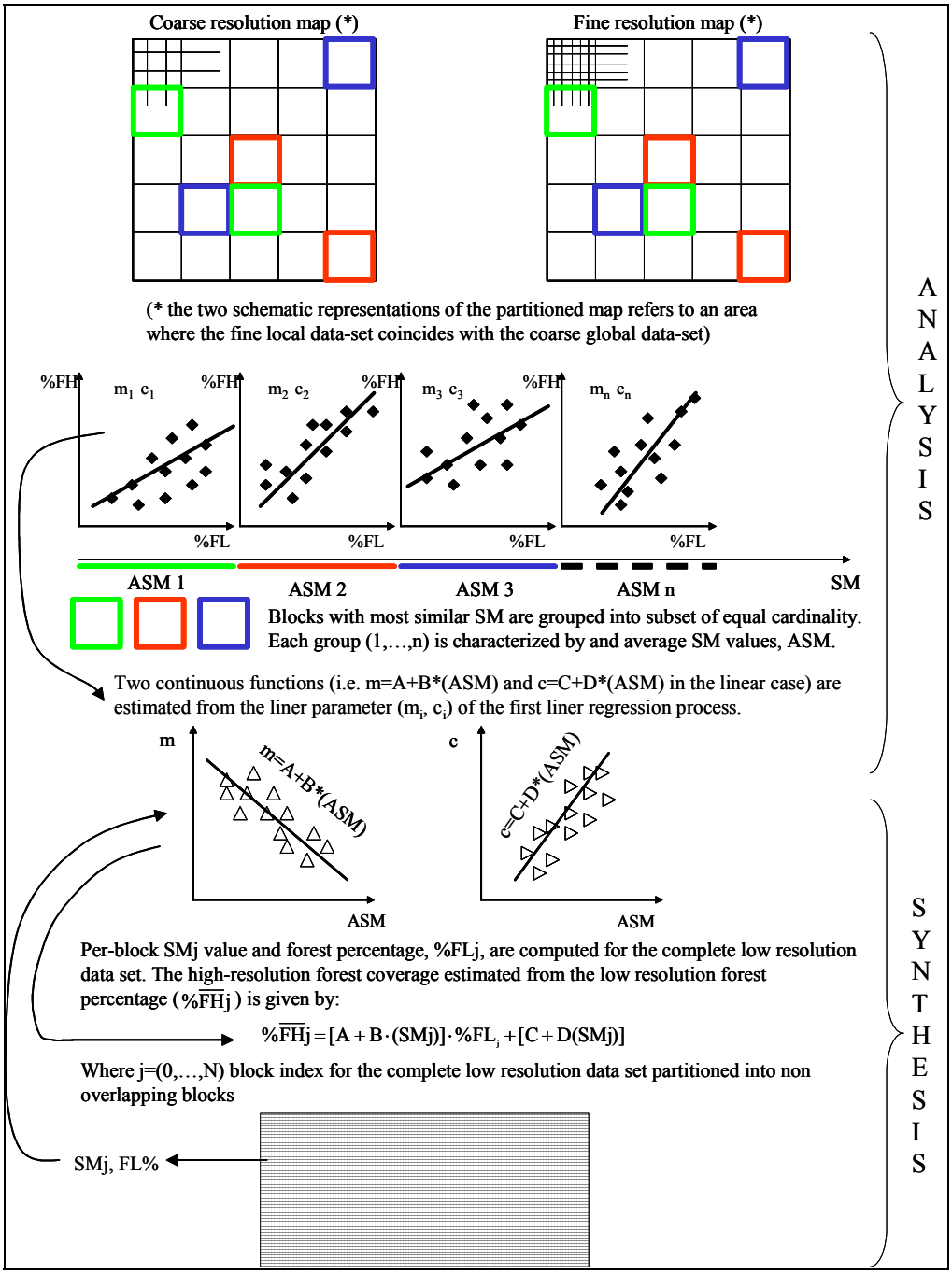

Figure B.27: Schematic representation of analysis and synthesis steps to estimate and apply the correction function to the low resolution SAR classification.

Figure B.28: Agricultural School "*Rainha Dos Apostolos*": the students can also learn aquaculture techniques.

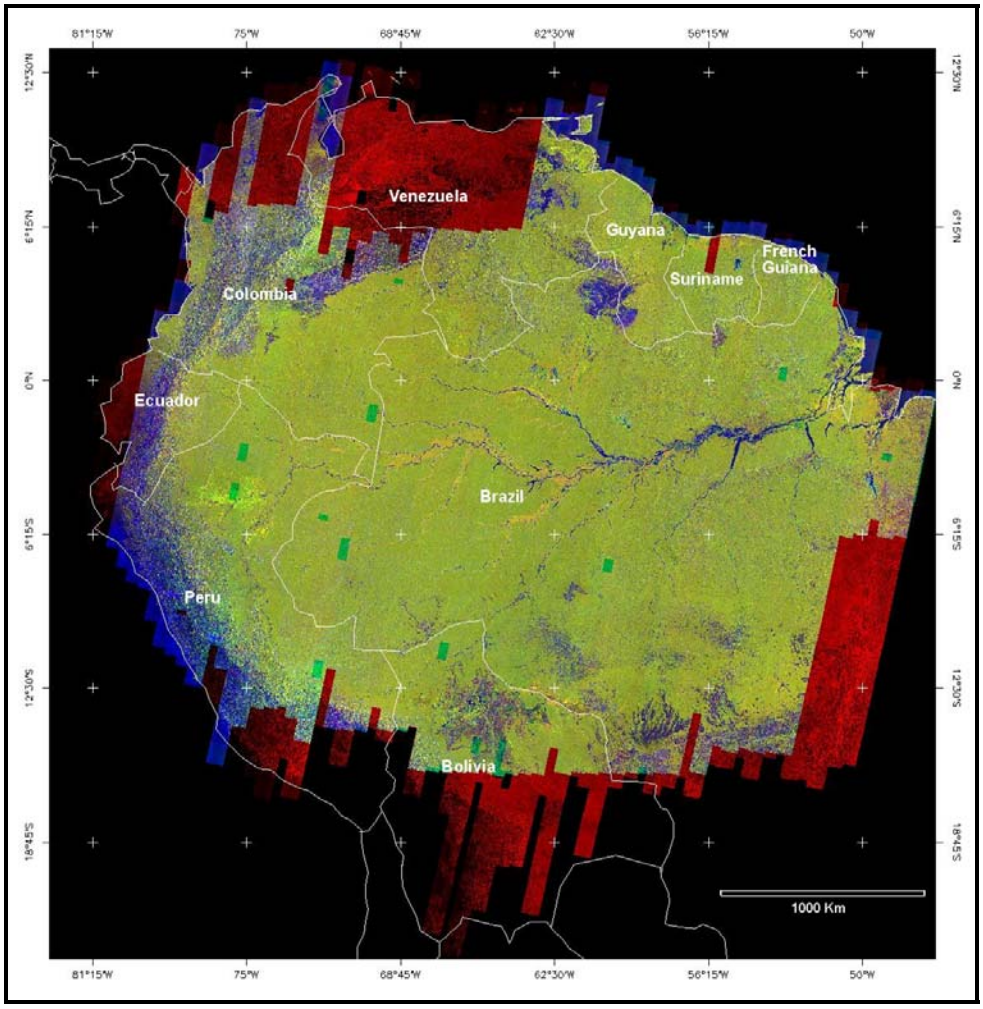

Figure B.29: Color composite of the GRFM radar mosaic layers. High water amplitude (red channel), low water amplitude (green channel), low water texture (blue channel).

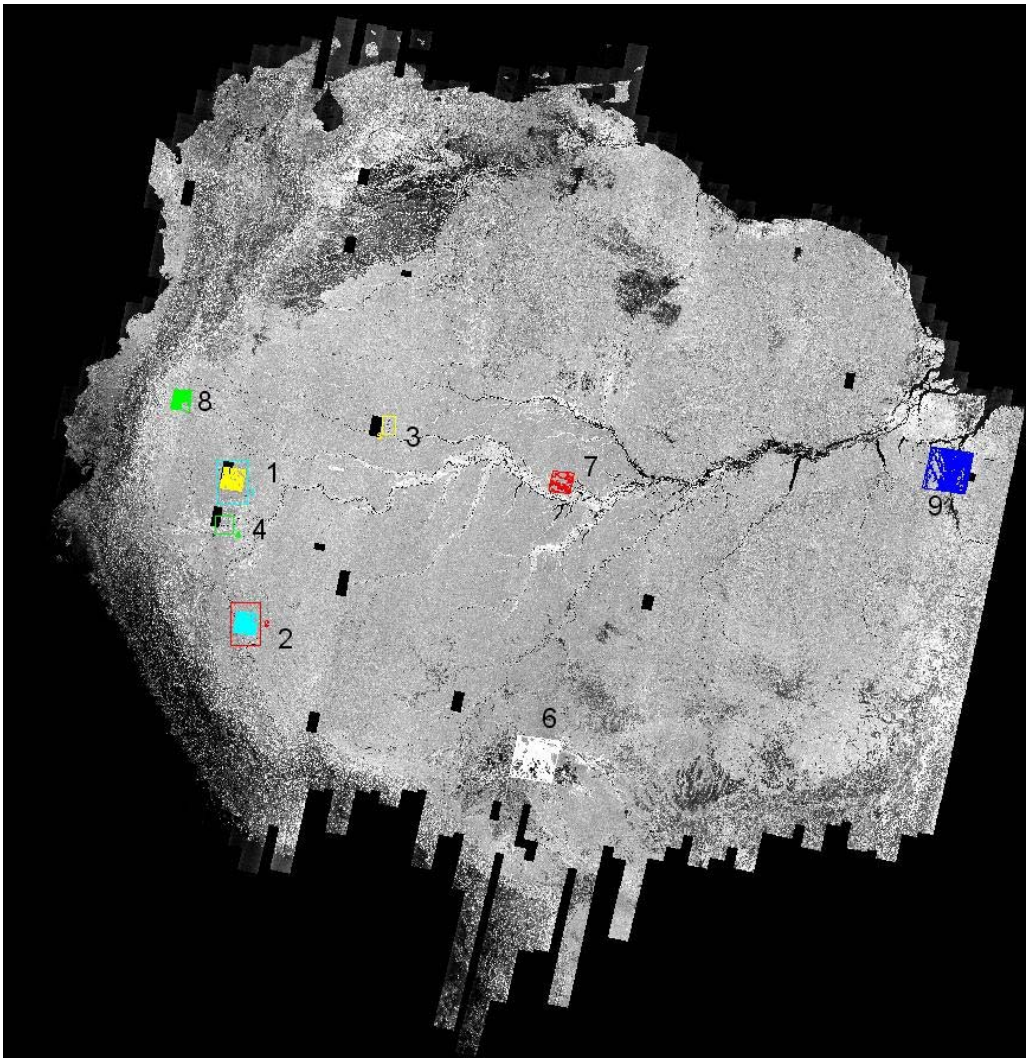

Figure B.30: The high water GRFM mosaic with 9 overlaid training/testing sites

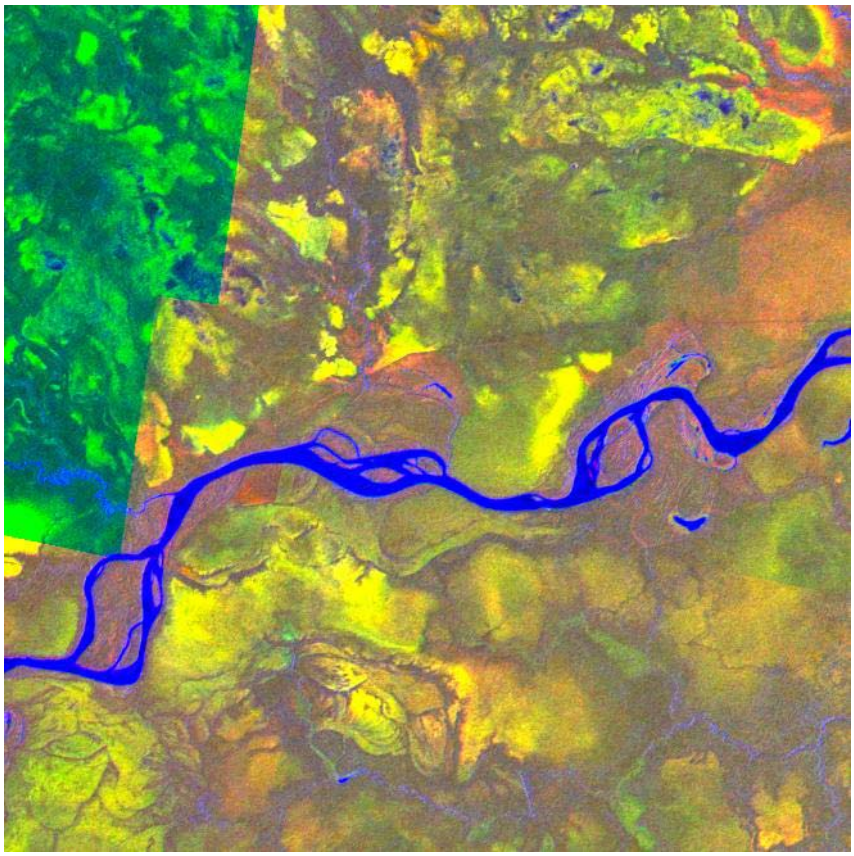

Figure B.31: The color composite of high water amplitude, low water amplitude and low water texture (wavelet filtered) GRFM images of the Peru site (training/testing site number 4).

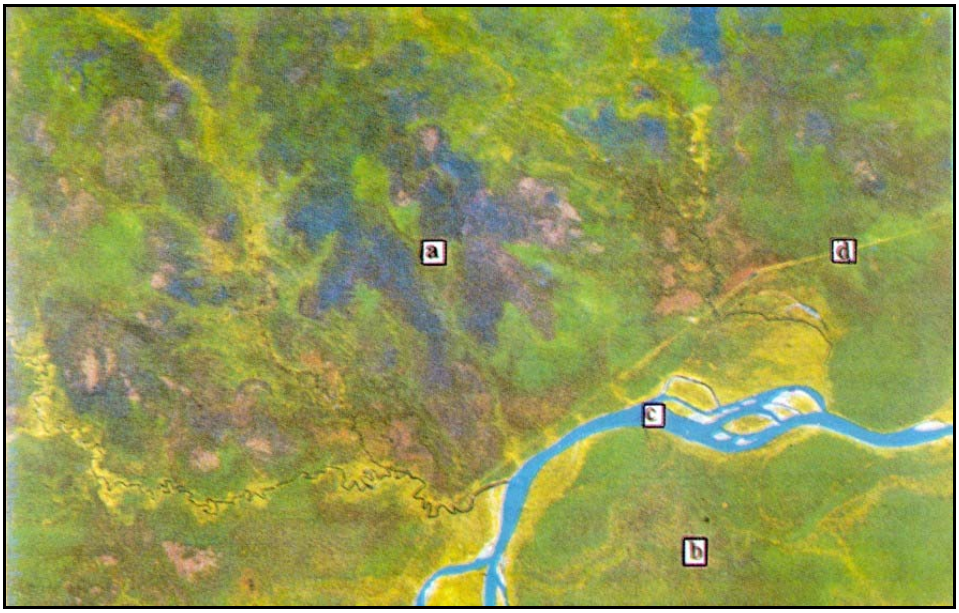

Figure B.32: Landsat TM auxiliary image available over the Peru site. Sites a) and b) are indicated from ground surveyors as permanently flooded forest.

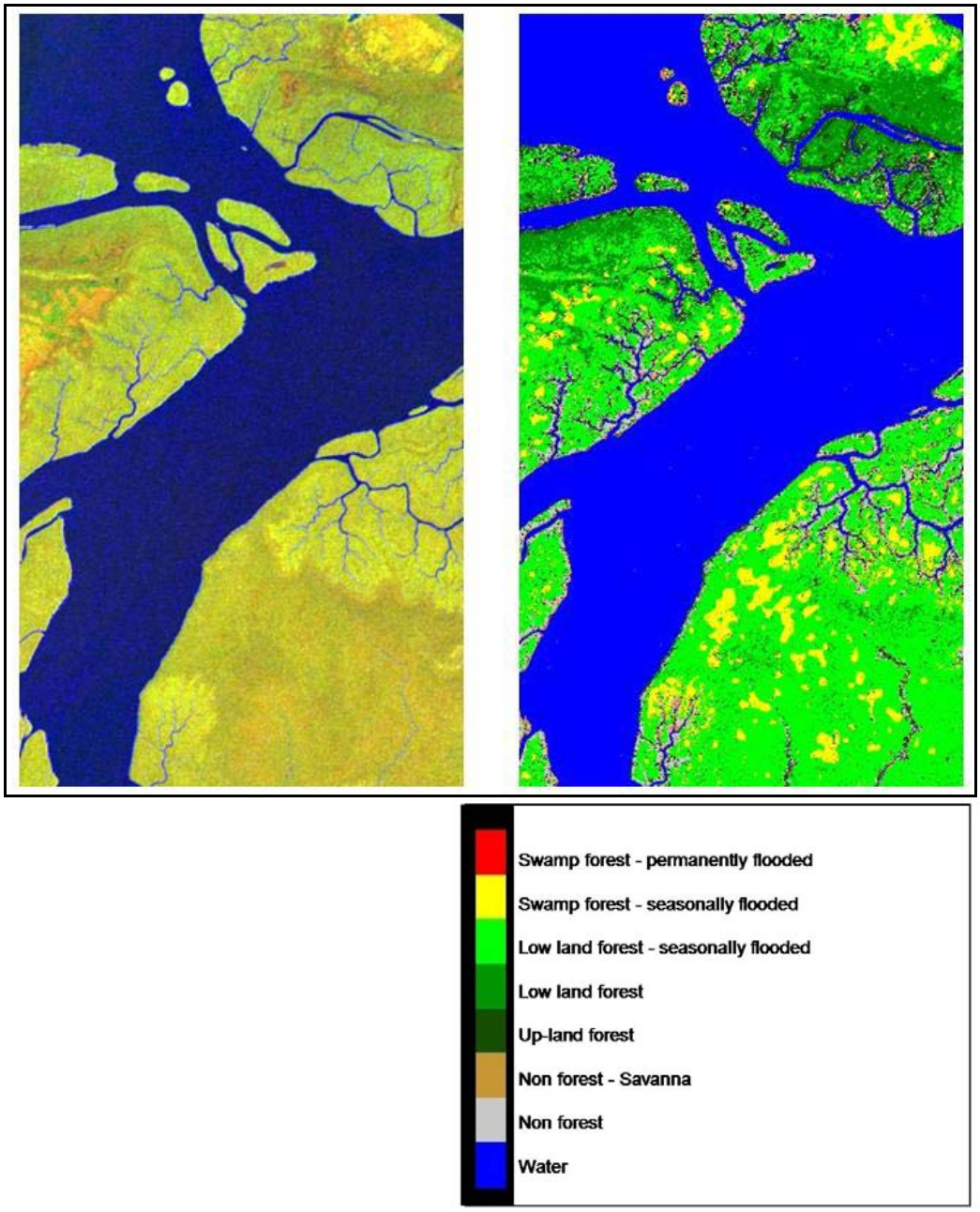

Figure B.33: GRFM color composite image and swamp forest map over the delta of the Amazon River.

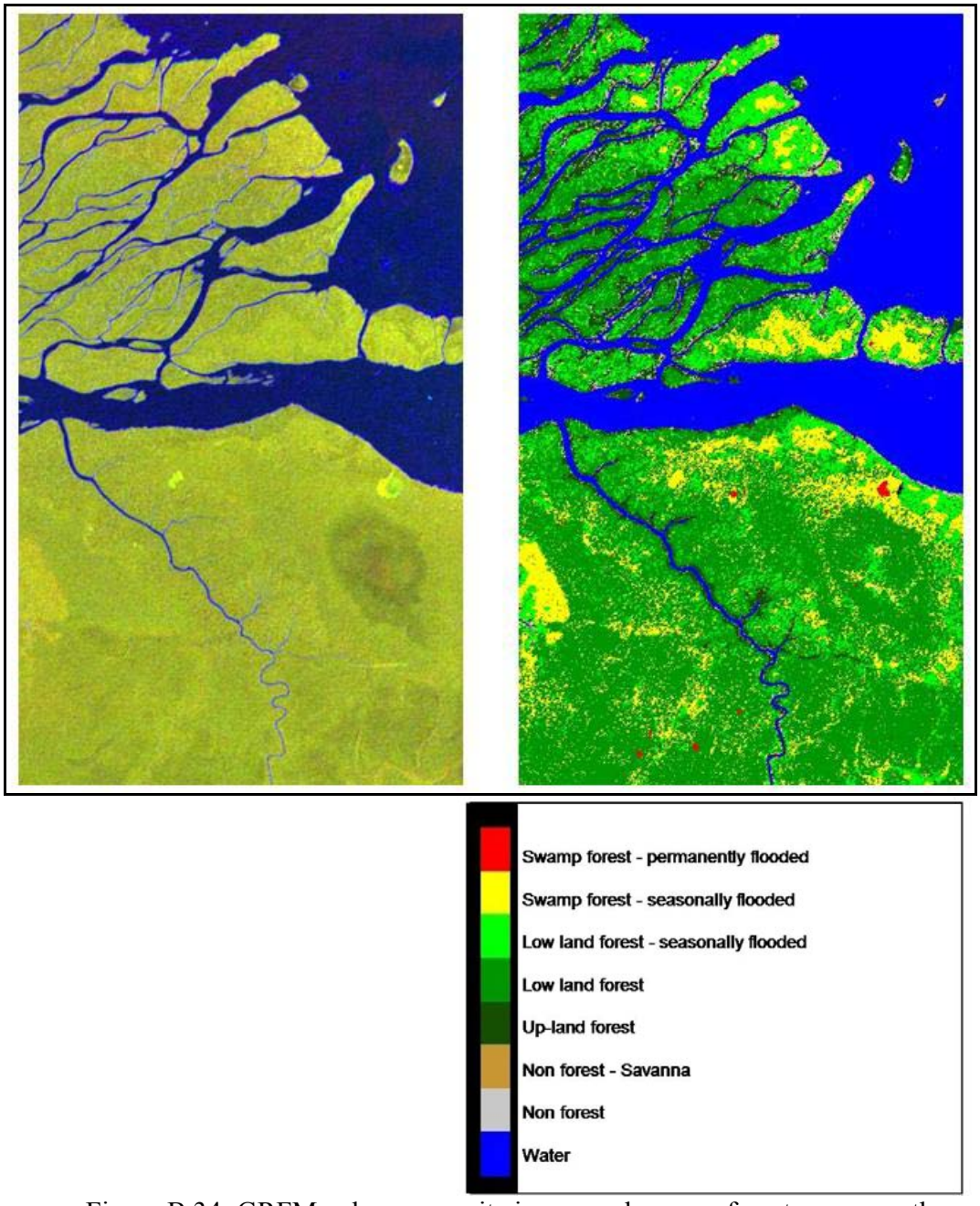

Figure B.34: GRFM color composite image and swamp forest map over the delta of the Orinoco River.

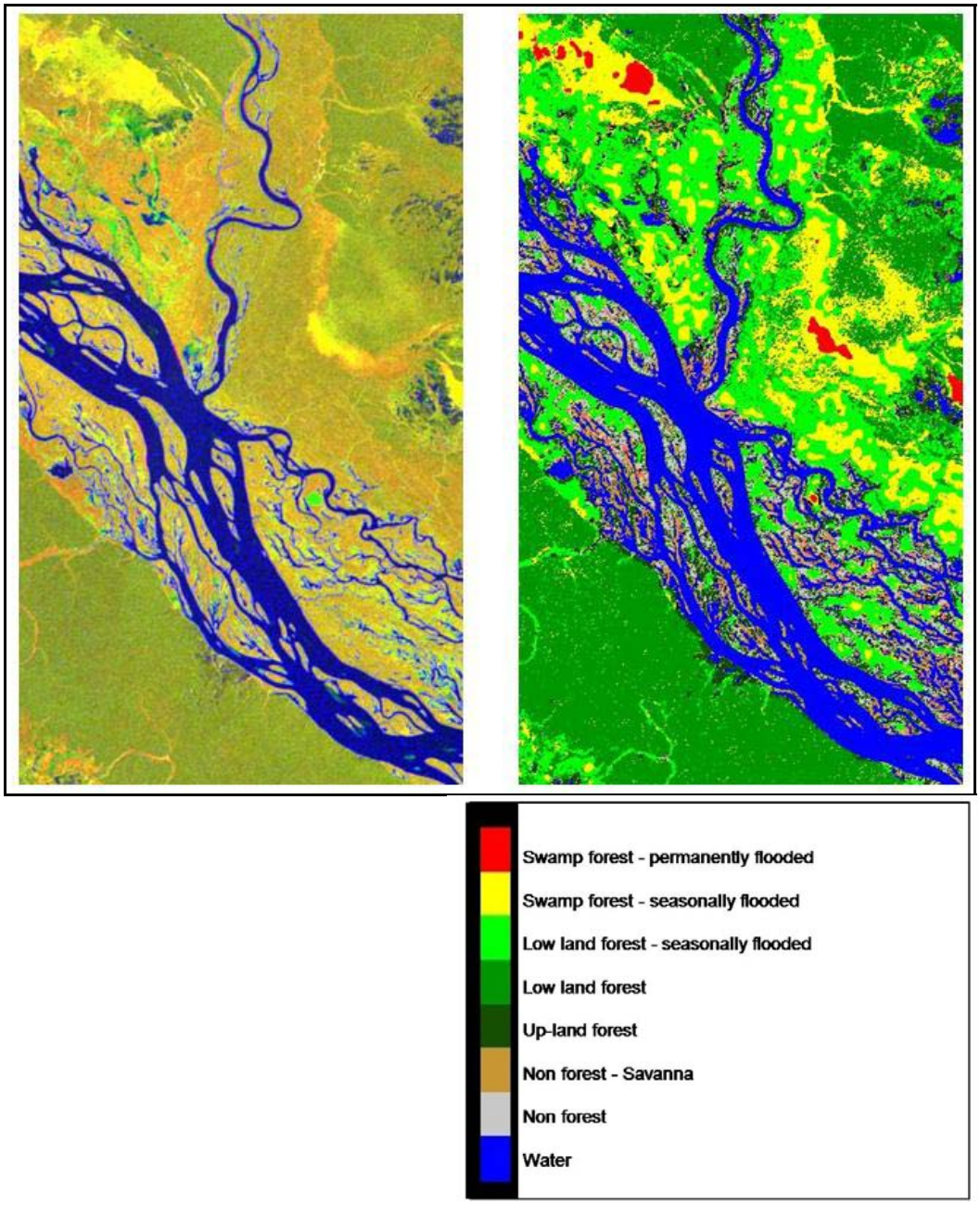

Figure B.35: GRFM color composite image and swamp forest map over an area around the Rio Negro River.

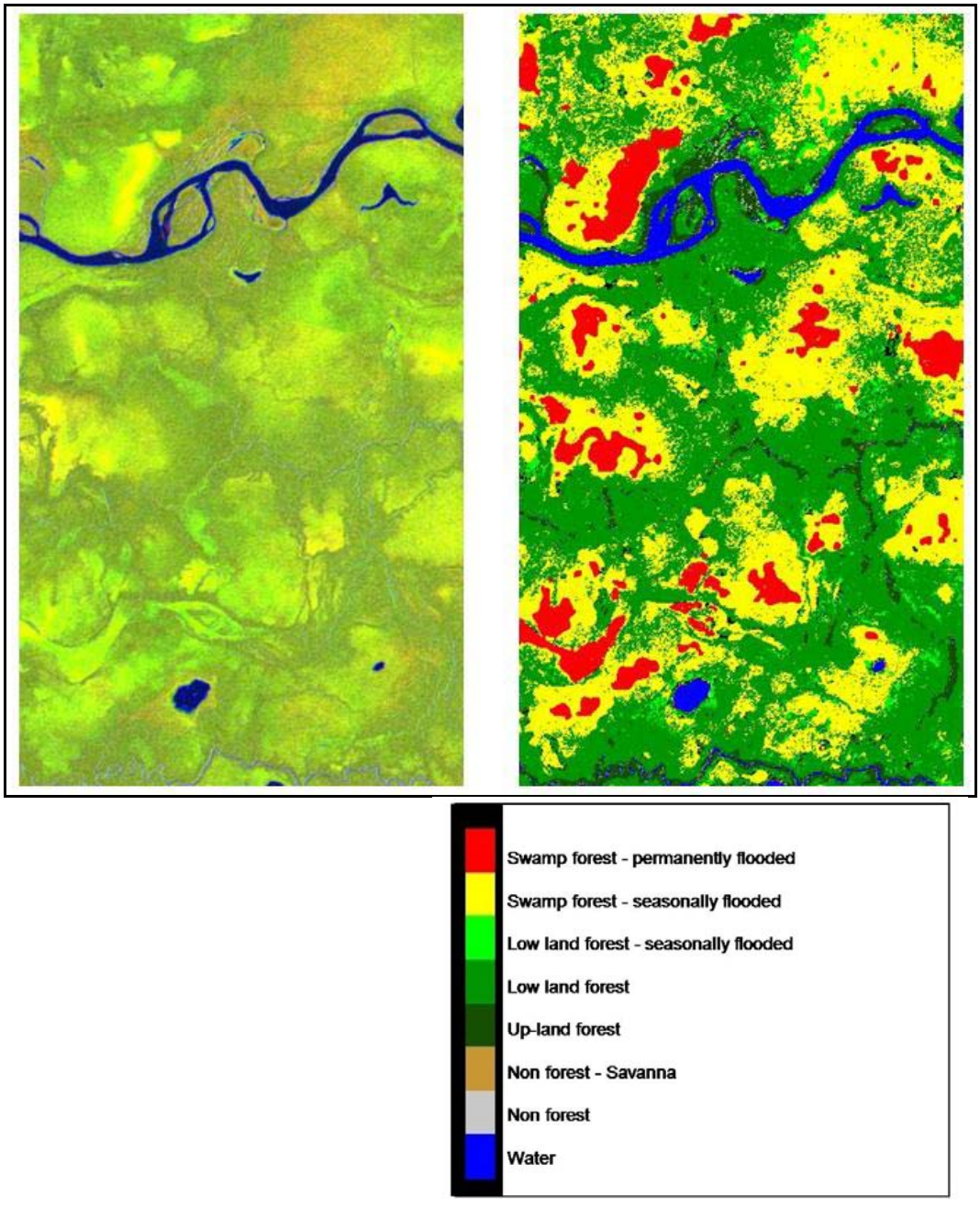

Figure B.36: GRFM color composite image and swamp forest map over a region in Peru state

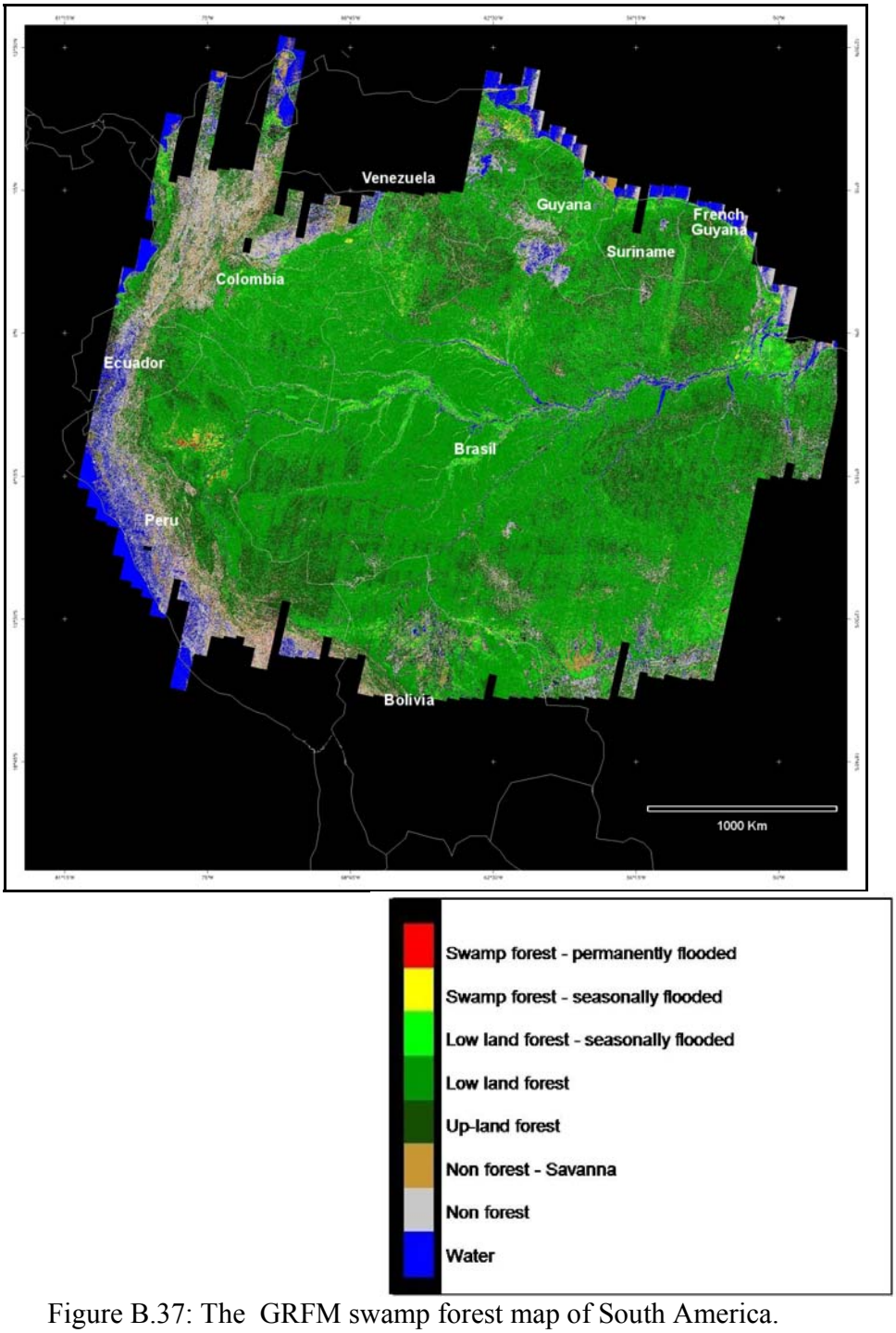

Figure B.37: The GRFM swamp forest map of South America.

References

Achard F., Eva H. D., Glinni A., Mayaux P., Stibig H.J., and Richards T., Identification of Deforestation Hot Spot Areas in the Humid Tropics, TREES Publications Series B4, European Commission, Luxembourg, EUR 18079 EN, 100, 1998.

Arbia G. and Haiming R., "Error propagation Through Map Operations", Technometrics, Vol.35, NO 35, pp. 293-305, 1993.

Baraldi A., Blonda P., Parmiggiani F., and Satalino G., "Contextual clustering for image segmentation," Optical Engineering, vol. 39, no. 4, pp. 1-17, April 2000.

Batista G.T. and Tucker C.J., "Accuracy of digital classification versus visual interpretation for deforestation in Amazon", In proceedings The 5th Latin America Remote sensing Symposium, Cusco, Perù, 1991.

Beaulieu N., Puig J., Fujisaka S., and Veneklaas E., "The Use of JERS-1 Images in CIAT's Benchmarks Sites in Puesto Lòpez, Colombia, and Pucallpa, Peru", JERS-1 Science Program '99 IP Reports, EORC-NASDA, March 1999.

Bicknell, T., "Alaska SAR Facility SAR Processor System User's Guide to Products", Report JPL D-9362, NASA JPL, Pasadena, CA, USA, 1992.

Bijker W. and Hoekman, D. H., "A remote sensing monitoring system for a settlement area in tropical rain forest", Geoscience and Remote Sensing Symposium, 1994. IGARSS '94. 'Surface and Atmospheric Remote Sensing: Technologies, Data Analysis and Interpretation', International , Volume: 1 , 8-12, Page(s): 97 -99 vol.1, Aug. 1994.

Bijker W. and Hoekman D. H., "Monitoring of tropical rain forest and pastures with ERS-1", Proceeding Final Workshop ERS-1 Study '94", EUR 17286 en, JRC, EU 1997.

Bijker W., Radar for rain forest: a monitoring system for land cover change in the Colombian Amazon. PhD thesis Wageningen Agricultural University; Summaries in Dutch, English and Spanish. PhD Thesis. ITC Publication 53. 192 p. ISBN 90-6164-139-X, 1997.

Carmona, R. A., “Extrema Reconstruction and Spline Smoothing: Variations on an Algorithm of Mallat & Zhong, in Wavelets and Statistics”, Lecture notes in statistics, A. Antoniadis, G. Oppenheim editors, Springer Verlag, Inc., 83-94, NY 1995.

Chomentowski W. S., Salas B. and Skole. D., “Landsat Pathfinder project advances deforestation mapping”, GIS World 7 (4): 34-8, 1994.

Cochrane M. A., Alencar A., Schulze M. D., Souza Jr. C. M., Nepstad D., Lefebvre P., and Davidson E. A., “Positive feedbacks in the fire dynamic of closed canopy tropical forests”, Science, vol. 284, pp. 1832-1835, 1999.

Collins N. M., Sayer J. A. & Whitmore T.C., The conservation Atlas of Tropical Forests: Asia and the Pacific, Macmillan Press, London, UK, pp. 256, 1991.
Congalton R.G. and Green K., Assessing the Accuracy of Remotely Sensed Data: Principles and Practices. Lewis Publishers, New York, 1999.

Conway J., Eva H.D., and D’Souza G., “Comparison of the detection of deforested areas using ERS-1 ATSR and the NOAA-11 AVHRR with reference to ERS-1 SAR data: a case study in the Brazilian Amazon”, International Journal of Remote Sensing, vol.17, pp. 3419-3440, 1996.

Conway J., “TREES ERS-1 Study 94 Workshop Final Report”, Proceeding Final Workshop ERS-1 Study ’94”, EUR 17286 en, JRC, EU 1997.

Corves C., Caves R., Quegan R., De Grandi G., and Nezry E., “ Evaluating multi temporal ERS-1 SAR data for mapping forests and detecting forest clearing in the Manaus region of Brazil”, Proceeding Final Workshop ERS-1 Study ’94”, EUR 17286 en, JRC, EU 1997.

Daily M., “Hue-Saturation- Intensity Split- Spectrum Processing of Seasat Radar Imagery”, Photogrammetric Engineering and Remote Sensing, Vol.49, no. 3, pp. 349-355, 1983.

Davis, P.J., Interpolation and Approximation, sec. 1, pp. 4-12, Dover Publications Inc., New York, ISBN 0-486-62495-1, 1975.

De Araujo L.S., dos Santos J.R., da Costa Freitas C., and Xaud H.A.M, “The use of microwave and optical data for estimating aerial biomass of the savanna and forest formations at Roraima State, Brazil”, in Proceedings, IGARSS’99, Hamburg, Germany, Vol. V .IEEE Catalog No. 99 CH36293, July, 1999.

De Grandi G. F, “Synthesis on Radar processing methods and tools”, Final Workshop ERS-1 Study ’94”, EUR 17286 en, JRC, EU 1997a.

De Grandi G.F., Leysen M., Lee J.S. and Schuler D., Radar Reflectivity Estimation Using Multiple SAR Scenes of the Same Target: Technique and Application, in proceeding IGARRS’ 97, Singapore, 1997b.

De Grandi G.F., Mayaux P., Rosenqvist A., Rauste Y., Saatchi S., Simard M., Leysen M., "Flooded Forest Mapping at Regional Scale in the Central Africa Congo River Basin: First Thematic Results Derived by ERS-1 and JERS-1 Radar Mosaics", Proc. Sec. Int. Workshop on "Retrieval of Bio- and Geo-physical Parameters from SAR Data", ESA ESTEC, 21-23 October 1998.

De Grandi G. F., Lee J.S., Schuler D., Kattenborn G., Holecz F., Pasquali P., Simard M., "Singularity analysis with wavelets in polarimetric SAR imagery for vegetation mapping applications", in proceedings IEEE IGARSS'99, paper EE05_06, Hamburg, Germany, 1999a.

De Grandi G. F., Simard M., Perna G., Franchino E., and Rosenqvist, A., “The GRFM-Africa Multi-resolution Image Products: Signal Processing and Statistical Characterization”, JERS Science Program ’99, PI Reports, (Earth Observation Research Center, NASDA), 55-62, 1999b.

De Grandi G.F., Malingreau J. P, and Leyesen M. “The ERS-1 Central Africa Mosaic: A New Perspective in Radar Remote Sensing for the Global Monitoring of Vegetation”, IEEE Transaction on Geoscience and Remote Sensing, Vol. 37, No. 3, May 1999c.

De Grandi G.F., Mayaux P., Malingreau J.P., Rosenqvist A., Saatchi S., Simard M., "New Perspectives on Global Ecosystems from Wide-area Radar Mosaics: Flooded Forest Mapping in the Tropics", Int. Journal of Remote Sensing, special issue on "Global and Regional Land Cover Characterization from Satellite Data, vol. 21, no. 6-7, pp. 1235-1250, Apr. 2000a.

De Grandi G.F., Mayaux P., Rauste Y., Rosenqvist A., Simard M. and Saatchi S., "The Global Rain Forest Mapping Project JERS-1 Radar Mosaic of Tropical Africa: Development and Product Characterization Aspects", IEEE Trans. on Geosci. and Remote Sensing, vol. 38, no. 5, pp. 2218-2233, 2000b.

De Grandi G. F., Lee J.S., Simard M. and Wakabayashi H., "Speckle Filtering, Segmentation and Classification of Polarimetric SAR Data: A Unified Approach Based on The Wavelet Transform", Proc. IEEE IGARSS'00, CD-ROM paper TU08_05, Honolulu, Hawaii, USA, 2000c.

De Grandi F. G., Lee J.S., Siqueira P., Baraldi A., and Simard M. "Segmentation and Labeling of Polarimetric SAR Data: Can Wavelets Help?", Proc. IEEE IGARSS'01, CD-ROM paper TU10_01, Sydney, Australia, 2001a.

De Grandi G. F,, Mayaux P., Massart M. Baraldi A., Sgrenzaroli M., "A vegetation Map of the Central Congo Basin Derived from Microwave and Optical Remote Sensing Data Using a Variable Resolution Classification Approach", In proceedings IGARSS 01 , Sydney, Australia. July 9-13, IEEE Catalog No. 01CH37217C, 2001b.

Devol A.H., Richey J.E., Clark W.A., and King. S.L., "Methane emissions to the troposphere from the Amazon floodplain", Journal of Geophys. Res. 93: pp. 1583-1592, 1998.

Dobson M. C., "Land cover Classification of Tropical Rain Forests suing Orbital SAR and Impacts of the Natural and Anthropogenic Disturbance in Species", JERS-1 Science Program '99 IP Reports, EORC-NASDA, March 1999.

D'Souza G., Malingreau J.P. H. Eva, "Tropical Forest Cover of South and Central America as Derived from Analyses of NOAA-AVHRR Data", TREES Series B: Research Report No 3, JRC: Ispra, pp.1-50, 1995.

Dutra L.V., dos Santos J. R., da Costa Freitas C., de Leao Novo E. M., Alves D. S., Hernandez Filho P., Rennò D. C., Sant'Anna S. J. S., d e Farias Costa M. P., Ribeiro C. M., Soares S. M., Lacruz M. S. P.," The Use of Jersò1 Data for Environment Monitoring and Resources Assessment in Amazonia", JERS-1 Science Program '99 IP Reports, EORC-NASDA, March 1999.

Dutra L.V., Hernandez F. P., Mazzocato M.E., De Souza R C. M., Oliver, "Land Cover Classification Based on Multi-Date JERS-1 Imagery as a Basis for Deforestation Detection, in proceedings IGARSS '99, Vol. V .IEEE Catalog No. 99CH36293, 1999.

Eva H.D., D'Souza G. and Malingreau, J.P., Potential of ATSR-1 data for detection of clearings within dense humid tropical forest, International Journal of Remote Sensing, 16: 2071-2079, 1995.

Eva H., Glinni A., Janvier P. and Blair-Myers, "Vegetation Map of Tropical South America at 1:5000000", TREES Publications Series D2, Luxembourg, European Commission, 1999.

Eva H., de Miranda E.E., Di Bella C.M., Gond V., Huber O., Sgrenzaroli M., Jones S., Coutinho A., Dorado A., Guimaraes M., Achard F., Belward A.S., Bartholomè E., Baraldi A., De Grandi G., Vogt P., Fritz S. and Hartley A., EUR 20159 EN, Luxembourg, European Commission, 2002.

FAO, Forest Resources Assessment 1990 – Global Synthesis, http: //www.fao.org/forestry/for/fra/fo124e/gep05.htm, 1990

FAO, Forest Resources Assessment 1990; Tropical countries, FAO Forestry Paper 112, FAO, Rome 1993.

FAO, "Forest resources assessment 1990; survey of tropical forest cover and study of change processes," FAO Forestry Paper 130, FAO, Rome, pp. 152, 1996.

FAO, a State of the World's Forests, FAO publications, pp. 200, Rome 1997.

Fearnside P. M., "Desmatamanto na Amazonia: Quemtem razao – o INPE ou a NASA?", Ciencia Hoje 16 (96), 6-8, 1993a.

Fearnside M. P., "Deforestation in Brazilian Amazonia: The effects of Population and Land Tenure", Ambio 22, 537-545, INPE, Brazil 1993b.

Fearnside P. M., "Global Warming and Tropical Land-Use Change: Greenhouse Gas Emissions from Biomass Burning, Decomposition and Soils in Forest Conversion, Shifting Cultivation and Secondary Vegetation", Climate Change 46, 115-158, 2000.

Ferretti A., Prati, C. and Rocca, F., "Multibaseline InSAR DEM Construction: The Wavelet Approach," IEEE Trans. Geosci. Remote Sensing, vol. 37, no. 2, pp. 705-715, 1999.

Fisher R., Melham T., Russ Ramsay C., Raven P. H., Urquhrt J. C., Emerald Realm: Earth' s Precious Rain Forests, National Geographic Society, 1990.

Freeman A., Kramer C., Alves M. and Chapman B., "Tropical Rain Forest Classification Using JERS-1 SAR data", Final Report of JERS -1/ERS-1 System Verification Program, II, 2-343-353, 1995.

Fukuda S. and Hirosawa H., “Smoothing Effect of Wavelet-Based Speckle Filtering: The Haar Basis Case,” IEEE Trans. Geosci. Remote Sensing, vol. 37, no. 2, p. 1164, 1999a.

Fukuda S. and Hirosawa, H., “A Wavelet-Based Texture Feature Set Applied to Classification of Multifrequency Polarimetric SAR Images”, IEEE Trans. Geosci. Remote Sensing, vol. 37, no. 5, pp. 2282-2286, 1999b.

Fukuda S., and Hirosawa H, “Suppression of speckle in synthetic aperture radar images using wavelet, Int. Journal of Remote Sensing”, 19, 507-519, 1998.

Furley P. A., Proctor J. and Ratter J. A., Nature and dynamics of the forest-savanna boundaries London, Chapman and Hall, 1992.

Gash H. J. and Nobre A. C., “Climatic Effects of Amazonian Deforestation: Some Results from ABRACOS”, Bulletin of the American Meteorological Society, Vol. 78, No. 5, May 1997.

Gonzales C. G., Richard E. W., Digital Image Processing, Addison-Wesley Publishing Company, 1992.

Grover K. D. Quegan R., Dutra L. V., Yanasse L.V., Hernandez C.C.F., Sant’Anna F., and Luckman A., “ ERS-1 observations and potential for use in tropical monitoring”, Proceeding Final Workshop ERS-1 Study ’94”, EUR 17286 en, JRC, EU 1997.

Grover K. D., Quegan S., and Costa Freitas C., “Quantitative Estimation of Tropical Forest Cover by SAR”, IEEE Transactions on Geosciences and Remote Sensing, Vol.37, NO 1, January 1999.

Harcourt C. S and Sayer J. A, The conservation Atlas of Tropical Forests: the Americas, London, UK: Macmillan: 333 pp., 1996.

Haschimoto Y. and Tsuchiya K. K., “Investigation of Tropical Rain Forest in Central Amazonia”, Brazil Based on Images, Journal of Geography, 104(6) 827-842, 1995.

Hess L. L., Novo E. V. L., Valeriano D. M., Holt J. W., Melack J. M., “ Large-scale Vegetation Features of the Amazon Basin Visible on the JERSò1 Low-water Amazon Mosaic”, JERS-1 Science Program ’99 IP Reports, EORC-NASDA, March 1999.

Hoekman D. H., Amar F.,Quinones, M.J., “Biomass and structure estimation of primary and secondary tropical rain forests using AirSAR data”, Geoscience and Remote Sensing Symposium, 1995. IGARSS '95. 'Quantitative Remote Sensing for Science and Applications', International , Volume: 1 , Page(s): 706 707 vol.1., 10-14 July 1995.

Hoekman D. H., “ERS-1 Observations of tropical rain forest in Araracuara, Colombia”, Proceeding Final Workshop ERS-1 Study ’94”, EUR 17286 en, JRC, EU 1997a.

Hoekman D. H., “Radar monitoring system for sustainable forest management in Indonesia”, Geoscience and Remote Sensing. IGARSS '97. 'Remote Sensing - A Scientific Vision for Sustainable Development”, IEEE International, Volume: 4 , 3-8 Aug. 1997, Page(s): 1731 -1733 vol.4, 1997b.

Hoekman D. H., “Synthesis for Latin American sites”, Proceeding Final Workshop ERS-1 Study ’94”, EUR 17286 en, JRC, EU 1997c.

Hoekman D.H. and Quiñones M.J, “Land cover type and forest biomass assessment in the Colombian Amazon”, Geoscience and Remote Sensing, 1997. IGARSS '97. 'Remote Sensing - A Scientific Vision for Sustainable Development”, 1997 IEEE International , Volume: 4, Page(s): 1728 -1730 vol.4, 3-8 Aug. 1997d.

Hoekman D.H. and Quiñones M.J., “Land cover type and biomass classification using AirSAR data for evaluation of monitoring scenarios in the Colombian Amazon”, Geoscience and Remote Sensing, IEEE Transactions on , Volume: 38 Issue: 2, Page(s): 685 -696, March 2000.

Hoekman D.H. and Varekamp C., “Observation of tropical rain forest trees by airborne high-resolution interferometric radar”, Geoscience and Remote Sensing, IEEE Transactions on , Volume: 39 Issue: 3, Page(s): 584 -594, March 2001.

Hoekman D.H. and Quiñones M.J, “Biophysical forest type characterization in the Colombian Amazon by airborne polarimetric SAR”, Geoscience and Remote Sensing Symposium, 2001. IGARSS '01. IEEE 2002 International , Volume: 3, Page(s): 1288 -1300, vol.3., 9-13 July 2002.

Huising E., and Lemoine G.G., “Costa Rica ERS-1 data analysis”, Proceeding Final Workshop ERS-1 Study ’94”, EUR 17286 en, JRC, EU 1997.

INPE (Instituto National de Pesquisas Espaciais), PRODES: assessment of deforestation in Brazilian Amazonia, Sau Paulo: INPE, 1996.

INPE, “INPE atualiza os dados do desflorestamento na Amazônia, de 95 a 97”. INPE Notícias 13, 1-2. São Paulo: Instituto Nacional de Pesquisas 1998.

Jain A. K. and Dubes R. C., Algorithms for Clustering Data. Englewood Cliffs, Prentice Hall, UK 1988.

Jain A. K. and Binford T. O., “Ignorance, myopia and naivete` in computer vision systems,” Comput. Vision, Graphics, Image Processing: Image Understanding, vol. 53, pp. 112-117, 1991.

Jerry H., The soil resource: Origin and behavior, Ecological Studies 37, 3d ed. Springer-Verlag, pp. 377, 1986.

Jhung Y. and Swain P. H., “Bayesian contextual classification based on modified M-estimates and Markov Random Fields,” IEEE Trans. Geosci. Remote Sensing, vol. 34, no. 1, pp. 67-75, 1996.

Johnston, C. A, Geographic Information Systems in Ecology, Oxford, Blackwell Science, 1998.

Keil M., Scales D. R., Schmidt M., Kux H., Dos Santos J. R., and Pereira M., “Investigation of SIR-C/X_SAR Data for Landcover Characterization in Southwest Amazon, SIR_C/X_SAR”, Final Report, NASA/JPL, March 1997.

Keil M., Scales D. R., Semmt D., Winter W., Honsch H., and Lohmann G., “Tropical rainforest investigation with ERS-1 SAR data in the region of Sena Maudureira, Acre/Brazil“, Proceeding Final Workshop ERS-1 Study ’94”, EUR 17286 en, JRC, EU 1997.

Krishnamachari S. and Chellappa R., “Multiresolution Gauss-Markov random filed models for texture segmentation,” IEEE Trans. on Image Processing, vol. 6, no. 2, pp. 251-267, 1997.

Kummer D.M., “Remote sensing and tropical deforestation: A cautionary note for Philippines”, Photogrammetric Engineering and Remote Sensing, Vol.58, no. 10, pp. 1469-1471, 1992.

Kunt M., “Comments on ‘Dialogue,’ a series of articles generated by the paper entitled ‘Ignorance, myopia and naivete` in computer vision systems’,” Comput. Vision, Graphics, Image Processing: Image Understanding, vol. 54, pp. 428-429, 1991.

Lammerts van Bueren E.M and Blom, E.M, “Hierarchical framework for the formulation of sustainable forest management standards”, Wageningen, The Tropenbos Foundation, 82 p., 1997.

Lanly J.P., Tropical Forest Resources. Rome, Italy: FAO, FAO Forestry Paper 30: 106 pp., 1982.

Looyen W.J., Zeppenfeldt F.O., Venema J.C., van der Burg G., Hoekman, D.H., van der Sanden J.J., Reichert P.G., Westinga E., “FAME: a forest assessment and monitoring environment scenario”, IGARSS '93. 'Better Understanding of Earth Environment', International, 18-21 Aug. 1993, Page(s): 1146 -1148, vol.3, 1993.

Malingreau J. P., Achard F., D’Souza G., Stibig H.J., D’Souza J., Estreguil C., and Eva H., “AVHRR for global tropical forest monitoring: the lessons of the TREES project”, Remote Sensing Reviews, vol.12, pp. 29-40, 1995.

Malingreau J. P., G. Duchossois, “The TREES ERS-1 SAR ’94 Project- Executive Summary, Final Workshop ERS-1 Study ’94”, EUR 17286 en, JRC, EU 1997.

Mallat S. and Hwang W., “Singularity Detection and Processing with Wavelets”, IEEE Trans. Information Theory, vol. 38, no. 2, pp. 617-642, 1992.

Mallat S. and Zhong S., “Characterization of Signals from Multiscale Edges”, IEEE Trans. Pattern Anal. Machine Intell., vol. 14, no. 7, pp. 710-732, 1992.

Mallat S., “A Theory for Multiresolution Signal Decomposition: The Wavelet Representation”, IEEE Trans. Pattern Anal. Machine Intell., vol. 2, no. 7, pp. 674-692, July 1989.

Mallat S., A Wavelet Tour of Signal Processing, 2nd edition, San Diego: Academic Press, pp. 163-219, 1999.

Martins D.S., de Benayon, C. B. Oliveira Filho, D. Bassi, “Agroforesta - Progetto per l’utilizzo eco-compatibile della Foresta Amazzonica mediante l’utilizzo di specie legnose autoctone da frutto e da legno”, Manaus (Amazzonia Brasile), Dec. 1999.

Mas J. F. and Ramirez I., “Comparison of land use classifications obtain by visual interpretation and digital processing”, ITC Journal n. 1996-3/4, pp. 278-283, 1996.

Mas J.F, “Monitoring land cover changes: a comparison of change detection techniques”, Int J. Remote Sensing, Vol. 20, n.1, pp.139-152, 1999.

Mather M. P., Computer Processing of Remotely Sensed Images, 5th ed., Chichester: John Wiley & Sons, 1987.

Mayaux P. and Lambin E., “Estimation of tropical forest area from coarse spatial resolution data: a two-step correction function for proportional errors due to spatial aggregation”, Remote Sensing of Environment, Vol. 53 (1), pp. 1-16, 1995.

Mayaux P. and Lambin E., “Tropical forest area measured from global land-cover classifications: inverse calibration models based on spatial textures”, Remote Sensing of Environment 59: 29-43, 1997.

Mayaux P., Achard F. and Malingreau J.P., "Global Tropical Forest Area Measurements Derived from Coarse Resolution Satellite Imagery: a Comparison with Other Approaches", Environmental Conservation, 25 (1), pp. 37-52, 1998.

Mayaux P., De Grandi G.F., and Malingreau J.P., "Central Africa Forest Cover Revisited: a Multisatellite Analysis", Remote Sensing of Environment, 71:183-196, 2000.

Mayaux P., De Grandi G. F., Rauste, Y., Simard, M., and Saatchi, S., 2000, “Regional Scale Vegetation Maps Derived from the combined L-band GRFM and C-band CAMP Wide Area Radar Mosaics of Central Africa”, International Journal of Remote Sensing, International Journal of Remote Sensing, Vol. 23 No.7, 2002.

Mellillo J. M., Houghton R. A., Kicklighter D. W. and Mcguire, A. D., Tropical deforestation and the global carbon budget, Annual Rev. Energy Environment, 21, 293-310, 1996.

Myers N., Deforestation Rates in Tropical Forests and Their Climatic Implications, London, UK: Friends of the Earth: 78 pp., 1989.

Myers N., “Conversion of Tropical Moist Forests”, Washington DC, USA: National Academy of Sciences: 205 pp., 1980.

Myers N., “The world's forests: problems and potentials”, Environmental Conservation, 23,156-169, 1996.

Myers N., “Tropical forests the main deforestation fronts”, Environmental conservation, 20, 9-16, 2000.

Nepstad C. D., Verissimo A., Alencart A., Nobre C., Lima E., Lefebvre P., Schlesinger P., Potter C., Moutinho P., Mendoza E., Cochrane M., and Brooks V., “Large-scale impoverishment of Amazonian forests by logging and fire,” Nature, vol. 398, pp. 505-508, April 1999.

Niedermeier A., Romaneeßen E. and Lehner S., 2000, “Detection of Coastlines in SAR Images Using Wavelet Methods,” IEEE Trans. Geosci. Remote Sensing, vol. 5, no. 38, pp. 2270-2281, 2000.

Nobre A. C., Sellers J. P., Shukla J., “Amazonian Deforestation and Regional Climate Change”, Journal of Climate, Vol. 4, October 1991.

Olmsted C., “Alaska SAR Facility Scientific SAR User’s Guide”, July 1993.

Pappas T. N., “An adaptive clustering algorithm for image segmentation,” IEEE Trans. on Signal Processing, vol. 3, no. 2, pp. 162-177, 1992.

Patane` G. and Russo M., “ELBG Implementation," Int. Journal of Knowledge based Intelligent Engineering Systems, vol. 4, pp. 94-109, 2000.

Patane` G. and Russo, M., “The Enhanced-LBG Algorithm,” Neural Networks, vol. 14, no. 9, pp. 1219-1237, Nov. 2001.

Patane` G. and Russo M., “Fully Automatic Clustering System,” IEEE Trans. Neural Networks, accepted for publication, 2002.

Peralta P. and Mather P., “An analysis of deforestation patterns in the extractive reserves of Acre, Amazonia from satellite imagery: a landscape ecological approach,” Int. J. Remote Sensing, vol. 21, no. 13-14, pp. 2555-2570, 2000.

Podest E. and Saatchi S., “Application of Multiscale Texture in Classifying JERS-1 Radar Data Over Tropical Vegetation”, International Journal of Remote Sensing, Vol. 23 No.7, 2002.

Prance G. T. and Lovejoy T. E., Environments: Amazonia, Oxford: Pergamon, 1985.

Rauste Y., De Grandi G. F., Pasquali P., Holectz F., Rosenqvist A., Perna G., and Franchino E., “Radiometric Calibration of JERS-1 SAR Data in Connection with the GRFM Africa Mosaic Compilation”, JERS Science Program ’99, PI Reports, (Earth Observation Research Center, NASDA), pp. 92-98, March 1999a.

Rauste Y, Richards, T., De Grandi, G. F., G., Franchino E., and Rosenqvist A., “Compilation and validation of the GRFM Africa (SAR) Mosaics using Multi Temporal Block Adjustment”, JERS Science Program ’99, PI Reports (Earth Observation Research Center, NASDA), 99-108, 1999b.

Rignot E. and Chellappa R., “A Bayesian classifier for change detection”, in Proc. Int. Conf. Acoust., Speech, Signal Processing ICASSP ’92, IEEE Cat. 92CH3101-9, San Francisco, CA, Vol., ,pp. 25-28, 1992.

Rignot E. J. M. and van Zyl J.J., “Change Detection Techniques for ERS-1 SAR Data”,IEEE Trans. on Geoscience and Rem. Sens.,Vol.31, No.4, pp. 896-1271, July 1993.

Rosenqvist A., "The Global Rainforest Mapping Project by JERS-1 SAR", Int. Archives of Photogramm. and Rem. Sens., Vol. 31, Part B7, pp. 594-598, ISPRS, Vienna, Austria, 1996.

Rosenqvist A., Forsberg B.R., Pimentel T., Richey J.E., "Using JERS-1 L-band SAR to estimate methane emissions from the Jau river floodplain", IEEE IGARSS'98. Seattle, USA, , pp. 1623-1625, Vol. III, 6-10 July 1998.

Rosenqvist A., Birket C., Bartholome' E. and De Grandi G.F., "Using Satellite Altimetry and Historical Gauge Data for Validation of the Hydrological Significance of the JERS-1 SAR (GRFM) Mosaics in Central Africa", Proc. IGARSS'99, Hamburg, Germany. IEEE Catalogue No. 99CH36293C, 1999.

Rosenqvist A., Shimada M., Chapman B., , Freeman A., De Grandi G.F., Saatchi S., and Rauste Y., "The Global Rain Forest Mapping Project - A Review", Int. Journal of

Remote Sensing, special issue on "Global and Regional Land Cover Characterization from Satellite Data, vol. 21, no. 6-7, pp. 1375-1388, Apr. 2000.

Saatchi S., De Grandi G.F., Simard M., Podest E., "Classification of JERS-1 Image Mosaic of Central Africa using A Supervised Multi scale Classifier of Texture Features", Proc. IEEE IGARSS'99, Hamburg, Germany, paper EE10_06, 1999.

Saatchi S., Soares J. V. and Alves. S. D., "Mapping Deforestation and Land Use in Amazon Rainforest by Using SIR-C Imagery", Remote Sens. Environ. 59: 191-202, 190, 1997.

Saatchi S., Nelson B., Podest E., and Holt J., "Mapping land cover types in the Amazon Basin using 1 km JERS-1 mosaic", International Journal of Remote Sensing, 6 & 7, 1201-1234, 2000.

Salas W. A., Rignot E., and Skole D., "Study of Land-use and deforestation in Central and West Africa Tropical Forest using High Resolution SAR Satellite Imagery", JERS-1 Science Program '99 IP Reports, EORC-NASDA, March 1999.

Salas W. A., Ducey MJ, Rignot E, Skole D., "Assessment of JERS-1 SAR for monitoring secondary vegetation in Amazonia: I. Spatial and temporal variability in backscatter across a chrono-sequence of secondary vegetation stands in Rondonia", International Journal of Remote Sensing, 23, 1357-1379, 2002.

Salvador R. and Pons X., "On the Riability of Landsat TM for Estimating Forest Variables by Regression Techniques: A Methodological Analysis" ", IEEE Trans. on Geoscience and Rem. Sens., Vol.36 , No.6, pp. 1888-1897, November 1998.

Sayer J. A., Harcourt C. S. and Collins N. M, The conservation Atlas of Tropical Forests: Africa, Macmillan, London, , pp. 258, UK 1992.

Schmidt M., Keil M., Scales D.R., Dos Santos J.R., Kux H., "Investigation of deforestation dynamics and land use changes by Ers-1 SAR data in Rondonia; Brazil", Proc. of International Seminar On The Use and Applications of ERS in Latin America, Vina do Mar, Chile, Nov. 1996 (ESA SP-405, March 1997).

Sgrenzaroli M., Eva H. and Achard F., "Assessment of resolution L-band radar mosaics for regional forest change detection in lowland tropical forests of South America", Proceedings of the Conference on Remote Sensing and Forest Monitoring,

T. Zawila-Niedzwiecki, M. Brach (Eds.), EUR 19530/EN (2000) 208-215, European Commission, Luxembourg, 2000.

Sgrenzaroli M., Baraldi A., De Grandi G.D., Eva H. and Achard F., 2002, “Forest Degradation Assessment in South America form Landsat TM Images Using a Contextual Clustering Technique for Image Labeling, IEEE Transactions on Geoscience and Remote Sensing”, vol. 40, August 2002a.

Sgrenzaroli M., De Grandi G.D., Eva H. and Achard F., “Tropical Forest Cover Monitoring Estimates and Validation form the GRFM JERS-1 Radar Mosaics Using Wavelets Zooming Technique”, International Journal of Remote Sensing, Vol. 23 No.7, 2002b.

Shimada M., "Radiometric and geometric calibration of JERS-1 SAR", Advances in Space Research, Vol. 17, No. 1, p. (1) 9-(1)88, 1996.

Shimada M., Wakabayashi H., Tadakono T., Isoguchi O., and Miyagawa,H., “Jers-1 SAR Mosaics over Southeast Asia”, in proceeding IGARSS 2000, Vol. I, pp. 1-3 IEEE Catalog No. 00CH37120, Hawaii, USA, 24-28 July, 2000.

Simard M., De Grandi G.F., Saatchi S., Leysen M., and Thomson K.P.B., "Processing and Analysis Techniques for Continental Scale Radar Maps of the Tropical Forest", Proc. IEEE IGARSS'97 Symp., pp. 1890-92, Singapore 1997.

Simard M., De Grandi G. F., and Thomson K., "Adaptation of the Wavelet Transform for the Construction of Multiscale Texture Maps of SAR images", Canadian Journal of Remote Sensing, Vol. 24, No. 3, pp. 264-285, September 1998a.

Simard M., De Grandi G. F., Thomson, K., Benie' G.B., "Analysis of Speckle Noise Contribution on Wavelet Decomposition of SAR Images", IEEE Trans. Geosci. Remote Sensing, Vol. 36, No. 6, pp. 1953-1962, Nov. 1998b.

Simard M., Saatchi S., De Grandi G.F., "Classification of the Gabon SAR Mosaic using a Wavelet Based Rule Classifier", Proc. IEEE IGARSS'99, paper EE10_07, Germany, Hamburg 1999.

Singh A., “Spectral separability of tropical forest cover classes,” Int. J. Remote Sensing, vol. 8, pp. 971-979, 1987.

Singh A., “Digital Change Detection Techniques using remotely sensed data”, Int. Journal of remote Sensing, Vol. 10, pp. 989-100, 1989.

Siqueira P., Hesley S., Shaffer S., Hess L., Mcgrarragh G., Chapman B., Holt J., and Freeman A., “A continental Scale Mosaic of the Amazon Basin using JERS-1 SAR”, IEEE Transactions on Geoscience and Remote Sensing, vol. 38, no. 6, 2637-2644. 2000.

Skole D. and Tucker C. J., “Evidence for tropical deforestation, fragmented habitat, and adversely affected habitat in the Brazilian Amazon: 1978-1988,” Science, vol. 260, pp. 1905-1910, 1993.

Smits P. C. and Dellepiane S. G., “Synthetic aperture radar image segmentation by a detail preserving Markov Random Field approach,” IEEE Trans. Geosci. Remote Sensing, vol. 35, no. 4, pp. 844-857, 1997.

Stewart C., Moghaddam B., Hintz K. and Novak L., "Fractional Brownian Motion Models for Synthetic Aperture Radar Imagery Scene Segmentation", Proc. of the IEEE, vol. 81, no. 10, pp. 1511-1522, Oct. 1993.

Stone A. and Lefebvre T. P., “Using multi-temporal satellite data to evaluate selective-logging in Pará, Brazil”, Int. J. Remote Sensing, vol. 19, n. 13, pp. 2517-2526, 1998.

Thome K. J., Biggar S.F., Gellman D.I. and Slater P.N., "Absolute Radiometric Calibration of Landsat-5 Thematic Mapper and the Proposed Calibration of the Advanced Spaceborne Thermal Emission and Reflection Radiometer", Proceedings of IGARSS-94, Vol. 4, pp. 2295-2297, Pasadena, California, 1994.

Teillet, P.M., J.L. Barker, B.L. Markham, and J.C. Storey, "Long-Term Consistency of the Landsat Data Record: Landsat-7 ETM+ and Landsat-5 TM Cross-Calibration Plan"; Version 1.0 (December 17, 1999), Landsat Project Science Office, Code 923, Bldg 33, Rm 425, NASA Goddard Space Flight Center, Greenbelt, MD 20771, 1999.

Tou J. T. and Gonzalez R. C., Pattern Recognition Principles, Addison-Wesley Publishing Company, Reading, Massachusetts, 1974.

TRFIC Tropical Rain Forest Information Center, NASA's Earth Science Information Partnership, http://bsrsi.msu.edu/trfic/index.html.

U.S. Geological Survey, professional Paper 1395, “Map Projections-A working manual”, Navtech Seminar & Navtech Book and Software Store, Inc., from U.S. Government document, November 1993.

Uhl C. and Vieira I. C., “Ecological impacts of selective logging in the Brazilian Amazon: a case study from the Paragominas region of the State of Pará”, Biotropica, vol. 21 (2), pp. 98-106, 1989.

UNEP/IUC, The Kyoto Protocol to the Convention on Climate Change, Geneva: UNEP/IUC Executive Center, 3rd Edition, 1999.

Unser M., Aldroubi A. and M. Eden, “B-Spline Signal Processing: Part I-Theory”, IEEE Trans. Signal Processing, vol. 41, no. 2, February 1993.

USDA Forest Service, “Interim Resource Inventory Glossary. File 1900”, Dated 14 June, 1989. Washington, DC: U.S. Department of Agriculture, Forest Service p.96, 1989.

Van der Sanden J. J. and Hoekman D. H., “Potential of Airborne Radar To Support the Assessment of Land Cover in a Tropical Rain Forest Environment”, Remote Sensing of Environment, Volume 68, Issue 1, Pages 26-40, April 1999.

Van der Sanden, J.J., and Hoekman, D.H., “Multiband polarimetric SAR in support of tropical forest resources assessment”, Geoscience and Remote Sensing Symposium, IGARSS '95. 'Quantitative Remote Sensing for Science and Applications', International , Volume: 2 , 10-14 July 1995, Page(s): 1207 -1209 vol.2, 1995.

Van der Sanden J. J., “Analysis of ERS-1 SAR data for Mabura Hill, Guyana”, Proceeding Final Workshop ERS-1 Study ’94”, EUR 17286 en, JRC, EU 1997a.

Van der Sanden J. J., “Radar remote sensing to support tropical forest management”, Tropenbos-Guyana Series 5, 1997b.

Varekamp, C., and Hoekman, D. H., “Segmentation of high-resolution InSAR data of a tropical forest using Fourier parameterized deformable models”, Int. J. Remote Sensing, vol. 22, pages 12-2399, 2001.

Wilding L. P., Smeck E. N., and Hall G. F., Pedogenesis and soil taxonomy. LFII: the soil orders”, developments in soil Science, Vol. LF11b, Elsevier, 410 pp., eds. 1983.

Williams M. L., “The influence of canopy shape on SAR speckle distributions over woodland”, Proc. IGARSS’97, Singapore, August 1997, Piscataway NJ IEEE, pp. 755-7, 1997.

Woodcock C. E. and Strahler A. H., “The factor of scale in remote sensing”, Remote Sensing of Environment 21: 311-25, 1987.

Woodhouse I.H. and Hoekman, D.H, “Tropical forest monitoring using data from the ERS-1 Wind Scatterometer’, Geoscience and Remote Sensing Symposium, 1996. IGARSS '96. 'Remote Sensing for a Sustainable Future”, n. 27-31, Page(s): 845 -847 vol. 2, May 1996.

Wooding M. G., and Batts A. J., “Assessment of ERS-1 SAR data for monitoring deforestation Rondonia, Brazil”, Proceeding Final Workshop ERS-1 Study ’94”, EUR 17286 en, JRC, EU 1997.

Yanasse C. da C. F., Sant’Anna S J. S., Frery C. A., Renno’ C. D., Soares J. V., and Luckman A. J., “Exploratory Study of the Relationship between Tropical Forest Regeneration Stages and SIR-C L and C data”, Remote Sens. Environ. 59: 180-190, 1997.

Zamperoni P., “Plus ça va, moins ça va,” Pattern Recognition Letters, vol. 17, no. 7, pp. 671-677, 1996.

Zhang H., McGuffie K. and Henderson-Sellers A., “Impacts of tropical deforestation. Part II: The role of large-scale dynamics”, Journal of Climate, 9, 2498-2521, 1996.

Abbreviations and Acronyms

AFS	Agro-Forest Systems
ELBG	Enhanced Linde-Buzo-Gray
FAO	Food Agriculture Organization
GRFM	Global Rain Forest Mapping
GVM	Global Vegetation Monitoring
INPA	Instituto Nacional de Pesquisas da Amazonia (Brazil's National Institute for Amazon Research)
INPE	Instituto Nacional de Pesquisas Espaciais (Brazilian Space Research Agency)
JERS – 1	Japanese Earth Resources Satellite 1
JPL	Jet Propulsion Laboratory
JRC	Joint Research Centre
Landsat TM	Landsat Thematic Mapper
MAP	Maximum A Posteriori
MI	Matheron indices
MPAC	Modified Pappas Adaptive Clustering
MRFs	Markov Random Fields
NASDA	National Space Development Agency of Japan
NMP	Nearest Multiple-Prototype
PA	Perimeter-over-area ratio indices
SA	South America
SAI	Space Applications Institute
SAR	Synthetic Aperture Radar
SM	Spatial Measurement
TREES	Tropical Forest Ecosystem Environments monitoring by Satellites.
TRFIC	Tropical Rain Forest Information Centre
IHS	Intensity-Hue-Saturation colour transformation
i.i.d.	independent and identically distributed
MSE	mean square error
RMS	root means square

List of publications

Carcano G. and Sgrenzaroli M., 1999, “Telerilevamento da satellite con tecnologia SAR: Individuazione delle risaie nel Sud-Est Asiatico”, Rivista Italiana di Telerilevamento n. 14/15 Sept. 98-Gen. 99.

Carcano G., Sgrenzaroli M. and Lechi G., “Telerilevamento da satellite con tecnologia SAR: individuzione delle risaie nel Sud Est Asiatico”, in proceeding Asita symposium, Parma 1999.

Carcano G., Casartelli G., Sgrenzaroli M., Sgrenzaroli R., Smiraglia A. and Vassena G., 1999, “L’impiego di strumentazione satellitare GPS in modalità RTK, per il calcolo delle variazioni di massa dei ghiacciai”, Communication at 8° Convegno Glaciologico Italiano Bormio 9-12 settembre 1999.

Sgrenzaroli M., De Grandi F., and Simard M., “Evaluation of the GRFM radar mosaic potential for quantitative assessment of deforestation in Amazonia” Communication at GRFM Meeting, INPE Brazil Nov. 8-12, S. Jose dos Campos, 1999.

Sgrenzaroli M., Eva H. and Achard F., “Assessment of resolution L-band radar mosaics for regional forest change detection in lowland tropical forests of South America”, in proceedings of the Conference on Remote Sensing and Forest Monitoring, T. Zawila-Niedzwiecki, M. Brach (Eds.), EUR 19530/EN (2000) 208-215, European Commission, Luxembourg, 2000.

De Grandi G. F, Mayaux P., Massart M. Baraldi A., Sgrenzaroli M., “A vegetation Map of the Central Congo Basin Derived from Microwave and Optical Remote Sensing Data Using a Variable Resolution Classification Approach”, In proceedings IGARSS 01 , Sydney, Australia. July 9-13, IEEE Catalog No. 01CH37217C, 2001.

Sgrenzaroli M., De Grandi G.D., Eva H. and Achard F., “Tropical Forest Cover Monitoring Estimates and Validation form the GRFM JERS-1 Radar Mosaics Using Wavelets Zooming Technique”, International Journal of Remote Sensing, Vol. 23 No.7, 2002.

Sgrenzaroli M., Baraldi A., De Grandi G.D., Eva H. and Achard F., “Forest Degradation Assessment in South America form Landsat TM Images Using a Contextual Clustering Technique for Image Labelling”, IEEE Transactions on Geoscience and Remote Sensing, , vol. 40, August 2002.

Wolfart E., Sgrenzaroli M., “Accurate texture mapped 3D Models for documentations, surveying and presentation purposes”, in proceeding CIPA symposium, Corfu 2002.

Drap P., Sgrenzaroli M., Canciani M., Cannata G., Seinturier J., “Laser Scanning and close range photogrammetry: Towards a single measuring tool dedicated to architecture and archaeology”, in proceeding ISPRS symposium, Antalia 2003.

Eva H.D., de Miranda E.E., Di Bella C.M., Gond V., Huber O., Sgrenzaroli M.,Jones S., Coutinho A., Dorado A., Guimarães M., Elvidge C., Achard F., Belward A.S., Bartholomé E., Baraldi A., De Grandi G., Vogt P., Fritz S., Hartley A., “A Vegetation map of South America”, EUR 20159/EN (2002), European Commission, Luxembourg 2002.

Sgrenzaroli M., Baraldi A., De Grandi G., Eva H. and Achard F., “A Novel Operational Approach to Tropical Vegetation Mapping at Regional Scale Using the GRFM Radar Mosaics”, IEEE Transactions on Geoscience and Remote Sensing (accepted first revision).

Curriculum Vitae

Matteo Sgrenzaroli was born in Italy in 1972. He received the degree in Environmental Engineering from Polytechnic of Milan, in 1997. In 1997, he was involved with South East Asia Radar Rice Investigation (SEARRI) project of the Space Application Institute (SAI), European Commission Joint Research Centre (EC-JRC), for the analyses ERS and JERS -SAR multi-temporal data sets.

In 1998, he participated to the organization of *Changri Nup* glacier monitoring expedition promoted by University of Brescia, within the context of EV-K2 Project of National Council of Research of Italy (CNR) for Himalayas glacier survey using G.P.S. system. In 1999, he was admitted to the Ph.D. Program of Wageningen Agricultural University (The Netherlands). He worked as a Ph.D. fellow at SAI (EC-EU) for the exploitation of JERS-1 Radar Mosaic for Tropical deforestation monitoring from 1999 to 2001. From October 2001 to February 2003, he has been with 3DVeritas, a spin-off from the EC-JRC founded in 2001, as project manager for developing software for complete 3D modelling through laser scanner data and digital images. Since March 2003 is Laser Scanner responsible within the Centre of Competence for Geomatic and Survey of the innovation technology consortium – Inn.Tec. - in Brescia (Italy). In September/October 2003, he participated to the Himalayan glacier monitoring expedition promoted by University of Brescia, Politecnico of Milano, Inn.Tec. and "*Umana Dimora*" Environmental Association, as responsible for Everest Glacier Laser Scanner survey.

The research work reported in this thesis was supported by the European Commission DG-JRC under a category 20 grant. Work was performed at the Global Vegetation Monitoring Unit, Institute for Environment and Sustainability, DG Joint Research Centre, Ispra (Varese, Italy).

Cover: Over the South America forest map derived from GRFM South America Mosaic, 4 sample tiles of different deforestation patterns within the Amazon Basin. Samples extracted from GRFM South America Mosaic.